UNICA

UNIVERSITÀ
DEGLI STUDI
DI CAGLIARI

Ph.D. DEGREE IN
PHYSICS

Cycle XXXVI

Nonsingular and deformed black holes

Fundamental aspects and phenomenology

Scientific Disciplinary Sector(s)

FIS/02

Ph.D. Student: Mauro Oi

Supervisor Prof. Mariano Cadoni

Final exam. Academic Year 2022/2023
Thesis defence: January 2024 Session

Abstract

Einstein's theory of gravity, general relativity, stands as one of the most successful and enduring pillars of modern physics. Its predictions have consistently aligned with a vast array of observed phenomena within our Universe. However, the enigmatic nature of gravity persists, particularly when examined at both extremely short and exceedingly vast distances. In this thesis, we explore several aspects of black hole physics, which could encode signatures of quantum gravity effects at different, even macroscopic, scales. We will investigate modifications and deformations of classical black-hole geometries in a model-independent manner. We start by deriving a general class of regular black holes sourced by an anisotropic fluid violating the strong energy condition and allowing for the circumvention of Penrose's theorems. The anisotropies are then assumed to parameterize some quantum effects, whose typical scale is encoded in an additional quantum parameter (hair) ℓ. We then turn our attention to the thermodynamics of these models, revealing a preference for the states with ℓ of the order of the horizon scale. This aspect is further investigated through theanalysis of semiclassical dynamics, i.e., the Hawking evaporation process, by using a simple two dimensional balck-hole model. We also test these models against orbits of stars around our galactic center, placing constraints on the strength of the quantum effects. In a separate developement, we study a general class of deformed, rotating, singular black holes, focusing on their phenomenology and, in particular, the superradiant amplification of test fields. We then consider the problem of describing the gravitational field generated by a quantum particle in a delocalized state. The resultant geometry resembles the first models we analyzed, allowing to reinterpret the smearing of the singularity in terms of the uncertainty principle. Finally, we analyze a model in which black holes are medelled as sets of oscillators whose typical frequencies are given by the quasinormal modes of the systems. Under some assumptions, we are able to obtain the Bekenstein-Hawking formula for the entropy and its first, logarithmic correction. Finally, we reinterpret this model in terms of the dual conformal field theory at the boundary, finding that the perturbations of two-dimensional regular black holes are related to a conformally-invariant generalization of the quantum harmonic oscillator, described by the de Alfaro-Fubini-Furlan theory.

Keywords: general relativity; quantum gravity; black holes; regular black holes; anisotropic fluids; singularity; Hawking radiation; evaporation; Kerr-like black holes; superradiance; phenomenology; tests of general relativity; S2-star.

Contents

Preface

In this thesis, we adopt natural units, where $c = \hbar = k_B = 1$, except for Chapter I.5, where we use geometric units where $c = G = 1$. For simplicity, we will remind the convention in each chapter. The signature of the metric is $(-,+,+,+)$, and greek indices indicate spacetime components of vectors and tensors, ranging from 1 to 4 and from 1 to 2 respectively for 4D and 2D metrics. We tried to keep each chapter as much self-contained as possible, sometimes at cost of some repetitions. For this reason, the acronyms will be redifined at the beginning of each chapter.

This thesis is based on the following works.

[1] M. Cadoni et al. "Effective models of nonsingular quantum black holes". *Phys. Rev. D* **106**.2 (2022), 024030. arXiv: 2204.09444 [gr-qc],

[2] M. Cadoni et al. "Evaporation and information puzzle for 2D nonsingular asymptotically flat black holes". *JHEP* **06** (2023), 211. arXiv: 2303.05557 [hep-th],

[3] M. Cadoni et al. "Are nonsingular black holes with super-Planckian hair ruled out by S2 star data?" *Phys. Rev. D* **107**.4 (2023), 044038. arXiv: 2211.11585 [gr-qc],

[4] E. Franzin et al. "Superradiance in Kerr-like black holes". *Phys. Rev. D* **103**.10 (2021), 104034. arXiv: 2102.03152 [gr-qc],

[5] A. Akil et al. "Semiclassical spacetimes at super-Planckian scales from delocalized sources". *Phys. Rev. D* **108**.4 (2023), 044051. arXiv: 2211.01657 [gr-qc],

[6] M. Cadoni et al. "Quasinormal modes and microscopic structure of the Schwarzschild black hole". *Phys. Rev. D* **104**.12 (2021), L121502. arXiv: 2109.10744 [gr-qc],

[7] M. Cadoni et al. "Quasi-normal modes and microscopic description of 2D black holes". *JHEP* **01** (2022), 087. arXiv: 2111.07763 [gr-qc].

Moreover, during my first year of PhD, I was also involved in a project in which we studied the Newtonian noise produced by turbulence in the atmosphere above a gravitational wave detector:

[8] D. Brundu et al. "Atmospheric Newtonian noise modeling for third-generation gravitational wave detectors". *Phys. Rev. D* **106**.6 (2022), 064040. arXiv: 2206.02610 [gr-qc].

Introduction

General relativity is one of the most successful theories the scientific community has been able to conceive. Its predictions have been accurately tested in a large range of scales, from millimetric to cosmological distances. Einstein's field equations, which describe the dynamics of the gravitational field generated by some matter source, stem from the Einstein-Hilbert action and were first solved in their full nonlinear complexity by Karl Schwarzschild in 1916, only one year after the publication of the theory of general relativity. The Schwarzschild solution describes the simplest static gravitational system, composed by a point-like, spherically-symmetric, uncharged particle of mass M [9]. This metric describes the exterior geometry of any nonrotating body and corresponds, as was later identified, to a static and spherically-symmetric black hole of mass M. The generalization to a rotating system appeared in literature only in 1964 when Kerr found its solution to Einstein's equations [10]. The Schwarzschild and the Kerr solutions provided, in the last century, a large number of accurate predictions. The former has been widely used to validate general relativity predictions in the Solar system (see Ref. [11], and references therein, for a comprehensive review), the most famous results being those related to the precession of Mercury's perihelion, the bending angle of light, and the gravitational redshift. The latter, instead, has been broadly tested [11], from X-ray observations [12] to the latest black-hole images [13–15] and gravitational-wave detections [16–18].

Despite being such a powerful tool, we know that general relativity and black holes cannot be the end of the story. For instance, the infrared phenomenology can be understood only assuming the presence of some exotic forms of matter and energy, interacting only via gravity and therefore called *dark*, whose origin is not clear. Dark matter have been first introduced while trying to explain the rotational curves of galaxies and some gravitational lensing observations. In these systems, general relativity predicts a large amount of extra matter that cannot be observed via electromagnetic observations. On the other hand, cosmological data clearly show that our universe is expanding at an accelerated rate. This can be explained, in the classical, general-relativistic framework, only by introducing some extra energy content, encoded in the cosmological constant Λ, whose origin is, again, poorly understood [19–21].

Over the years, several classical theories have been put forth to address the challenges associated with the long-distance behavior of Einstein's gravity. Alternative gravitational theories have also emerged in attempts to resolve certain issues within general relativity, such as its discrepancies with galactic and cosmological observations (see, e.g., Refs. [22, 23], and [24, 25] for reviews on the topic) and even its compatibility with quantum mechanics.

The infrared behavior of gravity is not the only problem of general relativity since Einstein's theory also shows some inconsistencies at short scales. Black holes, for example, are plagued by a severe problem: while being the simplest solutions of Einstein's theory, described by three parameters only [26], they hide a curvature singularity in their core, shielded behind an event horizon. Although the presence of a horizon saves the theory from being completely unpredictive in a neighbour of the singularity, its presence still shows our ignorance of the short scale, ultraviolet behavior of the theory. Indeed, a clear understanding of this regime would need a complete and consistent theory of quantum gravity, but its formulation remains elusive. While in literature there have been many attempts in capturing the essence of the quantum behavior of gravitational

systems beyond the semiclassical approximation, including string theory [27–29], the AdS/CFT correspondence [30–32], loop quantum gravity [33, 34], and, more recently, corpuscular quantum gravity [35–40] (for a more exhaustive discussion, see Chapter II.1), none of these attempts have been successful in providing a complete and satisfactory description of quantum gravity. What we know on a firm ground mostly relies on the semiclassical approximation, based on the pioneriing works of Hawking [41] in which he tackled, for the first time, the problem of studying the behavior of quantum fields in a curved spacetime. His main results indicate that a black-hole spacetime is not actually *black* but emits thermal radiation at some nonzero temperature. However, while this result represented a first step in understanding the small-scale behavior of gravity, at least on a semiclassical level, it also rised several problems regarding the incompatibility of general relativity with quantum mechanics [42, 43]. Moreover, black holes exhibit a large amount of entropy, indicating that these systems should have an intricate microscopic structure which we are currently uncapable of describing.

One of the reasons why research in quantum gravity is still incomplete, yet so florish, has been the lack of any experimental sign of quantumness in gravitational interactions. Indeed, theoretical arguments strongly indicate the breakdown of general relativity at short scales but the experimental guidance is still missing. This is due to the fact that quantum mechanics is expected to play a role only at scales comparable with the Planck length $\ell_{\rm P} = \sqrt{\hbar G/c^3} \simeq 10^{-35}$ m (in physical units). Therefore, if the typical length in a given system is L, quantum effects at the Planck scale should be suppressed as some power of the ratio $\ell_{\rm P}/L$ [44], making these effect really hard to detect at macroscopic scales. In recent times, however, the possibility of measuring Planck-scale effects has become more plausible. For instance, quantum gravity could induce some small modification in the dispersion relations of electromagnetic waves which, after a very long distance, could become measurable [45, 46]. Moreover, theoretical evidences indicate that, if the spacetime is not continuous and there exist some minimum length like, e.g., $\ell_{\rm P}$, then the uncertainty principle must be modified to accomodate a minimum indetermination in the position of a particle [47–50]. Quantum gravity effects could also be tested with particle accelerators since the cross sections of particles could be influenced by the modification of the uncertainty principle [45, 46]. Morover, even gravitational waves could be used to probe the quantum nature of gravity since the ringdown signal produced by the coalescence of two compact objects strongly depends on the nature of the systems and on their microscopic structure [51, 52].

Nonetheless, in recent times, there have been many indications supporting the possibility of having relevant quantum gravity effects even at scales much larger than $\ell_{\rm P}$, i.e., at horizon or cosmological scales. At the black-hole level, this new perspective gains motivation from different approaches: the firewall paradox [53], which triggered several recent advances in tackling the black-hole information puzzle (islands and replica wormholes [54–57], non-local modifications of effective field theory [58–60], fuzzball proposal [61–63]); the emergent gravity and corpuscular gravity scenarios [35–39, 64, 65], in which a black hole is considered as a coherent state of a large number of gravitons of typical wavelength $\sim R_{\rm S}$ [66–68]; finally, the quasi-normal modes (QNMs) spectrum of the Schwarzschild black hole, whose description is consistent with that of an ensemble of oscillators with typical frequency $\omega \sim 1/R_{\rm S}$ [6, 69]. Further evidence came from the galactic and cosmological framework, where deviations from Newtonian dynamics and the evolution of dark energy can be interpreted in terms of long-range quantum gravity effects, described by an exotic source of Einstein's equation in the form of an anisotropic fluid [64, 70–75].

In order to understand the possible deviations from general relativity, many alternatives to the standard black hole solutions have been proposed [76]. These compact objects, often referred to as mimickers, are usually indistinguishable from the standard Schwarzschild or Kerr solutions in the weak-field region, but they usually present strong deviations in their core or in the near-horizon region. Examples of mimickers include anisotropic and boson stars [77–80], gravastars [81], fuzzballs and firewalls [53, 61], wormholes [5, 82], and regular black holes [1, 83–85].

The latter, in particular, are among the most promising mimickers, being them singularity free. Now, singularity-free black-hole geometries can already be found in the context of pure general relativity coupled to some form of exotic matter. The latter is needed to circumvent the assumptions of Hawking and Penrose theorems [86, 87] which predict the inevitability of the formation of a singularity under a set of physically reasonable assumptions. However, one can think of some new-physics effects to be responsible for the smearing of the classical singularity.

This scenario is even more exiting when quantum effects are considered as solutions to the problem. In this sense, regular black holes could even represent a theoretical laboratory in which quantum effects are parameterized via, e.g., some additional *quantum hair*. The predictions extracted in this way could be, then, compared to experimental observations in order to test general relativity.

The main problem in testing possible deviations from Einstein's theory is that every theory gives a different set of predictions and, similarly, each black-hole mimicker parameterizes different deviations from general relativity. Therefore, in order to understand which theory, or mimicker, can better fit the observed phenomena one should, in principle, try all the possibilities, one at a time. This approach has the advantage of keeping all the physics completely under control, but requires an intense effort. Another possible way of tackling the problem is, instead, to modify some of the physical properties of the standard phenomenology with some additional parameters and constraint the latter with some experiment. This approach, often called *bottom-up*, has been pursued, for instance, in studying deviations in the quasinormal-mode spectrum [88, 89], in the parameterized-post-Newtonian formalism [11], and in the search for some classes of black-hole mimickers (see, e.g., Ref. [1] for static regular black holes and Refs. [90–92] for some parameterizations of deviations from the Kerr solution).

Another efficient way to study classical and quantum gravity is represented by lower-dimensional theories. Despite their simplicity, these models are expected, at least, to capture some of the dynamics of the full problem and their predictions could be then used as a *hint* to understand what the solution would look like in the full 4D scene. An example is the Jackiw-Teitelboim theory [93, 94], which is the simplest nontrivial model in a two-dimensional space. Not only is this model particularly interesting for its simplicity, but it also is capable of capturing a huge portion of classical and (putative) quantum effects expected in the full 4D scenario. For instance, it has been shown that the dynamics of near-extremal black holes, and their near-horizon physics, is well described by such two-dimensional theory (see, e.g., Ref. [95]). Moreover, it has been recently proved that Jackiw-Teitelboim gravity is dual to the SYK model [96, 97].

In this dissertation we focus on the main aspects introduced in this introduction. This work, divided into two parts, is devoted to the construction of models, interpretation and investigation of the possible phenomenology for regular and deformed singular black holes. We will focus both on the problem of constructing general classes of non singular and singular deformed black holes, the investigation of their physical properties and their implication for fundamental issues like, e.g., the information loss problem and the miscroscopic interpretation of Bekenstein-Hawking entropy. We will also look in detail to several phenomenological implications of our theoretical description, arguing that some of them can be presently tested or could be tested in the near future using black-hole imaging techniques and by third-generation GW detectors. The thesis is structured as follows.

In Part I we discuss the formulation, the classification, the theoretical implications and the phenomenology of some regular and singular models, whose deviations from Einstein's theory depend on a single parameter which can be identified as either a quantum hair or a simple deformation of the standard general-relativistic spacetimes. In particular, we study two classes of geometries. The first one is a two-parameter family of regular, static, asymptotically-flat black holes with a de Sitter core. These spacetimes are studied in detail in Chapter I.2, where we discuss the typical structure of the geometries pertaining to the general family, their thermodynamics and some of their most important phenomenological aspects. We show that their typical phenomenology correspond to the Schwarzschild one only when the quantum effects, parameterized by an effective length scale ℓ, are negligible at the horizon scale, i.e., when $\ell \ll R_{\rm S}$. However, when $\ell \simeq R_{\rm S}$, the situation changes drastically, and the phenomenology gets richer. In particular, the thermodynamic behavior of these objects suggests that configurations with $\ell \simeq R_{\rm S}$ are thermodynamically favored with respect to those where there are almost no quantum effects at the horizon scale. In Chapter I.3, we study in greater detail the thermodynamics and semiclassical dynamics of these objects, focusing in particular on the Hawking radiation emission and on the evaporation process. To do so, we work in a simplified two-dimensional framework, where we are able to show that the Hawking process leads to the stable configurations with $\ell \simeq R_{\rm S}$. In Chapter I.4, we discuss some phenomenological implications of our models and we test our metric with the

available S2-star orbital data. This star moves around the black hole placed at the center of the Milky way, Sagittarius A*, at relatively great distances. Under the hypothesis that this black hole is regular and its geometry is described by a specific model of the class derived in Chapter I.2, we derive a constraint for the quantum hair ℓ. Finally, in Chapter I.5, we discuss a family of axially-symmetric black holes, which represents a family of possible deformations of the Kerr black hole in general relativity, focusing on the superradiant scattering of massless and massive particles around these geometries. We find that the introduction of some deviations can, again, produce measurable deviations from general relativity. Moreover, we study the effect of these deviations on the superradiant instability, finding that these spacetimes are more unstable than the Kerr one.

In Part II, we describe two models in which we try to carefully insert some quantumness in general relativity. Indeed, without knowing the form of the (eventual) theory of gravitation at microscopic scales, we attempt to take into account the quantum nature of the sources of the gravitational field and to model the internal structure of 2D and 4D black holes in terms of an ensamble of harmonic oscillators. In Chapter II.2, we describe the effect of treating the source of the gravitational field as a quantum particle. We then derive, using a geometrical uplifting, the resulting space-time geometries. We find that the gravitational field generated by this quantum source is a black hole when the uncertainty on the position of the particle is much greater than the classical curvature radius $R_{\rm S}$. We also show that the L^2 integrability of the wavefunction describing the system guarantees asymptotic flatness, while smoothness conditions on its derivative implicate regularity at the core. As a simple realizaion of this model, we extensively study the case in which the probability distribution is Gaussian, finding an interesting and rich phenomenology which could be, in principle, tested in present or future experiments. In Chapter II.3, we investigate the internal structure of black holes focusing on possible microscopic models. In particular, we express this structure in terms of harmonic oscillators whose typical frequencies are given by the quasinormal modes of the black hole. This description, inspired by Maggiore's idea [69], allows us to recover the usual Bekenstein-Hawking entropy, and the subleading logarithmic term, in the limit in which the black-hole mass is large. Adopting the same approach, in Chapter II.4 we model a 2D black hole, solution of the Jackiw-Teitelboim theory, again as a set of oscillators with frequency equal to the modes of the system. Also in this case we reproduce the Bekenstein-Hawking entropy of the object. Additionally, we are able to connect this microscopic description to the De Alfaro-Fubini-Furlan conformal quantum mechanics at the boundary, in which we find a natural description of the modes as the response function of the conformally-invariant version of the quantum harmnonic oscillator.

Finally, in Conclusions, we draw our conclusions and we outline the future prospects.

Part I

Models of nonsingular and deformed black holes

Testing putative alternatives to Einstein's theory and to its black-hole solutions is particularly appealing to try to better understand the nature of the gravitational interactions. In this first part of the thesis, we discuss our effort in both modeling and testing singular and regular black-hole candidates which can be used to probe parametrical deviations from the usual general relativity phenomenology. In particular, we first study a general class of effective models of static and spherically symmetric regular black holes sourced by anisotropic fluids with equation of state $p_{\|} = -\rho$ presenting an additional hair ℓ. The central singularity of the Schwarzschild solution is replaced, in these models, by a de Sitter core. We also show that these models are thermodynamically stable when the deformation parameter is of $\mathcal{O}(R_S)$, the classical gravitational radius of the Schwarzschild black hole. We also explicitly study the evaporation of such objects using a 2D gravity model, namely the Jackiw-Teitelboim model, and we find strong evidence that the final state of this process describes a perfectly regular, zero entropy, extremal configuration. We then consider a specific example of the general class of 4D black holes, the Fan-Wang model, with the property of having the strongest possible corrections with respect to Schwarzschild at great distances. We then test this metric with S2-star data by studying the orbits of test particles around such black hole. Finally, we test deviations from the Kerr metric using the Konoplya-Zhidenko black hole as an example of a more general class of rotating objects, and we study the superradiant amplification of scalar and spin-1 particles off a black hole.

This part is mainly based on:

M. Cadoni et al. "Effective models of nonsingular quantum black holes". *Phys. Rev. D* **106**.2 (2022), 024030. arXiv: 2204.09444 [gr-qc] for Chapter I.2,

M. Cadoni et al. "Evaporation and information puzzle for 2D nonsingular asymptotically flat black holes". *JHEP* **06** (2023), 211. arXiv: 2303.05557 [hep-th] for Chapter I.3,

M. Cadoni et al. "Are nonsingular black holes with super-Planckian hair ruled out by S2 star data?" *Phys. Rev. D* **107**.4 (2023), 044038. arXiv: 2211.11585 [gr-qc] for Chapter I.4,

E. Franzin et al. "Superradiance in Kerr-like black holes". *Phys. Rev. D* **103**.10 (2021), 104034. arXiv: 2102.03152 [gr-qc] for Chapter I.5.

Chapter I.1

Regular and modified black holes as mimickers

Einstein's general relativity has been extensively tested in both weak and strong regimes [98–104]. While, nowadays, black holes are widely accepted as astrophysical systems (see, e.g., Refs. [105, 106] for a comprehensive review on black-hole related measurements) we still do not have the ultimate evidence of the existence of these objects. Indeed, although the measurements are in agreement with the presence of Kerr black holes in the universe, their uncertainties still leave room for some possible alternatives to the Kerr spacetime. Moreover, the final proof would be the observation of the defining property of these objects, i.e., the event horizon, which is, however, intrinsically not directly observable [51, 76, 107, 108].

For this reason (and many others more), there has been an intense effort in the literature to study alternative theories of gravity and black-hole mimickers. The latter, as we discussed in the Introduction, were proposed as possible alternatives to black holes since they usually show the same asymptotics of the Schwarzschild or Kerr spacetimes, but they differ in the near horizon or the interior region [84, 109–111]. These spacetimes often show an interesting set of physical features that makes them appealing candidates for tests of general relativity: they often need some kind of exotic matter to avoid the collapse to a singularity [112]; they show a different geodesic structure (even at great distances [3]); they can be thermodynamically stable [1, 2]; gravitational waves emitted by these objects can have a very distinct signature [51, 113]. Again, we stress that the scientific community has proposed numerous theories and models, resulting in the discovery of several mimicker solutions. These theories and models often yield different predictions, and likewise, diverse black hole mimickers lead to distinct observables. The great challenge, therefore, is to test all the theories and understand which candidates are the most promising. A different possibility is to follow a bottom-up approach, in which, we recall, at the cost of losing control over the dynamics of the theory, one encodes the deviations from general relativity in a set of additional parameters. Because of its generality, this approach is often more efficient to perform tests of general relativity and does not rely on any specific microscopic description.

In this part of the thesis, we focus on a particular class of mimickers represented by singularity-free, i.e., regular black holes. As we discussed in the Introduction, the need of a resolution of the singularity, inevitable in a classical framework [87, 114], can be traced back to the discovery of the Schwarzschild solution itself, since the divergence of the curvature invariants clearly implicates the breakdown of the theory in some neighborhood of the core. In order to save general relativity from completely losing its predictive power near the singularity, it has been conjectured that the latter are always hidden behind event horizons, shielding the singularities from being seen by any external observer [86]. However, the singularity may still play a role in processes in which quantum effects are nonnegligible anymore, like the final phases of the evaporation process. Hawking's and Penrose's theorems can be circumvented already in a pure general relativity framework simply by relaxing some of their main assumptions. For example, by violating the assumption on the validity of the strong energy condition, one can build some regular-black-hole solutions (see, e.g., Refs. [115–121]; for models with non-linearly coupled electromagnetic fields, see [122–127]). Alternatively, one can invoke quantum-gravity effects to prevent the formation of a singularity. In the past, the most widely adopted approach has been to assume that these quantum

corrections play a role at the Planck scale [128–142]. Since quantum gravity effects are expected to become important only when the Compton length of a pointlike mass M is comparable with its Schwarzschild radius, $R_{\rm S} = 2GM$, they should be irrelevant as long as gravitational interactions at Planck-scale distances are not considered, like the behavior of spacetime near their central singularity or the initial phases of the evolution of the universe.

Nonetheless, as discussed in the Introduction, in recent times there have been several indications that quantum corrections can be relevant even at the horizon scale, which is, for astrophysical systems, much larger than $\ell_{\rm P}$. We recall that, at the black-hole level, this new perspective gains motivation from different approaches: the firewall paradox [53]; the fuzzball proposal [143, 144]; the emergent- and corpuscular-gravity scenarios [35–39, 64–68]; finally, the quasi-normal modes (QNMs) spectrum of the Schwarzschild black hole, whose description is consistent with that of an ensemble of oscillators with typical frequency $\omega \sim 1/R_{\rm S}$ [6, 69].

A peculiar feature of these regular-black-hole spacetimes is that, when interpreted as solutions of Einstein's equations, they typically need an anisotropic fluid to source the gravitational field (see, e.g., Refs. [1, 84, 121, 132, 145, 146] for an incomplete list). This fluid has a long history and has been used in several different contexts. For instance, this description has been used in cosmological models [71, 73, 74, 147–149], to explain the rotational curves of galaxies [75], to build black-hole-mimicker solutions [77, 118, 150–155], and to study the primordial-black-hole formation [156]. Moreover, in Chapter I.2 we propose that the anisotropies can be thought as a parameterization of the quantum effects responsible for the smearing of the classical singularity in the black-hole cores with a short-distance de Sitter behavior (see also Ref. [1]).

Moreover, black holes behave as thermodynamical systems [1, 157, 158]. In particular, one can identify the surface gravity at the event horizon as the temperature of the black hole, and the entropy of the system with a suitable multiple of the horizon area. They emit thermal Hawking radiation similarly to black bodies [41]. This emission is also related to a very well known problem arising from semiclassical gravity, namely the information paradox [42, 43] (see also Ref. [159] for a comprehensive introduction to the topic). Indeed, semiclassical gravity suggests that the information about the state of matter that falls inside of a black hole is irretrievably lost, which is, therefore, in clear contrast with the principles of quantum mechanics since the former suggests a nonunitary evolution for any system. Several solutions have been proposed to solve this problem during the years: islands and replica wormholes [54–57], non-local modifications of effective field theory [58–60], and fuzzball proposal [61–63] are just some of the most famous proposals. Moreover, there are some theoretical arguments relating the information puzzle and the presence of a singularity in classical black holes [160–164]. In this sense, regular black holes could be useful also to address this long-time, unsolved puzzle in general relativity (see Chapter I.3 for a more extensive discussion on this topic).

Another class of mimickers can be obtained by studying deviations from general relativity that are small in the asymptotic region. A first attempt in this direction came in Refs. [90, 165, 166], where deviations the general-relativistic black-hole geometry are are expanded in powers of M/r, being M the black-hole mass and r some radial coordinate. The main problem of this formulation consist in the fact that a very large number of equally important coefficients remains undetermined, with the additional drawback of a lack of a hierarchy among them. Moreover, while it works sufficiently well for small deviations from general relativity, it fails for, e.g., Einstein-dilaton-Gauss-Bonnet with large coupling constants [167]. A successive and more reliable approach has been proposed in Refs. [91, 92]. In this parameterization, the deviations from Einstein's theory are again expressed in term of some expansion whose coefficients, this time, have a much more definite hierarchy and are able to reproduce well known solutions up to the desired accuracy with a relatively small number of parameters. Moreover, these parameters can be fixed by observations in the near-horizon and in the far, post-Newtonian regions. Such method, moreover, have been used to test the Kerr hypothesis via the iron-line method [168–170] and to produce black-hole shadows simulations [171, 172].

In this part of the thesis, we investigate two classes of black holes presenting an extra parameter. We first focus on a set of de Sitter core, asymptotically-flat, static and sperically symmetric black holes, sourced by an anisotropic fluid. This source is characterized by a new length scale ℓ which parameterize some unknown microscopic dynamics that will be interpreted in terms of some putative quantum effects. We study the thermodynamic behavior of this spacetimes and the

evaporation process, and we also test the phenomenology of these geometries against astrophysical data. Then, we move to a class of rotating singular spacetimes, namely the Konoplya-Rezzolla-Zhidenko class, characterized by a few additional functions encoding deviations from the Kerr spacetime. After specializing this metric to the simples case, the Konoplya-Zhidenko spacetime, we study the imprint of these modifications on the superradiant scattering of test particles on these objects.

Chapter I.2

Effective models of nonsingular black holes sourced by anisotropic fluids

Since the discovery of the Schwarzschild solution, the presence of a singularity inside black holes, together with the initial cosmological one, has represented a serious challenge to our current understanding of the fundamental laws of physics. This problem became even more serious after the groundbreaking Penrose and Hawking singularity theorems [87, 114]. They proved incontrovertibly that, under a set of a few, very general and physically motivated assumptions (the validity of the weak energy condition and either global hyperbolicity or the validity of the strong energy condition), these space-time singularities are unavoidable, at least in the classical general relativity (GR) framework. Despite this, it is conjectured that these singularities are always hidden behind a causal barrier, the event horizon, which prevents outside observers from seeing them and the theory from completely loosing its predictive power [86]. Semiclassical effects, like black hole evaporation [41], seem however to bring the singularity problem back on the table, as the final steps of the evaporation process, where the singularity role should be most prominent, are still poorly understood.

Although it is in principle solvable already in the classical GR framework by relaxing some assumptions of Penrose's theorem and constructing non-singular effective models (see, e.g., Refs. [115–121]; for models with non-linearly coupled electromagnetic fields, see [122–127]) the singularity problem calls for the need of a quantum description of gravitational interactions. As discussed in the Introduction and in Chapter I.1, the most widely adopted approach in the past has been to assume that these quantum corrections should only be relevant at Planck scale $\ell_{\rm P}$ [128–142]. Thus, they can be safely neglected as long as gravitational interactions at Planck-scale distances are not considered, like the final stages of the evaporation of black holes, the behavior of space-time near their central singularity or the initial phases of the evolution of the universe. However, several recent results [6, 35–39, 53, 64, 65, 69] indicate that these effects could be important even at scales much larger than the Planck one, namely at the horizon or at the cosmological level. This latter possibility is also interesting from a more phenomenological point of view. For instance, these effects are expected to be encoded in the QNMs spectrum and to be detected by the next generation of gravitational wave (GW) detectors, like the Einstein Telescope (ET), in the ringdown phase of two compact objects merging to form a single black hole. In some particular cases, a manifest signature could be the presence of echoes in the GW signal [173–175].

The starting idea of this chapter is that the resolution of the singularity problem could be related to the presence of quantum gravity effects at horizon scales. This is somehow natural because we expect quantum effects to be at work both in the smearing of the classical black-hole singularity and in generating an effective *quantum hair* at horizon scales. We parametrize the smearing of the classical singularity with a length-scale $\hat{L}$, whereas the quantum hair is represented by an extra length-scale ℓ. We assume that this smearing is sourced by an exotic form of matter having the form of an anisotropic fluid, which should give an effective description of quantum gravity effects. The analogy with galactic dynamics, where an infrared (IR) scale $R_0 = \sqrt{R_{\rm S} L}$ is generated out of $R_{\rm S}$ and the size of the cosmological horizon L [64], now suggests that, similarly, ℓ can be

interpreted as an IR scale generated from $R_{\rm S}$ and $\hat{L}$, for instance by the simple relation

$$\ell = R_{\rm S}^{a}\hat{L}^{b} \tag{I.2.1}$$

with $a+b=1$. Thus, the origin of the quantum hair ℓ should find an explanation in the multi-scale behavior of gravitational interactions.

Following the cosmological analogy, we can think of a non-singular black hole as a "reversed" Schwarzschild-de Sitter (SdS) space-time, in which the external cosmological horizon and the inner Schwarzschild one are interchanged, and for which the length-scale $\hat{L}$ becomes the de Sitter (dS) length. In this way, we are motivated to construct a general class of non-singular, static, asymptotically-flat black-hole solutions with a dS core, sourced by an anisotropic fluid, which endows the classical Schwarzschild solution with a quantum hair ℓ. Extending this similarity with the SdS case and with the dynamically generated scale R_0, we will explicitly show that ℓ is dynamically generated by $R_{\rm S}$ and $\hat{L}$ by $\ell \sim R_{\rm S}^{1/3}\hat{L}^{2/3}$, a relation which should hold in general for regular models with dS cores.

We find that imposing a regular dS core $a)$ always violates the strong energy condition in the interior of these objects, and therefore allows us to circumvent the singularity theorem, and $b)$ depending on the value of the parameter ℓ, our non-singular models can have two, one (extremal configuration) or no horizons. We then proceed by investigating the implications of the presence an extra parameter ℓ, assumed to be of the same order of magnitude as $R_{\rm S}$, on the thermodynamic properties of the black hole and on the phenomenology of the models, i.e., on photon orbits and on the QNMs spectrum.

By using the first law of thermodynamics, we show that the presence of ℓ causes deviations from the standard area law. We propose therefore an entropy formula to generalize the latter. Using this general entropy formula, we also find that the extremal configuration is a zero-temperature, zero-entropy state, a behavior drastically different from extremal Reissner-Nordström (RN) and Kerr black holes. This, together with the fact that the extremal, near-horizon, geometry factorizes as the tensor product of two-dimensional Anti-de Sitter (AdS_2) with a two-sphere, i.e., $AdS_2\times S^2$, indicates that these regular models could actually be relevant for tackling the information paradox [42, 43, 55, 96, 159, 176]. By investigating the behavior of the specific heat and the free energy of the hole, we find a second-order phase transition near extremality, i.e., for $\ell \sim R_{\rm S}$. In particular, black holes with $\ell \sim R_{\rm S}$ are energetically preferred with respect to those with $R_{\rm S} \gg \ell$, lending further support to the possible relevance of quantum corrections at the horizon scale.

On the phenomenological side, we find that for black holes with $\ell \ll R_{\rm S}$, deviations from standard results concerning photon orbits and the QNMs spectrum are negligibly small and not detectable, at least in the near future. Conversely, black holes with $\ell \sim R_{\rm S}$ are characterized by macroscopic deviations from the Schwarzschild behavior, whose signatures are potentially detectable by the next generation of GW detectors. In particular, by analytically computing the QNMs spectrum in the eikonal approximation, we find that, in the near-extremal limit, the imaginary part of the quasi-normal frequencies scale with the black-hole temperature as $c_1/\ell + c_2\ell T_{\rm H}^2$ (with $c_{1,2}$ constants), while in the near-extremal and near-horizon regimes, it goes to zero, in agreement with several results in the literature [7, 177–187]. This appears to be a general feature of non-singular black holes, common also to charged and/or rotating extension of regular models [188–190].

In the final part of the chapter, we check our results by revisiting two already-known models, namely the Hayward and Gaussian-core black-hole metrics, which represent particular cases of our general class of regular black holes.

The outline of the present chapter is the following. In Chapter I.2 we build up the grounds for our multi-scale description of gravity by drawing an analogy between the SdS solution and galactic dynamics from one side, and regular black-hole models for the other side.

In Section I.2.2, we find the exact, most-general, spherically-symmetric static solution of Einstein's field equations, sourced by an anisotropic fluid, and we outline the basic requirements needed to avoid the central singularity. We then focus on a subclass of such models by choosing a particular equation of state and analyze the null and strong energy conditions.

In Section I.2.3, we select the general class of regular black-hole solutions by imposing a set of minimal constraints, namely dS behavior in the interior, asymptotically flatness at infinity, and the presence of horizons. We also study the general thermodynamic behavior of these

models, discussing the first law of thermodynamics and the appearance of the second-order phase transition. Finally, we investigate photon orbits and the QNMs spectrum in the eikonal approximation.

In Section I.2.4 and Section I.2.5 the general discussion is applied and the results are confirmed by revisiting two previously-proposed regular black-hole models, the Hayward and the gaussian-core ones, which appear as particular cases of our general class of models.

In this chapter, we use units in which $c = \hbar = k_{\rm B} = 1$.

I.2.1 Unified description of spacetime and matter inside a black hole

In the present chapter, we adopt a description of gravitational interactions in terms of an effective multiscale field theory, characterized by the generations of hierarchically different length scales. This description is natural in the cosmological and galactic context, as gravity and baryonic matter are characterized by: the Planck length $\ell_{\rm P}$, the size of the cosmological horizon L, related to the cosmological constant by $L = \Lambda^{-1/2}$, and the gravitational radius of a clump of baryonic matter with mass M, $R_{\rm S} = \ell_{\rm P}^2 M$. Indeed, in this context, an intermediate (mesoscopic) IR length scale in the galactic regime

$$R_0 = \sqrt{R_{\rm S} L} \tag{I.2.2}$$

is dynamically generated from $R_{\rm S}$ and L. At this scale, gravity deviates from its Newtonian behavior as is evident from the rotational curves of galaxies. Moreover, R_0 can be seen as a scale at which long-range quantum gravity effects become relevant [64, 70–72]. This scenario allows for an effective description in the GR framework in terms of an anisotropic fluid, which can be seen as a two-fluid model of dark energy and matter [70–75]. The resulting spacetime is the SdS solution, in which dark energy dominates at very large scales. In this regime, we have a description in terms of the pure de Sitter (dS) spacetime and a related scale isometry [191]. When instead clustered matter with mass M is present and becomes nonnegligible, the scale invariance of the dS background is broken, the quantum scale R_0 is generated and we have an effective description in terms of the SdS spacetime. The latter is characterized by an internal Schwarzschild-like horizon, determined by the baryonic mass M, and by an external dS horizon, which, for small M, is located at the radial position $r = L$, being r the radial position in a spherical coordinate system. The short-scale regime, instead, is described by the Schwarzschild solution with a related scale $R_{\rm S}$, at which the matter contribution dominates over dark energy. The geometry is asymptotically dS.[1]

In the emergent gravity scenario of Ref. [64], these two regimes are assumed to be endowed with a microscopic description in terms of quantum gravity degrees of freedom (DOFs) entangled at short-scales (at $r \sim R_{\rm S}$) and at cosmological scales ($r \sim L$). Following Refs. [64, 70], the short-range entanglement is responsible for the holographic horizon-area scaling of the entropy. The long-range regime is, instead, characterized by the slow thermalization of IR, long-range interacting, quantum-gravity DOFs. These IR dynamics is responsible for an extensive, i.e., volume-dependent, contribution to the entropy. As argued in Ref. [64], the competition between the area- and volume-laws in the entropy generates a mesoscopic scale R_0 and an additional gravitational dark force explaining the deviations from the Newtonian dynamics at galactic scales. This multiscale description of gravity, with a "fast scale", $R_{\rm S}$ and a "slow scale" L, is reminiscent of thermodynamic systems characterized by a glass transition [64].[2]

Following this line of reasoning, one is led by analogy to use a similar multiscale description of matter and gravity for the BH interior, in particular, to solve the singularity problem. We will consider only macroscopic BHs, i.e., BHs whose horizon radius is hierarchically larger than $\ell_{\rm P}$. The short-distance behavior in the BH interior (near the singularity) is now dominated by the short-scale dynamics of the emergent spacetime DOFs. It is natural to assume that, similarly to the cosmological case at large scales, here the contribution of matter is negligible at short scales, where we have an effective GR description in terms of a pure dS spacetime. This regime is therefore characterized by an ultraviolet (UV) dS length $\hat{L}$, a related cosmological constant

[1] Notice that, in order to make contact with the BH spacetime, we need a static parameterization of the dS geometry.

[2] At short time scales, glassy systems have properties which cannot be distinguished from those of crystals: their effective descriptions are identical. However, the former are characterized by a long timescale behavior, which makes them completely different from crystals.

$\hat{\Lambda} = \hat{L}^{-2}$, and scale invariance. This description is fully consistent with the existence of a UV fixed point, predicted by the quantum-gravity asymptotic safety scenario (see, e.g., Refs. [192–194]; for a resolution of the classical singularity in the asymptotic safety scenario, see Ref. [195]; for recent results on scale invariance in the core of BHs, see Ref. [196]). Moreover, the dS behavior of the spacetime at short scales is consistent with the volume-law contribution to the entropy.

Introducing baryonic matter M breaks the scale and conformal invariance of the dS spacetime in the BH interior. Similarly to the galactic and cosmological regimes [72], in this case, a new quantum scale ℓ is generated in terms of $\hat{L}$ and $R_{\rm S}$ as shown in Eq. (I.2.1). Using an argument similar to that of Ref. [64], the generation of ℓ can be also explained in terms of the competition between the short-range, volume contribution, and the Bekenstein-Hawking area-law contribution to the entropy at the Schwarzschild radius $R_{\rm S}$, i.e., at great distances from the center of the object.

Such a multiscale description of gravitational interactions can be adopted to describe both BHs in a cosmological background and the interior of asymptotically flat regular BHs. In the two cases, however, the horizon positions are reversed. In the latter, the dS horizon is the internal one, whereas the matter-determined horizon is the external one. For this reason, even if we expect $\ell = f(\hat{L}, R_{\rm S})$, this relation needs not to be the same as that relating R_0, L and $R_{\rm S}$ in Eq. (I.2.2). Another difference from the cosmological SdS case is that here we have the possibility of an external description given by an asymptotic observer at $r \to \infty$. The latter sees "quantum" deviations from the Schwarzschild geometry, parametrized by ℓ. In this respect, it should be emphasized once again that the relation between the cosmological case, described by Eq. (I.2.2), and the BH case, described instead by Eq. (I.2.1), is simply of an analogy, which prevents us from finding any relation between the cosmological scales (L, R_0) and the new scales $(\hat{L}, \ell)$.

From this perspective, we have a new phase in the BH interior, in which the emergent-gravity DOFs and matter should allow for an effective two-fluid description, i.e., an effective description in terms of an anisotropic fluid [147]. In the next sections, we will construct a general class of GR models describing gravity sourced by an anisotropic fluid, which allows for nonsingular BH solutions with two event horizons and an internal dS core.

I.2.2 Spherically symmetric solutions sourced by anisotropic fluids

Our starting point is GR sourced by an anisotropic fluid. The stress-energy tensor $T_{\mu\nu}$ appearing in Einstein's equations $G_{\mu\nu} = 8\pi G T_{\mu\nu}$ will be that pertaining to an anisotropic fluid. The latter has a long history and has been fruitfully used in several different contexts in gravitational studies, including compact objects, singular and non-singular BH models, and cosmology (for an incomplete list, see, e.g., Refs. [71, 73–75, 77, 84, 118, 121, 132, 146–156, 197]).

We consider static, spherically symmetric solutions of the theory, whose metric part can be written in the form

$$\mathrm{d}s^2 = -\mathrm{e}^{\nu(r)}\mathrm{d}t^2 + \mathrm{e}^{\lambda(r)}\mathrm{d}r^2 + r^2\mathrm{d}\Omega^2. \tag{I.2.3}$$

where $\nu(r)$ and $\lambda(r)$ are metric functions, depending on the radial coordinate r only, and $d\Omega^2 = d\theta^2 + \sin^2\theta\, d\phi^2$. The stress-energy tensor describing the anisotropic fluid can be written as [197]

$$T_{\mu\nu} = (\epsilon + p_\perp)\, u_\mu u_\nu + p_\perp\, g_{\mu\nu} - \left(p_\perp - p_\parallel\right) w_\mu w_\nu, \tag{I.2.4}$$

where $\epsilon(r)$, $p_\parallel(r)$ and $p_\perp(r)$ are the energy density and the radial and tangential pressure components, respectively, while u_μ and w_μ are 4-vectors satisfying the normalization conditions $g^{\mu\nu}u_\mu u_\nu = -1$, $g^{\mu\nu}w_\mu w_\nu = 1$ and $u^\mu w_\mu = 0$. The independent Einstein's field and stress-energy tensor conservation equations read

$$\frac{1 - \mathrm{e}^{-\lambda} + r\mathrm{e}^{-\lambda}\lambda'}{r^2} = 8\pi G\epsilon; \tag{I.2.5a}$$

$$\frac{\mathrm{e}^{-\lambda} - 1 + r\mathrm{e}^{-\lambda}\nu'}{r^2} = 8\pi G p_\parallel; \tag{I.2.5b}$$

$$p_\parallel' + \frac{\nu'}{2}\left(\epsilon + p_\parallel\right) + \frac{2}{r}\left(p_\parallel - p_\perp\right) = 0, \tag{I.2.5c}$$

where the prime denotes derivation with respect to r. Integration of the first equation yields

$$\mathrm{e}^{-\lambda(r)} = 1 - \frac{8\pi G}{r}\int \epsilon\, r^2 dr \equiv 1 - \frac{2Gm(r)}{r} \tag{I.2.6}$$

where $m(r)$ is the Misner-Sharp (MS) mass

$$m(r) \equiv 4\pi \int_0^r d\tilde{r}\, \tilde{r}^2\, \epsilon(\tilde{r}). \tag{I.2.7}$$

Finally, Eq. (I.2.5b) can be recast, using Eq. (I.2.7), in the more useful form

$$\frac{\nu'}{2} = \frac{4\pi G p_\parallel r^3 + Gm}{r\,(r - 2Gm)}. \tag{I.2.8}$$

The system (I.2.5a)-(I.2.5c) is not closed. In order to determine the solution unambiguously, we must support Eqs. (I.2.5a) and (I.2.5c) with two further equations. The simplest and physically natural way to close the dynamical system is to provide a barotropic equation of state (EoS) for the radial pressure $p_\parallel = p_\parallel(\epsilon)$ and the matter density profile $\epsilon(r)$. In the following, we will fix the equation of state and the matter density profile by imposing absence of singularities, a Schwarzschild behavior at $r \to \infty$, i.e., asymptotic flatness, and exploiting the analogy with cosmology discussed in previously Section I.2.1.

I.2.2.1 Equation of state and energy conditions

The simplest and most natural EoS we can choose is

$$p_\parallel = -\epsilon. \tag{I.2.9}$$

This choice is physically well-motivated by the analogy with the cosmological and galactic regime since it allows for both the dS and SdS (cosmological) phases. It allows for a pure dS behavior near $r = 0$, which implies the absence of singularities in the BH interior. Moreover, the EoS also allows for asymptotically-flat solutions at $r \to \infty$, when both $p_\parallel \to 0$ and $\epsilon \to 0$. One can now easily check that, using Eq. (I.2.5a) and Eq. (I.2.5b), the EoS (I.2.9) implies $\lambda(r) = -\nu(r)$. In the remainder of the chapter, we will adopt the following parameterization of the metric functions $\mathrm{e}^{\nu} = \mathrm{e}^{-\lambda} = A(r)$.

Eq. (I.2.8) can be readily integrated, using Eqs. (I.2.7) and (I.2.9), and yields

$$A(r) = 1 - \frac{2Gm(r)}{r}. \tag{I.2.10}$$

Finally, using Eqs. (I.2.5c), (I.2.7) and (I.2.9), we can express the fluid anisotropy $p_\perp - p_\parallel$ as a function of the MS mass as follows

$$\frac{p_\perp - p_\parallel}{r} = \frac{1}{4\pi r^3}\left(m' - \frac{rm''}{2}\right). \tag{I.2.11}$$

It is useful to write down explicitly the energy conditions for the specific case in which the EoS (I.2.9) holds. We start with the null energy condition (NEC), which is satisfied when both $\epsilon + p_\parallel \geq 0$ and $\epsilon + p_\perp \geq 0$ hold globally [198]. While the first one is trivially satisfied by virtue of Eq. (I.2.9), the second one imposes

$$\epsilon'(r) \leq 0, \tag{I.2.12}$$

upon using Eqs. (I.2.7) and (I.2.11). The strong energy condition (SEC), instead, is fulfilled when $\epsilon + p_\parallel + 2p_\perp \geq 0$ holds at any radii. Again, using Eqs. (I.2.7) and (I.2.11), the SEC is equivalent to

$$2r\epsilon(r) + r^2\epsilon'(r) \leq 0. \tag{I.2.13}$$

I.2.2.2 Absence of singularity and behavior near $r = 0$

In order to avoid the presence of a central singularity at $r = 0$ we first impose a set of minimal, very general requirements on the form of the metric functions and on the density and pressure profiles.

- We require regularity of $\mathrm{e}^{-\lambda}$ in $r = 0$ which, together with Eqs. (I.2.6) and (I.2.10), implies $m(r)/r \to 0$ or $r \to 0$.
- We demand regularity of $p_\parallel$ in $r = 0$ which, together with Eq. (I.2.8), entails $r\nu'(r) \to 0$ for $r \to 0$.
- We require both $p_\parallel$ to be smooth in $r = 0$. From Eq. (I.2.5c), the condition on $p_\parallel$ also impose regularity on the tangential-pressure component

$$\lim_{r\to 0} \frac{p_\perp - p_\parallel}{r} = 0. \tag{I.2.14}$$

Equation (I.2.14), together with Eq. (I.2.11), implies the following behavior near $r = 0$ for the mass function $m(r)$

$$m(r \to 0) = m_1 + \frac{r^3}{2\ell_{\mathrm{P}}^2 \hat{L}^2} + \mathcal{O}\left(r^4\right), \tag{I.2.15}$$

with m_1 and $\hat{L}$ some integration constants. The absence of curvature singularities for the metric in $r = 0$ requires $m_1 = 0$. The other term, proportional to r^3, instead, gives a local dS solution with a dS length $\hat{L}$

$$A(r \to 0) = 1 - \frac{r^2}{\hat{L}^2} + \mathcal{O}\left(r^3\right). \tag{I.2.16}$$

This dS description of the solution core is fully consistent with both the EoS (I.2.9) and the analogy with the SdS solution in cosmology (see, e.g., Ref. [118] for a regular model with a Minkowski core).

I.2.2.3 Asymptotic flatness and behavior at $r \to \infty$

In the asymptotic ($r \to \infty$) region, we require our solution to be (almost) indistinguishable from the Schwarzschild spacetime. This implies the metric to be asymptotically flat, with a subleading $1/r$ term in the metric function $A(r)$. Moreover, the two pressure components $p_\parallel$ and $p_\perp$ must vanish in the limit $r \to \infty$. From Eq. (I.2.11), we see that the minimal condition to have $p_\perp \to 0$ in the asymptotic region is

$$m(r \to \infty) = \mathcal{C}_0 r^2 + \mathcal{C}_2 r + M + \mathcal{O}\left(\frac{1}{r}\right), \tag{I.2.17}$$

with $\mathcal{C}_0$, $\mathcal{C}_2$ and M integration constants. Asymptotic flatness and absence of conical defects require $\mathcal{C}_0 = \mathcal{C}_2 = 0$, whereas M becomes the Arnowitt-Deser-Misner (ADM) mass of the solution measured by the asymptotic observer, since

$$m(r \to \infty) = M + \mathcal{O}\left(\frac{1}{r}\right). \tag{I.2.18}$$

I.2.3 A general class of nonsingular quantum black-hole models

The absence of a central singularity and the requirement of Schwarzschild asymptotics strongly constrain, through Eqs. (I.2.16) and (I.2.18), the local form of the mass function $m(r)$ (or, equivalently, of the metric function A) in the limits $r \to 0$ and $r \to \infty$. However, the global behavior of $m(r)$, which interpolates between the internal and asymptotic regions, remains extremely poorly constrained. In this section, we will use the analogy with the cosmological SdS case to further

restrict its global form. As a result, we obtain a general class of regular BH models, which can be used to give an effective description of quantum BHs.

We assume that $m(r)$ depends only on the two parameters $\hat{L}$ and $R_{\rm S}$, which characterize its local behavior near $r = 0$ and near $r \to \infty$. This implies that the IR quantum scale ℓ can is a function of $\hat{L}$ and $R_{\rm S}$ only. The explicit relation between these three scales can be found using a simple argument. Indeed, our models interpolate between the scale-invariant dS behavior in the core and that of clustered matter, which gives the Schwarzschild solution at large radii. Therefore, there must be some scale ℓ at which these two effects balance out. By exploiting the same arguments used in Ref. [72], we expect this scale to correspond to the one at which the Compton length associated with a test particle of mass m, experiencing the effect of a dS potential $V_{\rm dS} = r^2/\hat{L}^2$, is of the order of the Compton length of the particle if it felt the Schwarzschild potential generated by the surrounding mass $V_{\rm Sch} = R_{\rm S}/r$. The former cures the singularity at the center and reads $\lambda_{\rm c,\,dS} \sim \hbar/(|V_{\rm dS}|m) = \hbar\hat{L}^2/r^2 m$. The latter, instead, is responsible for the quantum correction at the horizon scale and is given by $\lambda_{\rm c,\,S} = \hbar r/R_{\rm S} m$. We thus have

$$\frac{\lambda_{\rm c,\,dS}}{\lambda_{\rm c,\,S}} \sim \mathcal{O}(1) \Rightarrow r \sim \ell \sim R_{\rm S}^{1/3}\hat{L}^{2/3}, \tag{I.2.19}$$

which is a scaling relation of the form given in Eq. (I.2.1), with $a = 1/3$, $b = 2/3$. We will check these general results in two specific models in Sections I.2.4 and I.2.5.

The presence of a new IR quantum scale implies that we have two complementary descriptions of the quantum BH. A BH-interior description, based on the parameters $\hat{L}$ and M, and a BH-exterior one, based instead on ℓ and M. The second case corresponds to the classical description characterized by the classical hair M and by a quantum-deformation parameter, i.e., the hair ℓ.

A second requirement on the form of the function $m(r)$ comes from the analogy with the cosmological SdS spacetime case. The spacetime must allow for two horizons, a dS-like internal one at $r = r_-$ and a Schwarzschild-like external one at $r = r_+$. Depending on the value of the parameter ℓ (or, equivalently, of the parameter $\hat{L}$), the BH could pertain to one of the following three cases: (i) a BH with two horizons, (ii) an extremal BH with two coinciding horizons, and (iii) a horizonless compact object.

We can easily estimate the relation between the parameters in the extremal case (ii) using a very simple argument. For the internal observer, which describes its spacetime as dS, the energy density is constant and it is given by $\epsilon \simeq (\hat{L}\ell_{\rm P})^{-2}$. The total energy inside a sphere of radius r is $E(r) \simeq r^3(\hat{L}\ell_{\rm P})^{-2}$. If we take, for the extremal case, $r \simeq \hat{L} \simeq R_{\rm S}$, then the total energy inside the sphere becomes $E(L) \simeq \hat{L}\ell_{\rm P}^{-2}$. Moreover, $E(\hat{L})$ must match the BH mass M seen by the outside observer. Therefore, using Eq. (I.2.19), the new scale ℓ for the extremal case must be related to $R_{\rm S}$ and $\hat{L}$ as

$$\ell \simeq R_{\rm S} \simeq \hat{L}. \tag{I.2.20}$$

Here we can see that the new scale ℓ has a quantum origin, being related to $\hat{L}$ which is responsible for the smearing of the singularity and should also be of the same order as the Schwarzschild scale $R_{\rm S}$.

For $\ell \lesssim R_{\rm S}$, the presence of the dS core and asymptotic flatness force the metric to have an even number of horizons. In the following, we will limit ourselves to the case of only two horizons. In the limit $\ell \to 0$, corresponding to $\hat{L} \to 0$, the inner dS horizon is pushed towards $r = 0$, it disappears, and a singularity is generated in the center. The outer horizon, on the other hand, becomes the classical Schwarzschild one. This case corresponds to the classical limit of our model, in which the usual asymptotically-flat Schwarzschild solution is recovered and the quantum effects can be neglected. In view of Eq. (I.2.18), the simplest way to recover the Schwarzschild solution in the $\ell \to 0$ limit is to assume that

$$m(r) = m\left(\frac{r}{\ell},\, M\right). \tag{I.2.21}$$

Conversely, in the $\ell \to \infty$ limit, corresponding also to $\hat{L} \to \infty$, the outer horizon disappears and the spacetime becomes dS. Notice that also $M \to \infty$ in this case, consistently with the fact

that the energy density is constant. This is the cosmological regime of emergent gravity, in which dark energy in the form of the cosmological constant L^{-2} fully dominates [64]. Our description in terms of a quantum BH with a dS interior sourced by an anisotropic fluid breaks down in this limit. An effective description of gravitational interactions in terms of GR sourced by an anisotropic fluid is still valid. It can be used to describe galactic dynamics and the generation of the IR length of galactic size (I.2.2), giving rise to interesting effects, like the emergence of a dark force at galactic level [70–72]. Finally, for $\ell \gtrsim R_{\rm S}$, the solution has no horizons and can be thought of as a horizonless star.

Let us now write down the most general form of the metric function satisfying the conditions discussed above and in Sections I.2.2.2 and I.2.2.3. We first reparametrize the metric function $A(r)$ in terms of a smooth function F as

$$A(r) = 1 - \frac{R_{\rm S}}{\ell} F\left(\frac{r}{\ell}\right) \equiv 1 - \alpha F(y) \tag{I.2.22}$$

where we defined the dimensionless coupling $\alpha \equiv R_{\rm S}/\ell$ and radial coordinate $y \equiv r/\ell$. Furthermore, the function F must satisfy the following conditions:

1. At great distances the spacetime must asymptote Schwarzschild, therefore F must behave as

$$F(y \to \infty) = \frac{1}{y} + \mathcal{O}\left(y^{-2}\right). \tag{I.2.23}$$

2. In the limit $r \to 0$ the spacetime becomes dS and F behaves as

$$F(y \to 0) = y^2 + \mathcal{O}\left(y^3\right). \tag{I.2.24}$$

3. The equation $1 - \alpha F(y) = 0$ admits at most two real positive roots y_+, y_-. Moreover, parameter regions in which the equation allows for two distinct, two coinciding, or no real positive roots are present.

4. In the region $y \geq y_+$, $F'(y)/F$ has only one local extremum (a maximum).

When the roots are distinct, y_+ corresponds to an event horizon and y_- is the inner Cauchy horizon. The presence of the latter horizons raised several concerns in the literature regarding the stability and viability of such regular-BH solutions with two horizons. Indeed, according to Poisson, Israel, and Ori [199, 200], the Cauchy horizon is typically exponentially unstable under perturbations, an effect known as "mass inflation". In standard regular-BH approaches with $\ell \simeq \ell_{\rm P}$, this instability develops in a time of order of the Planck time, which is a much shorter timescale than the evaporation time. Mass inflation, therefore, seems to challenge these models' ability to describe the evaporation process completely [201–203]. However, it has been shown recently [204] that a more careful analysis is needed and that the mass instability does not occur in some specific regular models, like those of Refs. [84, 192] (see also Refs. [205, 206] for more recent results).[3] Condition 4., instead, constrains the form of the derivative of F and is needed to have the simplest thermodynamic phase portrait since the ratio F'/F is related to the BH temperature (see Section I.2.3.3).

Finally, imposing the quantum-corrected metric to comply precisely with certain effective field equations, derived from some action principle, could introduce additional restrictions on the behavior of F, a possibility that has been analyzed in Ref. [210]. The latter analysis is mainly concerned with possible quantum corrections to the Schwarzschild metric, assumed to be polynomial in $1/r$ at asymptotic infinity (even if the main results seem to hold even if the latter assumption is relaxed). These corrections are derived as asymptotic solutions of effective field equations derived from an Einstein-Hilbert action corrected by additional higher-order terms in the curvature. What is found is that algebraic forms of F, like those of Refs. [84, 118], are incompatible with a principle of least action unless either fine-tuning is assumed or strong infrared non-localities in the gravitational action are taken into account. Therefore, their feasibility as

[3] We point the reader to Refs. [207–209], in the corpuscular gravity framework, and Ref. [5] for an alternative regular model without the presence of inner Cauchy horizons.

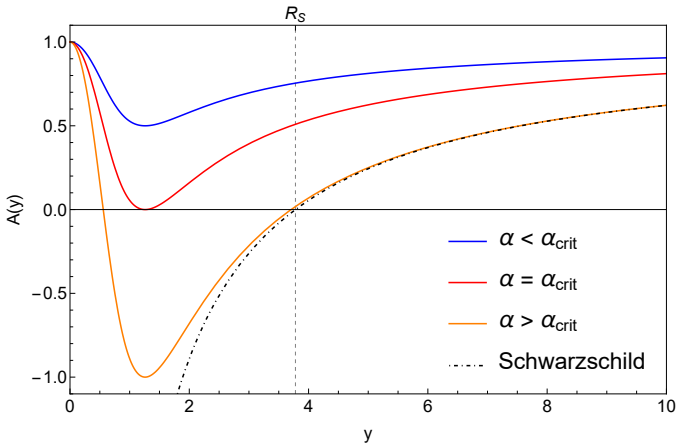

Figure I.2.1: Qualitative behavior of the metric function $A(r)$ as a function of the radial coordinate for different values of the parameter α. The solutions can show no horizons for $\alpha < \alpha_c$ (blue curve), be extremal for $\alpha = \alpha_c$ (red curve), or possess two horizons for $\alpha > \alpha_c$ (orange curve). We also show the Schwarzschild metric function (black dashed curve) for comparison.

quantum-deformed BHs may be questionable, at least if one requires these solutions to be derived from an Einstein-Hilbert action with higher-order terms in the curvature.

Condition 3. implies the existence of critical values α_c and y_c for α and y respectively, labeling the extremal case, when the two BH horizons merge. These critical values are determined by requiring the metric function to have a double-degenerate zero, i.e., by the system of equations

$$1 - \alpha_c F(y_c) = 0, \tag{I.2.25a}$$
$$F'(y_c) = 0. \tag{I.2.25b}$$

Notice that a simple principle of naturalness implies α_c and y_c being of order 1, so the critical values for ℓ and r are of order R_S. Therefore, α_c allows us to distinguish three regimes for our model.

(a) $\alpha \gg \alpha_c$, corresponding to $\ell \ll R_S$ (i.e., $\ell \sim \ell_P$), describes the Schwarzschild BH with small quantum corrections [131–142].

(b) $\alpha \sim \alpha_c$, corresponding to $\ell \sim R_S$, where ℓ parametrizes quantum gravity effects at horizon scales [6, 7, 35–39, 61–65, 69];

(c) $\alpha < \alpha_c$, corresponding to $\ell > R_S$, describes horizonless stars.

In the following, we will be mainly concerned with (a) and (b) regimes, though (c) can give interesting phenomenology as well as the other cases. Finally, we show the qualitative behavior of the metric function $A(r)$ in the three cases in Figure I.2.1.

I.2.3.1 Energy conditions revisited

Given the form (I.2.22) for the general metric function and taking into account (I.2.23) and (I.2.24), we can rewrite the two energy conditions (I.2.12) and (I.2.13) in terms of the function F and discuss their behavior near $r \sim 0$ and for $r \to \infty$. Using Eqs. (I.2.6) and (I.2.22) in (I.2.12) and (I.2.13), we get

$$\epsilon' = -\frac{\alpha F}{4\pi G \ell^3 y^3} + \frac{\alpha F''}{8\pi G \ell^3 y} \leq 0, \tag{I.2.26a}$$
$$2r\epsilon + r^2\epsilon' = \frac{\alpha\,(2F' + yF'')}{8\pi G \ell} \leq 0. \tag{I.2.26b}$$

Near $y = 0$ $\epsilon' = 0$, which satisfies the NEC. On the contrary, $2r\epsilon + r^2\epsilon' \sim 0^+$ for $y \to 0$, i.e., the SEC is violated somewhere deep in the core of the BH. This is expected since the SEC violation is

characteristic of the dS spacetime. On the other hand, for $y \to \infty$, using Eq. (I.2.23) we get $\epsilon' \to 0$ and $2r\epsilon + r^2\epsilon' \to 0$. Thus, both the NEC and the SEC are satisfied in the asymptotic region, a fact that is clearly related to the Schwarzschild asymptotics of the solutions.

Violation of the SEC in the inner core explains how the usual singularity theorems can be circumvented in our models. Even if the dS behavior near $r = 0$ assures the absence of a curvature singularity at $r = 0$, in principle it is not sufficient to guarantee the geodesic completeness of the spacetime described by the metric function (I.2.22). In Appendix I.A we explicitly show that in our models, caustics of time-like geodesics cannot form, proving therefore the geodesic completeness of spacetimes described by Eq. (I.2.22).

I.2.3.2 Extremal limit

As it is usually the case for standard charged and/or rotating BHs [211–214], in the extremal limit and in the near-horizon approximation, the local geometry of our spacetime behaves as $\mathrm{AdS}_2 \times \mathrm{S}^2$, i.e., as the tensor product of a two-dimensional (2D) AdS spacetime and a two-sphere, with both the AdS_2 length L_2 and the radius of S^2 of order R_S. In fact, in the extremal limit $r_+ = r_- = r_c$, the metric function $A(r)$ must have a double zero at $r = r_c$, determined by the solution of Eqs. (I.2.25). Expanding it near the horizon, i.e., in power series of $r - r_c$, we get at leading order

$$\mathrm{d}s^2 = -L_2^{-2}(r - r_c)^2\mathrm{d}t^2 + L_2^2(r - r_c)^{-2}\mathrm{d}r^2 + r_c^2\mathrm{d}\Omega^2, \tag{I.2.27}$$

where we have defined $L_2^{-2} = -\frac{1}{2}A''(r_c)$ and $r_c \sim R_\mathrm{S}$ owing to Eq. (I.2.20). Moreover, for purely dimensional reasons, the same equation implies $A(r_c)'' \sim R_\mathrm{S}^{-2}$, from which $L_2 \sim R_\mathrm{S}$ follows. A translation of the radial coordinate $r \to r + r_c$ brings the metric into the form

$$\mathrm{d}s^2 = -\frac{r^2}{L_2^2}\mathrm{d}t^2 + \frac{L_2^2}{r^2}\mathrm{d}r^2 + r_c^2\mathrm{d}\Omega^2, \tag{I.2.28}$$

which describes an $\mathrm{AdS}_2 \times \mathrm{S}^2$ spacetime, with the AdS_2 metric written in Poincaré coordinates.

As we shall show in the next sections, the extremal solution is a zero-temperature, zero-entropy solution. The extremal configuration will be then thermodynamically preferred. Even if a solution with two horizons could result from the astrophysical collapse of a compact object, it will decay in a much shorter time than the Hawking evaporation time into the extremal configuration. This process has been studied and proved for the 2D version of the Hayward BH in Ref. [2], which will be described in detail in Chapter I.3.

Let us conclude by noting that the extremal solution is stabilized by a particular profile for the energy density ϵ and for the pressures $p_\parallel$ and $p_\perp$. In the near-horizon approximation, when the metric takes the simple $\mathrm{AdS}_2 \times \mathrm{S}^2$ form, we expect them to be constant and to satisfy a simple EoS. In fact, combining Eqs. (I.2.5c), (I.2.6) and (I.2.22), the extremality conditions in Eqs. (I.2.25) and the EoS (I.2.9), we find that the leading terms for the near-horizon energy density and pressures are

$$\epsilon^{(\mathrm{NH})} = \frac{1}{8\pi G r_c^2}, \qquad p_\parallel^{(\mathrm{NH})} = -\epsilon^{(\mathrm{NH})}, \tag{I.2.29a}$$

$$\epsilon_{(\mathrm{AdS})}^{(\mathrm{NH})} = -\frac{1}{8\pi G L_2^2}, \qquad p_\perp^{(\mathrm{NH})} = -\epsilon_{(\mathrm{AdS})}^{(\mathrm{NH})}, \tag{I.2.29b}$$

where $\epsilon_{(\mathrm{AdS})}^{(\mathrm{NH})}$ is the (negative) constant energy density sourcing AdS_2. It is interesting to note that both the radial and perpendicular components of the pressure satisfy the simple equation of state $p = -\epsilon$. The (positive) energy density associated with the two-sphere acts as a source for the (negative) radial pressure, whereas the (negative) energy density associated with AdS_2 acts as a source for the (positive) perpendicular pressure. Thus, the stabilization of the $\mathrm{AdS}_2 \times \mathrm{S}^2$ near-horizon, extremal solution is achieved in a rather non-trivial way.

I.2.3.3 Black hole thermodynamics

From the metric function (I.2.22) and using standard formulae, we can compute both the Hawking temperature T_H and the BH mass for the quantum corrected BH, as functions of the outer horizon

radius $r_+ \equiv r_{\rm H}$ and of the quantum-deformation parameter ℓ

$$T_{\rm H}(r_{\rm H},\ell) = \frac{1}{4\pi}\frac{{\rm d}A(r)}{{\rm d}r}\bigg|_{r=r_{\rm H}} = -\frac{\alpha}{4\pi\ell}F'\bigg|_{y=y_{\rm H}}, \qquad M(r_{\rm H},\ell) = \frac{\ell}{2G}F^{-1}(y_{\rm H}). \tag{I.2.30}$$

An important point is that ℓ has to be considered as a quantum-deformation parameter which, contrary to M, is not associated with conserved charges. This makes our quantum BH solution drastically different from other two-parameter classes of solutions, e.g., the charged RN solution, for which *both* parameters are associated with thermodynamic potentials.

Owing to this feature, we look for a first law of thermodynamics of the form ${\rm d}M = T_{\rm H}{\rm d}S$, where S is the BH entropy. One can easily check that the area law, i.e., an entropy equal to a quarter of the area of the outer event horizon (in Planck units), cannot be valid for our class of BH models. In fact, using $S_A = \mathcal{A}_{\rm H}/4G = \pi r_{\rm H}^2/G$, we get ${\rm d}M - T_{\rm H}{\rm d}S_A = -(1/2G)({\rm d}F/{\rm d}y_{\rm H})F^{-1}\left(F^{-1} - r_{\rm H}/\ell\right){\rm d}r_{\rm H}$. This tells us that, once the area law is assumed, the first principle is satisfied only for $F(y) = \ell/r_{\rm H}$, i.e., only for the Schwarzschild BH.

Let us now look for a new definition of the BH entropy S, generalizing the area law, such that the first principle is satisfied. This generalized entropy can be found by noticing that Eq. (I.2.30) implies the validity of the following relation

$${\rm d}M = 4\pi M T_{\rm H}{\rm d}r_{\rm H}. \tag{I.2.31}$$

By defining the BH entropy as

$${\rm d}S = 4\pi M{\rm d}r_{\rm H}, \tag{I.2.32}$$

we see that the first principle ${\rm d}M = T{\rm d}S$ is satisfied. Moreover, the entropy (I.2.32) correctly reproduces the area law in the Schwarzschild case, $M = r_{\rm H}/2G$. Eq. (I.2.32) defines the entropy of the BH up to an integration constant, which can be fixed by requiring the entropy area law to be recovered in the limit $\ell \ll R_{\rm S}$, i.e., in the classical limit of our quantum model. This leads to

$$S(r_{\rm H}) = 4\pi\int_{r_m}^{r_{\rm H}} M(r'_{\rm H}){\rm d}r'_{\rm H}, \tag{I.2.33}$$

where r_m is the minimum value of the horizon radius. In the limit $\ell \ll R_{\rm S}$, we have $M(r_{\rm H}) = r_{\rm H}/2G$ and $r_m = 0$, so that Eq. (I.2.33) gives the area law $S = \pi r_{\rm H}^2/G$.

For a generic quantum deformed BH, r_m is given by the radius r_c of the extremal BH. This implies in particular that the extremal BH has zero entropy, i.e., $S(r_c) = 0$. The extremal limit for our quantum-deformed BH is, therefore, a state of non-vanishing mass but with zero temperature and entropy. Again, this behavior is drastically different from that of usual extremal BHs, for which the extremal configuration is a state with $T = 0$, but with $S \neq 0$.

For both large BH radii $r_{\rm H} \to \infty$ and in the extremal limit, the temperature goes to zero. This can be easily checked using Eq. (I.2.30) together with Eq. (I.2.24) and Eqs. (I.2.25). The smoothness of the function $F(y)$ then implies that the function $T_{\rm H}(r_{\rm H})$ has at least one local maximum in the range $[r_c, \infty)$. In order to avoid an oscillating behavior of $T_{\rm H}(r_{\rm H})$, we have restricted ourselves to the simplest case by imposing condition 4. on the form of the function F (see the beginning of Section I.2.3).

The temperature starts from zero in the extremal limit, then it reaches a maximum $T_{\rm H,max}$ for some $r_{\rm H,max}$ and then goes down to zero again for large values of $r_{\rm H}/\ell$. This implies that $T_{\rm H}$ is always bounded, $0 \leq T_{\rm H} \leq T_{\rm H,max}$. Only when we take the limit $\ell \to 0$ first, to recover the Schwarzschild BH, can the temperature become arbitrarily large when $r_{\rm H} \to 0$. Notice that a nonvanishing quantum deformation parameter, $\ell \neq 0$ solves, as expected, the singular thermodynamical behavior $T_{\rm H} \to \infty$ of the Schwarzschild BH for $r_{\rm H} \to 0$. The typical qualitative behavior of the temperature is shown in Figure I.2.2.

In order to study in detail the thermodynamic behavior of the BH near extremality, we expand $T_{\rm H}$ and M near r_c. At leading order, we get $T_{\rm H} = \gamma(r_{\rm H} - r_c)$, whereas $M = M_c + \beta(r_{\rm H} - r_c)^2$, where $\gamma = {\rm d}T_{\rm H}/{\rm d}r_{\rm H}|_{r_c}$, $\beta = (1/2){\rm d}^2M/{\rm d}r_{\rm H}^2|_{r_c}$ and $M_c = M(r_c)$. Notice that ${\rm d}M/{\rm d}r_{\rm H}$ is always positive and becomes zero at extremality, ${\rm d}M/{\rm d}r_{\rm H}|_{r_c} = 0$. For this reason, the linear term in the expansion

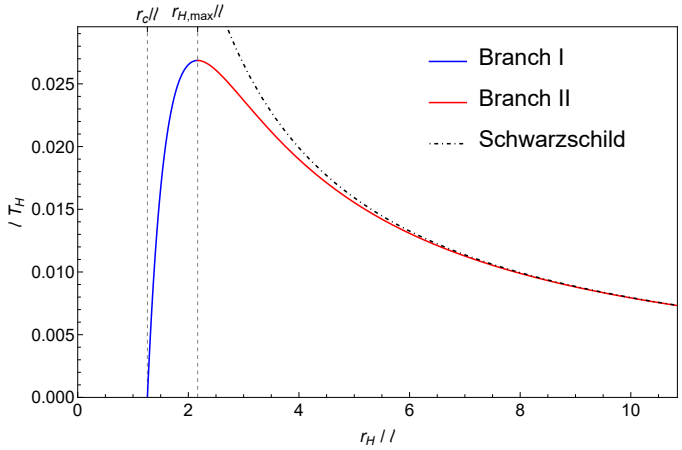

Figure I.2.2: Typical qualitative behavior of the BH temperature $T_{\rm H}$ as a function of the BH radius $r_{\rm H}$. We explicitly show the presence of the two branches (branch I in blue, with positive specific heat, and branch II in red, with negative specific heat), the critical horizon radius, and $r_{\rm H,max}$. We also show the typical behavior of the temperature of a Schwarzschild BH for comparison.

of M is absent. The previous expression implies a quadratic scaling with the temperature of the mass above extremality

$$M - M_c \sim \frac{\ell^3}{G} T_{\rm H}^2, \tag{I.2.34}$$

which is fully consistent with the $\mathrm{AdS}_2 \times \mathrm{S}^2$ near-horizon behavior of the extremal limit [215–217]. This means that, in the near-extremal limit, the BH allows for an effective description in terms of a 2D dilaton gravity theory, i.e., Jackiw-Teitelboim (JT) gravity, with the dilaton parametrizing the radius of the 2-sphere S^2 [93, 94, 218]. This in turn implies the possibility of using a dual 2D conformal field theory to describe the near-horizon regime of the near-extremal BH. This fact may be relevant for applications to the information puzzle in BH physics [42, 43, 54, 55, 96, 159, 176].

I.2.3.4 Phase transition

The nonmonotonic behavior of $T(r_{\rm H})$, which is common to a wide class of charged and/or AdS BHs, signalizes a non-trivial thermodynamic phase structure, the presence of two thermodynamic branches and a phase transition at the critical temperature $T_{\rm H,max}$ (see, e.g., Refs. [219–228]). This simply follows from the fact that there are two possible values of $r_{\rm H}$ for a given value of $T_{\rm H}$. This implies the presence of metastable states and the existence of two branches, I and II. The branch I corresponds to small, order 1 values of the dimensionless BH radius $y_{\rm H} = r_{\rm H}/\ell$ (the left-hand region of Fig. I.2.2). Here, $r_{\rm H}$ varies between the extremal value r_c and $r_{\rm H,max}$. Correspondingly, the parameter ℓ can take values between $\ell_{\rm H,max}$ and ℓ_c, both of order $R_{\rm S}$. Thus, branch I describes quantum BHs whose quantum deformation parameter ℓ is of the same order of magnitude as the classical Schwarzschild radius $R_{\rm S}$. Conversely, branch II corresponds to large values of $y_{\rm H}$ (the right-hand region of Fig. I.2.2). Here, $r_{\rm H}$ can take values much larger than $r_{\rm H,max}$. This corresponds to small values of the parameter ℓ. Hence, the far right region of branch II describes classical BHs, with quantum deformation parameter $\ell \ll R_{\rm S}$. A comparison with GR corroborates this interpretation. Indeed, in the limit $y_{\rm H} \gtrsim y_c$ the temperature shows a very different behavior with respect to its classical, GR analogous, while in the opposite case, $y_{\rm H} \to \infty$, we see that $T_{\rm H}$ asymptotes to the Schwarzschild value.

The phase transition and the stability of the different thermodynamic phases can be investigated by considering the specific heat of the BH, given by

$$C = \frac{\mathrm{d}M}{\mathrm{d}T} = \frac{\mathrm{d}M}{\mathrm{d}r_{\rm H}} \left(\frac{\mathrm{d}T}{\mathrm{d}r_{\rm H}} \right)^{-1}. \tag{I.2.35}$$

Typical values of C are shown in Fig. I.2.3 as a function of $r_{\rm H}$. Being $\mathrm{d}M/\mathrm{d}r_{\rm H}$ always positive, the non-monotonic behavior of $T_{\rm H}$ implies that

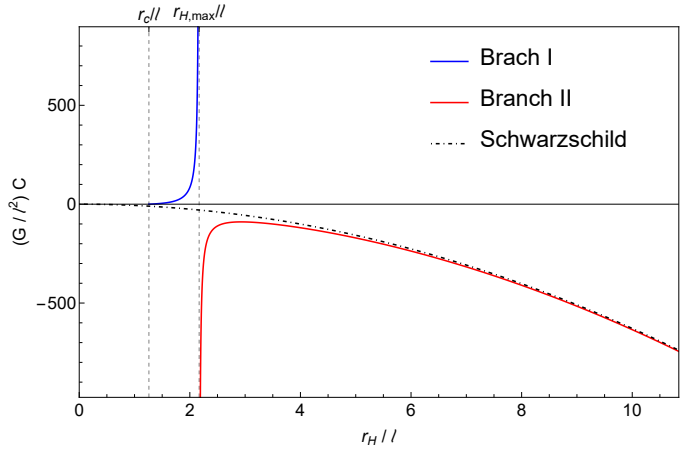

Figure I.2.3: Typical qualitative behavior of the BH specific heat C as a function of $r_{\rm H}$. The $r_{\rm H}$-axis starts from the value $C(r_{\rm H}=r_c)=0$, given by the solution of Eqs. (I.2.25). The point where C diverges corresponds to the temperature maximum, where $r_{\rm H}=r_{\rm H,min}$. The vertical dashed lines highlight the points $r_{\rm H}=r_c$ and $r_{\rm H}=r_{\rm H,max}$.

- For $r_c\leq r_{\rm H}<r_{\rm H,max}$, $\mathrm{d}T/\mathrm{d}r_{\rm H}$ is positive and thus $C>0$;
- For $r_{\rm H}>r_{\rm H,max}$, $\mathrm{d}T/\mathrm{d}r_{\rm H}$ is negative and thus $C<0$;
- For $r_{\rm H}=r_{\rm H,max}$, $\mathrm{d}T/\mathrm{d}r_{\rm H}=0$ and thus $C\to\infty$.

While in branch I the specific heat is always positive, indicating that the object is in equilibrium with its radiation, in branch II the BH has negative C. Since the latter states of the BH are thermodynamically disfavored with respect to the former, we see that the preferred configurations are those with $\ell\sim R_{\rm S}$. Moreover, as can be clearly seen in Fig. I.2.3, a second order phase transition occurs at $r_{\rm H}=r_{\rm H,max}$, where the object passes from branch II to branch I. Now, the states with $r_{\rm H}\lesssim r_{\rm H,max}$ also correspond to $\ell\sim\ell_c$, i.e., to near-extremal BHs with $\ell\sim GM$. This also shows that the outcome of the evaporation process will be a *cold* remnant at zero temperature and zero entropy. The latter, in particular, is again an intriguing property, as it could allow circumventing problems on the viability of remnants as possible solutions to the information paradox [229]. These thermodynamic aspects and the phase picture will be confirmed later when we will consider particular cases of our general class of models and we will study their free energy.

The non-trivial phase space structure analyzed above is a consequence of the multiscale description of our models, discussed in Section I.2.1. In light of the similarity between this description of gravitational interactions and glassy systems [64], one could ask whether our phase transition could be interpreted as a glass transition. Indeed, even the latter is characterized by a divergence in the specific heat at the transition point, but it is not generally classified as a second-order phase transition. To answer this question, one would need first to define some Ehrenfest equations, to describe variations of the specific heat and the derivatives of the volume between the two phases. For a second-order phase transition, both these equations are satisfied, while either both or one of them is violated in glassy systems. In the BH case, one can define Ehrenfest-like equations by replacing the volume with the electric charge and/or the angular momentum [230] (if the model is charged and/or rotating) and analyze their variations between the two phases.

Here, we can only speculate that the phase transition of our quantum-corrected BH could be very similar to a glass transition instead of a second-order one. In fact, the absence of any thermodynamic potentials related to ℓ or other physical observables prevents us from properly defining Ehrenfest-like equations and therefore performing an analysis similar to the one in Ref. [230]. Consequently, this does not allow us to assess quantitatively the nature of the phase transition in our models.

To summarize the results obtained so far, the stable configuration of our quantum-BH model, realized using an anisotropic fluid, will be represented by an extremal (or near-extremal, if we consider small deviations from extremality) BH. The geometry interpolates between a dS spacetime in the object's interior (near the location of the classical singularity), an $\mathrm{AdS}_2\times\mathrm{S}^2$

geometry in the near-horizon region, and flat spacetime in the asymptotic, $r \to \infty$, region. The dS behavior near $r = 0$ solves the singularity problem. At extremality, the two (dual) quantum scales characterizing the system (ℓ, $\hat{L}$) have the same order of magnitude of the classical BH radius $R_{\rm S}$. The scale ℓ, characterizing the quantum effects as seen by an external observer, is naturally of the order of magnitude of the classical Schwarzschild radius $R_{\rm S}$ of the BH. This opens the possibility of having potentially observable phenomenological quantum signatures in the near future through, e.g., the QNMs spectrum and the geodesic motion of particles near the horizon (see Chapter I.4). Moreover, the near-horizon $\mathrm{AdS}_2 \times \mathrm{S}^2$ behavior is very promising for tackling the BH information puzzle.

I.2.3.5 Null geodesics and photon orbits

To compute photon orbits in our class of models, we start from the geodesic equation together with the null-geodesic constraint (dot will refer to derivation with respect to some affine parameter)

$$\ddot{x}^\mu + \Gamma^\mu_{\nu\lambda}\dot{x}^\nu\dot{x}^\lambda = 0, \qquad g_{\mu\nu}\dot{x}^\mu\dot{x}^\nu = 0. \tag{I.2.36}$$

The isometries of the metric (spherical symmetry and invariance under time translations) imply two conservation equations, which by considering geodesics on the plane $\theta = \text{constant} = \pi/2$, take the form

$$\dot{\phi} = \frac{J}{r^2}, \quad \dot{t} = \frac{\sqrt{2\mathcal{E}}}{|A(r)|} \tag{I.2.37}$$

where J and $\mathcal{E}$ are integration constants and represent the total angular momentum and the energy of the test particle, respectively. The geodesic equation for the coordinate r can be integrated to give,

$$\frac{1}{2}\dot{r}^2 + V(r) = \mathcal{E}, \tag{I.2.38}$$

where $V(r)$ is the effective potential

$$V(r) \equiv \frac{J^2}{2r^2}A(r). \tag{I.2.39}$$

Notice that Eq. (I.2.38) represents the energy conservation equation for the system. Since the leading term of the metric function for $r \to 0$ is $A(r) \sim 1$, $V(r) \to \infty$ in this limit. This behavior differs from the Schwarzschild case, where $V \to -\infty$ for $r \to 0$, as a consequence of the dS behavior at the core. Conversely, for $r \to \infty$, $A(r)$ is dominated by the Schwarzschild-like $1/r$ term and $V(r) \to 0$. The shape of the effective potential $V(r)$ at intermediate distances depends crucially on the parameter α values.

The local extrema of V are the solution of the equation

$$rA'(r) - 2A(r) = 2\alpha F - 2 - \frac{\alpha r}{\ell}F' = 0. \tag{I.2.40}$$

Being F and F' both bounded, for any form of the function F it will exist a minimum value $\alpha_m = R_{\rm S}/\ell_m < \alpha_c$ such that for $\alpha \leq \alpha_m$ the equation has no real roots and bounded photon orbits cannot exist. For $\alpha > \alpha_m$, the equation allows instead for at most two real zeroes, corresponding to a local minimum and a local maximum for $V(r)$. On the other hand, for $\alpha_m < \alpha < \alpha_c$, stable and unstable photon orbits still exist, but the solution describes a horizonless compact object. In the extremal configuration ($\alpha = \alpha_c$), the minimum of the potential coincides with the horizon position. In this case, the potential shows the presence of an unstable photon ring, located at some $r > r_c$, and a stable orbit located at $r = r_c$. Finally, for $\alpha > \alpha_c$, the local minimum is inside the event horizon and there is only a bounded unstable photon orbit, similar to the Schwarzschild one. The qualitative behavior of the potential is shown in the left panel of Fig. I.2.4. The qualitative behavior of the position of the photon ring, instead, is plotted in the right panel of Fig. I.2.4 as a function of ℓ.

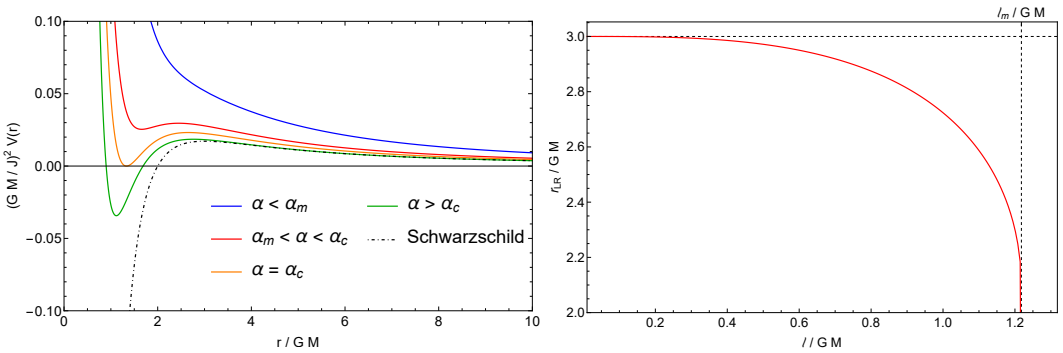

Figure I.2.4: Typical qualitative behavior of the effective potential V for null geodesics as a function of r for different values of the coupling α. The potential shows always two extrema for $\alpha > \alpha_m$, but none for $\alpha < \alpha_m$ (blue curve). Moreover, depending on the value of α compared to its critical value, the potential posses two distinct ($\alpha > \alpha_c$, green curve), two coinciding ($\alpha = \alpha_c$, orange curve) or no ($\alpha < \alpha_c$, red and blue curves) inversion points.

I.2.3.6 QNMs spectrum in the eikonal approximation

In this section, we consider QNMs for scalar perturbations in the fixed background given by our general black-hole solution. We will then use the eikonal approximation to give an analytical estimate of the QNMs frequencies.

The evolution of scalar perturbations Ψ, in the fixed gravitational background metric $g^{(B)}_{\mu\nu}$ described by the metric function (I.2.22), is determined by the Klein-Gordon equation

$$\Box\Psi = \frac{1}{\sqrt{-g^{(B)}}}\partial_\mu\left(\sqrt{-g^{(B)}}g^{\mu\nu}_{(B)}\partial_\nu\right)\Psi = 0. \tag{I.2.41}$$

Eq. (I.2.41) is separable into an angular and a radial part. By using the ansatz

$$\Psi = \frac{\psi(r)}{r}Y_{lm}(\theta,\phi)\mathrm{e}^{\mathrm{i}\omega t}, \tag{I.2.42}$$

where $Y_{lm}(\theta,\phi)$ is the (l,m)-th spherical harmonic, Eq. (I.2.41) becomes

$$\frac{\mathrm{d}^2\psi}{\mathrm{d}r_*^2} + \left[\omega^2 - V_{\mathrm{KG}}(r)\right]\psi = 0. \tag{I.2.43}$$

Here, the potential is

$$V_{\mathrm{KG}}(r) = (1-\alpha F)\left[\frac{l(l+1)}{r^2} - \alpha\frac{F'}{\ell r}\right], \tag{I.2.44}$$

and r_* is the tortoise coordinate, defined by $\mathrm{d}r_*/\mathrm{d}r = 1/(1-\alpha F)$. The qualitative behavior of the potential (I.2.44) is shown in Fig. I.2.5.

Analytical estimates of the QNMs frequencies can be obtained by using an intriguing relation between QNMs and the parameters characterizing null geodesics in the eikonal limit $l \gg 1$ first noted in Ref. [231]. The vibration modes of the BHs, whose energy is gradually being radiated away, are interpreted as photons moving along unstable null geodesics and slowly leaking out. This correspondence was more recently analyzed in Refs. [232–234] and shown to agree with WKB results [235, 236]. Specifically, the angular velocity Ω_m, computed at the maximum of the geodesic potential r_m, determines the real part of the QNMs spectrum, while the imaginary part is determined by the Lyapunov exponent λ. The latter, indeed, is related to the time scale of the null-orbit instability. The QNMs, in this approximation, read

$$\omega_{\mathrm{QNM}} = \omega_{\mathrm{R}} + \mathrm{i}\omega_{\mathrm{I}} = \Omega_m l - \mathrm{i}\left(n+\frac{1}{2}\right)|\lambda|, \tag{I.2.45}$$

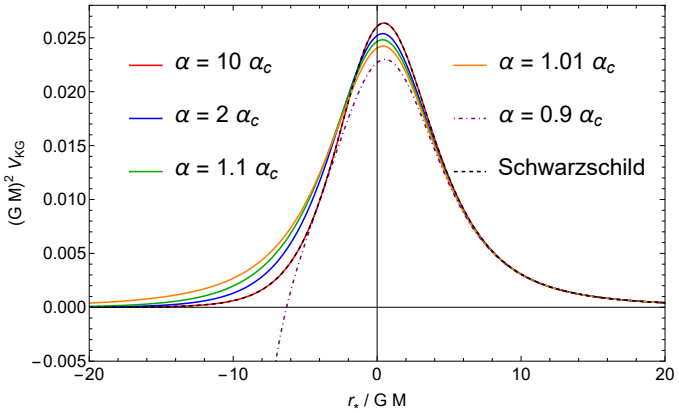

Figure I.2.5: Effective potential for scalar perturbations as a function of the tortoise coordinate r_* for scalar perturbations, $l = 0$ and different values of ℓ. We also show the same quantity computed with a Schwarzschild background metric (dashed black curve) as a comparison. The potential always shows a peak and goes to zero both at spatial infinity and at the horizon (if there is one), similarly to the Schwarzschild case. However, depending on the value of the quantum parameter ℓ (or, equivalently, of the ratio $\alpha = R_{\rm S}/\ell$), its behavior near the peak can be significantly different from the general relativistic vacuum solution.

where

$$\Omega_m = \left.\frac{\dot\phi}{\dot t}\right|_{r=r_m} = \frac{\sqrt{A(r_m)}}{r_m}, \tag{I.2.46a}$$

$$\lambda = \left.\sqrt{\frac{V''(r)}{2\dot t^2}}\right|_{r=r_m} = \frac{1}{\sqrt{2}}\sqrt{-\frac{r_m^2}{A(r_m)}\left(\frac{d^2}{dr_*^2}\frac{A(r)}{r^2}\right)_{r=r_m}}. \tag{I.2.46b}$$

Here V is the null-orbit potential given by Eq. (I.2.39) and r_m the position of the peak of the geodesic potential, i.e., the solution of Eq. (I.2.40).

Notice that, for extremal BHs, the potential V has an additional minimum exactly at the horizon. We will not consider this contribution, as small perturbations from extremality have the effect of moving this minimum towards the BH interior. The QNMs spectrum will be therefore entirely determined by the contribution at the maximum of V.

The general expressions (I.2.46a) and (I.2.46b) are valid for all spherically-symmetric, static, and asymptotically-flat solutions, in the eikonal limit. For our general class of models, using Eqs. (I.2.22), (I.2.46a) and (I.2.46b) we get

$$\omega_{\rm R} = \frac{l}{\ell y_m}\sqrt{1-\alpha F_m}, \tag{I.2.47a}$$

$$\omega_{\rm I} = -\frac{1}{\sqrt{2}\,\ell}\sqrt{\alpha\,(1-\alpha F_m)\,y_m\left|\left(\frac{F'}{y}\right)'_m\right|}\left(n+\frac{1}{2}\right), \tag{I.2.47b}$$

where the subscript $_m$ indicates that the corresponding quantity should be computed at $r = r_m$. It is important to stress that the QNMs frequencies depend both on the classical hair M and on the quantum hair ℓ. This dependence on two parameters of the QNMs spectrum will have a well-defined signature in the ringdown part of the gravitational wave. Next-generation gravitational-wave detectors are expected to be sensitive enough to detect such an effect.

In the generic case, $\omega_{\rm R}$ and $\omega_{\rm I}$ will be complicated functions of α. Simpler expressions can be obtained for near-extremal BHs, by expanding in powers of $(\alpha - \alpha_c)$. Taking into account that $|A|_m \neq 0$ (see the remark above), if we just consider the near-extremal expansion but not the near-horizon expansion, we will also have $\partial_r\left(\partial_r A(r)/r\right)_m \neq 0$. At first order in $(\alpha - \alpha_c)$ we get $\omega_{\rm I} = \text{constant}/\ell + \text{constant}\ (G/\ell^2)(M - M_c)$ and similarly for $\omega_{\rm R}$. Using Eq. (I.2.34), we can

express the QNMs frequencies in terms of the BH temperature

$$\omega_{\rm R} = \frac{a}{\ell} + b\,\ell\,T_{\rm H}^2, \tag{I.2.48a}$$

$$\omega_{\rm I} = \frac{c}{\ell} + d\,\ell\,T_{\rm H}^2, \tag{I.2.48b}$$

where a, b, c, d are dimensionless constants.

On the other hand, if we take the near-horizon limit together with the near-extremal limit, the metric satisfies $\partial_r\left(\partial_r A(r)/r\right) = 0$, identically, since the geometry becomes that of $\mathrm{AdS}_2 \times \mathrm{S}^2$. While the behavior of $\omega_{\rm R}$ remains that of Eq. (I.2.48a), we get a linear scaling of $\omega_{\rm I}$ with the temperature, owing to the absence of the constant term inside the square root:

$$\omega_{\rm I} \propto T_{\rm H}. \tag{I.2.49}$$

These results confirm partially Hod's conjecture, which asserts the complete absence of the imaginary damped part in the spectrum in the near-extremal case, both for RN and Kerr BHs [181–185]. In the case under consideration, Hod's conjecture seems to hold true only in the near-extremal, near-horizon case.

On the other hand, our results seem to confirm a general behavior found in Ref. [237] for the near-extremal Kerr spacetime, which is characterized by a branching in the QNMs spectrum. One family, corresponding to the simple near-extremal limit has indeed a nonvanishing imaginary part in the extremal limit, while the other branch shows that the damped part of the spectrum goes to zero in the near-extremal, near-horizon limit. Moreover, the temperature scaling (I.2.49) fully confirms previous derivation of the QNMs spectrum for two dimensional AdS_2 BHs [7, 177–180]. In fact, the latter allows for an explicit *analytical* treatment through different methods, which all point towards the same result: a linear scaling of the imaginary part $\omega_{\rm I}$ with the temperature of the hole. A quite interesting consequence of this scaling is the complete absence of the imaginary damped part in the spectrum in the extremal case, as the temperature becomes zero. These zero-damped (or nearly zero-damped) modes [181–187] would therefore represent a clear phenomenological signature of extremal BHs.

I.2.4 A minimal model: the Hayward black hole

One of the simplest examples of our general class of models is given by the Hayward-black-hole metric [84, 238], for which the metric function F in Eq. (I.2.22) reads

$$F(y) = \frac{y^2}{y^3 + 1}. \tag{I.2.50}$$

As already mentioned in Section I.2.3, the analysis of Ref. [210] shows that an algebraic form of F could be inconsistent with the semiclassical field equations derived from an action principle, at least if one requires the solutions to be derived from an Einstein-Hilbert action with higher-order terms in the curvature.

The horizon location and the extremality condition (I.2.25) are now

$$y^3 - \alpha y^2 + 1 = 0, \tag{I.2.51a}$$

$$-2\alpha y + 3y^2 = 0. \tag{I.2.51b}$$

Solving the equations above yields the critical values α_c and y_c

$$\alpha_c = \frac{3}{4^{1/3}}, \tag{I.2.52a}$$

$$y_c = \sqrt[3]{2}. \tag{I.2.52b}$$

The BH has two horizons for $\ell < 2 \times 4^{1/3} GM/3$, is extremal for $\ell = 2 \times 4^{1/3} GM/3$ and it becomes horizonless for $\ell > 2 \times 4^{1/3} GM/3$. The energy density ϵ and the mass function m sourcing the

BH are given by

$$\epsilon(r) = \frac{3}{4\pi}\frac{M\ell^3}{(r^3+\ell^3)^2}, \tag{I.2.53a}$$

$$m(r) = \frac{Mr^3}{r^3+\ell^3}. \tag{I.2.53b}$$

The NEC (see Eq. (I.2.12)) is always satisfied, while the SEC (see Eq. (I.2.13)) is violated deep inside the core of the object, for $r \leq \ell/\sqrt[3]{2}$. Moreover, in the limit $\ell \ll GM$ or $r \gg \ell$, $m(r) \to M$, i.e., the Hayward metric reduces to the Schwarzschild one. The deviation from the Schwarzschild case can be characterized by defining a new quantity $\Delta m(r)$ as the difference between the mass at infinity M and $m(r)$, which in the present case reads

$$\Delta m \equiv M - m(r) = \frac{M\ell^3}{r^3+\ell^3}. \tag{I.2.54}$$

In the limit $r \to \infty$, it behaves as

$$\Delta m \sim \frac{M\ell^3}{r^3} + \mathcal{O}\left(\frac{1}{r^4}\right). \tag{I.2.55}$$

The solution is asymptotically flat and satisfies the boundary conditions $\epsilon \sim p_{\parallel} \sim p_{\perp} \to 0$ for $r \to \infty$, while it has a dS behavior near $r = 0$ with the dS length $\hat{L}$ given by (see Eq. (I.2.15))

$$\hat{L} = \ell^{3/2} R_{\rm S}^{-1/2}, \tag{I.2.56}$$

which relates ℓ with the Schwarzschild radius and the dS length characterizing the small r behavior. Eq. (I.2.56) fully confirms the validity of our general scaling given by Eq. (I.2.19).

We note that the same result in Eq. (I.2.56) can be obtained in the limit of very large ℓ. In this case, however, we have an *exact* solution of Einstein's equations, sourced by a constant-density, *isotropic* and *homogeneous* fluid, with equation of state

$$p_{\parallel} = p_{\perp} = -\epsilon = -\frac{3}{8\pi G\hat{L}^2}. \tag{I.2.57}$$

Indeed, looking at the density profile (I.2.53a), the dS universe can be recovered in the limit $\ell \to \infty$ only if $M \to \infty$, so that the energy density sourcing the Hayward spacetime becomes constant.

For $\alpha > \alpha_c$, the cubic equation in Eqs. (I.2.51) has three real roots, out of which two are positive, r_+ and r_-, denoting the outer and inner horizons respectively, whereas the third, r_3, is negative. The metric function A factorizes as

$$A(r) = \frac{(r-r_+)(r-r_-)(r-r_3)}{r^3+\ell^3}. \tag{I.2.58}$$

In the extremal limit $r_+ = r_- \equiv r_c = \sqrt[3]{2}\ell$, after a translation of the radial coordinate $r \to r + r_c$, the metric becomes

$$ds^2 = -\tilde{A}(r)\mathrm{d}t^2 + \tilde{A}^{-1}(r)\mathrm{d}r^2 + (r+r_c)^2\mathrm{d}\Omega^2, \tag{I.2.59a}$$

$$\tilde{A}(r) = \frac{r^2(r+r_c-r_3)}{(r+r_c)^3+\ell^3}, \tag{I.2.59b}$$

describing an asymptotically flat region connected with an infinitely long throat of radius r_c. The near horizon (around $r = 0$) expansion of the metric (I.2.59) gives the $\mathrm{AdS}_2 \times \mathrm{S}^2$ spacetime (I.2.27), with an AdS_2 length $L_2 = (2/3)R_{\rm S}$. The fluid stabilizing the extremal solution is characterized by the equations of state (I.2.29), where now the AdS_2 length L_2 and the radius r_c of the two-sphere have the same value, $L_2 = r_c = (2/3)R_{\rm S}$.

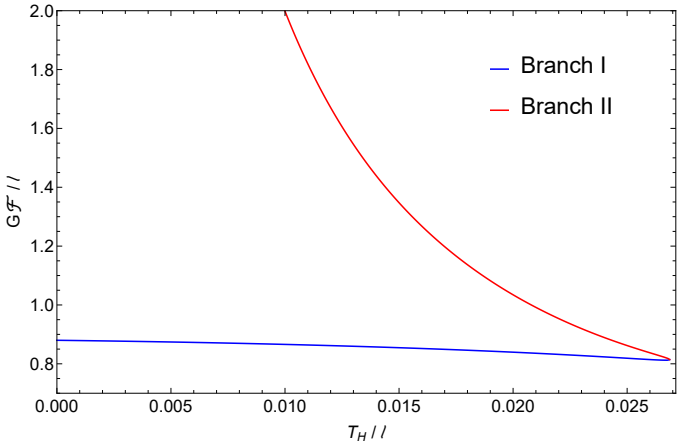

Figure I.2.6: Free energy $\mathcal{F}$, in units of ℓ^{-1}, as a function of the temperature, in units of ℓ^{-1}, for the two branches of the Hayward BH. We plot $\mathcal{F}$ for branch I, $\ell \sim R_{\rm S}$ (solid blue curve), and for branch II (solid orange curve) corresponding to $\ell \ll R_{\rm S}$. We see that "quantum deformed" BHs with $\ell \sim R_{\rm S}$ are always energetically preferred with respect to those with $\ell \ll R_{\rm S}$.

I.2.4.1 Thermodynamics and phase transition

Inserting F given by Eq. (I.2.50) into Eq. (I.2.30), we get the mass and temperature of the BH

$$T_{\rm H} = \frac{1}{4\pi\, r_{\rm H}}\frac{r_{\rm H}^3 - 2\ell^3}{r_{\rm H}^3 + \ell^3}, \quad M = \frac{1}{2G}\left(r_{\rm H} + \frac{\ell^3}{r_{\rm H}^2}\right). \tag{I.2.60}$$

The temperature behavior agrees with the expected qualitative one shown in Figure I.2.2. The maximum of $T_{\rm H}$ is obtained by solving the equation $y^6 - 10y^3 - 2 = 0$, giving $r_{\rm H} = \sqrt[3]{(5+3\sqrt{3})}\,\ell$.

Expanding Eq. (I.2.60) near extremality, one easily finds the quadratic scaling (I.2.34) of the mass with the temperature

$$M - M_c = 12\pi^2\frac{\ell^3}{G}T_{\rm H}^2. \tag{I.2.61}$$

The black-hole entropy satisfying the first principle of thermodynamics is easily obtained from Eq. (I.2.32)

$$S = \frac{\pi r_{\rm H}^2}{G} - \frac{2\pi\ell^3}{G r_{\rm H}}. \tag{I.2.62}$$

The first term is the standard area law, while the second term describes ℓ-dependent deviations.

The specific heat C can easily be calculated using Eq. (I.2.60) and agrees with the qualitative behavior shown in Figure I.2.3. It diverges for $r_{\rm H} = r_{\rm H,max} = (5+3\sqrt{3})^{1/3}\,\ell$, indicating the onset of the second order phase transition.[4]

The existence of this phase transition and related thermodynamical phase portrait can be checked by computing the free energy $\mathcal{F} = M - T_{\rm H}S$ as a function of the temperature. The free energy for the two branches I and II has to be calculated numerically by inverting the equation $T_{\rm H} = T_{\rm H}(r_{\rm H})$. We plot $\mathcal{F}(T_{\rm H})$ in Figure I.2.6, from which we see that branch I is always energetically preferred with respect to branch II, which further supports our interpretation in which the quantum effects are nonnegligible at the horizon scale. Here, branches I and II have the same meaning as in Section I.2.3.3. Branch I, we recall, corresponds to the configurations with $r_c \leq r_{\rm H} \leq r_{\rm H,max}$, thus describing quantum BHs with $\ell \simeq R_{\rm S}$. Branch II, instead, is populated by the "classical" BH states, where $\ell \ll R_{\rm S}$ and the quantum effects are negligible.

[4]The possibility of having a phase transition in the Hayward model has been previously recognized in Ref. [239].

I.2.4.2 Null geodesics and QNMs in the eikonal limit

Let us now consider geodesic motion and QNMs for the Hayward BH. The effective potential (I.2.39), which determines photon orbits in the black-hole background, in the present case reads

$$V(r) = \frac{J^2}{2r^2}\left(1 - \frac{R_{\rm S} r^2}{r^3 + \ell^3}\right). \tag{I.2.63}$$

The extrema of $V(r)$ are determined by Eq. (I.2.40) with A given by Eq. (I.2.58), i.e., by the roots of the equation $2y^6 - 3\alpha y^5 + 4y^3 + 2 = 0$. By solving this equation numerically, one can show that no real roots exist for $\alpha < \alpha_m \simeq 1.64$. The position of the maximum of the potential depends on the value of the parameter α with respect to α_m and $\alpha_c = 3/4^{1/3}$. Also here, we can distinguish between the four cases shown in Figure I.2.4. The QNMs frequencies in the eikonal approximation for the Hayward BH can be easily calculated by plugging Eq. (I.2.50) into Eqs. (I.2.47a) and (I.2.47b)

$$\omega_{\rm R} = \frac{l}{\ell y_m}\sqrt{1 - \alpha\frac{y_m^2}{y_m^3 + 1}}, \tag{I.2.64a}$$

$$\omega_{\rm I} = -\left(n + \frac{1}{2}\right)\frac{\sqrt{3\alpha}\, y_m^{3/2}}{\sqrt{2}\,\ell\,(1 + y_m)^2}\sqrt{|y_m^3 - 5|\,(1 + y_m^3 - \alpha y_m^2)}. \tag{I.2.64b}$$

By expanding around $\alpha = \alpha_c$, we get

$$\begin{aligned}\omega_{\rm R} &\simeq \frac{0.21\, l}{\ell} - \frac{0.11\, l}{\ell}(\alpha - \alpha_c)\\ &\simeq \frac{0.21\, l}{\ell} - 26.13\, l\, \ell\, T_{\rm H}^2;\end{aligned} \tag{I.2.65a}$$

$$\begin{aligned}\omega_{\rm I} &\simeq -\left(n + \frac{1}{2}\right)\frac{5.70}{\ell} + \left(n + \frac{1}{2}\right)\frac{1.44}{\ell}(\alpha - \alpha_c)\\ &\simeq -\left(n + \frac{1}{2}\right)\frac{5.71}{\ell} + \left(n + \frac{1}{2}\right) 340.07\, \ell\, T_{\rm H}^2,\end{aligned} \tag{I.2.65b}$$

where in the last equalities we used the definition of α and Eq. (I.2.61).

I.2.5 Gaussian-core black hole

Another explicit and simple realization of a regular quantum BH, sourced by an anisotropic fluid with EoS given by Eq. (I.2.9), and satisfying the conditions outlined in Section I.2.3, can be obtained by taking a Gaussian density distribution in the interior of the astrophysical object, peaked at $r = 0$

$$\epsilon(r) = \frac{M}{\pi^{3/2}\ell^3} e^{-r^2/\ell^2}, \tag{I.2.66}$$

The parameter ℓ represents here a smearing of the classical Schwarzschild-Dirac delta-density profile (the latter is recovered in the limit $\ell \to 0$). Such a density profile is motivated by several microscopic descriptions of BHs: non-commutative geometry [132, 240], loop quantum gravity (LQG) [136], corpuscular picture [241]. The NEC condition (see Eq. (I.2.12)) is always satisfied, while the SEC (see Eq. (I.2.13)) is again violated in the deep core of the body, i.e., for $r < \ell$.

Near $r = 0$, the spacetime behaves as dS, with a dS length $\hat{L}$ given by

$$\hat{L} = \sqrt{\frac{3}{4}}\pi^{1/4}\,\ell^{3/2} R_{\rm S}^{-1/2}, \tag{I.2.67}$$

confirming again our general result given by Eq. (I.2.19).

As we also pointed out in Section I.2.4, the same result can be obtained as an exact solution of Einstein's field equations, sourced by the fluid with EoS (I.2.57), in the limit $\ell \to \infty$. Indeed, looking at the density profile (I.2.66), the dS universe can be recovered in the limit $\ell \to \infty$ only if $M \to \infty$, and the energy density (I.2.66) behaves as a constant.

Let's turn our attention to the metric structure, by computing the MS mass at a generic r

$$\begin{aligned} m(r) &= 4\pi \int_0^r d\tilde{r}\, \tilde{r}^2\, \epsilon(\tilde{r}) \\ &= \frac{2M}{\sqrt{\pi}} \gamma\left(\frac{3}{2}, \frac{r^2}{\ell^2}\right) \\ &= M\left[1 - \frac{2}{\sqrt{\pi}} \Gamma\left(\frac{3}{2}, \frac{r^2}{\ell^2}\right)\right], \end{aligned} \tag{I.2.68}$$

where $\gamma(a,z) = \int_0^z dt\, e^{-t}\, t^{a-1}$ and $\Gamma(a,z) = \int_z^\infty dt\, e^{-t}\, t^{a-1}$ are the incomplete gamma functions. The first term in Eq. (I.2.68) is the mass measured at infinity (the Schwarzschild ADM mass), while the second term, parametrized by ℓ, encodes the quantum corrections, the effects of the smearing of the singularity. The deviation from the Schwarzschild solution, described by the mass deviation $\Delta m(r) \equiv M - m(r)$, is strongly suppressed outside the core of the compact object, as for $r \to \infty$ it behaves as

$$\Delta m \sim \frac{M}{\sqrt{\pi}} e^{-\frac{r^2}{\ell^2}} \left(\frac{\ell}{r} + \frac{2r}{\ell}\right) \tag{I.2.69}$$

which represents a stronger suppression with respect to that of the Hayward model (see Eq. (I.2.55)).

The metric components can be written in the form of Eq. (I.2.22) with the metric function $F(y)$ given by

$$F(y) = \frac{1}{y}\left[1 - \frac{2}{\sqrt{\pi}} \Gamma\left(\frac{3}{2}, y^2\right)\right]. \tag{I.2.70}$$

Contrary to the Hayward model, in the present case, the non-algebraic form of F allows to circumvent the viability constraints of Ref. [210].

Given the form of the metric functions, the position of the horizon(s) and the parameter range discriminating among the different possible configurations have to be computed numerically. In particular, the single-horizon, extremal case will satisfy both Eqs. (I.2.25). This translates into the conditions

$$1 - \frac{2GM}{y\ell} + \frac{4GM}{\ell\sqrt{\pi} y} \Gamma\left(\frac{3}{2}, y^2\right) = 0, \tag{I.2.71a}$$

$$1 - \frac{2}{\sqrt{\pi}} \Gamma\left(\frac{3}{2}, y^2\right) - \frac{4y^3}{\sqrt{\pi}} e^{-y^2} = 0. \tag{I.2.71b}$$

Solving these equations gives $y_{\text{min}} \simeq 1.51$, i.e., $r_{\text{min}} \simeq 1.5\,\ell$.[5] Now, substituting the solution into Eqs. (I.2.71), we observe that the critical value of α is $\alpha = \alpha_c \simeq 1.9$, where, we recall, $\alpha = R_{\text{S}}/\ell$ and $\alpha_c = R_{\text{S}}/\ell_c$. Therefore, when $\alpha < \alpha_c \simeq 1.9$ the configuration shows two distinct horizons, when $\alpha = \alpha_c \simeq 1.9$ the configuration is extremal and presents two coinciding horizons, and it becomes horizonless for $\alpha > \alpha_c \simeq 1.9$.

This condition can be expressed in terms of the critical value ℓ_c for the quantum parameter ℓ

$$\ell_c \simeq 0.53 R_{\text{S}}, \tag{I.2.72}$$

which is close to the classical gravitational radius of the object. Again, this critical value discriminates between the three classes of solutions. When ℓ is above, equal, or below ℓ_c we have a solution with two, one, or no horizons, correspondingly. ℓ_c, in turn, determines a critical value $\hat{L}_c$ for dS length through Eq. (I.2.67), which also turns out to be close to the classical Schwarzschild radius[6]

$$\hat{L}_c \simeq 0.31 R_{\text{S}}. \tag{I.2.73}$$

The most interesting case is the extremal BH, obtained for $\ell = \ell_c$ ($\hat{L} = \hat{L}_c$). As discussed in Section I.2.3, in the extremal case the near-horizon geometry factorizes as $\text{AdS}_2 \times \text{S}^2$, with the AdS_2

[5] We discard the trivial solution $r = 0$ since it does not represent a minimum.

[6] The fact that $\hat{L}_c < \ell_c$ is expected: the SEC is violated in the deep core of the object, namely for $r < \ell$. This is perfectly consistent with the fact that this energy condition is violated in a dS spacetime.

length given by $L_2^{-2} = -A''(r_c)/2$. L_2 can be calculated first using Eqs. (I.2.71a) and (I.2.71b), which give

$$e^{-y^2(r_c)} = \frac{\sqrt{\pi}\ell}{4R_{\rm S}y^2(r_c)}. \tag{I.2.74}$$

Using this equation together with Eqs. (I.2.68), (I.2.70), (I.2.71a) and (I.2.71b) enables us to find

$$-\frac{1}{2}A(r_c)'' \equiv \frac{1}{L_2^2} = \frac{1}{\ell^2} - \frac{1}{r_c^2}. \tag{I.2.75}$$

Now, since $\ell_c \simeq 0.53R_{\rm S}$, we see that $r_{\rm min} \simeq 0.78\, R_{\rm S}$ and

$$L_2 \simeq 0.70\, R_{\rm S}, \tag{I.2.76}$$

confirming the general result of Section I.2.3, in which we found that both the radius of the two-sphere and the AdS_2 length are of order $R_{\rm S}$.

As shown at the end of Section I.2.3.2, the extremal solution is stabilized by a particular profile for the energy density ϵ and for the pressures $p_\parallel$ and $p_\perp$, given by the expressions (I.2.29). In the present case, the negative energy density sourcing the AdS_2 spacetime reads

$$\epsilon^{\rm (NH)}_{\rm (AdS)} = -\frac{1}{8\pi G L_2^2} = -\frac{1}{8\pi G}\left(\frac{1}{\ell^2} - \frac{1}{r_c^2}\right). \tag{I.2.77}$$

I.2.5.1 Quantum black hole regimes

The parameter ℓ (or equivalently $\hat{L}$) controls the scale of quantum effects in our quantum black-hole model. In the usual, most conservative approach, which assumes quantum gravity effects to be relevant only at the Planck scale $\ell_{\rm P}$, ℓ is assumed to be of the same order of magnitude of $\ell_{\rm P}$. This assumption is surely justified when ℓ has an explicit origin in the microscopic description of gravity at the Planck scale. It is for instance the case of Refs. [132, 136, 240, 241], where the Gaussian model, and the parameter ℓ in particular, parametrizes UV non-commutative [132] or LQG [136] effects.

However, this is not the case in those approaches, like the one we are discussing here, in which an IR quantum scale, hierarchically larger than $\ell_{\rm P}$, is generated. Given the attention the model with $\ell \sim \ell_{\rm P}$ received in the past [131–139, 141], it is worthwhile to quantitatively compare the two different regimes 1) $\ell \sim \ell_{\rm P}$ and 2) $\ell \sim R_{\rm S}$ for the black-hole model with a Gaussian core, and analyze the possible impact on observable phenomenology in the two cases. Again, we remind the reader that we are considering macroscopic BHs, i.e., $R_{\rm S} \gg \ell_{\rm P}$.

$\ell \sim \ell_{\rm P}$

When $\ell \simeq \ell_{\rm P} \ll R_{\rm S}$, the BH has two horizons, is far from extremality, and the inner horizon is very close to $r = 0$. It is quite easy to understand that these quantum effects are completely irrelevant for macroscopic BHs, at least for what concerns the phenomenology accessible to external observers. In fact, the matter density is sensibly different from zero only at distances of order $\ell_{\rm P}$ from the classical singularity at $r = 0$. Therefore, the deviations from the Schwarzschild solution are expected to be incredibly small for the external observer. The only sensible deviations from $r_{\rm H} \sim R_{\rm S}$ appear when the black-hole mass is of order the Planck mass $m_{\rm P} = 1/\sqrt{G}$ and the event horizon is slightly smaller than $R_{\rm S}$ (the radius of the outer horizon is $r_{\rm H} \simeq 1.8\sqrt{G} = 0.9R_{\rm S}$). However, as the mass increases, the outer horizon becomes rapidly indistinguishable from $R_{\rm S}$. For example, for a solar mass BH, $M = 1\ M_\odot$, the outer horizon of the metric (I.2.70) is at $R_{\rm S}$ and the corrections are exponentially suppressed by a factor $\Gamma\left(\frac{3}{2}, \frac{r_{\rm H}^2}{\ell_{\rm P}^2}\right) \sim e^{-10^{76}}$. The mass deviation at the horizon $\Delta m(r_{\rm H})$ is of the same order of magnitude, which is effectively zero from the point of view of an external observer.

$\ell \sim R_{\rm S}$

As said in Chapter I.1, there are several indications pointing to the relevance of quantum effects at horizon scales. However, presently we do not have a precise microscopic description of these quantum effects, but only some quite interesting proposals, like fuzzballs, firewalls, non-local effects, and corpuscular models. An interesting explicit corpuscular black-hole model with a Gaussian core is the one given in Ref. [241], whose density profile is

$$\epsilon_{\rm corpuscular} = \frac{7^2 m_{\rm P}}{\sqrt{\pi} N} \frac{e^{-\frac{7}{2}\frac{r^2}{N\ell_{\rm P}^2}}}{\ell_{\rm P}^3} \tag{I.2.78}$$

where N is the number of gravitons building up the BH. Comparing this profile with our model (I.2.66), we can read the values of our parameters ℓ, M in terms of N

$$\ell = \ell_{\rm P}\sqrt{\frac{2N}{7}}, \qquad M = 49\pi \frac{\ell^3}{N\ell_{\rm P}^4}. \tag{I.2.79}$$

From these equations, one easily gets the expected holographic scaling of N, $N \propto \ell_{\rm P}^2 M^2$ and a value of ℓ which is $\ell = R_{\rm S}/28\pi \simeq 0.01 R_{\rm S} < \ell_c$. The BH has two horizons and is far from extremality. The outer horizon is quite close to the classical Schwarzschild one, being $r_{\rm H} \simeq 0.96 R_{\rm S}$. Therefore, the mass deviation is

$$\left.\frac{\Delta m}{M}\right|_{\rm H} = \frac{2}{\sqrt{\pi}}\Gamma\left(\frac{3}{2}, y_{\rm H}^2\right) \sim e^{-7733}. \tag{I.2.80}$$

We see that deviations from the classical behavior are still quite small for a value of ℓ which is about $1/100$ of the critical value ℓ_c.

However, when we consider a value $\ell < \ell_c$, but quite close to the critical value, e.g., $\ell = \ell_c/2$ the outer horizon is located at

$$r_{\rm H} \simeq 0.92 R_{\rm S}, \tag{I.2.81}$$

which is a small, but still important, difference with respect to the classical radius $R_{\rm S}$. In this case, the mass deviation is

$$\left.\frac{\Delta m}{M}\right|_{\rm H} = \frac{2}{\sqrt{\pi}}\Gamma\left(\frac{3}{2}, \frac{c^4 r_{\rm H}^2}{G^2 M^2}\right) \simeq \frac{2}{\sqrt{\pi}}\Gamma\left(\frac{3}{2}, 1.84^2\right) \simeq 0.07. \tag{I.2.82}$$

These results further show that the most interesting regime is that for which $\ell \sim R_{\rm S}$ from both a purely theoretical and a phenomenological point of view.

I.2.5.2 Thermodynamics and phase transition

Inserting the metric function (I.2.70) into Eq. (I.2.30), we get the temperature and the ADM mass of the Gaussian BHs

$$T_{\rm H}(r_{\rm H}) = \frac{1}{4\pi r_{\rm H}}\left(1 - \frac{8GM(r_{\rm H}) r_{\rm H}^2}{\ell^3} e^{-r_{\rm H}^2/\ell^2}\right), \tag{I.2.83a}$$

$$M(r_{\rm H}) = \frac{r_{\rm H}}{2G\left[1 - \frac{2}{\sqrt{\pi}}\Gamma\left(\frac{3}{2}, \frac{r_{\rm H}^2}{\ell^2}\right)\right]}. \tag{I.2.83b}$$

The temperature is given by the standard Hawking result plus an ℓ-dependent term, encoding quantum deviations from standard BH thermodynamics, which are, however, exponentially suppressed. The behavior agrees with the qualitative one depicted in Figure I.2.2. It starts from zero in correspondence with the extremal case. Then, it rises and reaches a maximum at $r_{\rm H,max} \simeq 2.38\ell$. Finally, it decreases and reaches zero as $r_{\rm H}/\ell \to \infty$, recovering the standard Schwarzschild results $T_{\rm H} = (4\pi r_{\rm H})^{-1}$ and $M = r_{\rm H}/2G$ in this limit. Also in this case, the quantum deformation parameter $\ell \neq 0$ solves the singular thermodynamic behavior of the Schwarzschild temperature

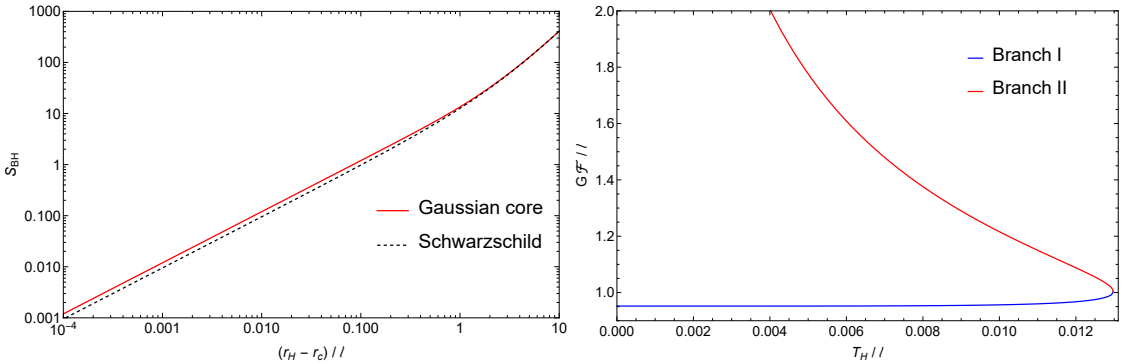

Figure I.2.7: **Left panel**: plot of the entropy of the quantum Gaussian BH (red curve) as a function of the horizon radius $r_{\rm H}$. As a comparison, we plot the standard Bekenstein-Hawking entropy (minus the corresponding value at $r_{\rm H} = r_c$) for a Schwarzschild BH (black dashed curve). **Right panel**: free energy $\mathcal{F}$ as a function of the temperature for the Gaussian model. We distinguish between two branches: one corresponding to BHs with $\ell \sim R_{\rm S}$ (blue curve), the other (red curve) corresponding to $\ell \ll R_{\rm S}$.

at $r_{\rm H} \simeq 0$. The value $\ell_{\rm H,max}$ of the quantum-deformation parameter can be obtained from $r_{\rm H,max}$ using Eqs. (I.2.71)

$$\ell_{\rm H,max} = \frac{1 - \frac{2}{\sqrt{\pi}}\Gamma\left(\frac{3}{2}, y^2_{\rm H,max}\right)}{y_{\rm H,max}} R_{\rm S} \simeq 0.42 R_{\rm S}. \tag{I.2.84}$$

Integrating Eq. (I.2.33) numerically and using the fact that the zero-entropy state is at the extremal radius $r_c/\ell \simeq 1.51$, we can study the black-hole entropy. The result of the integral is presented in the left panel of Figure I.2.7 and is compared to the standard result for the Schwarzschild BH. The entropy does not differ significantly from the standard area law at great horizon radii, as quantum deviations are expected to be exponentially suppressed [242–244] (see also Eq. (I.2.69)).

Expanding Eq. (I.2.83b) near extremality yields the quadratic scaling (I.2.34) of the mass above extremality with the temperature

$$M - M_c \simeq 15.55 \frac{\ell^3}{G} T^2_{\rm H}. \tag{I.2.85}$$

The specific heat can be computed using Eq. (I.2.35) and follows the qualitative behavior of Figure I.2.3: it diverges at $r_{\rm H,max} \simeq 2.38\,\ell$, indicating the onset of the second-order phase transition. Indeed, by computing numerically the free energy $\mathcal{F} = M - T_{\rm H} S$ and expressing it as a function of $T_{\rm H}$, we get the phase diagram depicted in the right panel of Figure I.2.7.

Again, we have two branches. Branch I corresponds to $r_{\rm H}$ taking values between the extremal value r_c and $r_{\rm H,max}$ (correspondingly, the parameter ℓ takes values between $\ell_{\rm H,max} \simeq 0.42 R_{\rm S}$ and $\ell_c \simeq 0.53 R_{\rm S}$), and therefore describes quantum BHs with $\ell \sim R_{\rm S}$. Conversely, branch II corresponds to $r_{\rm H}$ much larger than $r_{\rm H,max}$, corresponding to small ($< 0.42 R_{\rm S}$) values for the parameter ℓ. Thus, the far right region of branch II describes again classical BHs ($\ell \ll R_{\rm S}$).

Figure I.2.7 shows that the free energy of branch I is always smaller than that of branch II. This means that BHs in branch I, i.e., BHs with $\ell \sim R_{\rm S}$, are always energetically preferred.

I.2.5.3 Null geodesics and photon orbits

The effective potential (I.2.39) determining photon orbits in the Gaussian quantum BH reads

$$V(r) = \frac{J^2}{2r^2}\left[1 - \frac{2GM}{r} + \frac{4GM}{\sqrt{\pi} r}\Gamma\left(\frac{3}{2}, \frac{r^2}{\ell^2}\right)\right], \tag{I.2.86}$$

and its behavior for different values of the parameter $\alpha \equiv R_{\rm S}\ell^{-1}$ agrees with the qualitative plots shown in Figure I.2.4.

The extrema of the potential are given by the zeros of $\mathrm{d}V(r)/\mathrm{d}r$ (see Eq. (I.2.40)), i.e., by the solution of the equation

$$-r+3GM-\frac{4GM}{\sqrt{\pi}}\frac{r^3}{\ell^3}e^{-r^2/\ell^2}-\frac{6GM}{\sqrt{\pi}}\Gamma\left(\frac{3}{2},\frac{r^2}{\ell^2}\right)=0. \tag{I.2.87}$$

Notice that the presence of ℓ shifts the position of the photon sphere from the Schwarzschild case $r=3GM$. By solving Eq. (I.2.87) numerically, we distinguish again among three cases (two distinct, two coinciding, or no horizons)

- **T**wo horizons ($\alpha>\alpha_c$): the potential has multiple zeros, corresponding to a minimum in the black-hole interior and a maximum in the exterior, which corresponds to the position of the unstable photon orbit. We are interested in the latter. For instance, for $\alpha=2$ ($\ell=GM$), we get $y_m\simeq 2.99$, corresponding to a photon ring located at $r_m\simeq 2.99\ell=2.99GM$, very close to the Schwarzschild light-ring location $r_{\rm LR}^{\rm Sch}=3GM$.
- **O**ne horizon ($\alpha=\alpha_c$): this case is similar to the previous one. The potential has a minimum at $r=r_{\rm H}$ associated with a stable photon orbit, and a maximum representing the unstable photon orbit. Focusing again on the latter, we have $y_m\simeq 2.84$, corresponding to $r_m\simeq 2.98GM$, again pretty close to the Schwarzschild result.
- **N**o horizons ($\alpha<\alpha_c$): there are two possible cases. If α is large enough ($\alpha\sim[1.6,1.8]$), there exists a maximum corresponding to a photon ring. For example, for $\alpha=1.6$ we get $r_m\simeq 2.74GM$. However, if α falls below the aforementioned interval there are no extrema anymore, therefore the photon ring is absent.

I.2.5.4 QNMs spectrum in the eikonal limit

We can use the general arguments and results of Section I.2.3.6 to compute the expression of the QNMs frequencies for the quantum Gaussian BH in the eikonal limit. Applying the general formulae (I.2.47a), (I.2.47b) to the case of Eq. (I.2.70), we get

$$\omega_{\rm R}=\frac{l}{\ell y_m}\sqrt{1-\frac{\alpha}{y_m}\left[1-\frac{2}{\sqrt{\pi}}\Gamma\left(\frac{3}{2},y_m^2\right)\right]}, \tag{I.2.88a}$$

$$\omega_{\rm I}=-\left(n+\frac{1}{2}\right)\frac{1}{\sqrt{2}\ell}\sqrt{\alpha\left[y_m-\alpha+\frac{2}{\sqrt{\pi}}\Gamma\left(\frac{3}{2},y_m^2\right)\right]\left|\frac{3}{y_m^4}-\frac{4}{\sqrt{\pi}}\frac{1+2y_m^2}{y_m}e^{-y_m^2}-\frac{6}{\sqrt{\pi}y_m^2}\Gamma\left(\frac{3}{2},y_m^2\right)\right|}. \tag{I.2.88b}$$

By expanding around the critical value $\alpha_c\simeq 1.9$, we get

$$\omega_{\rm R}\simeq\frac{l}{\ell}\left[0.20-0.10(\alpha-\alpha_c)\right]\simeq 0.20\frac{l}{\ell}-3.36\,l\,\ell\,T_{\rm H}^2, \tag{I.2.89a}$$

$$\omega_{\rm I}\simeq\frac{1}{\ell}\left(n+\frac{1}{2}\right)\left[-0.19+0.05(\alpha-\alpha_c)\right]\simeq-\frac{0.19}{\ell}\left(n+\frac{1}{2}\right)+1.63\left(n+\frac{1}{2}\right)\ell\,T_{\rm H}^2. \tag{I.2.89b}$$

Chapter I.3

Evaporation of two-dimensional regular black holes

Despite the huge recent progress on the observational side, achieved through gravitational-wave detection [16, 245] and imaging [246, 247], black holes are still a source of challenges for theoretical fundamental physics. The usual black-hole solutions of general relativity (GR) harbour, shielded behind event horizons, spacetime singularities, i.e., regions where the classical and semi-classical descriptions break down [87, 114]. As discovered more than 50 years ago, black holes behave as thermodynamic systems, whose microscopic description remains, however, still mysterious [6, 35, 248–253]. They emit thermal radiation, but the description of the information flow during the evaporation has led to the information paradox, which most embodies the apparent incompatibility between quantum mechanics and GR [42, 43, 159].

A possible solution to the information puzzle, which has been pursued in the literature, is linking it to the singularity problem [1, 160–164]. The presence of a spacetime singularity makes the very notion of a global quantum state for matter fields in the black-hole background ill-defined. The loss of unitarity in the evolution of quantum states could be, therefore, traced back to the bad definition of the latter. The main objection to this argument is that the "unitarity crisis" shows up also for macroscopic black holes, i.e., those with masses hierarchically larger than the Planck mass $m_{\rm p} \simeq 10^{19}$GeV, that is at energy scales where the singularity cannot play any role. Also, the possibility to shift the solution of the problem to the late stages of the evaporation, for instance through the formation of Planck-scale remnants, seems untenable owing to the difficulty of storing or recovering the huge amount of information at these small scales [229, 254].

The recent reformulation and proposal for a solution to the information puzzle [54–56, 255] seem to bring further arguments against a close relationship between the singularity and the information problem. This is because this novel approach is focused *only* on reconstructing the correlations between early and late Hawking radiation and, thus, refers mainly to near-horizon physics.

There is, however, an important feature of black-hole solutions, which could change drastically the debate about the relationship between the singularity problem and the information paradox. The most commonly used spacetime setup is that of a black-hole solution with a single event horizon. Black holes with two (an inner and an outer) horizons introduce a new ingredient, which drastically changes the rules of the game. First of all, these black holes typically admit a ground state (GS) represented by an extremal configuration, in which the inner and outer horizons merge in a single one. Moreover, the radius of the extremal black hole could be hierarchically larger than the Planck scale [1, 3]. In the near-horizon region and in the extremal regime, the geometry factorizes as a two-dimensional (2D) anti-de Sitter (AdS_2) spacetime times a 2D sphere of constant radius. This opens the way to the intriguing possibility that the information issue could be solved in the final stages of the evaporation process using properties of AdS_2 quantum gravity, e.g., by reconstructing correlations between the two disconnected parts of AdS_2 spacetime [256] or by the topological properties of the fragmented GS [215]. Moreover, there is some evidence that, for black holes with two horizons and without a central singularity [84, 140, 257], the evaporation process could be unitary. Specifically, the presence of the inner Cauchy horizon could act as a trapping region for high energy modes, which could be responsible for the release of information

at late times, when the two horizons are about to merge [258, 259].

The most natural candidates for testing these ideas are four-dimensional (4D) nonsingular black holes with a de Sitter (dS) core [1, 84, 134, 136, 158, 238, 260–262]. They appear as static solutions of Einstein's equations sourced by an anisotropic fluid. The corresponding spacetime is asymptotically flat (AF) and at great distances is indistinguishable from the Schwarzschild solution, whereas the singularity at the origin of the radial coordinate is regularized due to inner dS behavior. The latter also produces an additional hair ℓ, which could have interesting observational signatures in the geodesics motion of massless and massive particles, quasinormal modes spectrum and gravitational waves (see, e.g., Refs. [1, 3, 263–266] and references therein). Another consequence of the dS core is the presence, depending on the value of ℓ, of two horizons and an extremal solution. From the thermodynamic point of view, these models are characterized by a second order phase transition: the spectrum has a branch of large unstable configurations and a stable branch of near-extremal solutions.

There are two main obstructions that prevent the direct use of such 4D models to address the information paradox. Firstly, we do not have a microscopic model describing the sources of the solutions. We can just give a coarse-grained description in terms of an anisotropic fluid, with equation of state $p = -\rho$, and a given profile for the energy density ρ. Secondly, there is the usual difficulty of describing semiclassical dynamics, including backreaction effects on the geometry, of quantum Hawking radiation in the 4D classical black-hole background.

Here, we show that both issues can be addressed by considering 2D dilaton gravity models of AF, nonsingular black holes with a dS core. As we shall show, these models can be formulated at Lagrangian level and describe, in a simplified setting, the S-wave sector (radial modes) of their 4D nonsingular counterparts. This will allow us to retain the qualitative features of the higher-dimensional models, keeping, however, under control their dynamics. For concreteness, our investigations will be focused on a particular, but quite relevant, case, namely the 2D Hayward black hole.

We will be able to capture the main thermodynamic features of 4D regular models and, at the same time, to describe their evaporation process and to solve the classical and semiclassical dynamics, including the backreaction of Hawking radiation on the geometry. Having under control the latter will allow us to partially answer some important questions regarding the endpoint of the evaporation process, the time evolution of the entanglement entropy, and the shape of the related Page curve [43, 267]. The main limitation of this approach is obviously represented by the limit of validity of the semiclassical approximation. Nonetheless, our results, together with some known features of AdS_2 quantum gravity, will allow us to have clear indications about the fate of information during the evaporation of nonsingular black holes with a dS core.

The structure of this chapter is as follows. In Section I.3.1, we review some general properties of 2D dilaton gravity models and we present our class of 2D, nonsingular, AF solutions with a dS core. In Section I.3.2, we introduce the prototype model we will use throughout this chapter, namely the 2D Hayward black hole. Section I.3.3 is devoted to the investigation of the thermodynamic properties of our 2D models. In Section I.3.4, we discuss black-hole evaporation using a quasistatic approximation. The coupling with conformal matter, in the form of N massless scalars, is introduced in Section I.3.5. We consider, in particular, classical solutions corresponding to a shock wave. In Section I.3.6, we discuss the evaporation process by quantizing matter in the classical gravitational background and by including backreaction effects. The semiclassical dynamics cannot be solved analytically, so we resort to numerical integration. The entanglement entropy of the Hawking radiation is computed in Section I.3.7 and its Page curve is presented. Some details of the calculations concerning the absence of divergences for the stress-energy tensor in the GS and the boundary conditions used for the numerical integration of the field equations are presented in Appendix I.C and Appendix I.D, respectively.

In this chapter, we use units in which $c = \hbar = k_{\rm B} = 1$.

I.3.1 Two-dimensional regular dilatonic black holes

The simplest black-hole models can be constructed in a 2D spacetime. However, the pure 2D Einstein-Hilbert action is a topological invariant and a metric theory of gravity has to be built by coupling the Ricci scalar with a scalar field ϕ, the dilaton. 2D dilaton gravity is generally described

by the action (see Ref. [218] for a review; for a generalization, see Ref. [268])

$$\mathcal{L} = \sqrt{-g}\left[\mathcal{D}(\phi)R + \mathcal{K}(\phi)g^{\mu\nu}\partial_\mu\phi\partial_\nu\phi + \mathcal{V}(\phi)\right], \tag{I.3.1}$$

where $\mathcal{D}$, $\mathcal{K}$, and $\mathcal{V}$ are functions of the dilaton, representing, respectively, the coupling with the Ricci scalar R (the dimensionless inverse Newton constant), the kinetic term of the scalar field and the potential. Using a Weyl transformation of the metric

$$g_{\mu\nu} = e^{\mathcal{P}(\phi)}\tilde{g}_{\mu\nu}, \qquad \mathcal{P} = -\int^{\phi} \mathrm{d}\psi \frac{\mathcal{K}(\psi)}{\mathcal{D}(\psi)}, \tag{I.3.2}$$

together with a field redefinition

$$\mathcal{D}(\phi) \to \phi, \tag{I.3.3}$$

it is always possible to set $\mathcal{K} = 0$ and to recast the lagrangian into the simpler form [269, 270]

$$\mathcal{L} = \sqrt{-g}\left[\phi R + \mathcal{V}(\phi)\right]. \tag{I.3.4}$$

This choice of the conformal (Weyl) frame is typically used when dealing with asymptotically AdS black holes, while for AF configurations (which is the focus of the present chapter), a conformal frame with $\mathcal{K} \neq 0$ is generally considered more appropriate [271–275]. This is particularly true when 2D dilatonic black holes are used to describe the S-wave sector of higher dimensional models (but see, e.g., Refs. [276–280]). However, as we shall see below, the description of also AF black holes is much simpler in the conformal frame (I.3.4) than in a frame with $\mathcal{K} \neq 0$. Moreover, the lagrangian (I.3.4) is fully characterized by the dilaton potential $\mathcal{V}(\phi)$; this allows for a simple classification of regular black-hole models in terms of the properties of $\mathcal{V}$. For these reasons, in the following, we will work in this frame, although this choice will introduce some difficulties concerning the physical interpretation of the parameters we use to describe black holes.

The equations of motion stemming from Eq. (I.3.4), in the absence of matter fields, read

$$R + \frac{\mathrm{d}\mathcal{V}}{\mathrm{d}\phi} = 0, \tag{I.3.5a}$$

$$\left(g_{\mu\nu}\Box - \nabla_\mu\nabla_\nu\right)\phi - \frac{1}{2}g_{\mu\nu}\mathcal{V} = 0. \tag{I.3.5b}$$

I.3.1.1 Linear dilaton solution

Let us now first consider static solutions of Eq. (I.3.5b). In this case, the dilaton can be used as a spacelike "radial" coordinate of the 2D spacetime,

$$\phi = \lambda r, \tag{I.3.6}$$

where λ is a constant, with dimensions of the inverse of a length, characterizing the potential $\mathcal{V}$. This parametrization of the dilaton is particularly useful when the 2D theory is used to describe the S-wave sector of 4D black holes. In this case, the dilaton is proportional to the radius of the transverse two-sphere. Notice also that the dilaton represents the inverse of the 2D Newton constant. This means that the region $r \ll \lambda^{-1}$ is in a strong coupling regime, whereas $r \gg \lambda^{-1}$ is a weak-coupling region. To be consistent, both interpretations of ϕ require to limit the range of variation of the radial coordinate to $r \in [0, \infty)$.

Eq. (I.3.6) allows us to write the most general static solution of Eqs. (I.3.5a) and (I.3.5b) as the linear dilaton solution (LDS)

$$ds^2 = -f(r)\mathrm{d}t^2 + \frac{\mathrm{d}r^2}{f(r)}, \quad f = c_1 + \frac{1}{\lambda}\int \mathrm{d}r\,\mathcal{V} \tag{I.3.7}$$

where c_1 is a dimensionless integration constant, which can be written in terms of the covariant mass $\mathcal{M}$, which can be defined for a generic 2D dilaton-gravity theory [281]. For a static spacetime, $\mathcal{M}$ is the conserved charge associated with the Killing vector $\chi^\mu = F_0\epsilon^{\mu\nu}\partial_\nu\phi$, generating time

translations[1]. F_0 is a constant, which is fixed by the normalization of χ^μ. As we will see in the following, to make contact with four-dimensional models, a convenient choice[2] is $F_0 = -1/\lambda$.

In our Weyl frame, $\mathcal{M}$ reads

$$\mathcal{M} = \frac{F_0}{2}\left[\int^\phi \mathrm{d}\phi\mathcal{V} - g^{\mu\nu}\partial_\mu\phi\partial_\nu\phi\right] = -\frac{F_0}{2}c_1\lambda^2. \tag{I.3.8}$$

Choosing appropriately the form of $\mathcal{V}$ allows to generate different solutions. In particular, we focus on dilaton gravity models allowing for AF nonsingular black holes.

A useful information for classifying different classes of models can be obtained from the existence of solutions characterized by a constant dilaton, the so-called constant dilaton vacua (CDV). Owing to the r-dependent parametrization of the dilaton (I.3.6), these solutions cannot be obtained as particular LDSs given by Eq. (I.3.7) and must be discussed separately.

I.3.1.2 Constant dilaton vacua

The CDV solutions of Eqs. (I.3.5) can be obtained by setting $\phi =$ constant $\equiv \phi_0$. According to Eq. (I.3.5b), these vacuum configurations must correspond to zeroes of the potential, $\mathcal{V}(\phi_0) = 0$. On the other hand, Eq. (I.3.5a) shows that they correspond to 2D spacetimes with constant curvature and can be classified according to the sign of $\mathrm{d}\mathcal{V}/\mathrm{d}\phi|_{\phi=\phi_0}$. There are three possible cases

1. If $\mathrm{d}\mathcal{V}/\mathrm{d}\phi|_{\phi_0} < 0$, $R > 0$, and the spacetime is de Sitter,

2. If $\mathrm{d}\mathcal{V}/\mathrm{d}\phi|_{\phi_0} > 0$, $R < 0$, and the spacetime is anti-de Sitter,

3. If $\mathrm{d}\mathcal{V}/\mathrm{d}\phi|_{\phi_0} = 0$, $R = 0$, and the spacetime is Minkowsky.

Notice that the condition for having a flat CDV is rather strong since it requires ϕ_0 to be both a zero and an extremum of $\mathcal{V}$. Asymptotic flatness, moreover, also implies that we always have $\mathcal{V}(\infty) = \mathrm{d}\mathcal{V}/\mathrm{d}\phi|_\infty = 0$. In this case, formally, we can consider $\phi = \infty$, which corresponds to a decoupled configuration (the 2D Newton constant vanishes), as a flat CDV. In the first case above, instead, we can define

$$\left.\frac{\mathrm{d}\mathcal{V}}{\mathrm{d}\phi}\right|_{\phi_0} \equiv -\frac{1}{L_{\mathrm{dS}}^2}. \tag{I.3.9}$$

From this, using Eq. (I.3.5a), we have

$$f(r) = 1 - \frac{r^2}{L_{\mathrm{dS}}^2}, \tag{I.3.10}$$

which describes two-dimensional dS (dS_2) spacetime, with an associated dS length L_{dS}.

In the second case, we define instead

$$\left.\frac{\mathrm{d}\mathcal{V}}{\mathrm{d}\phi}\right|_{\phi_0} \equiv \frac{1}{L_{\mathrm{AdS}}^2}. \tag{I.3.11}$$

Eq. (I.3.5a) now yields

$$f(r) = \frac{r^2}{L_{\mathrm{AdS}}^2}, \tag{I.3.12}$$

which describes the AdS_2 spacetime, with an associated AdS length L_{AdS}.

[1] In this case $\mathcal{M}$ corresponds to the ADM mass of the solution [282, 283].

[2] Note that this normalization differs only in the sign with respect to the expression of Ref. [281].

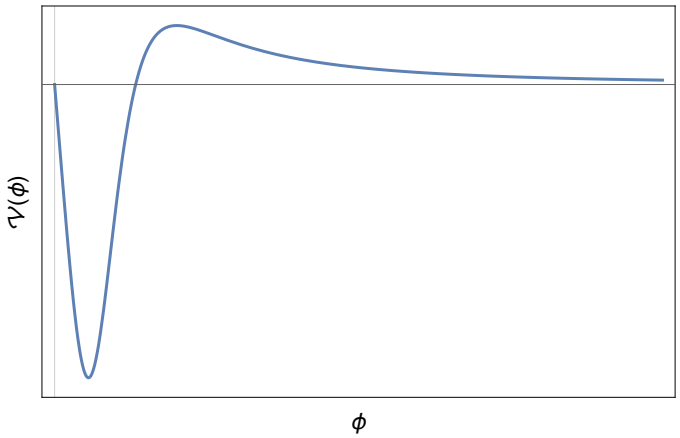

Figure I.3.1: Qualitative behavior of the potential, characterizing the broad class of the regular models satisfying the conditions (1), (2), (3). We restricted ourselves to the case of a single maximum and a single minimum. The horizontal and vertical lines correspond to $\mathcal{V} = 0$ and $\phi = 0$, respectively.

I.3.1.3 General class of 2D nonsingular, asymptotically-flat black holes with a de Sitter core

We are interested in 2D dilatonic black holes, which mimic the behavior of 4D regular black holes. Therefore we have to choose the form of the potential $\mathcal{V}$ such that: (a) the spacetime has one or at most two horizons; (b) the spacetime curvature remains everywhere finite, in particular the usual 4D curvature singularity at $r = 0$ is removed; (c) the spacetime is AF, with a Schwarzschild subleading behavior at $r \to \infty$, i.e., $f \sim 1 - c/r$, with c a constant.

Condition (a) requires $f(r)$ to have at least one zero and to stay positive outside the (outer) horizon, i.e.,

$$\int_{\phi_{\rm H}}^{\phi} \mathrm{d}\psi \mathcal{V}(\psi) \geq 0. \tag{I.3.13}$$

Condition (b) can be reformulated as a condition on the first derivative of $\mathcal{V}$. In two dimensions, the Ricci scalar is the only curvature invariant. Therefore, bounding it is sufficient to generate regular spacetime metrics. According to Eq. (I.3.5a), this translates into requiring regularity of $\mathrm{d}\mathcal{V}/\mathrm{d}\phi$. Regularity at $r = 0$ can be achieved in different ways. The simplest and more physical one, which has also been used for 4D models [1, 84, 134, 136, 158, 238, 260, 261], is to impose $\mathrm{d}\mathcal{V}/\mathrm{d}\phi|_0$ to be finite and

$$\mathcal{V}(0) = 0, \quad \left.\frac{\mathrm{d}\mathcal{V}}{\mathrm{d}\phi}\right|_0 < 0. \tag{I.3.14}$$

According to the general discussion of Section I.3.1.2, this implies that our model must allow for a dS_2 CDV at $\phi = 0$, given by Eq. (I.3.10), which will therefore describe the inner core of our black-hole solutions. Using Eq. (I.3.10), one can easily find the form of the potential in the $\phi \sim 0$ region is,

$$\mathcal{V} \sim -2\frac{\phi}{\lambda \hat{L}^2}. \tag{I.3.15}$$

Condition (c), i.e., asymptotic flatness and a Schwarzschild subleading behavior, can be implemented by fixing the asymptotic behavior for $\phi \to \infty$

$$\mathcal{V} \sim \frac{\lambda^2}{\phi^2}. \tag{I.3.16}$$

Eq. (I.3.14) implies the dilaton potential to be zero at $\phi = 0$, and to become negative and decrease near $\phi \sim 0$. However, it has to grow again, cross the ϕ-axis at a finite value $\phi = \phi_1$, and

develop at least one minimum and one maximum to guarantee the positive fall of $\mathcal{V}$ at asymptotic infinity, implied by Eq. (I.3.16). The model, therefore, must allow for three different CDV solutions at $\phi = 0$, $\phi = \phi_1$ and $\phi = \infty$, describing, respectively, a dS_2, AdS_2 and flat spacetimes.

In principle, the potential could show any number of oscillations, but for simplicity in the following we restrict ourselves to potentials with a single maximum and a single minimum. The qualitative behavior of the general form of our potential $\mathcal{V}$ is shown in Fig. I.3.1. Quantitatively, the potential will depend on some dimensional parameters. The most natural, minimal choice is a potential depending on two parameters. Since ϕ is dimensionless, the parameter λ, introduced above, is needed to give the right dimensions to $\mathcal{V}$. At least a second parameter, however, which we will call ℓ, is needed if we want to express the CDV ϕ_0 in terms of the parameters of the model. The values of such parameters will impact on the behavior of the metric function. Indeed, since $\mathcal{V} = \lambda \mathrm{d}f/\mathrm{d}r$ from Eq. (I.3.7), we see that the presence of two zeros for $\mathcal{V}$ implies the existence of a minimum for $f(r)$. Depending on the value of ℓ, this minimum can be above, below or exactly at the r-axis, producing horizonless, two-horizon or extremal configurations, respectively. The parameter λ, instead, does not affect the presence of extrema in $f(r)$, nor their location in the radial direction. Notice that the AdS_2 CDV describes the near-horizon behavior of the extremal black hole [284, 285].

One can easily construct dilatonic potentials $\mathcal{V}(\phi)$ behaving as in Fig. I.3.1. Basically, for every spherically-symmetric, regular 4D black hole, characterized by a single metric function f, one can easily construct the corresponding 2D dilaton gravity theory by solving Eq. (I.3.7), determining in this way the form of $\mathcal{V}$. For instance, notable models are those which can be obtained from the Hayward black hole [84], Gaussian-core black hole [134], the Fan-Wang model [158] or the Bardeen solution [260].

For the sake of concreteness, in the following we will focus on a 2D dilaton gravity model reproducing the Hayward black hole. However, all the considerations of the next sections can be extended to the general class of models described in this section.

I.3.2 Two-dimensional Hayward black hole

One of the simplest cases of potentials behaving as shown in Fig. I.3.1 is given by

$$\mathcal{V}(\phi) = \lambda^2 \frac{\phi^4 - 2\ell^3\lambda^3\phi}{(\phi^3 + \lambda^3\ell^3)^2}, \tag{I.3.17}$$

where ℓ is a parameter with dimensions of length. The potential has a zero at $\phi = 0$, which gives the dS CDV with a related dS length (I.3.9), given in this case by $L^2_{\rm dS} = \lambda\ell^3$, and goes to zero for $\phi \to \infty$. The other zero is at

$$\left(\frac{\phi}{\lambda}\right)^3 = 2\ell^3 \quad \Rightarrow \quad \phi_0 = \sqrt[3]{2}\lambda\ell, \tag{I.3.18}$$

which gives the AdS_2 CDV and, as we shall see below, describes extremal black holes in the near-horizon regime. The associated AdS length (see Eq. (I.3.11)) is $L^2_{\rm AdS} = 3\lambda\ell^3$.

With the potential (I.3.17), solving Eq. (I.3.7) yields

$$f = \frac{2\mathcal{M}}{\lambda} - \frac{1}{\lambda}\frac{r^2}{r^3 + \ell^3}, \tag{I.3.19}$$

which interpolates between the Schwarzschild spacetime at great distances and the dS one at $r \sim 0$, modulo a rescaling of the coordinates t and r by the constant quantity $2\mathcal{M}/\lambda$. This peculiar behavior, in which the mass term in the line element dominates at great distances, was analyzed in $2D$ very recently in Ref. [286] and termed "mass-dominated" dilaton gravity.

The 4D Hayward black hole [84] is described by the metric element $\mathrm{d}s^2_4 = -f_{\rm H}(r)\,\mathrm{d}t^2 + f^{-1}_{\rm H}(r)\,\mathrm{d}r^2 + r^2\mathrm{d}\Omega_2$, with the metric function given by

$$f_{\rm H}(r) = 1 - \frac{2Gmr^2}{r^3 + \ell^3}, \tag{I.3.20}$$

where m is the 4D ADM mass.

One can easily check that the (constant) Weyl rescaling of the 2D metric, together with a rescaling of the time coordinate

$$g_{\mu\nu} \to \frac{\lambda}{2\mathcal{M}} g_{\mu\nu}, \quad t \to \frac{\lambda}{2\mathcal{M}}\, t \tag{I.3.21}$$

brings the metric into the form

$$\mathrm{d}s_2^2 = -\left(1 - \frac{1}{2\mathcal{M}}\frac{r^2}{r^3+\ell^3}\right)\mathrm{d}t^2 + \left(1 - \frac{1}{2\mathcal{M}}\frac{r^2}{r^3+\ell^3}\right)^{-1}\mathrm{d}r^2. \tag{I.3.22}$$

This transformation leaves the 2D dilaton gravity action invariant up to a constant factor, which does not alter the equations of motion.

If we now write the covariant mass of the 2D solution in terms the mass m of the 4D black-hole solution (I.3.20) we get

$$\frac{1}{2\mathcal{M}} \equiv \frac{2m}{\lambda^2}. \tag{I.3.23}$$

The 4D metric element of the Hayward black hole can be simply written in terms of the 2D one (I.3.22) and the dilaton as $\mathrm{d}s_4^2 = \mathrm{d}s_2^2 + (\phi/\lambda)^2\mathrm{d}\Omega_2$.

The peculiar relation (I.3.23) can be seen as a consequence of both the specific conformal frame chosen here (see the discussion at the beginning of Section I.3.1), which is particularly suited for asymptotically AdS spacetimes, and of the normalization of the Killing vector F_0 adopted in Section I.3.1.1. As we shall see, the minus sign in F_0 implies that an asymptotic observer in 2D spacetime measures the energy of the system with the opposite sign with respect to the asymptotic observer in the 4D spacetime. Hence, when the 2D mass becomes bigger, the corresponding 4D mass decreases and viceversa, which is reflected in the inverse relation (I.3.23). We will further confirm this below when studying the thermodynamic properties of the 2D model.

In the remainder of the chapter, we will consider the metric function f in the form (I.3.19). It has a minimum at

$$r_{\min} = \sqrt[3]{2}\ell. \tag{I.3.24}$$

If $f(r_{\min}) < 0$, the metric has two horizons, solutions of $f(r) = 0$, while if $f(r_{\min}) > 0$, it has no horizons. If $f(r_{\min}) = 0$, the two horizons merge, become degenerate and the configuration becomes extremal, with an event horizon located at $r_{\min} \equiv r_{\text{ext}}$. Using the latter and setting $f(r_{\text{ext}}) = 0$ yields the critical value of ℓ at extremality

$$\ell_c = \frac{1}{3\sqrt[3]{2}\mathcal{M}}. \tag{I.3.25}$$

Thus, for $\ell < \ell_c$ the black hole has two horizons; for $\ell = \ell_c$ the two horizon merge in a single one; whereas for $\ell > \ell_c$ the spacetime has no horizons.

Interestingly, the value of r_{ext} in Eq. (I.3.24) is the same at which the potential (I.3.17) changes sign (see Eq. (I.3.18)). Indeed, as it is usually the case for two-horizon models [1, 211, 212], the extremal, near-horizon metric is that of AdS_2 spacetime.

I.3.3 Black-hole thermodynamics

I.3.3.1 Thermodynamic potentials and the first principle

Our 2D black-hole solutions can be considered as thermodynamic systems, characterized by a Hawking tempertaure T_{H}, an internal energy E and an entropy S. The Hawking temperature is given by the standard formula

$$T_{\text{H}} = \frac{f'(r_{\text{H}})}{4\pi} = \frac{\mathcal{V}(\phi_{\text{H}})}{4\pi} = \frac{r_{\text{H}}^4 - 2\ell^3 r_{\text{H}}}{4\pi\lambda\left(r_{\text{H}}^3+\ell^3\right)^2}, \tag{I.3.26}$$

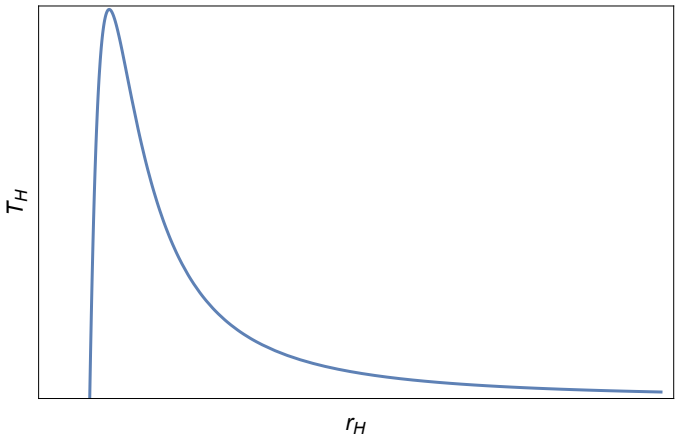

Figure I.3.2: Qualitative behavior of the temperature of the 2D black hole, according to Eq. (I.3.26).

where $r_{\rm H}$ is the radius of the (outer) event horizon. The temperature becomes zero both at extremality, i.e., for $r_{\rm H} = r_{\rm ext} = \sqrt[3]{2}\ell$, and for $r_{\rm H} \to \infty$, whereas it reaches a maximum at

$$r_{\rm H,\,peak} = \frac{\ell}{\sqrt[3]{2}} \sqrt[3]{7 + \sqrt{45}}. \tag{I.3.27}$$

The qualitative behavior of $T_{\rm H}$ is shown in Fig. I.3.2.

The internal energy is usually identified with the black-hole mass. However, in our case, we have chosen a negative normalization of the Killing vector generating time translation, opposite to the usual positive one. Consistency with this normalization requires $E = -\mathcal{M}$. Using Eq. (I.3.19), we can express $\mathcal{M}$ as a function of the outer event horizon radius

$$E = -\mathcal{M} = -\frac{1}{2}\frac{r_{\rm H}^2}{r_{\rm H}^3 + \ell^3}. \tag{I.3.28}$$

A negative internal energy is somehow unusual for black holes, but it is perfectly consistent with their description (and normalizations) as thermodynamic systems. Indeed, we will confirm this below by using the euclidean action approach and proving the consistency of the first law of thermodynamics. The energy E, thus, is always negative and goes to its maximum value $E = 0$ as $r_{\rm H} \to \infty$, whereas it reaches its minimum value $E_{\rm ext} = -(3\sqrt[3]{2}\ell)^{-1}$ for the extremal black hole, whose radius is given by Eq. (I.3.24)[3]. Moreover, for $r_{\rm H} \geq r_{\rm ext}$, as expected, $E(r_{\rm H})$ is a monotonic increasing function.

Let us now calculate the entropy of the 2D Hayward black hole using the Euclidean action formalism, which allows us to calculate the partition function $\mathcal{Z}$ of the thermodynamic ensemble in terms of the Euclidean action $\mathcal{I}$, i.e., $\mathcal{I} = -\ln \mathcal{Z}$. By a Wick rotation of the time t, the action of the lagrangian (I.3.4) becomes the euclidean bulk action $\mathcal{I}_{\rm b}$. It has been shown that, in order to have a well-defined variational principle for "mass-dominated" dilaton gravity theories, the action must be supported by (one half) the usual Gibbons-Hawking-York (GHY) boundary term $\mathcal{I}_{\rm GHY}$ plus an additional one, containing the normal derivative of the dilaton [286].

The action reads

$$\mathcal{I} = \mathcal{I}_{\rm b} + \mathcal{I}_{\rm GHY} + \mathcal{I}_{\partial\phi} = -\frac{1}{2}\int {\rm d}^2x\sqrt{-g}\,(\phi R + \mathcal{V}) - \frac{1}{2}\int_{r=r_\infty} {\rm d}\tau\sqrt{h}\,[\phi\mathcal{K} - n^\mu\partial_\mu\phi]\,. \tag{I.3.29}$$

We enclose the system into a hypersurface at constant $r = r_\infty$, where we define an induced, one-dimensional, metric h, whose extrinsic curvature is described by $\mathcal{K}_{\mu\nu}$ ($\mathcal{K}$ is its trace). τ is the euclidean time, which is periodic with period equal to the inverse of the temperature $T_{\rm H}^{-1} \equiv \beta$. All quantities on the boundary will be evaluated at the cutoff $r = r_\infty$ and then we will let r_∞ go to infinity.

[3]Notice that, according to Eq. (I.3.23), $E = 0$ corresponds to the 4D Hayward black hole with an infinite mass m, whereas the $E_{\rm ext}$ corresponds to the mass $m_{\rm ext}$ of the extremal 4D black hole.

Moreover, one could add a purely topological, Einstein-Hilbert term of the action $\mathcal{I}_{\rm topo} \propto \phi_0 \int d^2x\sqrt{-g}R$, with ϕ_0 a constant, which only changes the value of the entropy by an additional constant S_0, depending on ϕ_0. This constant value can be identified as the entropy of the extremal configuration.

Let us now evaluate the boundary term on the LDS. The induced metric with euclidean signature reads $h_{\mu\nu} = h_{00} = f$. The extrinsic curvature is defined in terms of the normal vector to the hypersurface n_μ as $\mathcal{K}_{\mu\nu} \equiv \frac{1}{2}\nabla_\mu n_\nu + \frac{1}{2}\nabla_\nu n_\mu$, where the normal vector reads, in this case, $n_\mu = f^{-1/2}\delta^r_\mu$. Therefore, when evaluated on the solution for the dilaton, we have $\mathcal{I}_{\rm GHY} = -\frac{\lambda}{4}\beta r f'|_{r=r_\infty}$, which vanishes in the limit $r_\infty \to \infty$ when f is given by Eq. (I.3.19). The remaining boundary term, instead, gives

$$\mathcal{I}_{\partial\phi} = \frac{\beta}{2}\lambda f\Big|_{r=r_\infty} = \beta\mathcal{M}. \tag{I.3.30}$$

Usually, one has to add a counterterm to the boundary action, needed to regularize divergences arising in the limit $r_\infty \to \infty$. This counterterm is written in terms of the extrinsic curvature of the boundary embedded in flat spacetime. In our case, such term is not needed because there are no divergences. Moreover, there is no contribution from flat spacetime ($f(r) = 1$) since Eq. (I.3.29) gives $\mathcal{S}_{\rm flat} = 2\int dtdr\phi''$, which is zero for the LDS (I.3.7).

We now evaluate the bulk action. Using Eqs. (I.3.6) and (I.3.7), we have

$$\mathcal{I}_{\rm b} = -\frac{1}{2}\int \mathrm{d}^2x\sqrt{-g}\,(-\phi f'' + \mathcal{V}) = -\frac{\beta\lambda}{2}\left[-rf' + 2f\right]_{r_{\rm H}}^{r_\infty} = -2\beta\mathcal{M} - 2\pi\lambda r_{\rm H}, \tag{I.3.31}$$

where we used $f(r_{\rm H}) = 0$, $r_\infty f'(r_\infty) \to 0$ and $f(r_\infty) \to 2\mathcal{M}/\lambda$ for $r_\infty \to \infty$, and $f'(r_{\rm H}) = 4\pi T_{\rm H} = 4\pi/\beta$.

Combining Eqs. (I.3.30) and (I.3.31) yields $\mathcal{I} = -\beta\mathcal{M} - 2\pi\lambda r_{\rm H} = -\ln\mathcal{Z}$, where $\mathcal{Z}$ is the partition function. The internal energy and entropy, thus, read

$$E = -\partial_\beta \ln\mathcal{Z} = -\mathcal{M}, \tag{I.3.32a}$$

$$S = \beta\partial_\beta \ln\mathcal{Z} - \ln\mathcal{Z} = 2\pi\lambda r_{\rm H} = 2\pi\phi(r_{\rm H}). \tag{I.3.32b}$$

Eq. (I.3.32a) confirms Eq. (I.3.28), as expected.

The black-hole entropy, instead, scales as the dilaton, i.e., as the inverse 2D Newton constant, evaluated at the horizon. This is the usual formula for the entropy of 2D black holes [287, 288] and represents the extension to two spacetime dimensions of the usual area law in higher dimensions. This is also quite evident when the 2D black hole is derived from the dimensional reduction of the 4D one, with the dilaton playing the role of the radius of the transverse S^2 sphere, as it is here the case.

Contrary to standard $4D$ regular black-hole solutions [1], here the entropy naturally follows the area law. This is because our 2D solutions do not require external matter sources and, therefore, are not coupled to a stress-energy tensor, which in the 4D case describes an anistropic fluid. In general, for regular models, the latter is characterized by a density that depends on the ADM mass of the model, which introduces extra (bulk) terms altering the area-scaling of the entropy [1, 289].

Adding the contribution S_0 of the topological action leads to

$$S = S_0 + 2\pi\lambda r_{\rm H}. \tag{I.3.33}$$

Because of the minus sign in Eq. (I.3.28), we need to check the consistency of our derivation with the first principle of thermodynamics. By differentiating E and S, given respectively by Eqs. (I.3.28) and (I.3.32b), with respect to $r_{\rm H}$, and using Eq. (I.3.26) for $T_{\rm H}$, we can easily check that the identity $dE = T_{\rm H}\mathrm{d}S$ is satisfied.

The previous results allow us to compute the energy difference between two configurations, characterized by the two values ϕ_1 and ϕ_2 of the dilaton, in terms of the integral of the dilaton potential. This can be done in all generality by integrating the first law, considering Eqs. (I.3.26) and (I.3.32b)

$$\Delta E_{1,2} \equiv E(\phi_1) - E(\phi_2) = \frac{1}{2}\int_{\phi_2}^{\phi_1} \mathcal{V}(\phi_{\rm H})\mathrm{d}\phi_{\rm H}. \tag{I.3.34}$$

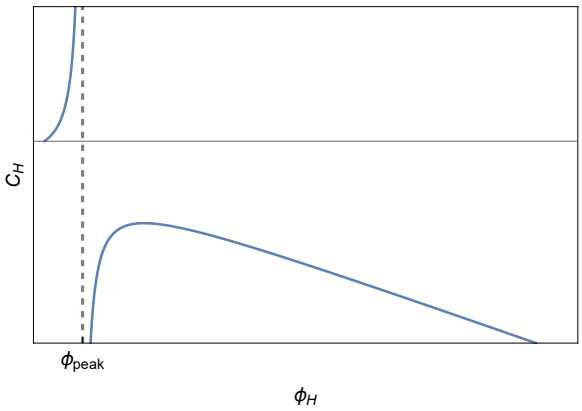

Figure I.3.3: Qualitative behavior of the specific heat of the 2D black hole. The vertical dashed line corresponds to the peak of the potential, ϕ_{peak}.

Let us assume $\phi_2 < \phi_1$ and that ϕ_2 represents a black-hole configuration. Then, for ϕ_2, the condition (I.3.13) holds, whether or not ϕ_1 represents a black hole. Therefore, $\Delta E_{1,2} > 0$ and the black-hole energy increases monotonically, as already seen by analysing Eq. (I.3.28). The consequence of this is that the configuration retaining the least internal energy will be the one with the least dilaton, i.e., the extremal configuration.

I.3.3.2 Thermodynamic stability and second order phase transition

Let us now investigate the thermodynamic stability of our regular black-hole solutions. This can be done by studying the specific heat and the free energy.

The specific heat of our solutions is given by

$$C_{\rm H} = \frac{{\rm d}E}{{\rm d}T_{\rm H}} = \frac{{\rm d}E}{{\rm d}\phi_{\rm H}}\left(\frac{{\rm d}T_{\rm H}}{{\rm d}\phi_{\rm H}}\right)^{-1} = 4\pi\frac{{\rm d}E}{{\rm d}\phi_{\rm H}}\left(\frac{{\rm d}\mathcal{V}}{{\rm d}\phi_{\rm H}}\right)^{-1}. \tag{I.3.35}$$

In Section I.3.3.1, we showed that the internal energy of black-hole configurations is always increasing with ϕ_H. Therefore, the sign of $C_{\rm H}$ is determined by the sign of ${\rm d}\mathcal{V}/{\rm d}\phi_{\rm H}$. As already discussed in Section I.3.1, requiring the potential to satisfy the minimal requirements listed in Section I.3.1.3 implies $\mathcal{V}$ to be necessarily nonmonotonic. Moreover, imposing a dS-like behavior in the interior constrains the potential to have another zero at $\phi_{\rm H} = \phi_0$, which further restricts the interval to $\phi_{\rm H} \in [\phi_0, \infty)$ where we have at least an extremum. The specific heat, thus, shows a single maximum in this interval, located at ϕ_{peak} (see Fig. I.3.1). Here, ${\rm d}\mathcal{V}/{\rm d}\phi_{\rm H}$ changes sign (from positive to negative) as the potential falls monotonically at infinity. Therefore, we have

- For $\phi_0 \leq \phi_{\rm H} < \phi_{\text{peak}}$, ${\rm d}\mathcal{V}/{\rm d}\phi_{\rm H} > 0$ and therefore $C_{\rm H} > 0$. This correspods to a branch of thermodynamically stable configurations;
- For $\phi_{\rm H} > \phi_{\text{peak}}$, ${\rm d}\mathcal{V}/{\rm d}\phi_{\rm H} < 0$ and therefore $C_{\rm H} < 0$. This is, instead, the branch of thermodynamically unstable configurations;
- For $\phi_{\rm H} = \phi_{\text{peak}}$, ${\rm d}\mathcal{V}/{\rm d}\phi_{\rm H} = 0$ and $C_{\rm H} \to \infty$, which signals the onset of a second order phase transition.

This general discussion also applies to the 2D Hayward black hole, described by the potential (I.3.17). Using Eqs. (I.3.26) and (I.3.28), Eq. (I.3.35) reads

$$C_{\rm H} = \frac{\pi\lambda\left(\ell^3 + r_{\rm H}^3\right)\left(2\ell^3 r_{\rm H} - r_{\rm H}^4\right)}{\ell^6 - 7\ell^3 r_{\rm H}^3 + r_{\rm H}^6}, \tag{I.3.36}$$

which diverges at the peak temperature (I.3.27). In terms of the event horizon radius we have

- An unstable branch of large black holes ($r_{\rm H} \gg r_{\text{ext}}$), with negative specific heat;

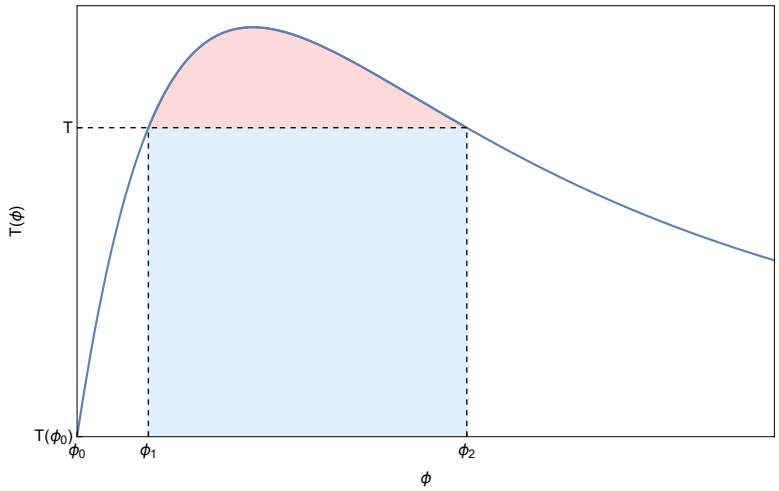

Figure I.3.4: Temperature $T(\phi)$ as a function of ϕ. Here, we highlighted the two configurations corresponding to ϕ_1 and ϕ_2, respectively in the stable and unstable branch and their common temperature $T = T(\phi_1) = T(\phi_2)$. The areas representing $(\phi_2 - \phi_1)T$ and the right-hand side of Eq. (I.3.38), are coloured in blue and red, respectively.

- A stable branch of black holes close to extremality ($r_{\rm H} \gtrsim r_{\rm ext}$) with positive specific heat.

$C_{\rm H}$ goes to zero at extremality and, near $r_{\rm H} \sim r_{\rm ext}$, it behaves as

$$C_{\rm H} \sim 2\pi\lambda(r_{\rm H} - r_{\rm ext}) + \mathcal{O}\left[(r_{\rm H} - r_{\rm ext})^2\right], \tag{I.3.37}$$

which scales linearly with $r_{\rm H}$, as the specific heat of AdS_2 black holes [290]. This is fully consistent with the AdS_2 behavior of the 4D LDS Hayward metric in the near-extremal, near-horizon regime. However, differently from its four dimensional counterpart, for which the AdS_2 spacetime represents only an approximate solution, the AdS_2 appears also as an exact CDV solution for the 2D model.

The analysis of the specific heat allows us to distinguish between stable and unstable branches, but it is not sufficient to select the energetically preferred configurations. To this end, we need to analyze the difference in the free energy between different configurations sharing the same temperature. We will consider LDS on different thermodynamic branches, with the same temperature, but different dilaton (and, therefore, different horizon radius). In our analysis, we will not consider the CDV solutions, but only LDS. The inclusion of the CDV will be discussed in the next subsection.

We consider the situation depicted in Fig. I.3.4, where we present a qualitative plot of the temperature $T(\phi)$ of our 2D black holes. We focus on two different configurations, ϕ_1 and ϕ_2, in the stable and unstable branches, respectively, but with the same temperature $T(\phi_1) = T(\phi_2) \equiv T$. We now evaluate the free energy difference $\Delta F_{2,1} \equiv F(\phi_2) - F(\phi_1) = \Delta E_{2,1} - T\Delta S_{2,1}$. Using Eqs. (I.3.32b) and (I.3.34), we have

$$\Delta F_{2,1} = 2\pi \int_{\phi_1}^{\phi_2} [T(\phi) - T]\, {\rm d}\phi. \tag{I.3.38}$$

From a geometric point of view, $\Delta F_{2,1}/2\pi$ represents the area limited by the graph of $T(\phi)$ (solid blue line in Fig. I.3.4) and the straight line T (dashed horizontal line in Fig. I.3.4). Since $T(\phi)$ shows a single maximum located at $\phi = \phi_{\rm peak}$ and $\phi_1 < \phi_{\rm peak} < \phi_2$, then the relation $T(\phi) > T$ holds true in the interval $[\phi_1, \phi_2]$. This implies $\Delta F_{2,1}$ to be strictly positive, i.e., $F(\phi_2) > F(\phi_1)$. Therefore, generic configurations in the stable branch are energetically preferred with respect to configurations in the stable branch. These results show that configurations in the stable branch retain the least free energy and are, thus, thermodynamically favoured.

I.3.3.3 Including the constant dilaton vacuum

So far, in our thermodynamic considerations, we have considered only the LDSs. We have already seen in Section I.3.1, however, that our dilaton gravity model allows, in its spectrum, a solution with constant dilaton describing an AdS_2 spacetime, the CDV. This solution represents a GS of the theory, with different asymptotics not only with respect to the "excited" LDS, but also to the extremal one. In fact, the LDS, including the extremal one, are metrically AF and the dilaton depends linearly on r. Conversely, the CDV describes an AdS_2 spacetime and the dilaton is identically constant. Extremal LDSs, in the near-horizon approximation, are described by an AdS_2 spacetime, endowed, however, with a linear dilaton, the so called linear dilaton vacuum (LDV) [285].

The situation described above is very common for 4D charged black holes [291], for which we have both an extremal, AF solution, described in the near-horizon approximation by AdS_2 with a linear dilaton, and an $AdS_2 \times S^2$ solution (our CDV).

Working in the context of 2D dilaton gravity, it has been shown that the AdS_2 CDV does not admit finite energy excitations, i.e., it is separated from the AdS_2 LDV by a mass gap [217]. Moreover, there is the additional difficulty that the two spacetimes have different asymptotics (linearly varying versus constant dilaton). The latter point makes it conceptually problematic to compare the free energies of the two configurations and to assess which one is thermodynamically favored. These difficulties can be circumvented, and one can show, computing the free energy, that the AdS_2 CDV is energetically preferred with respect to the AdS_2 LDV [285]. Here, we will use a similar procedure for the solutions of the 2D Hayward model and compare the free energy of the AdS_2 CDV with that of the extremal LDS.

Let us first note that we can formally consider zero mass, thermal excitations of the CDV using a Rindler-like coordinate transformation, which generates a horizon with a related temperature

$$\mathrm{d}s^2 = -\left(\frac{r^2}{L_{\mathrm{AdS}}^2} - 4\pi^2 T_{\mathrm{H}}^2 L_{\mathrm{AdS}}^2\right)\mathrm{d}t^2 + \left(\frac{r^2}{L_{\mathrm{AdS}}^2} - 4\pi^2 T_{\mathrm{H}}^2 L_{\mathrm{AdS}}^2\right)^{-1}\mathrm{d}r^2. \tag{I.3.39}$$

We can now evaluate the bulk Euclidean action of the CDV (I.3.39), considering that the dilaton is constant $\phi = \phi_{\mathrm{CDV}}$ and the potential is zero when evaluated in the CDV. We have[4]

$$\mathcal{I}_{\mathrm{b}}^{\mathrm{CDV}} = -\frac{1}{2}\int \mathrm{d}^2x\sqrt{-g}\,(-\phi_{\mathrm{CDV}} f'') = -\frac{\beta\phi_{\mathrm{CDV}}}{2}4\pi T_{\mathrm{H}} = -2\pi\phi_{\mathrm{CDV}}. \tag{I.3.40}$$

The free energy $F^{\mathrm{CDV}} = -T\ln\mathcal{Z}$ reads

$$F^{\mathrm{CDV}} = -2\pi\phi_{\mathrm{CDV}}T_{\mathrm{H}}. \tag{I.3.41}$$

We can now compute the difference in the free energy between a generic black-hole configuration of the LDS and the CDV. Using the result of Eq. (I.3.32b) for the entropy of the LDS and the equation $F = E - T_{\mathrm{H}}S$ we obtain

$$\Delta F^{\mathrm{BH-CDV}} \equiv F^{\mathrm{BH}} - F^{\mathrm{CDV}} = -\mathcal{M} - 2\pi T_{\mathrm{H}}\left(\phi_{\mathrm{H}} - \phi_{\mathrm{CDV}}\right). \tag{I.3.42}$$

Since, for every black-hole solution, $\phi_{\mathrm{H}} > \phi_{\mathrm{CDV}}$, we have $F^{\mathrm{BH}} < F^{\mathrm{CDV}}$, and thus the black-hole configuration is always thermodynamically preferred.

However, this is true whenever $T_{\mathrm{H}} \neq 0$. At $T_{\mathrm{H}} = 0$, we do not have thermal contributions to the free energy anymore and ΔF reduces to the difference of the masses contributions. On the other hand, at $T_{\mathrm{H}} = 0$ the semiclassical approximation is broken, as signalized by the generation of the mass gap (see Section I.3.4.3) [215, 217, 285], and thus we cannot rely on the euclidean action approach anymore. This does not allow to define a proper mass for the CDV, consistently with the fact that pure AdS_2 spacetime does not admit finite energy excitations. One could argue, following the argument of Ref. [285], that at $T_{\mathrm{H}} = 0$ the only contribution to $\Delta F^{\mathrm{BH-CDV}}$ comes from the mass difference, which, due the absence of finite energy excitations, should diverge, which makes the CDV energetically preferred with respect to the extremal LDV.

[4] We are implicitly considering also a renormalization contribution to the action, to renormalize the divergent contribution at infinity due to the AdS asymptotics.

I.3.4 Black-hole evaporation in the quasistatic approximation

In the following, we will describe the evaporation process of our regular 2D black hole working in the quasistatic approximation and in the semiclassical regime, in which the mass is slowly varying with time so that it can be considered almost constant for each individual evaporation step. In this way, the backreaction of the geometry due to the radiation is not taken into account in a fully dynamic way, but it is described in a very simplified, rough manner. The dynamic character of this backreaction will be, instead, fully taken into account in the next section, where we will consider the coupling of gravity to the matter fields describing Hawking radiation. We expect our quasistatic approximation to hold for black holes very far from extremality and to break down in the near-extremal regime, where the semiclassical approximation is not capable of describing the dynamics.

Since our black holes behave as black bodies with a Planckian thermal spectrum, we use the Stefan-Boltzmann (SB) law to describe the time variation of the internal energy, which in arbitrary $d+1$ dimensions reads [292]

$$\frac{\mathrm{d}E}{\mathrm{d}t} = \sigma \mathcal{A}_{d-1} T_{\mathrm{H}}^{d+1}, \qquad \sigma = \frac{d\Gamma\left(\frac{d}{2}\right)\zeta\left(d+1\right)}{2\pi^{d/2+1}}, \qquad \mathcal{A}_{d-1} = \frac{2\pi^{d/2}}{\Gamma\left(\frac{d}{2}\right)} r^{d-1}, \tag{I.3.43}$$

where σ is the SB constant, $\mathcal{A}_{d-1}$ is the $(d-1)$-dimensional emitting surface, $\Gamma(x)$ and $\zeta(s)$ are the gamma and Riemann zeta functions, respectively. In the present case, $d=1$, and thus

$$\frac{\mathrm{d}E}{\mathrm{d}t} = -\frac{\mathrm{d}\mathcal{M}}{\mathrm{d}t} = -\frac{\pi}{6} T_{\mathrm{H}}^2, \tag{I.3.44}$$

where we used the fact that $E = -\mathcal{M}$.

I.3.4.1 Evaporation time

To compute the evaporation time, we express $\mathcal{M}$ as a function of the event horizon radius and use $\mathrm{d}\mathcal{M}/\mathrm{d}t = (\mathrm{d}\mathcal{M}/\mathrm{d}r_{\mathrm{H}})(\mathrm{d}r_{\mathrm{H}}/\mathrm{d}t)$ together with Eqs. (I.3.26), (I.3.28) and (I.3.44), to obtain

$$\frac{\mathrm{d}r_{\mathrm{H}}}{\mathrm{d}t} = -\frac{1}{12\lambda} T_{\mathrm{H}}. \tag{I.3.45}$$

Inverting and integrating yields the evaporation time required to pass from an initial configuration with event horizon radius $r_{\mathrm{H},0} \gg r_{\mathrm{ext}}$ to a final one with radius $r_{\mathrm{H,final}}$

$$\Delta t = -12\lambda \int_{r_{\mathrm{H},0}}^{r_{\mathrm{H,final}}} \frac{\mathrm{d}r_{\mathrm{H}}}{T_{\mathrm{H}}}. \tag{I.3.46}$$

From this expression, it is already evident that, as $T_{\mathrm{H}} \to 0$, i.e., as we approach extremality, $\Delta t \to \infty$. In other words, reaching the extremal configuration, in the quasistatic semiclassical approximation, requires an infinite time, consistently with the thermodynamic stability analysis of the previous subsections.

For the particular model under investigation described by Eq. (I.3.19), Eq. (I.3.46) reads

$$\Delta t = -48\pi\lambda^2 \int_{r_{\mathrm{H},0}}^{r_{\mathrm{H,\,final}}} \mathrm{d}r_{\mathrm{H}} \frac{(r_{\mathrm{H}}^3+\ell^3)^2}{r_{\mathrm{H}}^4 - 2\ell^3 r_{\mathrm{H}}} = -8\pi\lambda^2 \left[2r_{\mathrm{H}}^3 - 3\ell^3 \ln r_{\mathrm{H}} + 9\ell^3 \ln\left(r_{\mathrm{H}}^3 - 2\ell^3\right)\right]_{r_{\mathrm{H},0}}^{r_{\mathrm{H,\,final}}}. \tag{I.3.47}$$

In the extremal limit $r_{\mathrm{H,\,final}} \to \sqrt[3]{2}\ell = r_{\mathrm{ext}}$ we have a logarithmic divergence, as expected. This is consistent with the behavior of 4D regular models (see [5, 202, 293] and references therein).

I.3.4.2 Time variation of mass and entropy

Let us now compute how the mass of our 2D Hayward black hole evolves in time due to the emission of Hawking radiation, according to the SB law (I.3.44). This can be done by first inverting r_{H} and T_{H}, to express them as functions of $\mathcal{M}$ and then by numerically solving Eq. (I.3.44) written

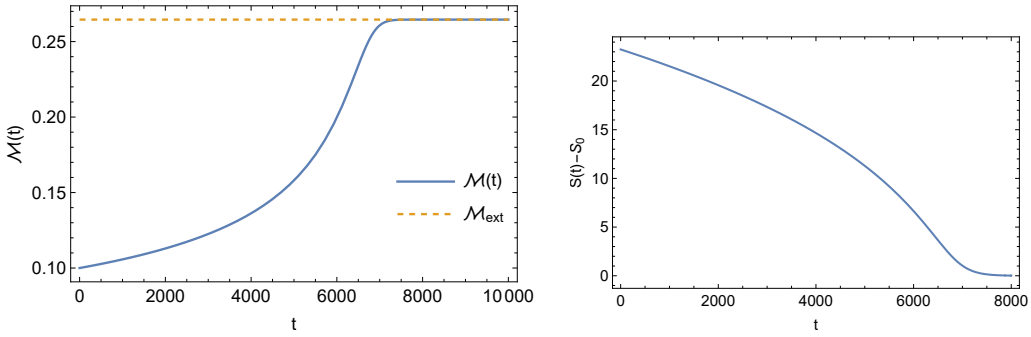

(a) (b)

Figure I.3.5: **Panel (a)**: Numerical solution of Eq. (I.3.44) (blue solid line), which shows the time evolution of the mass of an evaporating black hole as a function of time, in the quasistatic approximation. We see that at large times, the numerical solution asymptotes the extremal mass (orange dashed line). For the numerical integration, we set $\mathcal{M}(t=0)=0.1\lambda$ as an initial condition. **Panel (b)**: Time variation of the entropy of the black hole according to Eq. (I.3.33). At late times, the entropy goes to zero, after subtracting the topological term S_0. In both figures, we set $\lambda=\ell=1$.

in the form $\mathrm{d}\mathcal{M}/\mathrm{d}t=\pi T_{\rm H}^2(\mathcal{M})/6$. As a boundary condition, we impose $\mathcal{M}(t=0)=0.1\lambda$. We also set $\lambda=\ell=1$. Using the expression for $r_{\rm H}$ as a function of the mass obtained by inverting Eq. (I.3.28), for $\mathcal{M}=0.1$, we have $r_{\rm H}\simeq 4.96$, which is about twice as large as that pertaining to the temperature peak (I.3.27) ($r_{\rm H,\,peak}\simeq 1.9$ with $\ell=1$), which confirms that the initial state belongs to the unstable branch. We have also checked that the final results are independent of the value of the initial mass.

The result of the numerical integration is shown in Fig. I.3.5a. We see that, at large times, the mass asymptotes the extremal one. The mass increases during the evaporation due to the negative normalization of the Killing vector generating time translations. Indeed, the internal energy $E=-\mathcal{M}$ is decreasing, as it should be during the evaporation.

We can also derive the time evolution of the black-hole entropy. This can be done by simply combining the solution of Eq. (I.3.44) together with the function $r_{\rm H}(\mathcal{M})$ (obtained by inverting Eq. (I.3.28)) and Eq. (I.3.33). The result is reported in Fig. I.3.5b and confirms the fact that, as the solution asymptotes the extremal one, the entropy reduces to zero. This is true only if we subtract the contribution S_0 of Eq. (I.3.33).

These results will be extended in Section I.3.6, where we will go beyond the quasistatic approximation and we will consider the full dynamics of the backreaction of Hawking radiation on the background geometry. We will show that the inclusion of the latter causes the evaporation process to take place in a *finite* time.

I.3.4.3 Approaching extremality and breakdown of the semiclassical approximation

The divergence of the evaporation time for black holes approaching extremality, found in the previous section, signalizes the breakdown of the semiclassical approximation. Let us now study in details how an excited configuration approaches the extremal limit, by solving Eq. (I.3.45) at leading order around extremality, i.e., around $r_{\rm H}\sim\sqrt[3]{2}\ell$.

Near extremality, at leading order, the temperature varies linearly with $r_{\rm H}$,

$$T_{\rm H}\simeq\frac{r_{\rm H}-\sqrt[3]{2}\ell}{6\pi\lambda\ell^3}+\mathcal{O}\left[\left(r_{\rm H}-\sqrt[3]{2}\ell\right)^2\right], \tag{I.3.48}$$

which gives, after solving Eq. (I.3.45), the time-dependence of $r_{\rm H}$

$$r_{\rm H}(t)\simeq\sqrt[3]{2}\ell+\alpha_1 e^{-\frac{t}{72\pi\lambda^2\ell^3}}, \tag{I.3.49}$$

where α_1 is an integration constant.

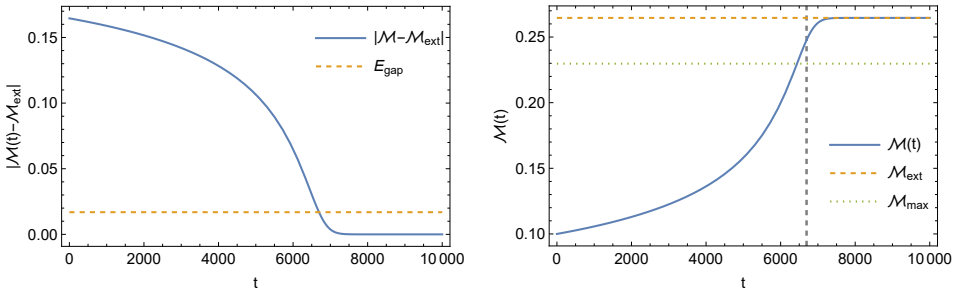

(a) (b)

Figure I.3.6: **Panel (a)**: Plot of ΔE as a function of time (solid blue line). The horizontal dashed orange line corresponds to the value of the mass gap (I.3.52). The intersection point between the two curves gives the time when the semiclassical approximation breaks down. **Panel (b)**: Mass evolution in time (solid blue line). The horizontal dashed orange line corresponds to the value of the mass of the extremal configuration. The horizontal dotted green line corresponds to the value of the mass at the temperature peak (I.3.27). The vertical dashed line, instead, signals the instant of time where $|\mathcal{M}-\mathcal{M}_{\rm ext}| \sim E_{\rm gap}$, with $E_{\rm gap}$ given by Eq. (I.3.52). As can be seen, the breakdown of the semiclassical approximation happens after the evaporation process reaches the temperature peak. For both figures, we set $\mathcal{M}(t=0)=0.1\lambda$ and $\ell=\lambda=1$.

Moreover, $\mathcal{M}(t)$ behaves, near extremality, as

$$\mathcal{M} \simeq \frac{\left(\sqrt[3]{2}\ell + \alpha_1 e^{-\frac{t}{72\pi\lambda^2\ell^3}}\right)^2}{2\left[\ell^3 + \left(\sqrt[3]{2}\ell + \alpha_1 e^{-\frac{t}{72\pi\lambda^2\ell^3}}\right)^3\right]}, \tag{I.3.50}$$

which reduces to $\frac{1}{3\sqrt[3]{2}\ell} = \mathcal{M}_{\rm ext}$ only for $t \to \infty$, confirming the numerical results of the previous subsection. The entropy, instead, approaches exponentially that of the extremal configuration at $t \to \infty$, according to Eq. (I.3.49).

However, one must question the validity of the semiclassical approximation near extremality. The latter breaks down when the energy of Hawking quanta, which is of order $T_{\rm H}$, becomes comparable with the energy of the black-hole energy above extremality $\Delta E = |\mathcal{M}-\mathcal{M}_{\rm ext}|$ (see, e.g., Ref. [215]). The energy scale at which this breakdown occurs determines the mass gap separating the CDV from the continuous part of the spectrum (the LDS) [215, 217].

This mass gap can be determined by expanding Eq. (I.3.28) near extremality, which yields

$$\Delta E \simeq \frac{\left(r_{\rm H} - \sqrt[3]{2}\ell\right)^2}{6\ell^3} = 6\pi^2\lambda^2\ell^3 T_{\rm H}^2. \tag{I.3.51}$$

From $\Delta E \simeq T_{\rm H}$, we easily find the energy gap

$$E_{\rm gap} \simeq \frac{1}{6\pi^2\ell^3\lambda^2}. \tag{I.3.52}$$

This result is consistent with those obtained for 4D black holes with two horizons merging into a single one, in particular for charged black holes. For instance, in the Reissner-Nordström case, the energy gap behaves as $E_{\rm gap} \propto Q^{-3}$, where Q is the black-hole charge [215]. As one can expect, here the role of Q is played by ℓ.[5] Fig. I.3.6a shows the time variation of $\Delta E = |\mathcal{M}-\mathcal{M}_{\rm ext}|$: the intersection with the horizontal dashed line, corresponding to $\Delta E \sim E_{\rm gap}$, identifies the time at which the semiclassical approximation breaks down.

It is interesting to notice that the limit of validity of the semiclassical approximation sets also the limit of validity of the quasistatic one, which cannot be valid when the former is broken. In fact, the quasistatic approximation is valid in the initial stages, when the black hole is macroscopic,

[5] An important difference is that, contrary to Q, ℓ is not related to any conserved quantity at infinity and thus it is not associated to any thermodynamic potential.

which essentially evaporates as a GR one. It remains also valid for most of the evaporation process because the evaporation time is much larger than the typical black-hole time scale $1/\Delta E$ (see also, e.g., Refs. [192, 202]). Only at extremality, when ΔE goes to zero, the two time scales become comparable.

Moreover, it should be considered that the time at which the semiclassical approximation breaks down (which can be read from Fig. I.3.6a) is close to the time at which the evaporation process reaches the maximum of the temperature (I.3.27), where we expect the system to go through a second order phase transition (see Fig. I.3.6b).

I.3.5 Coupling to conformal matter

In the previous section, we described the black-hole evaporation process in the semiclassical and quasistatic approximations. Within these approximations, the backreaction effects of the geometry on the presence of Hawking radiation is completely encoded in the change in time of the black-hole mass $\mathcal{M}$. As we have seen above, this may be a good approximation in the early stages of the evaporation, but it is expected to fail at later times. Another shortcoming of the approximation is that the backreaction is not fully dynamic, since it does not involve the full metric solution. Its role is simply encoded in the variation of the black-hole mass.

In this section, we will give an exact semiclassical description of the evaporation process by studying the coupling of our 2D model to quantum conformal matter, in the form of N massless scalar fields. This coupling is most easily analyzed in the conformal gauge, where the 2D metric reads

$$\mathrm{d}s^2 = -e^{2\rho(x^+,x^-)}\mathrm{d}x^+\mathrm{d}x^-, \tag{I.3.53}$$

where $e^{2\rho}$ is the conformal factor of the metric. The transition from the metric in the Schwarzschild gauge (I.3.7) to that in the form Eq. (I.3.53) is realized by using the coordinates, $x^\pm = t \pm r_*$, where $r_* \equiv \int \mathrm{d}r/f$ is the tortoise coordinate. The system of coordinates $x^\pm$ does not cover the interior of the black hole, but only the region outside the outer horizon. Indeed, $x^+ - x^- \to -\infty$ corresponds to the horizon ($x^+ \to -\infty$ gives the past horizon, while $x^- \to \infty$ future horizon), while $x^+ - x^- \to \infty$ corresponds to asymptotic infinity.

The field equations stemming from Eq. (I.3.4) are now

$$8e^{-2\rho}\partial_+\partial_-\rho = -\frac{\mathrm{d}\mathcal{V}}{\mathrm{d}\phi}, \tag{I.3.54a}$$

$$\partial_+^2\phi - 2\partial_+\rho\partial_+\phi = 0, \tag{I.3.54b}$$

$$\partial_-^2\phi - 2\partial_-\rho\partial_-\phi = 0, \tag{I.3.54c}$$

$$\partial_+\partial_-\phi + \frac{\mathcal{V}}{4}e^{2\rho} = 0. \tag{I.3.54d}$$

The solution reads

$$e^{2\rho} = f = \frac{2\mathcal{M}}{\lambda} + \frac{1}{\lambda^2}\int^\phi \mathrm{d}\psi\mathcal{V} \equiv \frac{2\mathcal{M}}{\lambda} + \mathcal{J} \tag{I.3.55a}$$

$$\int^\phi \frac{\mathrm{d}\psi}{e^{2\rho}} = \int^\phi \frac{\mathrm{d}\psi}{\frac{2\mathcal{M}}{\lambda} + \mathcal{J}} = \lambda r_* = \frac{\lambda}{2}\left(x^+ - x^-\right), \tag{I.3.55b}$$

where we defined $\mathcal{J} = \lambda^{-2}\int^\phi \mathrm{d}\psi\mathcal{V}(\psi)$.

I.3.5.1 Coupling to matter: shock wave solution

We now couple 2D dilaton gravity to the N massless scalar fields describing conformal matter. The full action reads

$$\mathcal{S} = \frac{1}{2}\int \mathrm{d}^2x\sqrt{-g}\left[\phi R + \mathcal{V} - \frac{1}{2}\sum_{i=1}^{N}\left(\nabla f_i\right)^2\right]. \tag{I.3.56}$$

The stress-energy tensor of matter fields is given by

$$T_{\mu\nu} = -\frac{1}{4} g_{\mu\nu} \sum_{i=1}^{N} g^{\rho\sigma} \partial_\rho f_i \partial_\sigma f_i + \frac{1}{2} \sum_{i=1}^{N} \partial_\mu f_i \partial_\nu f_i. \tag{I.3.57}$$

The field equations (I.3.54) now become

$$8e^{-2\rho} \partial_+ \partial_- \rho = -\frac{\mathrm{d}\mathcal{V}}{\mathrm{d}\phi}, \tag{I.3.58a}$$

$$\partial_+^2 \phi - 2\partial_+ \rho \partial_+ \phi = -T_{++} = -\frac{1}{2} \sum_{i=1}^{N} \partial_+ f_i \partial_+ f_i, \tag{I.3.58b}$$

$$\partial_-^2 \phi - 2\partial_- \rho \partial_- \phi = -T_{--} = -\frac{1}{2} \sum_{i=1}^{N} \partial_- f_i \partial_- f_i, \tag{I.3.58c}$$

$$\partial_+ \partial_- \phi + \frac{\mathcal{V}}{4} e^{2\rho} = 0, \tag{I.3.58d}$$

$$\partial_+ \partial_- f_i = 0. \tag{I.3.58e}$$

Notice that Eq. (I.3.58e) can be readily solved and implies $f_i = f_{i,+}(x^+) + f_{i,-}(x^-)$. The matter-coupled field equations above admit an exact solution if we consider an ingoing shock wave starting at $x^+ = x_0^+$ and propagating in the x^- direction, while no energy flux is present in the x^+ direction

$$T_{++} = -\mathcal{M}\delta\left(x^+ - x_0^+\right) = \frac{1}{2} \sum_{i=1}^{N} \partial_+ f_i \partial_+ f_i, \qquad T_{--} = 0. \tag{I.3.59}$$

The minus sign in T_{++} is again due to the normalization of the Killing vector of the metric.

From Birkhoff's theorem, we can write the full solution by patching, on the infall line $x^+ = x_0^+$, the vacuum solution together with the one after the shock wave [279].

$\boldsymbol{x^+ \leq x_0^+}$—At the end of Section I.3.3.1, we showed that, in the linear dilaton case, the GS of the theory, i.e., the state retaining the least internal energy, is the extremal black-hole configuration, characterized by a mass $\mathcal{M}_{\text{ext}}$ given by Eq. (I.3.25).

The vacuum solution (before the shock wave) therefore is equivalent to Eqs. (I.3.55) with $\mathcal{M} = \mathcal{M}_{\text{ext}}$

$$e^{2\rho} = \frac{2\mathcal{M}_{\text{ext}}}{\lambda} + \mathcal{J}, \qquad \int^{\phi} \frac{\mathrm{d}\psi}{\frac{2\mathcal{M}_{\text{ext}}}{\lambda} + \mathcal{J}} = \frac{\lambda}{2}\left(x^+ - x^-\right). \tag{I.3.60}$$

$\boldsymbol{x \geq x_0^+}$—Since $T_{--} = 0$, now the solution is (see Ref. [279])

$$e^{2\rho} = \left(\frac{2\mathcal{M}}{\lambda} + \mathcal{J}\right) F'(x^-), \tag{I.3.61}$$

$$\int^{\phi} \frac{\mathrm{d}\psi}{\mathcal{J} + \frac{2\mathcal{M}}{\lambda}} = \frac{\lambda}{2}\left[x^+ - x_0^+ - F(x^-)\right], \tag{I.3.62}$$

$$F'(x^-) \equiv \frac{\mathrm{d}F(x^-)}{\mathrm{d}x^-} = \frac{\mathcal{J}_0 + \frac{2\mathcal{M}_{\text{ext}}}{\lambda}}{\mathcal{J}_0 + \frac{2\mathcal{M}}{\lambda}}, \tag{I.3.63}$$

where $\mathcal{J}_0 \equiv \mathcal{J}|_{x^+ = x_0^+}$ and $F(x^-)$ is a function needed to map the old coordinate x^- of the observer in the GS solution into a new coordinate, which pertains to an observer in the excited solution. Its form is fixed by requiring continuity of the metric function across the shock wave at $x^+ = x_0^+$. This defines the function up to an integration constant, which is fixed by requiring the continuity of the dilaton across the shock wave.

As usual, and as we will see in more detail in Section I.3.6.2, the function $F(x^-)$ generates the Hawking flux of particles, which can be described in terms of the change of the coordinate

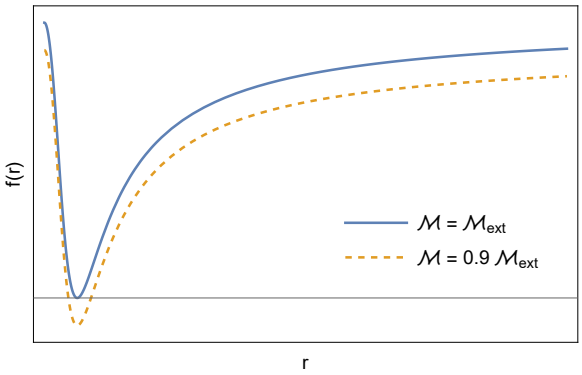

Figure I.3.7: Metric functions for different values of the black-hole mass $\mathcal{M}$. The blue solid line refers to the extremal configuration with $\mathcal{M} = \mathcal{M}_{\rm ext}$. The orange dashed line, instead, refers to an excited state (after the shock wave) with $\mathcal{M} = 0.9\mathcal{M}_{\rm ext}$, which presents two event horizons.

x^- defined by F. In fact, in 2D, the flux of Hawking particles can be described in terms of the Schwarzian derivative of the function $F(x^-)$ (see, e.g., Refs. [279, 294]).

Due to the sign of the shock wave (I.3.59) and to the minus sign in Eq. (I.3.28), the mass $\mathcal{M}$ of the excited states is *less* than the extremal mass, as the shock wave increases the internal energy of the system. The physical picture we expect is therefore the following (see also Fig. I.3.7). The shock wave increases the internal energy of the initial system, i.e., the GS, extremal configuration: the degenerate horizon splits into two apparent horizons. According to the thermodynamic analysis and the results of Section I.3.4.2, we then expect that, when dynamically evolving the system, these two horizons will meet again at the end of evaporation, and merge to give again the extremal configuration. We will confirm this in the next section by keeping into account the dynamic contributions of backreaction effects of the radiation on the geometry and dynamically describing the evaporation process by numerically integrating the field equations.

I.3.6 Black hole evaporation and backreaction

The evaporation and its backreaction effects on the spacetime geometry, are studied by quantizing the conformal matter on the curved 2D background. An important consequence of the curvature of the spacetime is that the otherwise classically traceless stress-energy tensor acquires a nonzero trace, proportional to the Ricci scalar, which is the so-called conformal anomaly [295]

$$\langle T^\mu_\mu \rangle = \frac{N}{24} R, \tag{I.3.64}$$

where N is the number of matter fields. This can be accounted for by adding, to the classical action, the nonlocal Polyakov term

$$\mathcal{S}_{\rm Pol} = -\frac{N}{96} \int \mathrm{d}^2x \sqrt{-g} R \Box^{-1} R, \tag{I.3.65}$$

where $\Box^{-1}$ is the scalar Green function.

Using Eq. (I.3.64), we can derive the expectation value of T_{+-}, which in the conformal gauge is entirely local

$$\langle T_{+-} \rangle = -\frac{N}{12} \partial_+ \partial_- \rho. \tag{I.3.66}$$

The nonlocal effects stemming from the action (I.3.65) are, instead, encoded in the other components of the stress-energy tensor $\langle T_{\pm\pm} \rangle$, which can be obtained from covariant conservation of the latter

$$\langle T_{--} \rangle = -\frac{N}{12} \left[\partial_- \rho \partial_- \rho - \partial_-^2 \rho + t_-(x^-) \right], \tag{I.3.67a}$$

$$\langle T_{++} \rangle = -\frac{N}{12} \left[\partial_+ \rho \partial_+ \rho - \partial_+^2 \rho + t_+(x^+) \right]. \tag{I.3.67b}$$

Here, $t_\pm(x^\pm)$ are integration functions, which depend on the boundary conditions and therefore encode the nonlocal effects of the Polyakov action (I.3.65). These functions are also sensitive to the choice of the coordinates. Indeed, under a conformal transformation of the coordinates $x^\pm \to y^\pm(x^\pm)$, the conformal factor transforms as

$$\rho(y^+, y^-) = \rho(x^+, x^-) - \frac{1}{2}\ln\frac{\mathrm{d}y^+}{\mathrm{d}x^+}\frac{\mathrm{d}y^-}{\mathrm{d}x^-}, \tag{I.3.68}$$

which, plugged into Eqs. (I.3.66), (I.3.67a) and (I.3.67b), yields the anomalous transformation of the stress-energy tensor with the Schwarzian derivative

$$\left(\frac{\mathrm{d}y^\pm}{\mathrm{d}x^\pm}\right)^2 T_{\pm\pm}(y^\pm) = T_{\pm\pm}(x^\pm) - \frac{N}{12}\left\{y^\pm, x^\pm\right\}, \qquad \{y, x\} = \frac{y'''}{y'} - \frac{3}{2}\frac{y''^2}{y'^2}, \tag{I.3.69}$$

where the prime indicates a derivative with respect to x. The form of the stress-energy tensor in the new coordinate system is preserved if the $t_\pm$'s trasform as

$$\left(\frac{\mathrm{d}y^\pm}{\mathrm{d}x^\pm}\right)^2 t_\pm(y^\pm) = t_\pm(x^\pm) + \left\{y^\pm, x^\pm\right\}. \tag{I.3.70}$$

Including the conformal anomaly, the field equations (I.3.58) become

$$8e^{-2\rho}\partial_+\partial_-\rho = -\frac{\mathrm{d}\mathcal{V}}{\mathrm{d}\phi}, \tag{I.3.71a}$$

$$\partial_+^2\phi - 2\partial_+\rho\partial_+\phi = \mathcal{M}\delta\left(x^+ - x_0^+\right) + \frac{N}{12}\left[\left(\partial_+\rho\right)^2 - \partial_+^2\rho + t_+(x^+)\right], \tag{I.3.71b}$$

$$\partial_-^2\phi - 2\partial_-\rho\partial_-\phi = \frac{N}{12}\left[\left(\partial_-\rho\right)^2 - \partial_-^2\rho + t_-(x^-)\right], \tag{I.3.71c}$$

$$\partial_+\partial_-\phi + \frac{\mathcal{V}}{4}e^{2\rho} = -\frac{N}{12}\partial_+\partial_-\rho, \tag{I.3.71d}$$

$$f_i = f_{i,+}(x^+) + f_{i,-}(x^-). \tag{I.3.71e}$$

Eqs. (I.3.71) can be solved once suitable initial conditions to fix the functions $t_\pm(x^\pm)$ are imposed. These can be determined assuming the GS as the initial state. In conventional AF models, like the CGHS one [271], the GS is pure Minkowski spacetime. One can therefore define a global coordinate transformation in which the conformal metric (I.3.53) is manifestly flat, i.e., we can define a system of coordinates in which $e^{2\rho} = \text{constant} = 1$. One can then assume that there is no incoming radiation (except from the classical shock wave) and that there is no net outcoming flux, so that

$$\langle T_{\mu\nu}\rangle_{\mathrm{GS}} = 0 \tag{I.3.72}$$

identically, which implies $t_\pm = 0$ on the GS in this system of coordinates. One can then transform back to the original coordinates and exploit the anomalous transformation (I.3.70) to obtain their final form in the new coordinates.

In the case under consideration, however, we saw that the GS does not correspond to Minkowski spacetime (which is only reached asymptotically), but it is given by the extremal configuration (I.3.60). This, of course, prevents from defining a global coordinate transformation which brings $e^{2\rho} \to$ constant. Despite this difficulty, we can still use Eq. (I.3.72) as a boundary condition, similarly to the CGHS model.

Once the boundary conditions on the GS have been imposed, the solution before the shock wave ($x^+ < x_0^+$) is Eq. (I.3.60), the vacuum one, while after the shock wave ($x^+ > x_0^+$) it is given by an evaporating black-hole solution.

I.3.6.1 Adding counterterms and fixing the boundary conditions

In order to preserve the physically motivated boundary condition (I.3.72), we can follow Refs. [279, 282] and modify the usual Polyakov action (I.3.65) by adding the most general local covariant counterterms with no second order derivatives

$$\mathcal{S}_{\mathrm{Pol}} = -\frac{N}{96}\int \mathrm{d}^2x\sqrt{-g}\left[R\Box^{-1}R - 4\mathcal{A}(\phi)R + 4\mathcal{B}(\phi)\left(\nabla\phi\right)^2\right], \tag{I.3.73}$$

where $\mathcal{A}$ and $\mathcal{B}$ are functions of the scalar field. The presence of these new terms, of course, does not alter the classical limit $N \to 0$. Also notice that the addition of new counterterms was already employed in, e.g., the CGHS model, in order to make the theory exactly solvable [296, 297].

In Ref. [279], the addition of the counterterms was necessary to prevent $\langle T_{\mu\nu}\rangle_{\rm GS}$ from diverging for $\phi \to \infty$. In the present case, it can be shown that divergences are absent due to the peculiar properties of the potential outlined in Section I.3.1.3 (see Appendix I.C). Nevertheless, adding counterterms is needed to implement the boundary condition (I.3.72) in a consistent way. With the new terms, the components of the stress-energy tensor (I.3.66), (I.3.67a) and (I.3.67b) become

$$\langle T_{+-}\rangle = -\frac{N}{12}\left(\partial_+\partial_-\rho + \partial_+\partial_-\mathcal{A}\right), \tag{I.3.74a}$$

$$\langle T_{\pm\pm}\rangle = -\frac{N}{12}\left[\partial_\pm\rho\partial_\pm\rho - \partial_\pm^2\rho + 2\partial_\pm\rho\partial_\pm\mathcal{A} - \partial_\pm^2\mathcal{A} - \mathcal{B}\partial_\pm\phi\partial_\pm\phi + t_\pm(x^\pm)\right]. \tag{I.3.74b}$$

We now impose the boundary condition (I.3.72). Requiring $t_\pm(x^\pm) = 0$ on the GS completely fixes the two functions $\mathcal{A}$ and $\mathcal{B}$ (see also Ref. [279])

$$\mathcal{A}(\phi) = -\frac{1}{2}\ln\left(\frac{2\mathcal{M}_{\rm ext}}{\lambda} + \mathcal{J}_{\rm GS}\right) = -\rho_{\rm GS}, \tag{I.3.75a}$$

$$\mathcal{B}(\phi) = -\left(\partial_\phi\rho_{\rm GS}\right)^2 = -\frac{1}{4\left(\frac{2\mathcal{M}_{\rm ext}}{\lambda} + \mathcal{J}_{\rm GS}\right)^2}\left(\frac{d\mathcal{J}_{\rm GS}}{d\phi}\right)^2, \tag{I.3.75b}$$

where the subscript GS indicates that $\mathcal{J}$ is computed at extremality.

Eqs. (I.3.74a) and (I.3.74b) now read

$$\langle T_{+-}\rangle = -\frac{N}{12}\left(\partial_+\partial_-\rho - \frac{\partial_+\partial_-\mathcal{J}_{\rm GS}}{2\left(\frac{2\mathcal{M}_{\rm ext}}{\lambda} + \mathcal{J}_{\rm GS}\right)} + \frac{\partial_-\mathcal{J}_{\rm GS}\partial_+\mathcal{J}_{\rm GS}}{2\left(\frac{2\mathcal{M}_{\rm ext}}{\lambda} + \mathcal{J}_{\rm GS}\right)^2}\right), \tag{I.3.76}$$

$$\langle T_{\pm\pm}\rangle = -\frac{N}{12}\left[\partial_\pm\rho\partial_\pm\rho - \partial_\pm^2\rho - \frac{\partial_\pm\rho\partial_\pm\mathcal{J}_{\rm GS}}{\frac{2\mathcal{M}_{\rm ext}}{\lambda} + \mathcal{J}_{\rm GS}} + \frac{\partial_\pm^2\mathcal{J}_{\rm GS}}{2\left(\frac{2\mathcal{M}_{\rm ext}}{\lambda} + \mathcal{J}_{\rm GS}\right)} + \right. \tag{I.3.77}$$

$$\left. - \frac{\partial_\pm\mathcal{J}_{\rm GS}\partial_\pm\mathcal{J}_{\rm GS}}{2\left(\frac{2\mathcal{M}_{\rm ext}}{\lambda} + \mathcal{J}_{\rm GS}\right)^2} + \frac{\partial_\pm\phi_{\rm GS}\partial_\pm\phi_{\rm GS}}{4\left(\frac{2\mathcal{M}_{\rm ext}}{\lambda} + \mathcal{J}_{\rm GS}\right)^2}\left(\frac{d\mathcal{J}_{\rm GS}}{d\phi}\right)^2\right]. \tag{I.3.78}$$

Since the scalar field is a function of x^+ and x^-, while we are treating $\mathcal{J}$ as a function of ϕ, it is convenient to rewrite all derivatives of $\mathcal{J}$ with respect to the coordinates as derivatives with respect to ϕ (to lighten the notation, we indicate derivation with respect to ϕ with a subscript $_{,\phi}$). With the new components of the stress-energy tensor (I.3.76) and also using Eq. (I.3.60), the field equations (I.3.71) become

$$8e^{-2\rho}\partial_+\partial_-\rho = -\mathcal{V}_{,\phi}, \tag{I.3.79a}$$

$$\partial_+^2\phi - 2\partial_+\rho\partial_+\phi = \mathcal{M}\delta\left(x^+ - x_0^+\right) + \frac{N}{12}\left[\partial_+\rho\partial_+\rho - \partial_+^2\rho - \frac{\lambda}{2}\partial_+\rho\mathcal{J}_{{\rm GS},\phi} + \right.$$
$$\left. + \frac{\lambda^2}{8}\left(\frac{2\mathcal{M}_{\rm ext}}{\lambda} + \mathcal{J}_{\rm GS}\right)\mathcal{J}_{{\rm GS},\phi\phi} + \frac{\lambda^2}{16}\left(\mathcal{J}_{{\rm GS},\phi}\right)^2\right], \tag{I.3.79b}$$

$$\partial_-^2\phi - 2\partial_-\rho\partial_-\phi = \frac{N}{12}\left[\partial_-\rho\partial_-\rho - \partial_-^2\rho + \frac{\lambda}{2}\partial_-\rho\mathcal{J}_{{\rm GS},\phi} + \frac{\lambda^2}{8}\left(\frac{2\mathcal{M}_{\rm ext}}{\lambda} + \mathcal{J}_{\rm GS}\right)\mathcal{J}_{{\rm GS},\phi\phi} + \frac{\lambda^2}{16}\left(\mathcal{J}_{{\rm GS},\phi}\right)^2\right], \tag{I.3.79c}$$

$$\partial_+\partial_-\phi + \frac{\mathcal{V}}{4}e^{2\rho} = -\frac{N}{12}\left[\partial_+\partial_-\rho + \frac{\lambda^2}{8}\left(\frac{2\mathcal{M}_{\rm ext}}{\lambda} + \mathcal{J}_{\rm GS}\right)\mathcal{J}_{{\rm GS},\phi\phi}\right]. \tag{I.3.79d}$$

I.3.6.2 Hawking flux and apparent horizon trajectory

We now derive the asymptotic form of the Hawking flux in our model. This can be done by studying the behavior of $\langle T_{\mu\nu}\rangle$ at future null infinity $x^+ \to \infty$. In this region, we are considering

$\phi \to \infty$. We are, therefore, in the decoupling regime, where the gravitational coupling is weak, so that the effects of backreaction can be approximately neglected. This means that the solution in the region of interest ($x^+ > x_0^+$) corresponds to the classical one (I.3.63). In this limit, $\mathcal{J} \to 0$, $\mathcal{J}_{,\phi} \to 0$ and $\mathcal{J}_{,\phi\phi} \to 0$. We have thus

$$\langle T_{+-} \rangle \to 0, \tag{I.3.80a}$$

$$\langle T_{++} \rangle \to 0, \tag{I.3.80b}$$

$$\langle T_{--} \rangle \to \frac{N}{24} \left\{ F, x^- \right\}, \qquad \left\{ F, x^- \right\} = \frac{F'''}{F'} - \frac{3}{2} \left(\frac{F''}{F'} \right)^2, \tag{I.3.80c}$$

where now $'$ indicates differentiation with respect to x^-. This result agrees with that of Ref. [279], as it is naturally expected. As it is noted there, this expression diverges once the (outer) event horizon is reached, due to the choice of coordinates adopted. One way to solve this problem is to redefine the x^- coordinate as $\hat{x}^- \equiv F(x^-)$ and exploit the anomalous transformation (I.3.69). This leads to a well-behaved expression at the horizon, which reads

$$\langle \hat{T}_{--} \rangle = \frac{N}{24} \frac{\{F, x^-\}}{F'^2}. \tag{I.3.81}$$

Using the form of F given by Eq. (I.3.63), we obtain, approaching the horizon

$$\langle \hat{T}_{--} \rangle = \frac{N}{192} \left[\mathcal{V}(\phi_{\rm H}) \right]^2 \propto T_{\rm H}^2. \tag{I.3.82}$$

The proportionality relation is the same as the SB law (I.3.44), which confirms the Planckian nature of the emitted spectrum. Here, however, the flux is modified with respect to standard singular models due to the specific form of the potential (I.3.17).

Since the outgoing flux of Hawking radiation is positive, we expect the (outer) apparent event horizon to recede. To see this, we closely follow the approach adopted in Ref. [298]. The apparent horizon trajectory $\hat{x}^- = \hat{x}^-(x^+)$ can be derived using the definition of apparent horizon, which satisfies $\partial_+ \phi = 0$. This implies

$$0 = \frac{\mathrm{d}}{\mathrm{d}x^+} \partial_+ \phi \Big|_{x^- = \hat{x}^-} = \partial_+^2 \phi + \left(\frac{\mathrm{d}\hat{x}^-}{\mathrm{d}x^+} \right) \partial_+ \partial_- \phi, \tag{I.3.83}$$

from which follows

$$\partial_+ \partial_- \phi = -\partial_+^2 \phi \left(\frac{\mathrm{d}\hat{x}^-}{\mathrm{d}x^+} \right)^{-1}. \tag{I.3.84}$$

Combining Eqs. (I.3.79a), (I.3.79b) and (I.3.79d) into the above yields

$$\frac{\mathrm{d}\hat{x}^-}{\mathrm{d}x^+} = \frac{N}{12} \frac{\partial_+ \rho \partial_+ \rho - \partial_+^2 \rho - \frac{\partial_+ \rho}{2\lambda} \mathcal{V}_{\rm GS} + \frac{e^{2\rho_{\rm ext}}}{8} \mathcal{V}_{{\rm GS},\phi} + \frac{\mathcal{V}_{\rm GS}^2}{16\lambda^2}}{\frac{\mathcal{V}}{4} e^{2\rho} + \frac{N}{96} \left(e^{2\rho_{\rm ext}} \mathcal{V}_{{\rm GS},\phi} - e^{2\rho} \mathcal{V}_{,\phi} \right)}. \tag{I.3.85}$$

The qualitative behavior of the trajectory of the apparent horizon is determined by the sign of the right hand side of the expression above. In order to assess the latter, we would need the full solution of Eqs. (I.3.79a) and (I.3.79d), which however can only be solved numerically. This will be done in the next section. Here, as a first test, we exploit the fact that the full solution of the field equations approaches the classical one in the asymptotic region $\phi \to \infty$, where the coupling with matter fields and backreaction effects become negligible. In this region, the solution is then given by Eq. (I.3.63). Using this solution into Eq. (I.3.85), it can be shown that $\mathrm{d}\hat{x}^-/\mathrm{d}x^+$ is indeed positive. This implies a receding outer apparent horizon, as expected. Moreover, it confirms the qualitative picture we expect from evaporation, outlined in Section I.3.4 and at the end of Section I.3.5.1: the outer horizon recedes and approaches the horizon of the extremal GS.

Notice that, due to the limitations caused by the adopted system of coordinates, we are able to describe the behavior of the outer horizon only.

I.3.6.3 Numerical results

We now numerically solve the equations of motion given in Eqs. (I.3.79). This will allow us to capture the full dynamics of the evaporation process, keeping into account also backreaction effects. A numerical study of evaporating 2D models was performed in the past for the CGHS [299–301] and other (singular or regular) 2D models [278, 302].

To numerically integrate the equations of motion, we construct a spacetime lattice by means of a grid of null lines and we impose two different sets of boundary conditions, one along x^+ and one along x^-:

- At the shock wave, i.e., at $x^+ = x_0^+$, we require the solution to coincide with the GS, given by Eq. (I.3.60);
- Above the shock wave, along $\mathcal{I}^-$, i.e., at $x^- \to -\infty$, where backreaction effects are expected to be negligible, we require the solution to match Eq. (I.3.63), the classical one. Of course, we cannot numerically set a condition at infinity, so we choose a reasonably large negative value. Here we set $x_\infty^- = -220$. This value is found to be the minimal one for which the numerical solution coincides, in the classical limit $N \to 0$, with Eq. (I.3.63), for every value of x^+ and x^-, within a reasonably small numerical error. For values of x_∞^- greater than -220, the numerical solution deviates from the expected analytical one, while for smaller values the results are the same as the one obtained with $x_\infty^- = -220$, but with a much higher integration time.

Both the boundary conditions at $x^+ = x_0^+$ and at $x^- \to -\infty$ are given in implicit form. We therefore first need to integrate and invert the corresponding expressions (the details of this computation are reported in Appendix I.D).

To numerically integrate the field equations, we also need to select an appropriate integration interval along x^+, from the shock wave at x_0^+ up to a maximum value x^+_{max}. We chose the interval $x^+ \in [x_0^+, 5]$ (where we set $x_0^+ = 1$). We expect the general results to hold also for larger values of x^+_{max}. We chose it equal to 5 to have a reasonable integration time interval. For larger values of x^+_{max}, the time required to complete a computation increases considerably, given the high computational cost of the algorithm.

The interval on the x^+-axis is then discretized into a number n_{steps} of small intervals, with length $\Delta x = (x^+_{\text{max}} - x_0^+)/n_{\text{steps}}$. The number of steps was set equal to $n_{\text{steps}} = 1000$. We checked that, for larger values of n_{steps}, the results of the integration remain qualitatively the same, at the price of having, again, a much longer computational time.

Each point of the discretized x^+-axis is labeled by an index i. We choose to discretize the derivatives in the x^+ direction accordingly,

$$\partial_+ \phi = \frac{\phi(x^+_{i+1}, x^-) - \phi(x^+_i, x^-)}{\Delta x} + \mathcal{O}(\Delta x), \tag{I.3.86}$$

$$\partial_+ \rho = \frac{\rho(x^+_{i+1}, x^-) - \rho(x^+_i, x^-)}{\Delta x} + \mathcal{O}(\Delta x). \tag{I.3.87}$$

Notice that, with this choice, our algorithm converges to the solution only at first order in Δx. However, since we are interested in the qualitative behavior of the solutions, Eqs. (I.3.86) and (I.3.87) represent a good approximation for the derivatives of ϕ and ρ.

Along x^- at fixed x^+, the field equations reduce to ordinary differential equations. Therefore, for each step in the x^+ direction, we numerically integrate the equations along x^- by means of a 4th-order Runge-Kutta algorithm. The outcome, thus, is a list of x^--profiles of ϕ and ρ for each point of the discretized interval on x^+ (see Fig. I.3.8).

For all the cases considered here, the values of the parameters are set equal to $\lambda = 1$ and $\ell = 1$. The mass of the evaporating solution is fixed equal to $\mathcal{M} = 0.1$ (in these units).

As a first test, we have verified the accuracy of the integration algorithm in the absence of backreaction, i.e., for $N = 0$, by comparing the numerical solution with the analytical classical one (I.3.63). Overall, we find that the relative difference between the numerical and the analytical solutions is smaller than 1% as long as we consider large negative values of x^-, while it increases for $x^- \to 0$, staying however $\lesssim 20\%$ (see Fig. I.3.9). We checked that increasing n_{steps} leads to

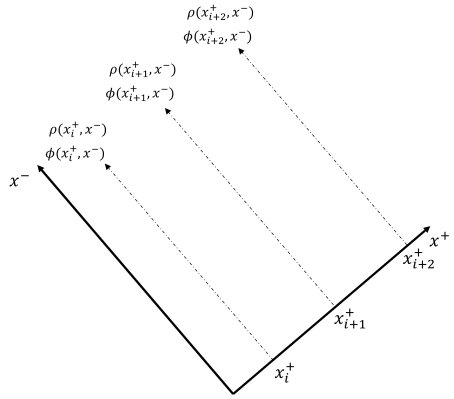

Figure I.3.8: Schematic representation of the numerical algorithm adopted to numerically integrate Eqs. (I.3.79a) and (I.3.79d). We discretize the x^+-axis, and for each interval on the latter, we numerically integrate the field equations along x^- using a Runge-Kutta algorithm.

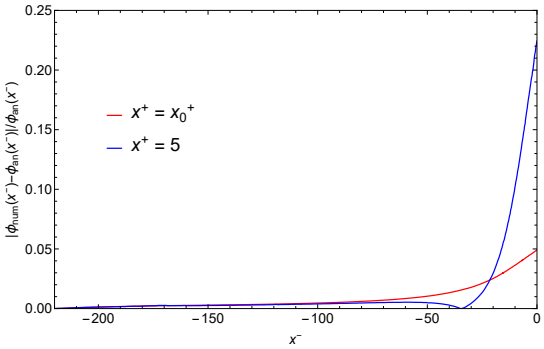

Figure I.3.9: Relative difference between the numerical (obtained by setting $N = 0$) and the exact (I.3.63) solutions at $x^+ = x_0^+$ and $x^+ = 5$. As it can be seen, the difference increases as we move towards small negative values of x^-. The numerical integration has been carried out on an x^+ interval of $[x_0^+, x_{\rm max}^+] = [1, 5]$, while on the x^- direction, in the interval $[-220, 0]$. The parameters of the integration are the following: $\lambda = \ell = 1$, $\mathcal{M} = 0.1$ (in these units), $n_{\rm steps} = 1000$, so that $\Delta x = 4 \cdot 10^{-3}$. We checked that, for higher values of $n_{\rm steps}$, the relative differences decrease, without however altering the qualitative final results and with a much higher computational time.

an improvement in the accuracy of the integration algorithm (the relative differences decrease), without, however, altering the qualitative final results and at the price of having a much longer computational time. Although a relative discrepancy of 20% may seem quite important, one should consider that, in the presence of backreaction (see below), the extremal solution is reached at values of x^- for which the relative discrepancy stays always below 5%. As in the following we are not interested in the exact details of the evaporation process, but rather in its qualitative evolution and outcome, we will adopt $n_{\rm steps} = 1000$ anyway, favouring time efficiency over high precision.

After this preliminary test, we analyse three different cases of increasing N: $N = 0$, $N = 24$ and $N = 2400$, to study the backreaction effects in different regimes.

The x^--profiles of ϕ and ρ, together with their variations $\Delta\phi = |\phi(x^-) - \phi_{\rm ext}(x^-)|$, $\Delta\rho = |\rho(x^-) - \rho_{\rm ext}(x^-)|$ with respect to the extremal configurations, are computed numerically for several values of x^+ in the range $x^+ \in [x_0^+, 5]$. At $x^+ = x_0^+$, the numerical solutions match exactly the extremal ones, as it should be according to the boundary condition imposed at the shock wave. For simplicity, in Figs. I.3.10 to I.3.12, we only show the plots for $x^+ = 5$ and $N = 0, 24, 2400$. The plots for the other values of x^+ in the range considered here have the same qualitative behavior. Moreover, given the increase in computational errors near $x^- \sim 0$, we performed the integration in the range $x^- \in [-220, 0]$ for convenience. We have checked that the results do not differ from those shown, even if we extend the x^- axis to positive values: the convergence to the extremal solution either does not occur in the entire axis or always occurs in the $x^- < 0$ region.

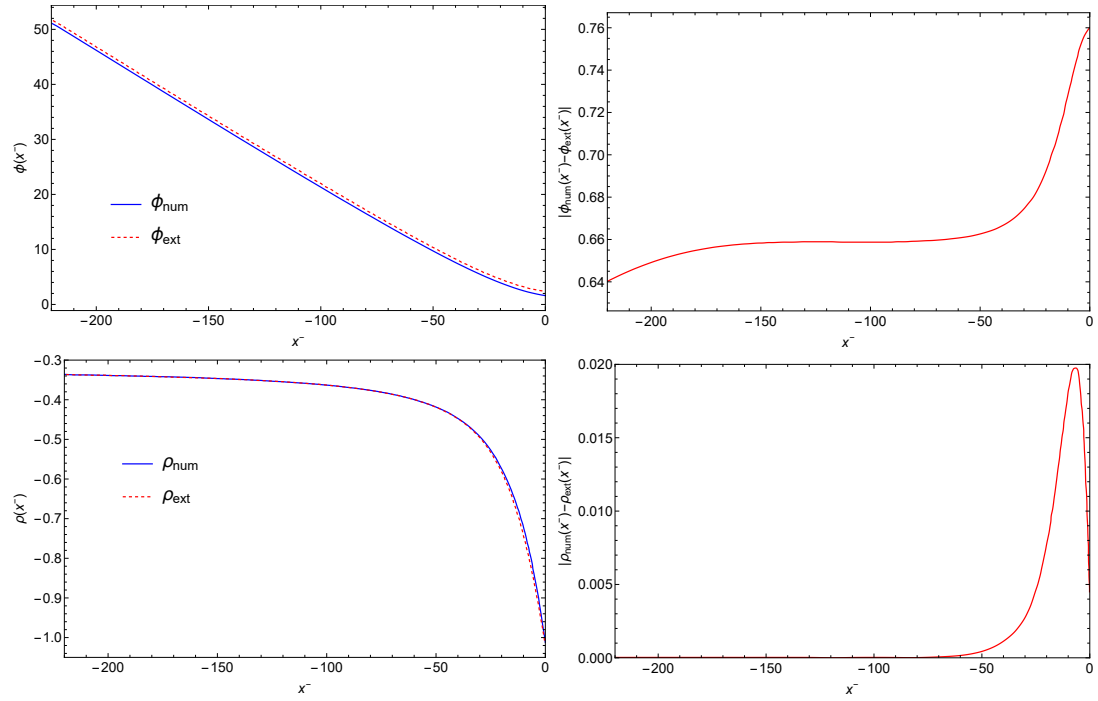

Figure I.3.10: **Upper panels**: Comparison between the numerical (solid blue line) and analytical extremal (dashed orange line) dilaton solutions (left figure), and difference between the two (right figure), as functions of x^-. **Lower panels**: Comparison between the numerical (solid blue line) and analytical extremal (dashed orange line) metric solution (left figure), and difference between the two (right figure), as functions of x^-. All figures are evaluated at $x^+ = 5$ and with $N = 0$, in units where $\lambda = \ell = 1$.

For $N = 0$, i.e., in the absence of backreaction, we see, as expected, that the black-hole solution remains different from the extremal one for every value of the coordinate x^-. For $N = 24$, namely when backreaction effects begin to become relevant, we see that, although $\Delta\phi$ and $\Delta\rho$ remain different from zero for all values of x^-, they begin to decrease towards zero after reaching a maximum. For $N \gg 24$, i.e., $N \sim 2400$, when backreaction effects become stronger, we see that $\Delta\phi$ and $\Delta\rho$ become always zero at some finite (negative) value of x^-. In general, the larger N, i.e., the stronger backreaction effects, the faster the evaporating configuration reaches the extremal GS. As remarked above, the convergence to the extremal configuration occurs at values of x^- for which relative numerical errors are less than 5%.

It is very important to notice that the convergence of the excited, evaporating solution towards the extremal one is non-monotonic. As one can see clearly from the plots shown (but the same happens also for other values of N not shown here), $\Delta\phi$ and $\Delta\rho$ stay almost flat in the region of large ϕ (corresponding to $x^- \ll 0$). Then, they reach a sharp maximum at relatively large values of x^- before falling rapidly toward zero. This behavior cannot be traced back to backreaction effects, since it is present also in the $N = 0$ case. The sharp maximum seems to be related to the presence of the maximum in the potential $\mathcal{V}$ at (relatively) small values of the dilaton (see Fig. I.3.1), thus to a self-interaction effect of the dilaton. On the other hand, this maximum in $\mathcal{V}$ is also responsible for both the presence of two horizons (instead of only one) and for the phase transition small/large black holes (see Sections I.3.1.3 and I.3.3).

Summarizing, the numerical integration of Eqs. (I.3.79) clearly shows that, differently from what we obtained in the rough quasistatic description, the effect of the backreaction is to bring the excited, evaporating solution back to the extremal state after a *finite* time, when N is chosen to be sufficiently large, i.e., at least $N \sim \mathcal{O}(10^2 - 10^3)$.

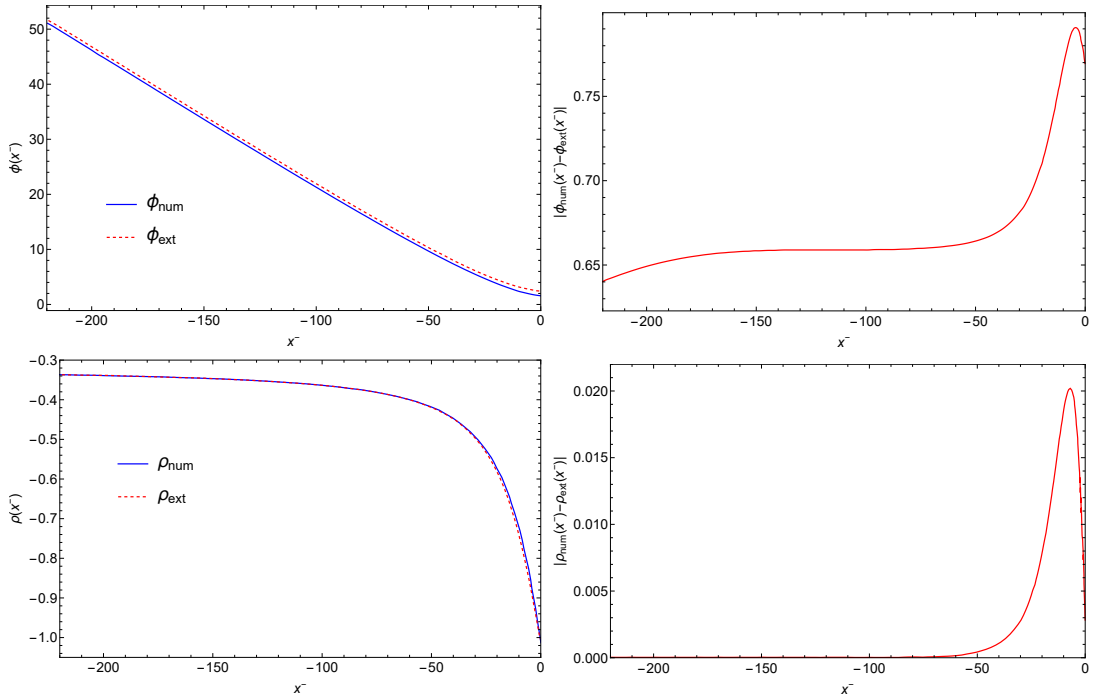

Figure I.3.11: **Upper panels**: Comparison between the numerical (solid blue line) and analytical extremal (dashed orange line) dilaton solutions (left figure), and difference between the two (right figure), as functions of x^-. **Lower panels**: Comparison between the numerical (solid blue line) and analytical extremal (dashed orange line) metric solution (left figure), and difference between the two (right figure), as functions of x^-. All figures are evaluated at $x^+ = 5$ and with $N = 24$, in units where $\lambda = \ell = 1$.

I.3.7 Entanglement Entropy and the Page curve

In this section, we compute the entanglement entropy (EE) of Hawking radiation, described here as a collection of N massless scalar fields, in the 2D nonsingular black-hole geometry. By assuming that the evaporation process is quasistatic, we also determine the time variation of the EE and construct the related Page curve.

The EE of the radiation can be computed by using Kruskal coordinates, covering the region outside the outer event horizon of the black hole,

$$\kappa X^{\pm} = \pm e^{\pm \kappa x^{\pm}} \longleftrightarrow x^{\pm} = \pm \frac{1}{\kappa} \ln\left(\pm \kappa X^{\pm}\right), \tag{I.3.88}$$

where κ is the surface gravity at the outer event horizon. In these coordinates, the conformal factor of the metric (I.3.53) can be written as

$$e^{2\rho} = \frac{f(r)}{-\kappa^2 X^+ X^-}. \tag{I.3.89}$$

The entanglement entropy of N massless scalar fields in two spacetime dimensions on a line can be evaluated by tracing out the degrees of freedom in a spacelike slice $[x, y]$ connecting two points. The resulting expression is[6] (see, e.g., Refs. [54, 55, 303, 304])

$$S_{\text{matter}} = \frac{N}{6} \ln d^2(x, y), \tag{I.3.90}$$

where $d(x, y)$ is the geodesic distance between x and y. In principle, Eq. (I.3.90) is valid for a QFT on a flat spacetime [305], but it has been generalized to *static* curved spacetime [303], where

[6] This expression should depend also on ultraviolet cutoffs, which are here considered as additive constants.

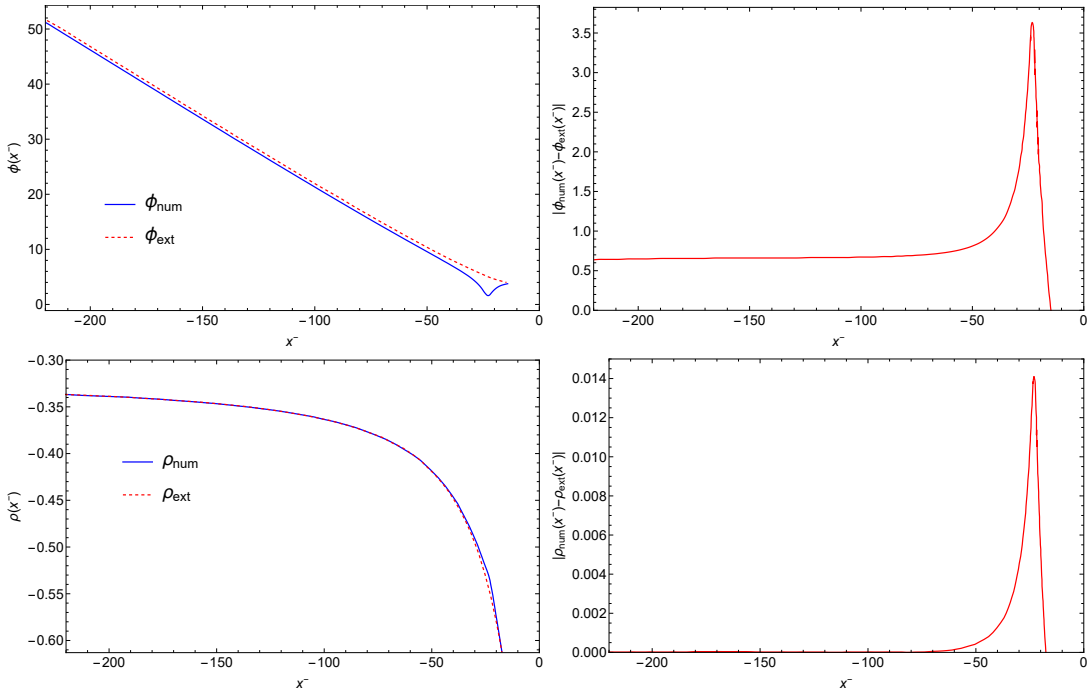

Figure I.3.12: **Upper panels**: Comparison between the numerical (solid blue line) and analytical extremal (dashed orange line) dilaton solutions (left figure), and difference between the two (right figure), as functions of x^-. **Lower panels**: Comparison between the numerical (solid blue line) and analytical extremal (dashed orange line) metric solution (left figure), and difference between the two (right figure), as functions of x^-. All figures are evaluated at $x^+ = 5$ and with $N = 2400$. The x^- axis has been cut at the point where the numerical solution matches the extremal one.

$d^2(x, y)$ reads

$$d^2(x,y) = -\left[X^+(x) - X^+(y)\right]\left[X^-(x) - X^-(y)\right] e^{\rho(x)} e^{\rho(y)}. \tag{I.3.91}$$

To compute the entanglement entropy, we construct a spacelike surface encompassing different regions of the black hole. In Fig. I.3.13, this surface is $\Sigma_{\rm L} \cup I \cup \Sigma_{\rm R}$, where $\Sigma_{\rm L}$ and $\Sigma_{\rm R}$ are two hypersurfaces on the *outside* regions of the two copies of the black hole, where an observer collects Hawking radiation. They are the portion of the hypersurface, where the radiation degrees of freedom are defined. They are anchored to two timelike surfaces (dashed black lines in Fig. I.3.13) at the points $b_+ = (t_b, b)$ (right wedge) and $b_- = (-t_b + \mathrm{i}\beta/2, b)$ (left wedge). The surface $\mathcal{J}$ defines, instead, the interior region of the black hole. The radiation quantum state over the whole hypersurface $\Sigma_{\rm L} \cup I \cup \Sigma_{\rm R}$ is pure. When tracing out the interior degrees of freedom in I, we obtain the mixed state of the radiation described by the density matrix $\rho_{\rm rad}$, which can therefore be used to compute the entanglement entropy. This is reminiscent of the thermofield double state of the black hole [256, 306]: the entanglement entropy takes into account the correlations between the two disjointed copies of the black hole (right and left wedges). Since we have radiation outside the black hole, there will be two copies of this thermal bath (the two regions $\Sigma_{\rm L}$ and $\Sigma_{\rm R}$).

In our case, Eq. (I.3.91) reads

$$d^2(b_+, b_-) = -\frac{1}{\kappa^2}\left[e^{\kappa t_b + \kappa b} - e^{-\kappa t_b + \kappa b} e^{i\kappa\beta/2}\right]\left[-e^{-\kappa t_b + \kappa b} + e^{\kappa t_b + \kappa b} e^{-i\kappa\beta/2}\right]\frac{f(b)}{e^{2\kappa b}}. \tag{I.3.92}$$

This is valid off-shell. On shell $\kappa \to \kappa_{\rm H}$, we have $\frac{\beta\kappa_{\rm H}}{2} = \pi$, and thus

$$d^2(b_+, b_-) = \frac{4f(b)}{\kappa_{\rm H}^2}\cosh^2(\kappa_{\rm H} t_b). \tag{I.3.93}$$

Finally, the EE of the matter fields is

$$S_{\rm matter} = \frac{N}{6}\ln\left[\frac{4f(b)}{\kappa_{\rm H}^2}\cosh^2(\kappa_{\rm H} t_b)\right]. \tag{I.3.94}$$

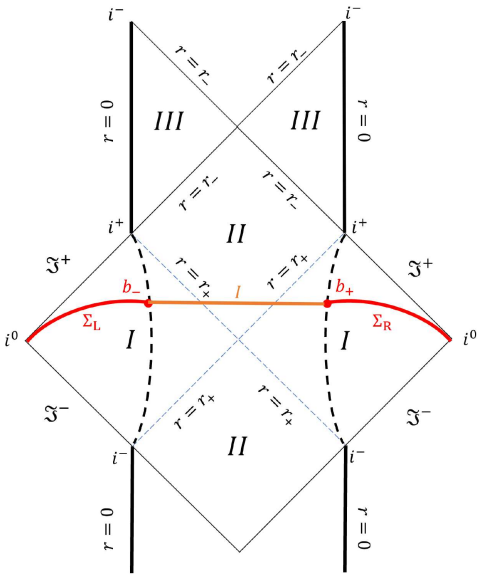

Figure I.3.13: Penrose diagram of the maximally extended spacetime of the nonextremal configuration. The two points b_+ and b_-, belonging to the right and left wedges, respectively, are highlighted, and represents points anchored to two timelike curves (dashed black lines in the two wedges). The union between the three hypersurfaces $\Sigma_{\rm L} \cup I \cup \Sigma_{\rm R}$ (the red and orange curves) is a spacelike surface and the state defined on it is pure. The radiation is defined on $\Sigma_{\rm L}$ and $\Sigma_{\rm R}$ and its state is mixed.

As stressed above, this is valid as long as we consider the static case. However, $\kappa_{\rm H}$ varies due to the evaporation process. To get a qualitative picture of the behavior of the entropy in time, we can assume that the evaporation process happens in an adiabatic way, so that we can use a quasistatic approximation. The evaporation is thus again modelled in terms of a sequence of static states with decreasing mass. As we have seen explicitly in Section I.3.4.3, the quasistatic approximation is reliable as long as the semiclassical one is valid. In a first approximation, therefore, we can use the time variation of the event horizon $r_{\rm H} = r_{\rm H}(t)$, computed as a solution of the SB law (I.3.45), and plug it into the expression of the surface gravity

$$\kappa_{\rm H}(r_{\rm H}) = \frac{f'(r_{\rm H})}{2} = \frac{r_{\rm H}^4 - 2\ell^3 r_{\rm H}}{2\lambda\left(\ell^3 + r_{\rm H}^3\right)^2}. \tag{I.3.95}$$

The qualitative result (obtained neglecting the irrelevant constants $\frac{N}{6}\ln\left[4f(b)\right]$) is plotted in Fig. I.3.14. As in singular black-hole models, initially the entanglement entropy of the radiation grows. However, this growth reaches a maximum at the "Page time" $t_{\rm P}$ and then the entropy starts decreasing, due to the peculiar form of the surface gravity, which is related to the absence of a singularity.

It is interesting to note that $t_{\rm P}$ physically coincides with the onset time of the second order phase transition (graphically, the intersection point between the solid blue and the horizontal dotted lines in Fig. I.3.6b). This feature was found before for nonsingular black holes in Ref. [258], where it was noted that the presence of the dS core traps Hawking modes, which cause a decrease in entropy once freed from the trapping region. This indeed happens as we get closer to the extremal configuration, right after the onset of the second order phase transition, as the role of the inner horizon becomes increasingly important. This release of information could also be related to the peculiarities of the latter, which has negative surface gravity, causing an outburst of energy in the final stages of the evaporation [259], a process similar to the mass inflation.

The mechanism described above is qualitative similar to that taking place in the island proposal [54–56, 255] (for an application to two-horizon models, both singular and regular, see, e.g.,

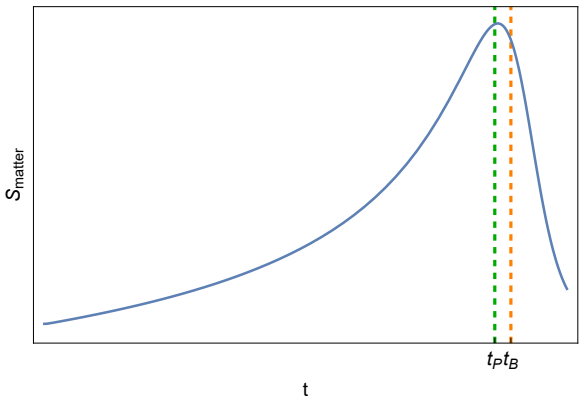

Figure I.3.14: Qualitative time variation of the entanglement entropy of matter fields, according to Eq. (I.3.94), where we considered the time variation of the surface gravity, calculated using the solution of Eq. (I.3.45). The vertical, dashed green line corresponds to the maximum of the curve (the Page time $t_{\rm P}$), while the vertical dashed orange one indicates the time $t_{\rm B}$ at which the semiclassical approximation should break down.

Refs. [307–309]; for an application to dS spacetime, see, e.g., Refs. [310, 311]), where the resolution of the information paradox is traced back to a transition in the behavior of the entanglement entropy functional. At late times (right after the Page time), this functional starts receiving contributions from nontrivial configurations in the black hole interior (the "islands"). This allows to correctly keep track of the entanglement structure of both the black hole and the radiation subsystems and to reconstruct the Page curve. Our approach provides, at qualitative level, a physical explanation for the appearance of such configurations in the black-hole interior. In our description, the islands correspond to the inner horizon, while the transition in the entropy functional is physically realized by the second order phase transition[7]. In this work we have only considered nonsingular black holes with two horizons, characterized therefore by a timelike singularity. It is, therefore, currently unclear if and how the results of the present work compare with the island rule applied to black holes possessing spacelike singularities (see, e.g., Refs. [312–314])[8]. In general, we expect the single-horizon case to be qualitatively different from the two-horizon one. On the other hand, at least in some particular cases, the behavior of regular models with a *single* event horizon could be not so drastically different from that of two-horizon black holes (see, e.g., Refs. [5, 119, 275, 276]).

The assumptions used so far are the validity of the quasistatic and the semiclassical approximations. As we have seen in Section I.3.4.3, the semiclassical approximation (and hence also the quasistatic one) breaks down near extremality, when we reach the energy gap (I.3.52). This happens at the time corresponding to the vertical dashed orange line in Fig. I.3.14. Therefore, we have to cut the Page curve when the semiclassical approximation breaks down. What happens beyond this point cannot be inferred from our semiclassical description of the dynamics. In particular, we cannot assess whether the decrease in EE continues until it becomes zero at extremality, as it would be expected for an evaporation process that leaves behind a quantum pure state. Results from AdS_2 quantum gravity indicate the occurrence of a quantum phase transition from the LDS vacuum to the AdS_2 CDV [285]. Similarly to what happens in the case of extremal charged black holes, the near-extremal, near-horizon state of 4D nonsingular Hayward black holes, described by the $AdS_2 \times S^2$ spacetime, could have a purely topological entropy content, explained in terms of AdS_2 fragmentation [215].

[7] As it was noted in Ref. [308], the expression for the entanglement entropy in the island, when applied to singular two-horizon models, becomes mathematically ill-defined for the extremal configurations, as the boundary of the islands necessarily ends at the singularity at $r = 0$. This problem is naturally avoided when dealing with regular models, as we do in this work.

[8] It was shown in Ref. [314] that the quantum extremal surface, identifying the position of the island, could meet the singularity during the evaporation, leading to the impossibility of following the evaporation process until completion, at least in this setup. The absence of the singularity could possibly lead to a resolution of this problem.

Chapter I.4

Testing regular BHs with S2 orbits

Since its formulation, General Relativity (GR) has been widely tested in several different contexts. In particular, one of its most intriguing predictions is the existence of black holes, whose possible presence has been tested both directly [16, 246, 247] and indirectly [315, 316]. Although black-hole imaging, gravitational wave and iron-line observations are compatible with the presence of Kerr black holes [12, 15, 16, 246, 317], there is still room for small deviations, which could be tested with present and future experiments. For this reason, there has been an increasing interest in studying black-hole mimickers. These objects share some properties with GR solutions but allow for a different phenomenology at the horizon scale, which, if observed, would represent a smoking gun for deviations from GR.

Regular black holes are among the most fascinating mimickers. Contrary to classical black holes which present a singularity at their core [87, 114], indicating the breakdown of the classical theory, these objects are completely regular everywhere. This point is particularly significant, since we expect a quantum theory of gravity to resolve the classical singularity problem. Although there have been some attempts to capture the main properties of the fundamental theory [61, 318, 319], a clear understanding of its dynamics and of the mechanism leading to the formation of these regular spacetimes is still lacking. Consequently, mainly bottom-up approaches have been followed until now [1, 84, 118, 120, 206, 260, 320–322], in which one usually modifies GR solutions to test possible deviations in a phenomenological fashion. This is particularly suitable, for instance, to study orbits of test particles [323, 324], and it has been used to investigate modifications to the black-hole shadow, gravitational waves and X-ray emission (see, e.g., Refs. [13, 15, 90, 92, 171, 325–328] and references therein). An intriguing feature of nonsingular black-hole models is the presence of a new length scale (hair) ℓ, which can be hierarchically larger than the Planck scale [1]. An important question to be answered is whether such models with super-Planckian hair can be excluded by present experimental data.

In this chapter, following this type of approach, we consider the Fan-Wang regular black-hole metric [158], a particular case of the general class of models explored in Ref. [1]. The reason for this choice is that the corrections to the Schwarzschild spacetime decrease sufficiently slowly to be experimentally observable also at great distances from the horizon. Therefore, we test our model with the orbital motion of the S2 star around the compact radio source Sagittarius A* (SgrA* [247]) in the Galactic Center (GC) [329, 330]. If this spacetime cannot be tested with current S2-star data, no other models belonging to the same class can.

In this chapter, we use units in which $c = \hbar = k_{\rm B} = 1$.

I.4.1 The model

In this chapter, we discuss how to constrain the deformation parameter ℓ introduced in Chapter I.2, responsible for the smearing of the classical singularity. Again, The starting point is the general class of dS-core BHs, which can be parameterized in spherical coordinates, as (cfr. Eqs. (I.2.3), (I.2.6), (I.2.7), (I.2.10) and (I.2.22))

$$\mathrm{d}s^2 = -A(r)\mathrm{d}t^2 + \frac{\mathrm{d}r^2}{A(r)} + r^2\mathrm{d}\Omega^2, \tag{I.4.1}$$

where $\mathrm{d}\Omega^2 = \mathrm{d}\theta^2 + \sin^2\theta \mathrm{d}\phi^2$ is the line element on the unitary 2-sphere, and

$$A(r) = 1 - \frac{R_\mathrm{S}}{\ell} F\left(\frac{r}{\ell}\right). \tag{I.4.2}$$

We recall that the function F can be written in terms of the MS mass as

$$m(r) = \frac{r R_\mathrm{S}}{2G\ell} F\left(\frac{r}{\ell}\right). \tag{I.4.3}$$

As discussed in the previous chapter, one way to avoid the presence of the classical curvature singularity at $r = 0$ is to require a dS-like behavior at the BH core. One way of achieving this is by requiring the function $F(r/\ell)$ to behave as $F \simeq \alpha r^2/\ell^2 + \mathcal{O}\left(r^3/\ell^3\right)$, with $\alpha > 0$, when $r \ll R_\mathrm{S}$. On the other hand, asymptotic flatness requires $F(r/\ell) \simeq \ell/r + \beta\ell^2/r^2 + \mathcal{O}\left(\ell^3/r^3\right)$ for $r \gg R_\mathrm{S}$. The parameters α and β are two dimensionless parameters related to the dS length scale and to the strength of the corrections at infinity, respectively.

In the past, there have been several proposals to test GR predictions against other possibilities, the latter coming from theories beyond GR or from phenomenological modifications of the Schwarzschild and Kerr metrics (see, e.g., Ref. [105] and references therein for tests with electromagnetic signals, and Refs. [15, 18]). In this chapter, we discuss our recent tests of the metric of a spherically-symmetric, static spacetime with the orbits of stars around supermassive BHs. In particular, the most accurate and complete dataset of this kind is the one relative to the motion of the S2 star around Sagittarius A*. Indeed, the S2-star motion happens sufficiently far away from the central BH that the effects of the spin of the latter are completely negligible, a fact that makes this system suitable for testing our regular BH models and constraining the quantum-deformation parameter ℓ.

To do so, we consider a particular case of the Fan-Wang regular-black-hole metrics [158], i.e.,

$$F\left(\frac{r}{\ell}\right) = \frac{\ell r^2}{(r+\ell)^3}, \tag{I.4.4}$$

for which $\alpha = 2GM/\ell$ and $\beta = 6GM/\ell$.

The main reason to choose this metric is that it gives $\mathcal{O}\left(\ell^2/r^2\right)$ corrections to the Schwarzschild geometry at great distances, which are the strongest possible admitted in the general class described in Chapter I.2 and compatible with the Schwarzschild asymptotics, reason why we expect this spacetime to show important phenomenological differences with respect to the GR classical solution (at least when $\ell \gg \ell_\mathrm{P}$). Moreover, any other solution will be less constrained, when tested against the S2-star data, due to the weaker asymptotics. Therefore, if this simple model cannot be tested with this system, no other models belonging to the same class can. In addition, while other metrics (with corrections of $\mathcal{O}\left(\ell^3/r^3\right)$ or $\mathcal{O}\left(\ell^4/r^4\right)$, corresponding to the Bardeen and the Hayward spacetimes, respectively) have been extensively investigated, this model is relatively less studied. Finally, the metric has also a nice astrophysical analogy. Indeed, the density associated with the MS mass that generates the considered spacetime is

$$\rho = \frac{3M\ell}{4\pi(r+\ell)^4}, \tag{I.4.5}$$

whose large r behavior resembles that of some density profiles of dark matter in elliptical and spherical galaxies [331, 332] with different characteristic scales involved.

Also in this case, as already discussed in the previous chapter, the spacetime structure is the same as the general class to which this model pertains. It has an outer event horizon and an inner Cauchy horizon, respectively located at $r = r_\mathrm{H}$ and $r = r_-$, where r_H and r_- are the positive roots of $A(r) = 0$. The two horizons coincide in the extremal configuration where $r_\mathrm{H} = r_- = r_c = 2\ell_c$ and $\ell_c = 8GM/27$. Moreover, when $\ell > \ell_c$, the horizon disappears and the configuration represents a compact horizonless object.

I.4.2 Black hole thermodynamics

Analogously to the spacetime structure, the Fan-Wang model's thermodynamic behavior is similar to the general one discussed in Section I.2.3.3. We start by defining the Hawking temperature of

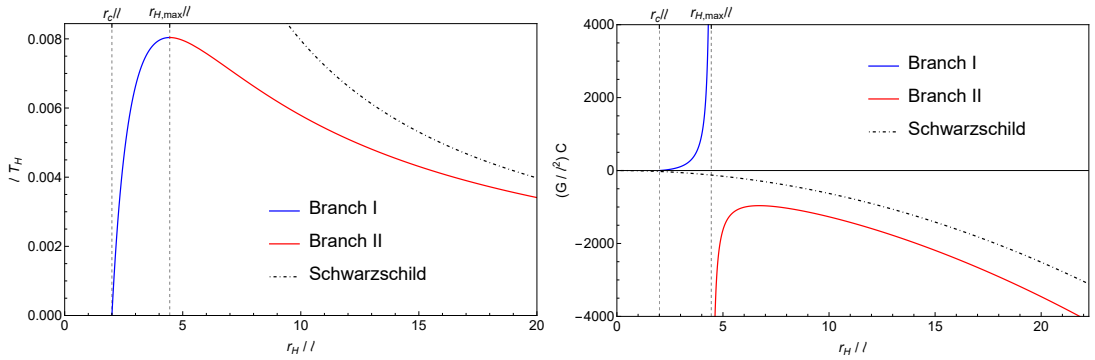

Figure I.4.1: **Left panel**: Temperature as a function of the horizon radius for the Fan-Wang minimal model. As for the general case discussed in Section I.2.3.3, also this model shows a nonmonotonic behavior of the temperature, which is peaked for $r_{\rm H} = r_{\rm H,max} = (2+\sqrt{6})\ell$. We also highlight the presence of the two branches I and II, where the temperature is respectively an increasing and a decreasing function of the horizon radius. **Right panel**: Specific heat as a function of the horizon radius for the Fan-Wang model. Again, the behavior of this quantity is analogous to the one shown in Section I.2.3.3. The specific heat is positive for $r_c < r_{\rm H} < r_{\rm H,max}$, it diverges for $r_{\rm H} = r_{\rm H,max}$ and is negative for $r_{\rm H} < r_{\rm H,max}$. The divergence at $r_{\rm H} = r_{\rm H,max}$ signals the onset of a second-order phase transition.

the BH in terms of the event horizon radius as

$$T_H = \frac{1}{4\pi}\,\frac{{\rm d}A(r)}{{\rm d}r}\bigg|_{r=r_{\rm H}} = \frac{r_{\rm H}-2\ell}{4\pi r_{\rm H}(\ell+r_{\rm H})}, \tag{I.4.6}$$

and we rewrite the BH mass in terms of its outer horizon location as

$$M = \frac{(\ell+r_{\rm H})^3}{2Gr_{\rm H}^2} \tag{I.4.7}$$

for convenience. Notice that the behavior of the temperature is nonmonotonic (see Fig. I.4.1: it has a peak at $r_{\rm H} = r_{\rm H,max} = (2+\sqrt{6})\ell$ and goes to zero for $r_{\rm H}\to\infty$ and $r_{\rm H}\to r_c$, exactly as the other models analyzed in Section I.2.3.3. This behavior indicates the presence of metastable states, with the same temperature but with different radii and thermodynamic properties. Indeed, by inspecting the specific heat of this model, given by

$$C_{\rm H} = \frac{{\rm d}M}{{\rm d}T_{\rm H}} = -\frac{2\pi(r_{\rm H}-2\ell)(\ell+r_{\rm H})^4}{Gr_{\rm H}(r_{\rm H}^2-4\ell r_{\rm H}-2\ell^2)}, \tag{I.4.8}$$

we can clearly see the presence of two different branches. The first branch (branch I) is characterized by quantum black holes with $r_{\rm H}\simeq r_c\simeq\ell$ and a positive specific heat (because of the increasing behavior of the temperature). Branch I also include the extremal configuration, for which $C_{\rm H}=0$. The second branch (branch II), instead, is characterized by a more Schwarzschild-like, classical behavior (at least for great values of the horizon radius), large horizon radii $r_{\rm H} > r_{\rm H,max}$ and a negative specific heat closely resembling that of the vacuum general-relativity solutions. At $r_{\rm H} = r_{\rm H,max}$, the specific heat diverges since ${\rm d}T_{\rm H}/{\rm d}M = 0$: this signals the onset of a second-order phase transition that separates the quantum-like branch from the classical one. The separation between the two branches can also be translated in terms of the quantum-deformation parameter ℓ. Quantum-like black holes, indeed, correspond to those having $\ell_{\rm H,max}\lesssim\ell\leq\ell_c$, being $\ell_{\rm H,max} = 4(3-\sqrt{6})/9\simeq 0.245GM$, while the classical ones are those with $\ell<\ell_{\rm H,max}$. This behavior is shown in the right panel of Fig. I.4.1.

In order to assess which branch is thermodynamically favored we compute the free energy $\mathcal{F} = M - T_{\rm H}S$, where M and T are given respectively by Eqs. (I.4.6) and (I.4.7), while the entropy can be computed with the generalized formula in terms of the integral of the mass given by Eq. (I.2.33). As shown in Fig. I.4.2, the quantum configurations, corresponding to $r_c\leq r_{\rm H} < r_{\rm H,max}$, are thermodynamically favored with respect to their classical counterparts, corresponding to $r_{\rm H}\geq r_{\rm H,max}$, since they retain the least free energy.

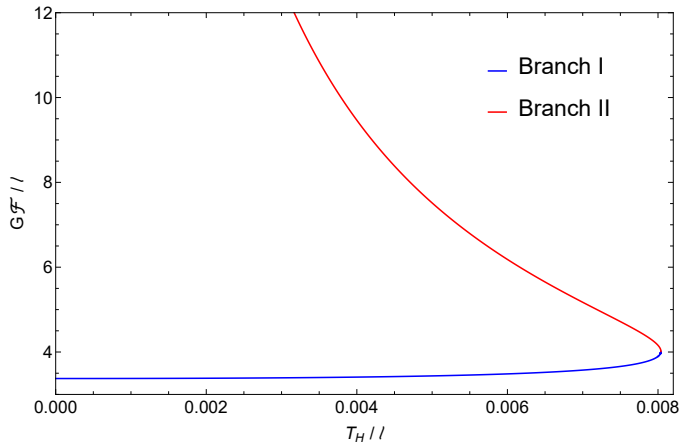

Figure I.4.2: Free energy as a function of the BH temperature. We explicitly show the presence of two branches, I (in blue) and II (in red), corresponding to stable, quantum black holes and to classical, unstable black holes.

I.4.3 Orbits of test particles

In order to test the Fan-Wang metric with the S2-star orbital data, we first need to analyze the orbits of a generic test particle in this spacetime. Here, we study such orbits using a standard procedure (see, e.g., Ref. [333] for a more extensive presentation of the method). Although we already discussed the behavior of null orbits in Section I.2.3.5, here we show a different method for obtaining the equations of motion for both massive and massless particles in a spherically symmetric spacetime and we finally specialize the formalism to the Fan-Wang model.

We start by writing the Lagrangian for the geodesic motion around this spacetime

$$\mathcal{L} = \frac{1}{2} g_{\mu\nu} \dot{x}^\mu \dot{x}^\nu = \frac{1}{2} \left[-A(r)\dot{t}^2 + \frac{\dot{r}^2}{A(r)} + r^2 \dot{\theta}^2 + r^2 \sin^2\theta \, \dot{\phi}^2 \right]. \tag{I.4.9}$$

Here, x^μ expresses the position of the particle in the specified coordinate system, and the dot indicates differentiation with respect to some affine parameter λ. We can simplify Eq. (I.4.9) by using the isometries of the spacetime. Indeed, the quantities

$$p_t = \partial_t \mathcal{L} = -A(r)\dot{t} = -\mathcal{E}, \tag{I.4.10a}$$

$$p_\phi = \partial_\phi \mathcal{L} = r^2 \sin^2\theta \, \dot{\phi} = L, \tag{I.4.10b}$$

are the conserved momenta related to the symmetries under time translations and rotations in the equatorial plane, respectively, while $\mathcal{E}$ is the energy of the particle and L is its angular momentum. Moreover, using the Euler-Lagrange equations, the equation of motion for the θ component reads

$$r^2\ddot{\theta} + 2r\dot{r}\dot{\theta} - r^2 \sin\theta \cos\theta \dot{\phi}^2 = 0. \tag{I.4.11}$$

We can easily see, from Eq. (I.4.11), that by rotating the reference frame to set $\theta(\lambda = 0) = \pi/2$ and $\dot{(}\lambda = 0) = 0$, then $\theta = \text{const.} = \pi/2$ for any value of the affine parameter λ. Therefore, without loss of generality, we can focus on equatorial orbits only. Finally, since the Lagrangian does not depend explicitly on the affine parameter, we see that the Hamiltonian

$$\mathcal{H} = \mathcal{L} = -\frac{1}{2}\epsilon^2 \tag{I.4.12}$$

is also conserved. Here, the parameter $\epsilon = \pm 1$ for timelike orbits and $\epsilon = 0$ for null trajectories.

Now, using Eqs. (I.4.10) and (I.4.12) and fixing the reference frame to $\theta = \pi/2$, we get an equation for the radial coordinate r

$$\dot{r}^2 + A(r)\left(\epsilon^2 + \frac{L^2}{r^2}\right) = \mathcal{E}^2. \tag{I.4.13}$$

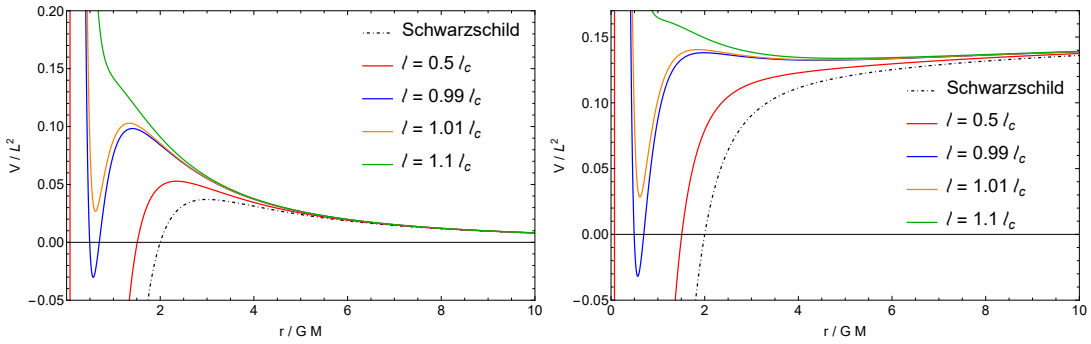

Figure I.4.3: **Left panel**: effective potential as a function of the radial coordinate for different values of the angular momentum L and $\epsilon^2 = 0$ (null orbits). **Right panel**: effective potential as a function of the radial coordinate for different values of the angular momentum L and $\epsilon^2 = 1$ (timelike orbits).

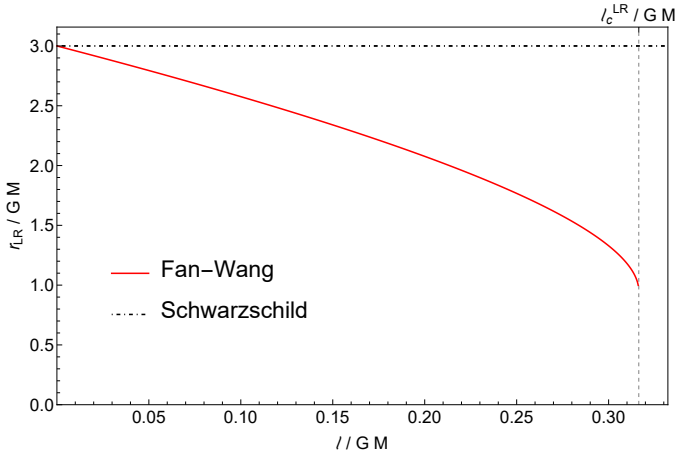

Figure I.4.4: Light-ring location for the Fan-Wang model as a function of the quantum-deformation parameter ℓ. We also highlight the light-ring radius for the Schwarzschild spacetime, located at $r = 3GM$.

Notice that Eq. (I.4.13) can be interpreted as the energy conservation law for the motion in the spacetime described by the metric function A. Indeed, the term

$$V_{\text{eff}} = A(r)\left(\epsilon^2 + \frac{L^2}{r^2}\right) \tag{I.4.14}$$

plays the role of an effective potential whose properties determine the trajectory of the particle. The qualitative behavior of the effective potential is shown in Fig. I.4.3. When $\epsilon = 0$, the potential behaves as described in Section I.2.3.5. V_{eff} has a minimum in the region $r_- < r < r_{\text{H}}$ and a maximum at $r > r_{\text{H}}$, the latter corresponding to an unstable circular orbit, i.e., the light ring. The light-ring radius, in particular, decreases when ℓ increases and disappears when $\ell > \ell_c^{\text{LR}} \simeq 0.317$. The photon-ring location, as measured by an asymptotic observer, is shown in Fig. I.4.4. On the other hand, when $\epsilon = \pm 1$, i.e., for timelike geodesics, the potential can have up to three extrema, depending on the angular momentum. The first one is again located between the two horizons, at some $r \in (r_-, r_{\text{H}})$. The other two correspond to a maximum and a minimum that represent the marginally bound and the stable circular orbits, respectively.

To proceed in our analysis and study the orbits of stars around such a BH, we rewrite Eq. (I.4.13) in terms of the new variable $u = 1/r$. Moreover, since we want to describe the trajectory on the orbital plane, we compute the derivatives in terms of the azimuthal angle ϕ. The equation becomes

$$\left(\frac{\mathrm{d}u}{\mathrm{d}\phi}\right)^2 + A(u)\left(\frac{\epsilon^2}{L^2} + u^2\right) = \frac{\mathcal{E}^2}{L^2}, \tag{I.4.15}$$

where $A(u)$ reads now

$$A(u) = 1 - \frac{2GMu}{(1+u\ell)^3}. \tag{I.4.16}$$

In order to further simplify Eq. (I.4.15), we differentiate with respect to ϕ and we get

$$\frac{\mathrm{d}^2u}{\mathrm{d}\phi^2} + A(u)u + \frac{\mathrm{d}A}{\mathrm{d}u}\left(\frac{\epsilon^2}{L^2} + u^2\right) = 0. \tag{I.4.17}$$

In the following, we will focus on timelike geodesics, therefore we set $\epsilon^2 = 1$. For simplicity, we also introduce the dimensionless quantities $\sigma = (GM/L)^2$, $\bar{\ell}$, and the new variable $\xi = GMu/\sigma^3$. The advantage of these new variables is that, when σ is small, Eq. (I.4.17) can be solved perturbatively. This analysis is well motivated for the S2-star orbits since $\sigma = 1.9 \times 10^{-4}$. Therefore, we expand the solution as $\xi = \xi_0 + \sigma\xi_1 + \mathcal{O}\left(\sigma^2\right)$. At zeroth order we obtain

$$\frac{\mathrm{d}^2\xi_0}{\mathrm{d}\phi^2} + \xi_0 = 1, \tag{I.4.18}$$

which gives the well-known Newtonian orbits given by $\xi_0 = 1 + e\cos\phi$, where e is the eccentricity of the orbit. Here, $\mathcal{C}_{1,2}$ are constants of integration, to be fixed with the boundary conditions. We are more interested in the first correction which solves the equation

$$\frac{\mathrm{d}^2\xi_1}{\mathrm{d}\phi^2} + \xi_1 = 3\xi_0\left(\xi_0 - 2\bar{\ell}\right). \tag{I.4.19}$$

The linear term in the right-hand side of the equation depends on the particular asymptotics of the Fan-Wang spacetime and is present, at this order, only if the corrections to the large-r behavior of the metric is $A(r \gg \ell) \simeq 1 - 2GM/r + \beta\ell^2/r^2 + \mathcal{O}\left(\ell^3/r^3\right)$. Moreover, notice that the quantum deformation introduced by the parameter ℓ enters in Eq. (I.4.19) with an opposite sign with respect to the usual Schwarzschild equation. This strongly impacts the behavior of orbits in this model since it modifies the precession angle by a quantity proportional to ℓ, as we shall show in the following.

Eq. (I.4.19) can be solved using standard methods and gives

$$\xi_1 = \frac{3}{2}\left(e^2 - 4\bar{\ell} + 2\right) + 3e\gamma\cos\phi - \frac{1}{2}e^2\cos 2\phi + 3e\gamma\phi\sin\phi, \tag{I.4.20}$$

where $\gamma = 1 - \bar{\ell}$. As in the Schwarzschild case, the dominant term is clearly the one proportional to $\phi\sin\phi$ since after a few orbits it becomes large while the others stay bounded. For this reason, neglecting subdominant contributions, we can rewrite the solution as

$$\xi = 1 + e\cos\left[(1 - 3\gamma\sigma)\phi\right], \tag{I.4.21}$$

from which we see that the precession angle is given by $\Delta\phi \simeq 6\pi\sigma\gamma = 6\pi\sigma(1-\bar{\ell})$. While the usual Schwarzschild result is obtained in the limit $\ell \to 0$, we see that $\Delta\phi$ decreases linearly with the quantum deformation, and the precession becomes retrograde for $\bar{\ell} > 1$, i.e., for $\ell > GM$. This interesting feature is not present in the orbits of the Schwarzschild spacetime, therefore can be used to strongly constrain the model.

I.4.4 Numerical integration of the equations of motion

In order to probe the possible existence of the hair ℓ in Section I.4.1, we have developed an orbital model for the S2 star in the galactic center based on the numerical integration of Eq. (I.4.17). In particular, one can recast the energy $\mathcal{E}$ and the angular momentum L in Eq. (I.4.17) in terms of the classical Keplerian elements: the semi-major axis a, the eccentricity e, the time of pericenter passage t_p and the orbital period T (which can, in fact, be derived from M and a through Kepler's third law). A choice of these parameters uniquely identifies a Keplerian ellipse on the equatorial plane, that we assume to osculate the real trajectory of the star at a given time. We hence make

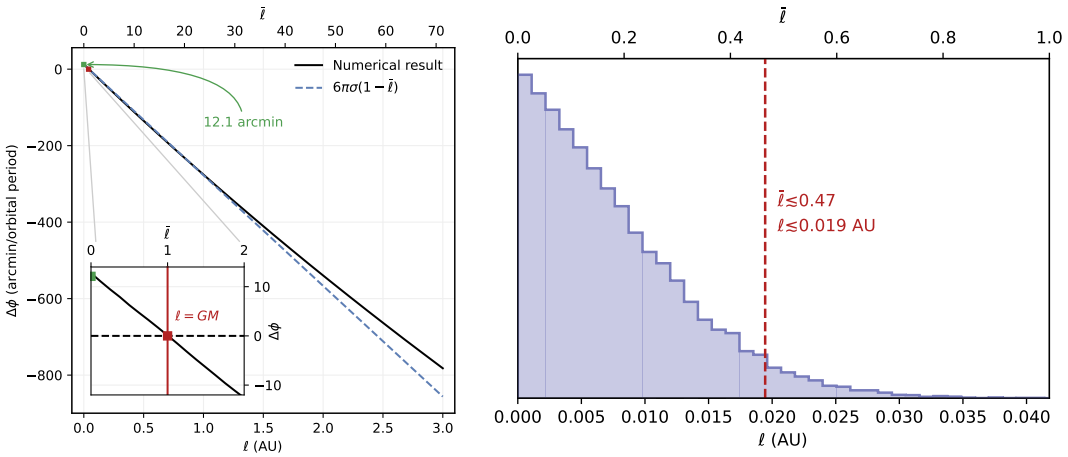

Figure I.4.5: **Left panel**: orbital precession for the S2 star for our model as a function of ℓ. The black solid line reports the results of our numerical integration of the geodesic equations in Eq. (I.4.17), and the blue dashed line represents our first-order perturbative prediction for the precession angle. For $\ell = 0$ we obtain the Schwarzschild precession of 12.1 arcmin per orbital period observed in Ref. [335]. Moreover, we are able to confirm the perturbative result for small values of ℓ up to a few tens of gravitational radii, where departure from the linear trend in $\Delta\phi$ is exhibited by the numerical prediction. Finally, we confirm numerically that for $\ell \geq GM$, the orbital precession becomes retrograde. **Right panel**: marginalized posterior probability distribution for the parameter ℓ resulting from our MCMC analysis. We are able to constrain the parameter ℓ by providing a 95% confidence level upper limit of $\ell \lesssim 0.019$ AU, corresponding to $\ell \lesssim 0.47GM$.

use of such ellipse to set the initial conditions at a time t_0 that, without loss of generality, we fix to be the last time of apocentre passage for S2 in ∼2010.35.

Starting from such initial conditions, we integrate the geodesic equations numerically by means of a fourth-order Runge-Kutta scheme, over approximately two orbital periods, covering the time range that spans from 1990 to 2017. The use of an adaptive step size in our integration algorithm ensures control over the integration relative error that we fix to be $\lesssim 10^{-12}$. Finally, to compare our synthetic orbit with public data, we need to reconstruct the observable quantities for S2, i.e., the astrometric sky-projected position over time for an Earth-based observatory and the spectroscopically-measured line-of-sight velocity of the star. To this aim, we perform a geometric projection of the star's trajectory in the observer reference frame by means of the Thiele-Innes formulas computed from the three angular orbital elements: i, the orbital inclination; Ω, the longitude of the ascending node; ω, the argument of the pericenter. Additionally, for the spectroscopic observables, we take into account the post-Newtonian time-dilation effects on the light emitted by the star, namely the special-relativistic transverse and longitudinal Doppler effect and the general-relativistic gravitational redshift (for more details on how such quantities can be appropriately accounted for, we refer to previous works on the subject [266, 324]).

The orbital precession is naturally taken into account on our synthetic orbits since we directly integrate the fully-relativistic geodesic equation (I.4.17). As a matter of fact, our numerically-integrated orbit allows us to effectively validate the perturbative results for the precession angle by computing $\Delta\phi$ as the angle spanned by the star between two subsequent radial turning points. In Fig. I.4.5 we report a comparison between the numerically computed orbital precession (black solid line) for the S2 star as a function of the parameter ℓ, once all the other Keplerian elements have been fixed to the ones of S2, as derived from the analysis in Ref. [334] (based on a Newtonian orbital model). For $\ell = 0$ we obtain the Schwarzschild precession of 12.1 arcmin per orbital period observed in Ref. [335]. The linearly decreasing trend predicted by our perturbative analysis (dashed blue line) is confirmed up to a few tens of gravitational radii for the parameter ℓ, where our numerical predictions start to depart. Moreover, we are able to confirm numerically the prediction that the orbital precession becomes retrograde for $\ell \geq GM$.

I.4.5 Constraining the model with S2 orbital data

We have explored the parameter space of our orbital model for the S2 star, using the publicly available orbital data for S2. In particular, we have used near-infrared astrometric positions and radial velocities, coming from 25 years of uninterrupted monitoring of stellar orbits in the GC between ~ 1992 and ~ 2017, presented in [334]. These data do not cover the last S2 pericenter passage in May 2018 nor its subsequent motion observed by the GRAVITY Collaboration [335, 336]. Information provided by such portion of the orbit is crucial in the deed of constraining the gravitational field of SgrA* [337]. However, as demonstrated in previous works [266, 323], one can consider orbital data that do not cover the pericenter passage and, then, add as a single datapoint the precession measurement ($f_{\rm SP} = 1.10 \pm 0.19$ from [335], where $f_{\rm SP} = 0$ corresponds to a non-preceding ellipse from Newtonian gravity and $f_{\rm SP} = 1$ corresponds to the GR rate of orbital precession for the Schwarzschild spacetime).

Besides the knowledge of ℓ, the full orbital model requires the knowledge of the seven Keplerian parameters, (i.e., the time of pericenter passage, t_p; the orbital period, T; the semi-major axis, a, which implies leaving the mass of the central object, M, as a free parameter, as well; the eccentricity, e; the orbital inclination, i; the longitude of the ascending node, Ω; and the argument of the pericenter, ω), along with the observer galactocentric distance D and 5 reference frame parameters to take into account potential offsets and drifts of the astrometric reference frame [334, 338]. The 14-dimensional parameter space has been explored through a Markov-Chain Monte Carlo (MCMC) algorithm. More specifically, we employed the affine invariant ensemble samplers [339] implemented in [340]. For the sake of generality, we have employed uniform priors on all the Keplerian parameters of our orbital model corresponding to an interval centered on the best-fit values from [334], with amplitude being 10 times the corresponding observational uncertainty. For the reference frame parameters, on the other hand, we have taken priors from the independent analysis in [338]. The interval for the hair ℓ has been set heuristically between 0 and 5 AU, corresponding to over 100 gravitational radii of the central source. The likelihood adopted for our analysis is the following

$$\log\mathcal{L} = -\frac{1}{2}\sum_i \left[\left(\frac{\text{R.A.}_i - \text{R.A.}_{\text{obs},i}}{\sqrt{2}\sigma_{\text{R.A.},i}} \right)^2 + \left(\frac{\text{Dec}_i - \text{Dec}_{\text{obs},i}}{\sqrt{2}\sigma_{\text{Dec},i}} \right)^2 + \left(\frac{\text{RV}_i - \text{RV}_{\text{obs},i}}{\sqrt{2}\sigma_{\text{RV},i}} \right)^2 + \left(\frac{\Delta\phi/\Delta\phi_{\rm GR} - f_{\rm SP}}{\sqrt{2}\sigma_{f_{\rm SP}}} \right)^2 \right], \tag{I.4.22}$$

where R.A., Dec, and RV correspond to the sky-projected right ascension and declination of S2 and its radial velocity, respectively, while $\Delta\phi_{\rm GR}$ is the precession angle predicted for the Schwarzschild spacetime. The subscript *obs* represents the observed quantity at the i-th epoch, and the σ's are the corresponding observational uncertainties. As done in [323], the factors $\sqrt{2}$ in the denominators are introduced in order not to double count data points when considering the last term with the orbital precession (that has been derived with the same dataset).

The results of our posterior analysis are presented in Table I.4.1 (while a detailed, full posterior distribution is shown in Fig. I.6.1 of Appendix I.B) where the medians and the 68% confidence level intervals for each bounded parameter are reported. They agree within 1σ with previous results in the literature [334]. We are able to place an upper limit $\ell \lesssim 0.019$ AU (corresponding to $\ell \lesssim 0.47\,GM$) at 95% confidence level on the additional hair, whose marginalized posterior distribution is shown in Fig. I.4.5. Finally, we tested deviations from a Schwarzschild black hole using a mock catalog (for more details see [266]) that mirrors future GRAVITY observations of S2, and we proved the ability of GRAVITY to improve the upper limit on the hair ℓ derived in this chapter by a factor ~ 10.

Our results rule out most horizonless solutions but allow the existence of thermodynamically stable regular black holes, i.e., models with $0.254 \leq \ell/GM \leq 0.296$. Our results show that regular black holes with super-Planckian hair are not excluded by the S2 star observational data. The actual proof of the existence of our nonsingular black holes requires the measurement of ℓ-dependent deviations from GR, which could be detected by observations at the light-ring scale, e.g., with the black hole shadow or gravitational wave experiments. Nonetheless, we expect our

Parameter (units)	**Best-fit**	**Parameter (units)**	**Best-fit**
D (kpc)	8.24 ± 0.22	ω (°)	$65.23^{+0.78}_{-0.77}$
T (yr)	16.050 ± 0.028	x_0 (mas)	0.26 ± 0.16
t_p (yr)	2018.379 ± 0.024	y_0 (mas)	$-0.04^{+0.19}_{-0.20}$
a (as)	$0.1249^{+0.0011}_{-0.0010}$	$v_{x,0}$ (mas/yr)	$0.071^{+0.053}_{-0.052}$
e	0.8828 ± 0.0024	$v_{z,0}$ (mas/yr)	0.092 ± 0.062
i (°)	$134.42^{+0.48}_{-0.49}$	$v_{z,0}$ (km/s)	-3.4 ± 4.5
Ω (°)	$226.75^{+0.83}_{-0.82}$	$\bar{\ell}$	$\lesssim 0.47$ (95% c.l.)

Table I.4.1: Results of our posterior analysis for the 14 parameters of our orbital model for the S2 star. In particular, for the bounded parameters, we derived and reported the 68% confidence interval around the median of the marginalized distributions. On the other hand, for the parameter ℓ, our analysis yields an upper limit which, at 95% confidence level, is given by $\ell \lesssim 0.019$ AU (corresponding to the dimensionless value $\bar{\ell} \lesssim 0.47$).

model not to be a good approximation at that scale, and that a rotating generalization could be necessary.

Chapter I.5

Probing deviations from Kerr with superradiance

While nowadays observations agree with numerical simulations based on Einstein gravity, the current uncertainties on the measurements of the black-hole parameters leave room for alternatives. A possible framework is to describe this freedom by introducing suitable parametrized deviations from the Kerr geometry. The observed interval values for the black-hole mass M and angular momentum $J = aM$ can be therefore translated in an allowed range for the deviation parameters. Of course, we do not expect these deviations to be exceedingly large or they would be observable in the weak-field regime as well. But, for instance, one can consider non-negligible deviations from Kerr and obtain the same quasinormal frequencies. If the geometry of the spacetime is different from Kerr only in a small region near the would-be horizon, asymptotically the geometry would be barely distinguishable from Kerr, leaving a weak signature in the form of gravitational-wave echoes at late times [51, 341–345].

From this point of view, instead of testing a specific theory against general relativity case by case and/or a specific black-hole alternative, it could be more convenient to work in a model-independent framework describing the most generic black holes in any metric theory of gravity. The idea of this framework is similar to the parametrized post-Newtonian (PPN) formalism [11] but in this case, it is valid in the whole space outside the event horizon.

In Refs. [90, 165, 166], deviations from general relativity and the general-relativistic black-hole geometry are written in terms of an expansion in M/r being r some radial coordinate. Some coefficients are easily constrained with the PPN parameters, while a very large number of equally important coefficients remains undetermined in the near-horizon region, with the additional drawback of a lack of a hierarchy among them. Even if this formulation works well for small deviations from general relativity, it fails for, e.g., Einstein-dilaton-Gauss-Bonnet with large coupling constants [167].

A more robust general parametrization to describe, respectively, spherically symmetric and axisymmetric asymptotically flat black holes has been introduced by Konoplya, Rezzolla and Zhidenko in Refs. [91, 92], and tested to constrain deviations from the Kerr hypothesis with the iron-line method [168–170] and to produce black-hole shadows simulations [171, 172]. In this framework, deviations from general relativity and the Kerr metric are given again as an expansion whose coefficient values can be fixed from observations in the strong-gravity regime (close to the horizon) and in the post-Newtonian region (far from the black hole). This parametrization also allows for non-spherical deformations of the horizon, provides a faster convergence of the series, and typically requires a small number of parameters to approximate known solutions to the desired precision. Besides, there exists a hierarchy among the parameters.

A different perspective is to modify each mass and spin term in the Kerr metric and test whether the magnitude of the spacetime curvature matches with that predicted by general relativity [346]. More recently, the work of Ref. [165] has been extended to the most general stationary, axisymmetric and asymptotically flat spacetime with separable geodesic equations [347]. However, even if these parametrizations may depend on a large number of parameters to be fixed with data, it is natural to think that astrophysical observables—e.g., quasinormal frequencies, orbits of particles, accretion, parameters of the shadow, electromagnetic radiation—depend only on a few

of them [348].

A common feature of rotating spacetimes is the multifaceted phenomenon of superradiance [349–351]: in a gravitational system and under certain conditions, the scattering of radiation off absorbing rotating objects produces waves with amplitude larger than the incident one. For a monochromatic wave of frequency ω scattering off a body with angular velocity Ω, the superradiant condition is satisfied as long as $\omega < m\Omega$, being m the azimuthal number with respect to the rotation axis.

When rotating black holes are surrounded with matter, superradiance gives rise to exponentially growing modes, i.e., black-hole bombs [352, 353]. The scattering of massive fields produces a similar effect: the mass term can effectively confine the field giving rise to floating orbits and superradiant instabilities which extract rotational energy away from the black hole [354–356]. The observation or the absence of effects related to these instabilities can be used to impose bounds on the mass of ultralight bosons, see, e.g., Refs. [357–361].

Similarly to the Kerr black hole, Kerr-like spacetimes dissipate energy as well as any classical dissipative system, and the aim of this chapter is to investigate differences and analogies for these objects with respect to the superradiant scattering around Kerr black holes. We stress that these spacetimes are not solutions to the field equations of any specific gravitational theory, meaning that we can only study test fields propagating in these backgrounds while the gravitational-wave dynamics is excluded. However, in extended theories of gravity exact rotating solutions are difficult to derive and in some cases they are known only perturbatively in the spin parameter, or numerically. To our knowledge, there are no studies of superradiant amplification in these extended theories, neither for those which admit general-relativistic solutions [362, 363] but predict different dynamics.

In the most general parametrization, there is no reason to believe that the separability property of the Kerr metric is guaranteed, not even for the Klein–Gordon equation. In particular, the class of Kerr-like spacetimes which allows for the separation of variables in the Klein–Gordon and Hamilton–Jacobi equations has been derived in Ref. [364], which is a subclass of the Johannsen metrics [165]. In this chapter we show that, under given conditions, a subclass of the metrics presented in Ref. [364] also allows for the separation of variables in the Maxwell equation.

The results presented in this chapter are mostly relative to the Konoplya-Zhidenko black hole [365], which introduces a single extra parameter. Despite its simplicity, this model preserves a lot of features of the Kerr spacetime: the asymptotic properties, the post-Newtonian expansion coefficients, the relation between quadrupole moment and mass, the spherical horizon, and the mirror symmetry. Yet, it allows for significant differences in the near-horizon region [366–368].

The scope of this chapter is twofold: first we analyze the structure of the Konoplya-Zhidenko spacetime, and second we study superradiant scattering of test fields. In particular, the chapter is organized as follows. In Section I.5.1 we review the family of spacetimes which admits separability of the perturbative equations for massless spin-0 and spin-1 fields, with a particular focus on the Konoplya-Zhidenko rotating black hole. In Section I.5.2 we present our results regarding the superradiant emission in the Konoplya-Zhidenko spacetime for massless and massive bosonic test fields. In Appendix I.E we derive the angular and radial equations for a general non-Kerr black-hole parametrization and study their boundary conditions. In Appendix I.F we provide helpful formulas for the Konoplya-Zhidenko spacetime, namely the Einstein tensor, the geodesic equations, and the four-velocity of a zero-angular-momentum observer. In Appendix I.G we study the instability of the Konoplya-Zhidenko black hole against massive scalar fields in the low-frequency, small-mass, and small-deformation limit. Throughout this chapter, we use $G = c = 1$ units.

I.5.1 Deformed Kerr spacetimes and the Konoplya-Zhidenko black hole

The metric of a generic axially symmetric, stationary, and asymptotically flat spacetime can be written as

$$\mathrm{d}s^2 = -\frac{N^2 - W^2\sin^2\theta}{K^2}\,\mathrm{d}t^2 - 2Wr\sin^2\theta\,\mathrm{d}t\,\mathrm{d}\varphi + K^2 r^2\sin^2\theta\,\mathrm{d}\varphi^2 + \frac{\Sigma}{r^2}\left(\frac{B^2}{N^2}\,\mathrm{d}r^2 + r^2\,\mathrm{d}\theta^2\right), \tag{I.5.1}$$

where N, W, K, Σ and B are in general functions of r and θ. In this chapter, we focus on deformed Kerr spacetimes which possess Kerr-like symmetries and admit separable Klein-Gordon equations for test fields [364]. As in Ref. [364], we are not interested in the general conditions for the separability of variables, which are related to the symmetry of the background and the choice of appropriate coordinates. Being our pragmatic objective to test strong-gravity effects in an asymptotically flat and axisymmetric spacetime describing a Kerr-like black hole, we can simplify the above spacetime metric leaving only three arbitrary functions of the radial coordinate, so that

$$B(r,\theta) = R_B(r), \qquad \Sigma(r,\theta) = r^2 R_\Sigma(r) + a^2\cos^2\theta, \tag{I.5.2a}$$

$$W(r,\theta) = \frac{a R_M(r)}{\Sigma(r,\theta)}, \qquad N^2(r,\theta) = R_\Sigma(r) - \frac{R_M(r)}{r} + \frac{a^2}{r^2}, \tag{I.5.2b}$$

$$K^2(r,\theta) = \frac{1}{\Sigma(r,\theta)}\left[r^2 R_\Sigma^2(r) + a^2 R_\Sigma(r) + a^2\cos^2\theta\, N^2(r,\theta)\right] + \frac{a\,W(r,\theta)}{r}. \tag{I.5.2c}$$

For further convenience, we define $\Delta \equiv r^2 N^2 = r^2 R_\Sigma - R_M r + a^2$ and we observe that for this class of spacetimes the event horizon is defined by the largest positive root of $\Delta = 0$.

Asymptotic flatness and current PPN parameters imply $R_M \to 2M + O\left(1/r^2\right)$ as $r \to \infty$. With a suitable change of the radial coordinate it is possible to set R_B or R_Σ to 1, so only two of the three radial functions are independent. The Kerr metric is recovered for $R_\Sigma = R_B = 1$ and $R_M = 2M$. Eq. (I.5.2) describe a Petrov D spacetime, and as a consequence, the Hamilton–Jacobi equation is separable with a generalized Carter constant [364]—see also Appendix I.F. In Appendix I.E, we show that the subclass of this spacetime such that $R_B = 1$ and $R_\Sigma = (1+\xi/r)^2$ also admits separable Maxwell equations for test fields.

A minimal deformation for the Kerr spacetime was introduced by Konoplya and Zhidenko in Ref. [365] and can be obtained from Eq. (I.5.2) by setting $R_\Sigma = R_B = 1$ and $R_M = 2M + \eta/r^2$. In the following, we consider this background geometry, although we expect the results to hold, though with some differences, for the whole class of models.

I.5.1.1 Event horizons and causal structure

For the Konoplya-Zhidenko metric the event horizon radius is given by the largest positive real root of $\Delta = r^2 - 2Mr + a^2 - \eta/r = 0$, which in general admits three (possibly complex-valued) solutions

$$r_k = \frac{2M}{3} + \frac{2}{3}\sqrt{4M^2 - 3a^2}\cos\left(\beta - \frac{2k\pi}{3}\right), \tag{I.5.3}$$
$$\beta = \frac{1}{3}\cos^{-1}\frac{16M^3 - 18Ma^2 + 27\eta}{2\left(4M^2 - 3a^2\right)^{3/2}}, \quad k = 0,1,2\,.$$

We immediately notice that the Kerr limit $\eta \to 0$ is not continuous, as in looking for the roots of $\Delta = 0$ we pass from solving a cubic to a quadratic equation. Nevertheless, for $a < M$ and in the small η/M^3 limit, we have

$$r_0 = r_+ + \frac{\eta}{r_+(r_+ - r_-)} - \frac{\eta^2(2r_+ - r_-)}{r_+^3(r_+ - r_-)^3} + O\left(\eta^3\right), \tag{I.5.4}$$

where $r_\pm = M \pm \sqrt{M^2 - a^2}$ are the radii of the event and Cauchy horizon for the Kerr spacetime. For $|\eta|/M^3 \lesssim 7/100$ the difference between r_0 calculated as a linear correction to r_+ and the exact value as in Eq. (I.5.3) is less than 1% for values of $a \lesssim 0.9M$. Eq. (I.5.4) does not apply in the extremal limit, which must be treated separately, as in this case the leading order correction is $O\left(\eta^{1/2}\right)$ and r_0 is given by

$$r_0 = M + \sqrt{\frac{\eta}{M}} - \frac{\eta}{2M^2} + O\left(\eta^{3/2}\right). \tag{I.5.5}$$

Under these assumptions, the compactness of the spacetime for $a < M$ is

$$\mathcal{C} = \mathcal{C}_{\rm Kerr}\left(1 - \frac{\eta}{r_+^2(r_+ - r_-)}\right) + O\left(\eta^2\right), \tag{I.5.6}$$

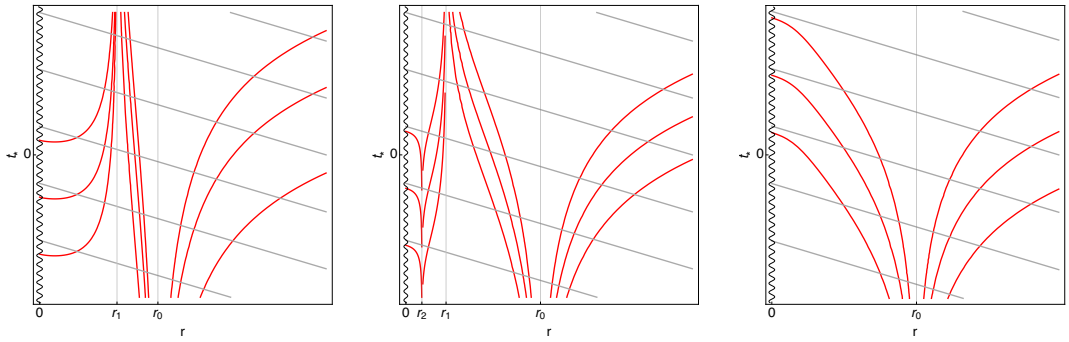

(a) Region (II) with $\eta_- < \eta < 0$. (b) Region (II) with $0 < \eta < \eta_+$. (c) Region (III) with $\eta \geq \eta_+$.

Figure I.5.1: Light-cone structure in advanced coordinates for a Konoplya-Zhidenko black hole below the Kerr bound.

being $\mathcal{C}_{\rm Kerr} = M/r_+$ the compactness of the Kerr black hole, while in the extremal case ($\mathcal{C}_{\rm Kerr} = 1$)

$$\mathcal{C} = 1 - \sqrt{\frac{\eta}{M^3}} + \frac{3\eta}{2M^3} + O\left(\eta^{3/2}\right). \tag{I.5.7}$$

Eq. (I.5.6) indicates that positive (negative) values of η corresponds to less (more) compact configurations.

For $a < M$, instead of working with η, deviations from the Kerr spacetime can be parametrized in terms of the quantity δr, such that the position of the event horizon can be written as $r_0 = r_+ + \delta r$—cfr. Eq. (I.5.4), although δr can account for large values of η/M^3 and it is not limited to a perturbative expansion. This writing is obviously coordinate-dependent but since we are using asymptotic Boyer–Lindquist coordinates, a significant deviation from Kerr should be similarly acknowledged by different observers.

Differently from the Kerr case, in the Konoplya-Zhidenko spacetime there exists no maximum value for a beyond which the spacetime always describes a naked singularity. As a always enters quadratically in Eq. (I.5.3), without loss of generality, in the following we consider positive a.

Although this spacetime belongs to a class of metrics which are constructed to describe the spacetime *outside* the event horizon, it is instructive to explore the implications *inside* the horizon. This should be taken with great care and interpreted prudently, but it might give insights about what a small difference at infinity entails about the structure of the spacetime inside the horizon. This being said, in what follows we do not limit our analysis to the largest positive real root of $\Delta = 0$ but we give a more comprehensive discussion.

The Ricci scalar of the Konoplya-Zhidenko metric is non-vanishing, $R = 2\eta/\left[r^3\left(r^2 + a^2\cos^2\theta\right)\right]$, from which we infer that $r = 0$ is a physical singularity.

To classify the solutions of $\Delta = 0$ it is helpful to introduce

$$\eta_\pm = \frac{2}{27}\left[9Ma^2 - 8M^3 \pm \left(4M^2 - 3a^2\right)^{3/2}\right], \tag{I.5.8}$$

and to define three separate parameter regions as (I) $\eta < \eta_-$; (II) $\eta_- \leq \eta \leq \eta_+$; (III) $\eta \geq \eta_+$. Then we sort configurations according to the value of the spin parameter: *below the Kerr bound*, $a < M$; *highly spinning* $M \leq a < a_* \equiv 2M/\sqrt{3}$; and *ultra spinning* $a \geq a_*$.

Below the Kerr bound: In region (I), there is only one real solution given by r_2 in Eq. (I.5.3) which is always negative and hence the spacetime describes a naked singularity. In region (II), the equation $\Delta = 0$ admits three real solutions, and the event horizon is r_0. The root r_1 is always positive while r_2 is negative (positive) for $\eta_- < \eta < 0$ ($0 < \eta < \eta_+$). In particular for $\eta = \eta_-$, $r_0 = (1/3)(2M + \sqrt{4M^2 - 3a^2})$,[1] while for $\eta = \eta_+$, $r_0 = (2/3)(M + \sqrt{4M^2 - 3a^2})$. In region (III), r_0 is the only positive-definite real root.

[1] Notice, however, that $\partial r_0/\partial\eta$ diverges as $\eta \to \eta_-$.

Highly spinning: For $a = M$ and $\eta > 0$ the event horizon is $r_0 = (2/3)\left[1 + \cos\left(\frac{1}{3}\arccos\left(27\eta/2 - 1\right)\right)\right]$. The other solutions r_1 and r_2 are generically complex-valued but for $0 < \eta < 4M^3/27$ the imaginary part goes to zero and the real part is positive. For $M < a < a_*$, η_- is positive and in the subregion of region (I) such that $0 < \eta < \eta_-$, the only real positive root is r_2. In region (II) the three real roots are positive and the event horizon is given by r_0, while in region (III) the only real solution is r_0. Notice that for each value of η in the range $0 < \eta < 8M^3/27$, there exists a value of a

$$a_+ = \frac{M}{\sqrt{3}}\left(1 + 2\sqrt{1 + \frac{27\eta}{M^3}}\cos\beta_+\right)^{1/2}, \tag{I.5.9}$$

with

$$\beta_+ = \frac{1}{3}\cos^{-1}\frac{8M^6 - 540\eta M^3 - 729\eta^2}{8\left(M^4 + 27\eta M\right)^{3/2}},$$

for which the largest root of $\Delta = 0$ passes from r_0 to r_2 discontinuously. Alternatively, for a fixed a, the largest root of $\Delta = 0$ passes from r_2 to r_0 at $\eta = \eta_-$. Depending on the specific values of the parameters the ratio r_0/r_2 can be of several orders of magnitude, and the compactness of the black hole changes accordingly.

Ultra spinning: For the particular case $a = a_*$ with $\eta > 0$, $r_0 = 2M/3 + \sqrt[3]{\eta - 8M^3/27}$ and r_1 and r_2 are complex-valued unless $\eta = 8M^3/27$, for which $r_0 = r_1 = r_2 = 2M/3$. For $a > a_*$, $\eta_\pm$ in Eq. (I.5.8) become complex-valued and independently on the value of η, r_0 and r_2 are complex-valued, while r_1 is positive for $\eta > 0$.

The light-cone structure of these configurations can be richer and significantly different than that of a Kerr black hole. As an example, consider a Konoplya-Zhidenko black hole below the Kerr bound. Following a standard procedure, we define advanced coordinates and we plot null rays in Fig. I.5.1, where $t_* = t + r - r_*$ being r_* a tortoise coordinate defined by $\mathrm{d}r_*/\mathrm{d}r = (r^2 + a^2)/\Delta$. In the external regions, i.e., for $r > r_0$, we observe a peeling structure, typical of black-hole horizons. In region (II), for $\eta_- < \eta < 0$, the light-cone structure is nearly similar to that of a Kerr black hole, there are an outer and an inner horizon and a timelike singularity. In region (II) but for $0 < \eta < \eta_+$, a null trajectory encounters a black-hole horizon, a white-hole-like horizon, and then again a black-hole-like horizon to eventually reach a spacelike singularity. In region (III) there is only one horizon and the light-cone structure looks like the Schwarzschild one with a spacelike singularity.

For further convenience, we introduce the angular velocity $\Omega_k = -g_{t\varphi}/g_{\varphi\varphi}|_{r=r_k}$ at the horizon reads

$$\Omega_k = \frac{a}{r_k^2 + a^2} = \frac{a}{2Mr_k + \eta/r_k}, \tag{I.5.10}$$

where the value of k depends on the specific values of the black-hole parameters.

I.5.1.2 Ergoregions

An ergosurface is a static limit surface, i.e., no static observer is allowed beyond this surface. Ergosurfaces in these black-hole spacetimes are defined as the roots of the equation $g_{tt} = 0$, or equivalently $r^2 - 2Mr + a^2\cos^2\theta - \eta/r = 0$, which read

$$r_k^{\rm erg} = \frac{2M}{3} + \frac{2}{3}\sqrt{4M^2 - 3a^2\cos^2\theta}\,\cos\left(\beta^{\rm erg} - \frac{2k\pi}{3}\right), \tag{I.5.11}$$

$$\beta^{\rm erg} = \frac{1}{3}\cos^{-1}\frac{27\eta + 16M^3 - 18Ma^2\cos^2\theta}{2\left(4M^2 - 3a^2\cos^2\theta\right)^{3/2}}, \quad k = 0, 1, 2\,.$$

For configurations below the Kerr bound in regions (II) and (III), the location of the ergosurface is $r_0^{\rm erg}$ (see Fig. I.5.2). For highly spinning configurations, the ergosurface is again $r_0^{\rm erg}$ in regions

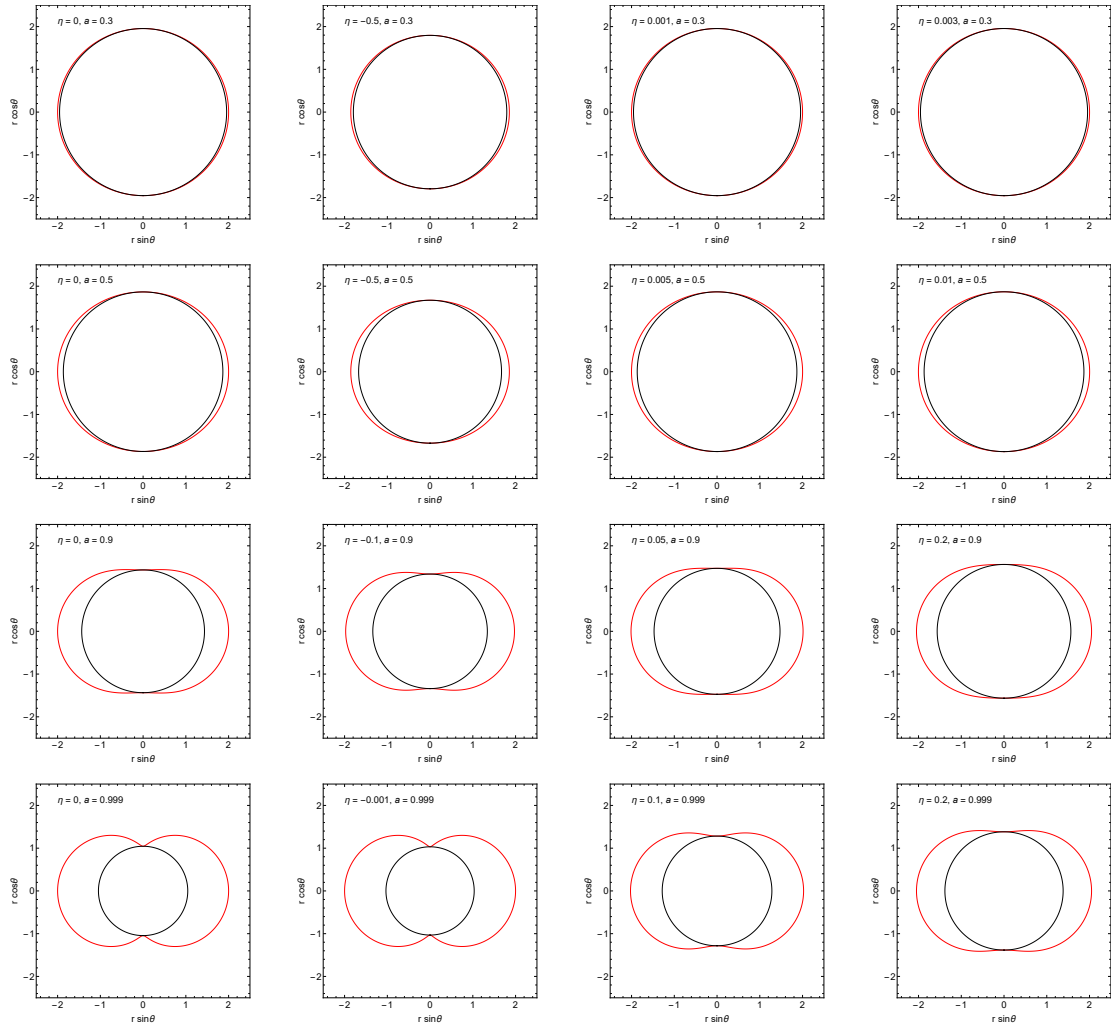

(a) Kerr BH ($\eta = 0$). (b) Region (I) ($\eta_- < \eta < 0$). (c) Region (II) ($0 < \eta < \eta_+$). (d) Region (III) ($\eta \geq \eta_+$).

Figure I.5.2: Position of the event horizon and of the surface of the ergosphere for a Kerr and a Konoplya-Zhidenko black hole and for different values of the deformation parameter and in the three different regions of the parameter space.

(II) and (III), but it is piecewise and non-continuous in region (I): it is given by $r_0^{\rm erg}$ in the angular interval $[\theta_1, \theta_2]$ and $r_2^{\rm erg}$ in the complementary interval, $[0, \theta_1) \cup (\theta_2, \pi]$ where $\theta_{1,2}$ ($\theta_2 = \pi - \theta_1$) are the solutions of

$$\eta = \frac{2}{27}\left[9Ma^2\cos^2\theta - 8M^3 - \left(4M^2 - 3a^2\cos^2\theta\right)^{3/2}\right], \tag{I.5.12}$$

once the values of M, a and η are fixed; the maximum value of θ_1 is $\cos^{-1}(M/a)$, attained for $\eta \to 0^+$. This means that when passing from a configuration in region (I) to one in region (II), the volume between the ergosurface and the event horizon, the ergoregion, can change dramatically.

Notice that for configurations below the Kerr bound and highly spinning and values of η in regions (II) and (III) the volume of the ergoregion is maximum for $\eta = \eta_-$ and it decreases for larger values.

For the particular case $a = a_*$, the location of the ergosurface is $r_0^{\rm erg}$ as long as $\eta \geq 8M^3/27$, but piecewise and discontinuous for $0 < \eta < 8M^3/27$ as described above. For superspinning configurations, let θ_* the smallest root of $\cos^2\theta = a_*^2/a^2$. For $0 < \eta < 8M^3/27$ the ergoregion is piecewise and discontinuous: it is given by $r_1^{\rm erg}$ for $[0, \theta_*) \cup (\pi - \theta_*, \pi]$, $r_2^{\rm erg}$ for $[\theta_*, \theta_1) \cup (\theta_2, \pi - \theta_*]$, and $r_0^{\rm erg}$ for $[\theta_1, \theta_2]$ where $\theta_{1,2}$ are again the solutions of Eq. (I.5.12). For $\eta \geq 8M^3/27$ the ergoregion

is still piecewise but no longer discontinuous: it is given by $r_0^{\rm erg}$ in the interval $[\theta_1, \theta_2]$ and $r_1^{\rm erg}$ in the complementary interval $[0, \theta_1) \cup (\theta_2, \pi]$.

The fact that superspinning configuration for some values of the deformation parameter can have a piecewise and non-continuous ergoregion, i.e., no longer an ergosurface, poses a serious problem on the viability of these particular configurations as black-hole mimickers. We expect these particular solutions to be dynamically unstable, but this analysis is beyond the scope of this thesis and is left for future work.

I.5.1.3 Photon orbits

Photon orbits for the Konoplya-Zhidenko black hole can be studied starting from the geodesic equations derived in Appendix I.F. In particular, the radial null geodesic in the equatorial plane is

$$\dot{r}^2 = E^2 + \frac{a^2E^2 - L^2}{r^2} + \frac{2M\left(L - aE\right)^2}{r^3} + \frac{\eta\left(L - aE\right)^2}{r^5}\,, \tag{I.5.13}$$

where the dot indicates derivative with respect to an affine parameter, while E and L are, respectively, the energy and the angular momentum of the photon, although it is more convenient to characterize the geodesic by the impact parameter $D \equiv L/E$.

The radius of photon orbits r_c and its corresponding impact parameter D_c are determined by Eq. (I.5.13) and its derivative evaluated at $r = r_c = \text{const}$. The problem is well-known for the Kerr black hole [333], but the term introduced by the deformation parameter η makes the equation no longer amenable to analytical methods for all values of L and E. Therefore, we decide to adopt a small η/M^3 approximation and work below the Kerr bound. This guarantees some level of analyticity and exploits known results to be compared with. In what follows, the sign of a is important to distinguish between direct ($a > 0$) and retrograde ($a < 0$) orbits, so uniquely for the remainder of this subsection we allow $a \in [-M, M]$.

In practice, we expand the light ring radius r_c and the impact parameter D_c around the Kerr values in powers of η/M^3. Here we report the leading-order corrections for the most familiar cases, i.e. $a = -M,\ 0,\ M$. When $a = -M$ we find

$$r_c \simeq 4M + \frac{13\eta}{72M^2}, \quad D_c \simeq 7M + \frac{\eta}{6M^2}\,. \tag{I.5.14}$$

In the non-rotating limit, i.e., for $a = 0$, we get

$$r_c \simeq 3M + \frac{5\eta}{18M^2}, \quad D_c \simeq 3\sqrt{3}M + \frac{\sqrt{3}\eta}{6M^2}\,. \tag{I.5.15}$$

For $a = M$ the leading order correction is milder,

$$r_c \simeq M + \sqrt{\frac{4\eta}{3M}}, \quad D_c \simeq 2M + \sqrt{\frac{3\eta}{M}}\,. \tag{I.5.16}$$

For general values of the deformation parameter, and to allow the spin parameter above the Kerr bound, the radius of the photon orbits and the corresponding impact parameter can be determined numerically. For $|\eta|/M^3 \lesssim 1/10$, r_c and D_c have maximum deviations from the Kerr values, respectively, of $\sim 3\%$ and $\sim 4\%$ for $0 \leq a < 0.9M$, which reduce to less than 1% for $-M \leq a < 0$. We have also checked that the light ring is always outside the horizon for $\eta > \eta_-$ and $a \leq a_*$.

I.5.1.4 The Konoplya-Zhidenko black hole as a solution of general relativity

Although these parametrically deformed metrics are built *not* to be exact solutions to any gravitational theory,[2] it is an interesting exercise to figure out what kind of matter distribution one would need in general relativity to obtain the Konoplya-Zhidenko black hole as an exact solution, and which energy conditions must be violated.

[2] In Refs. [369, 370] it is shown that the Konoplya-Zhidenko metric is an exact solution of a (non-analytical) mixed scalar-$f(R)$ gravitational theory.

We start by defining the stress-energy tensor out of the Einstein tensor, i.e., $T_{\mu\nu} = G_{\mu\nu}/8\pi$, whose non-zero components are given in Appendix I.F. To characterize the would-be matter content of this spacetime, a first possibility is to compute the eigenvalues of T^{μ}_{ν}. In particular, we identify the energy density with the opposite of the eigenvalue relative to the timelike eigenvector,[3]

$$\rho = -\frac{\eta}{4\pi r\left(r^2+a^2\cos^2\theta\right)^2}\,. \tag{I.5.17}$$

This matter distribution is concentrated close to the singularity and mainly along the equatorial plane, but it extends beyond the event horizon although it decays quite fast for large values of the radius.

Alternatively, the distribution of energy can be characterized in an observer-dependent way by analysing the contraction of the stress-energy tensor with the velocity of a physical observer, i.e., $\rho = T_{\mu\nu}u^{\mu}u^{\nu}$. In view of the angular distribution of Eq. (I.5.17), for simplicity, consider a zero-angular-momentum observer (ZAMO) in the equatorial plane, whose four-velocity in given in Appendix I.F. It can be verified that

$$\rho_{\rm ZAMO}|_{\theta=\pi/2} = -\frac{\eta\left(2r^2+5a^2\right)}{8\pi r^7}\,. \tag{I.5.18}$$

Inspection of Eqs. (I.5.17) and (I.5.18) reveals that the sign of these energy densities is purely determined by the sign of η: negative (positive) values of η correspond to a positive (negative) energy density; assuming $a < M$ and in the small η/M^3 regime, they also correspond to configurations more (less) compact than a Kerr black hole with the same spin—cfr. Eq. (I.5.6). These results further imply that, for positive values of η, this matter distribution violates—at least—the weak energy condition.

Within this effective description, it is possible to relate the above matter distribution to the flux contribution to the Komar mass [371],

$$2\int_{\Sigma}\mathrm{d}^3y\,\sqrt{h}\left(T_{\mu\nu}-\frac{1}{2}\,T g_{\mu\nu}\right)n^{\mu}\xi^{\nu}, \tag{I.5.19}$$

where Σ is a spacelike hypersurface that extends from the event horizon to infinity, n^{μ} the unit normal, h the determinant of the induced metric on Σ, T the trace of the stress-energy tensor, and ξ^{ν} the timelike Killing vector. Explicit evaluation of Eq. (I.5.19) indicates that this contribution can be of the same magnitude of M for some specific values of the black-hole parameters, although for configurations below the Kerr bound it is typically of order $\pm 20\%$ of M, where the sign depends on the sign of η. It would be interesting to explore whether this amount of putative matter can be used to model "dirty" black holes as well.

Configurations on the edge of $\eta = \eta_{-}$, i.e., configurations between regions (I) and (II)—which describe black holes for $a > M$—seem particularly unstable. As the radius of the event horizon and the volume of the ergoregion can change abruptly and widely, one passes from small to enormous violations of the energy conditions. Together with the odd piecewise and disconnected ergosurface for some values of the parameter space, this might suggest that not every configuration can mimic actual Kerr black holes.

Nonetheless, if we drop the assumption that general relativity is the correct gravitational theory, the discussion above might be extremely different.

I.5.2 Superradiance from the Konoplya-Zhidenko black hole

In the Konoplya-Zhidenko background, the scalar ($s = 0$) and electromagnetic ($s = \pm 1$) wave equations are separable with the angular part described by the spin-weighted spheroidal harmonics equation and the radial part by

$$\Delta^{-s}\frac{\mathrm{d}}{\mathrm{d}r}\left(\Delta^{s+1}\frac{\mathrm{d}R_s}{\mathrm{d}r}\right)+\left(\frac{K^2-2\mathrm{i}s\left(r-M+\frac{\eta}{2r^2}\right)K}{\Delta}+4\mathrm{i}s\omega r-\lambda-\frac{s(s+1)\eta}{r^3}\right)R_s=0\,, \tag{I.5.20}$$

[3] Being $v_t = \{a + r^2/a, 0, 0, 1\}$, $v_r = \{0, 1, 0, 0\}$, $v_\theta = \{0, 0, 1, 0\}$, and $v_\varphi = \{a\sin^2\theta, 0, 0, 1\}$ the eigenvectors of T^{μ}_{ν}, the timelike vector is v_t for $\Delta > 0$ and v_r otherwise.

where $K \equiv (r^2+a^2)\omega - am$ and $\lambda \equiv A + a^2\omega^2 - 2ma\omega$, being A the eigenvalue of the angular equation, ω the frequency of the perturbation and m its azimuthal number. The angular eigenvalue is also characterized by the harmonic number l. As discussed in Appendix I.E, the physical information contained in the solution with spin-weight s is equivalent to that with spin-weight $-s$. This property will be particularly important when computing the energy fluxes of electromagnetic waves at infinity.

I.5.2.1 Boundary conditions

To integrate Eq. (I.5.20) we need to supply it with boundary conditions. We first introduce a tortoise-like coordinate $\mathrm{d}r_*/\mathrm{d}r \equiv (r^2+a^2)/\Delta$ and a new radial function $Y_s(r) = \sqrt{r^2+a^2}\,\Delta^{s/2}\,R_s(r)$ such that the radial equation becomes

$$\frac{\mathrm{d}^2 Y_s}{\mathrm{d}r_*^2} + \left(\frac{K^2 - 2\mathrm{i}s\left(r - M + \frac{\eta}{2r^2}\right)K + (4\mathrm{i}rs\omega - \lambda)\Delta}{\left(r^2+a^2\right)^2} - \frac{\mathrm{d}G}{\mathrm{d}r_*} - G^2 - \frac{s(s+1)\eta\Delta}{r^3\left(r^2+a^2\right)^2} \right) Y_s = 0, \tag{I.5.21}$$

where $G = r\Delta/(r^2+a^2)^2 + s\Delta'/2(r^2+a^2)$. Asymptotically ($r \to \infty$), Eq. (I.5.21) becomes

$$\frac{\mathrm{d}^2 Y_s}{\mathrm{d}r_*^2} + \left(\omega^2 + \frac{2\mathrm{i}s\omega}{r}\right) Y_s \simeq 0\,, \tag{I.5.22}$$

whose solutions are $Y_s \sim r^{\pm s}\mathrm{e}^{\mp \mathrm{i}\omega r_*}$ where the plus (minus) sign refers to outgoing (ingoing) waves.

Near the event horizon r_0 ($r_* \to -\infty$), let $k \equiv \omega - m\Omega_0$, Ω_0 being defined in Eq. (I.5.10), then Eq. (I.5.21) becomes

$$\frac{\mathrm{d}^2 Y_s}{\mathrm{d}r_*^2} + (k - \mathrm{i}s\sigma)^2\, Y_s \simeq 0\,, \quad \sigma = \frac{a^2 + r_0(3r_0 - 4M)}{2r_0\left(r_0^2 + a^2\right)}\,, \tag{I.5.23}$$

and the purely ingoing solution at the horizon is $Y_s \sim \exp\left[-\mathrm{i}\left(k - \mathrm{i}s\sigma\right) r_*\right] \sim \Delta^{-s/2}\mathrm{e}^{-\mathrm{i}kr_*}$.

I.5.2.2 Amplification factors

The asymptotic solutions to Eq. (I.5.22) can be used to define the energy fluxes of bosonic fields at infinity. Since the Konoplya-Zhidenko spacetime shares the same asymptotic behaviour and symmetries of the Kerr spacetime, the derivation of this section is very similar to what happens for Kerr [372].

Consider an incident wave of amplitude $\mathcal{I}$ from infinity producing a reflected wave of amplitude $\mathcal{R}$, the asymptotic solution to Eq. (I.5.22) can be written as

$$Y_s \sim \mathcal{I}\,\mathrm{e}^{-\mathrm{i}\omega r_*} r^s + \mathcal{R}\,\mathrm{e}^{\mathrm{i}\omega r_*}/r^s\,. \tag{I.5.24}$$

The total energy flux at infinity per unit solid angle can be computed out of the stress-energy tensor of the test fields as

$$\frac{\mathrm{d}^2 E}{\mathrm{d}t\,\mathrm{d}\Omega} = \frac{\mathrm{d}^2}{\mathrm{d}t\,\mathrm{d}\Omega}\left(E_{\rm in} + E_{\rm out}\right) = \lim_{r\to\infty} r^2 T^r_t\,, \tag{I.5.25}$$

where the ingoing and outgoing fluxes $\mathrm{d}E_{\rm in/out}/\mathrm{d}t$ are proportional, respectively, to $|\mathcal{I}|^2$ and $|\mathcal{R}|^2$ [372]. When energy is extracted from the black hole, the flux of energy through the horizon is negative and energy conservation implies $\mathrm{d}E_{\rm in}/\mathrm{d}t < \mathrm{d}E_{\rm out}/\mathrm{d}t$. It is then possible to define the quantity $Z_{s,l,m} = \mathrm{d}E_{\rm out}/\mathrm{d}E_{\rm in} - 1$ which gives the amplification or absorption factor for bosonic waves of spin-weight s and quantum numbers (l,m) off a black hole.

In our case of interest, the amplification factors are

$$Z_{0,l,m} = \frac{|\mathcal{R}|^2}{|\mathcal{I}|^2} - 1\,, \quad Z_{\pm 1,l,m} = \frac{|\mathcal{R}|^2}{|\mathcal{I}|^2}\left(\frac{16\omega^4}{B^2}\right)^{\pm 1} - 1\,, \tag{I.5.26}$$

where $B^2 = [\lambda + s(s+1)]^2 + 4ma\omega - 4a^2\omega^2$. Notice that the expressions in Eq. (I.5.26) are the same as for Kerr as the asymptotic behavior and the symmetries of the Konoplya-Zhidenko black hole are the same. However, the deformation parameter η changes the geometry of the near-horizon region and is responsible for a different amplification factor, as shown in the next section.

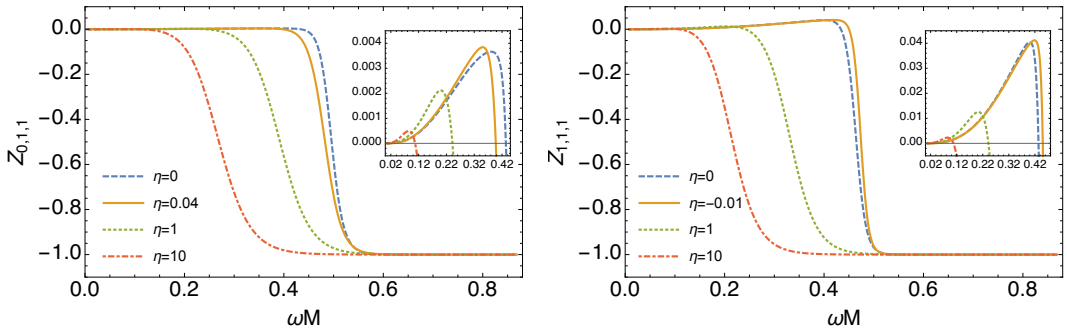

Figure I.5.3: Spectra of the amplification factor for a scalar (left panel) and electromagnetic (right panel) field with $l = m = 1$ off a Konoplya-Zhidenko black hole with $a = 0.99M$ for selected values of η in units of M^3. Inset: Zoom in the superradiant region.

I.5.2.3 Numerical results

For general ω we need to numerically integrate the angular and radial equations. Our numerical routine works as follows. For each value of the spin-weight s, the quantum numbers (l, m) and $a\omega$, we first determine the angular eigenvalue using the Leaver method [373]. Second, fixed a value for η, we integrate Eq. (I.5.21) from the horizon onwards until a sufficiently large radius. Then we compare our numerical solution and its radial derivative to the asymptotic behavior in Eq. (I.5.24) and its derivative to extract the coefficients $\mathcal{I}$ and $\mathcal{R}$. Finally, we compute the amplification factor using Eq. (I.5.26). To increase the accuracy of this numerical procedure, we consider a higher-order expansion near the horizon and in the asymptotic region which reduces to those reported in the previous section at the leading order. The routine is repeated for several values of the frequency (typically) in the interval $0 < \omega < 2m\Omega_0$. Modes with $m \leq 0$ are not superradiant and as a consequence of the symmetries of the angular and radial equation, the amplification factor is symmetric under $Z_{s,l,m}(\omega) = Z_{s,l,-m}(-\omega)$ we can consider positive frequencies only.

We now define our working assumptions for what follows. We allow the deformation parameter in the range $\eta \geq \eta_-$ and we mainly exclude superspinning configurations from our investigation, i.e., we focus on black holes below the Kerr bound and highly spinning in regions (II) and (III) introduced above. This has a practical advantage: the event horizon and the ergosurface are always given by r_0 and $r_0^{\rm erg}$. Despite the lack of observational evidence for rotating black holes beyond the Kerr bound [374], it cannot be excluded that some highly spinning objects can be produced in high-energy astrophysical phenomena that dynamically evolve in less spinning configurations. Hence it makes sense to explore a bit this parameter region.

Some of our results are presented in Fig. I.5.3 and more are available online [375]. Both for scalar and electromagnetic fields with quantum numbers $l = m = 1$, scattered off a black hole with spin $a = 0.99M$, we observe in the insets of Fig. I.5.3 that the position of the maximum of the amplification factor is close to the superradiant threshold $\omega = m\Omega_0$ where the curve becomes very steep, as in the Kerr case.

In absolute values, the maximum amplification factor is about 0.4% and 4.4% for scalar and electromagnetic waves, as for Kerr. However, in the left panel of Fig. I.5.4 we notice that for scalar waves scattering off a deformed black hole with $\eta/M^3 \simeq 4/100$ the maximum amplification factor is about 6% larger than in the non-deformed Kerr case, while for electromagnetic waves, we observe a maximum amplification factor roughly 1% larger than in the Kerr case for $\eta/M^3 \simeq -1/100$.

These values of η/M^3 are not universal but depend on the value of a/M. For smaller values of a/M, the maximum value of $Z_{s,l,m}$ gets smaller, the position of the peak moves towards smaller values of η/M^3 and the frequency range for which the amplification factor is positive shrinks. For configurations with higher spin, say at the Thorne limit $a = 0.998M$, the scalar (electromagnetic) amplification factor can be up to 15% (1%) larger than in the Kerr case. This bigger amplification factor does not mean that these deformed spacetimes are more superradiant

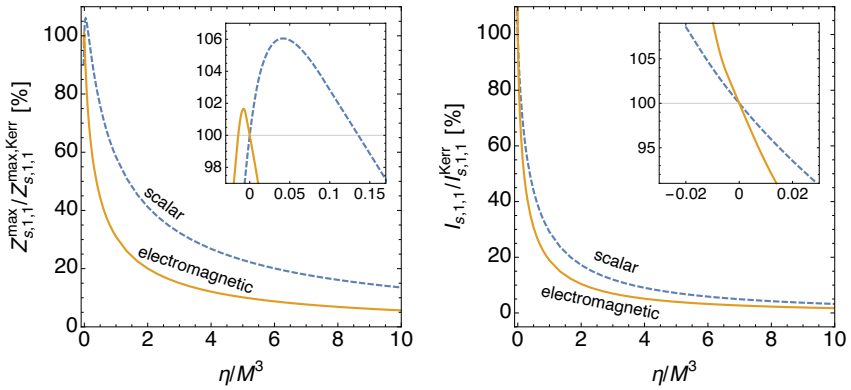

Figure I.5.4: Maximum value of the amplification factor $Z_{s,1,1}$ (left panel) and integral of the superradiant spectrum $I_{s,1,1}$ (right panel) for a scalar and electromagnetic field with $l = m = 1$ as functions of η, normalized to the maximum value in the Kerr case, i.e., $\eta = 0$, for $a = 0.99M$.

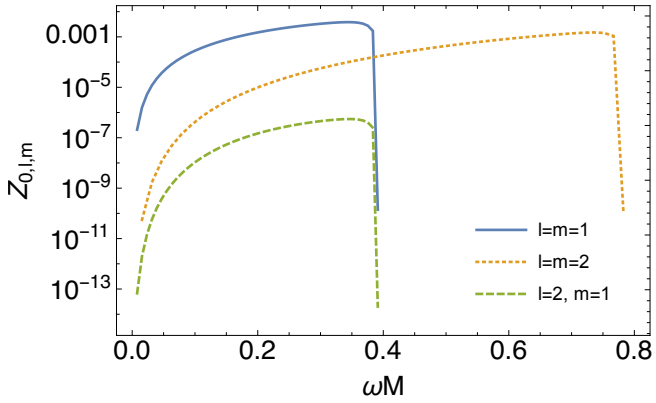

Figure I.5.5: Typical spectra of the amplification factor $Z_{0,l,m}$ for different superradiant scalar field modes off a Konoplya-Zhidenko black hole with $a = 0.99M$ and $\eta = 5M^3/100$.

than the Kerr spacetime, as the quantity

$$I_{s,l,m} = \int_0^{m\Omega_0} \mathrm{d}\omega \, Z_{s,l,m} \,, \tag{I.5.27}$$

is always smaller than in Kerr, for positive values of η, as shown in the right panel of Fig. I.5.4. However, a bosonic wave with frequency close to the superradiant threshold can be significantly more enhanced in a deformed Kerr background. For negative values of η, which correspond to more compact configurations, $I_{s,l,m}$ is typically bigger than in Kerr and maximal close to $\eta = \eta_-$. For large enough positive values of the deformation parameter the maximum value of the amplification factor and the range of superradiant frequencies are always smaller than in the Kerr case. The physical explanation to this result is that, typically, for values of $\eta/M^3 \neq 0$ the volume of the ergoregion is smaller and hence the energy that can be extracted. In the non-rotating limit, i.e., $a = 0$, superradiance disappears and we recover the recent results on absorption in deformed Schwarzschild backgrounds [376, 377].

In the inset of the left panel of Fig. I.5.4, we observe that the same maximum value of the amplification factor for a scalar field is obtained for Kerr ($\eta = 0$) and for $\eta/M^3 \simeq 12/100$. This is nothing but an apparent degeneracy, as the spectra and the superradiant ranges of frequency are significantly different.

In Fig. I.5.5 it is evident that the most superradiant mode corresponds to the minimum allowed value of $l = m$, as in the Kerr case. Modes with different values of $(l, m > 0)$ qualitatively share the same behavior with the $l = m = 1$ mode, though the maximum amplification factor is hierarchically smaller than the dominant one. For example, in the range $0.5M \lesssim a < M$, for

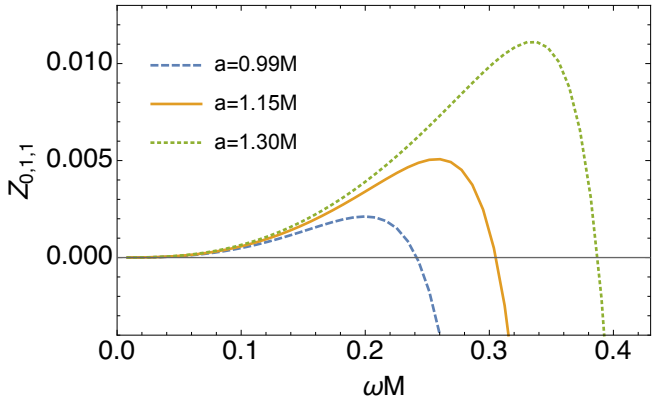

Figure I.5.6: Spectra of the amplification factor for a scalar field with $l = m = 1$ off a superspinning Konoplya-Zhidenko black hole with $\eta = M^3$ for selected values of a.

both scalar and electromagnetic fields we find $Z^{\max}_{s,2,1}/Z^{\max}_{s,2,2} \sim 10^{-3}$ while $Z^{\max}_{s,2,2}/Z^{\max}_{s,1,1} \sim 0.1$ for $a \gtrsim 0.8M$. For the $l = m = 2$ modes, $Z^{\max}_{s,2,2}$ and $I_{s,2,2}$ are always smaller than in the Kerr case for positive values of η and $a < M$, but for negative values, the amplification factor can be bigger than in Kerr. Again, this could be interpreted as a consequence of the fact that, for a given a, the ergoregion is larger than the Kerr ergoregion for negative values of η. On the other hand, the $l = 2$, $m = 1$ modes can be more superradiant than in the Kerr case, in the sense of Eq. (I.5.27), even for positive values of η when $a \gtrsim 0.8M$. For the remaining modes, i.e., with $m \leq 0$, we have verified that the amplification factor is always negative, meaning that these modes are not superradiant.

As previously discussed, the Konoplya-Zhidenko black hole also admits superspinning configurations, i.e., with spin parameter $a > M$. If the rotation parameter is (slightly) above the Kerr bound, in principle, such energy extraction could rapidly spin down these configurations to produce a black hole with $a < M$.

For completeness, we consider the scattering of a scalar field off a superspinning black hole. We observe in Fig. I.5.6 that for $\eta/M^3 = 1$ and selected values of the black-hole spin, the maximum value of the amplification factor can grow (in principle indefinitely), as well as the range of frequency for which the process is superradiant. But to obtain amplification factors larger than 100% one needs configurations with very large spin parameter or very small positive deformation parameter, which are unlikely to describe astrophysical black holes. Moreover, as discussed in Section I.5.1.1, one needs to be careful with these configurations, as in the range $0 < \eta < 8M^3/27$ the position of the event horizon is not always given by r_0 for all values of a, and perhaps even more gravely, the ergosurface can be piecewise and non-continuous.

I.5.2.4 Massive scalar fields

The extension to a massive scalar field with mass $\mu_s\hbar$ is quite simple: such mass term in the Klein-Gordon equation introduces, after separation, a quantity $-\mu_s^2 r^2\Delta/\left(r^2+a^2\right)^2$ in the coefficient of Y_0 in Eq. (I.5.21) and shifts the frequency of the angular equation as $\omega^2 \to \omega^2 - \mu_s^2$.

The boundary conditions are slightly modified. In particular, purely ingoing solutions at the horizon still require $Y_0 \sim \mathrm{e}^{-\mathrm{i}kr_*}$, while the asymptotic behaviour at infinity is

$$Y_0 \sim r^{-M\mu_s^2/\varpi}\,\mathrm{e}^{\varpi r_*} \sim r^{M\left(\mu_s^2-2\omega^2\right)/\varpi}\,\mathrm{e}^{\varpi r}\,, \quad \varpi = \pm\sqrt{\mu_s^2-\omega^2}\,. \tag{I.5.28}$$

Massive waves can be superradiant for frequencies in the range $\mu_s < \omega < m\Omega_0$, while they are trapped near the horizon and exponentially suppressed at infinity for $\omega < \mu_s$.

The numerical routine for the computation of the amplification factor is adapted from that used for massless waves, correcting the asymptotic behaviours accordingly. We limit this analysis to the $l = m = 1$ mode for which, in analogy with the massless case, we expect the dominant contribution. We repeat the routine for several values of the frequency in the interval $\mu_s < \omega < 2\Omega_0 - \mu_s$. Our results, as those in the left panel of Fig. I.5.7, show that superradiance grows with

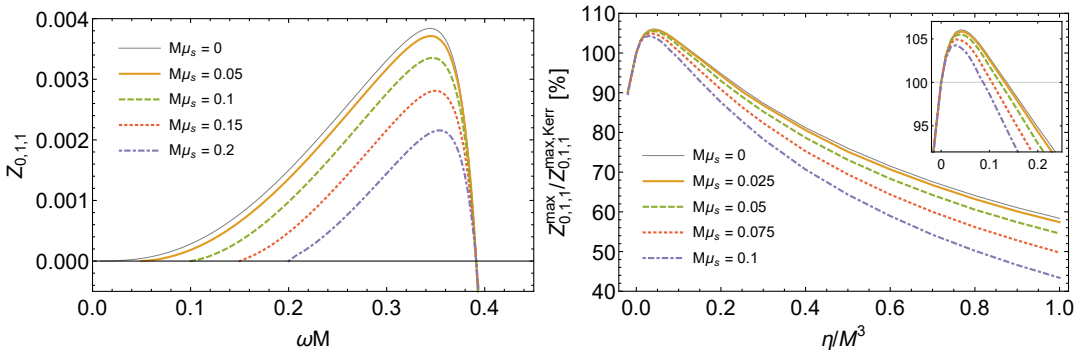

Figure I.5.7: **Left panel**: Spectra of the amplification factor for massive scalar fields with $l = m = 1$ off a Konoplya-Zhidenko black hole with $a = 0.99M$ and $\eta = 5M^3/100$, for selected values of the mass parameter. **Right panel**: Maximum value of the amplification factor $Z_{0,1,1}$ for a massive scalar field with $l = m = 1$ as a function of η normalized to the maximum value in the Kerr case, i.e., $\eta = 0$, for $a = 0.99M$ and for selected values of the mass parameter.

the spin parameter a and is less pronounced for more massive fields, as in the Kerr spacetime. The right panel of Fig. I.5.7 shows that massive waves can be more amplified than in a Kerr background with the same spin parameter for some values of the deformation parameter, analogously to what we found for massless fields, though waves with larger masses are still less enhanced. Even in this case, for positive values of η, the Konoplya-Zhidenko black hole is less superradiant than Kerr in the sense of Eq. (I.5.27) with the interval of integration adapted to $[\mu_s, m\Omega_0]$.

Kerr black holes develop superradiant instabilities against massive fields [378] which can be used to constraint the existence and the mass of ultralight bosons, i.e., using black holes as "particle detectors" [379]. In addition, the bosonic cloud can produce long-lasting, monochromatic gravitational-wave signals observable, in principle, in the sensitive band of current detectors [358, 359, 380]. We do not expect this picture to be considerably changed for deformed rotating black holes. Small values of the deformation parameter unveiled an interesting feature in the massless case, and we also expect a good black-hole mimicker not to turn upside-down the Kerr metric. This motivates us to investigate the stability of the Konoplya-Zhidenko spacetime against massive scalar fields in the small η/M^3 limit. Remarkably, in this limit, in the low-frequency regime, i.e., for $\omega M \ll 1$ and $a\omega \ll 1$ and in the small mass approximation $M\mu_s \ll 1$, the problem can be tackled with analytical methods—see Appendix I.G for details.

At leading order, the growth time of instability τ for a Kerr black hole perturbed by an axion with mass $m_{\rm axion} = \mu_{\rm axion}\hbar = 10^{-20}$ eV is

$$\tau = \left(1.58 \times 10^6 \text{ s}\right) \left(\frac{\mu_{\rm axion}}{\mu_s}\right) \frac{M}{a} \frac{1}{(M\mu_s)^8} , \tag{I.5.29}$$

to which the deformation parameter adds the contribution (valid as long as η/M^3 is small)

$$\delta\tau = -\left(7.89 \times 10^3 \text{ s}\right) \left(\frac{\mu_{\rm axion}}{\mu_s}\right) \left(\frac{\eta/M^3}{0.01}\right) \left(\frac{M}{a}\right)^3 \frac{1}{(M\mu_s)^8} . \tag{I.5.30}$$

Eq. (I.5.30) implies that for positive (negative) values of the deformation parameter (within a perturbative regime), the growth time of instability is shorter (longer), i.e., the Konoplya-Zhidenko black hole is more (less) unstable than Kerr. For an axion cloud around a supermassive black hole with $M = 10^9 M_\odot$, $M\mu_{\rm axion} \approx 10^{-1}$, and the growth time of instability would be shorter but comparable with the age of the Universe. Yet, this timescale should also be shorter than the decay time of the particle for the instability to be really effective.

As this preliminary result relies on several assumptions, it is to be confirmed by an exhaustive computation of quasi-normal modes and bound states, which is left for future work. In fact, this result is valid for slowly rotating black holes hence we cannot conclude whether highly spinning configurations are more unstable or not.

Chapter I.6

Summary of part I

In this part of the thesis we analyzed some potential black-hole mimicker candidates, putting a particular emphasis on regular black-hole models, the interpretation of the sources of their gravitational field and their rich phenomenology. Here we report a brief summary of what discussed so far, and we present some ideas left for future research.

In Chapter I.2, we presented and discussed a general class of black holes that are regular everywhere, being the central singularity resolved by the presence of a de Sitter core. The regularity of these spacetimes is then linked to the presence long-range quantum-gravity effects at the horizon scale. The quantum corrections are effectively accounted in the source term, which has the form of an anisotropic fluid with equation of state $p_{\|} = -\epsilon$ and described by a single parameter ℓ. This also avoids the assumptions of Penrose's theorem by violating the strong energy condition somewhere in the black-hole core, naturally smearing the classical Schwarzschild singularity. Because of the presence of this additional quantum hair, black holes pertaining to our class of models present interesting and rich thermodynamical and phenomenological features. Indeed, in Section I.2.3.3 we showed that, differently from their classical counterpart, objects presenting quantum corrections at the horizon scale, for which $\ell \simeq R_{\rm S}$, are thermodynamically stable, providing further evidence for the relevance of quantum effects at horizon scale. From a phenomenological point of view, instead, we showed that when the quantum hair ℓ is comparable with the classical gravitational radius, both the quasinormal modes spectra and the null orbits manifest measurable departures from the general-relativistic solutions (see Sections I.2.3.5 and I.2.3.6).

Chapter I.3 is devoted to the study of the thermodynamical properties and the evaporation process of 2D asymptotycally-flat regular models. The choice of working in two dimensions is dictated by the fact that, in this simplified environment, we cab solve the semiclassical dynamics, at least at numerical level, following the evaporation process until the point where the semiclassical approximation breaks down. Both the numerical and the analytical results of this chapter indicate that regular black holes decay to an extremal, zero-entropy state in a finite amount of time due to the Hawking effect. We have also been able to reconstruct the Page curve, which clearly shows a maximum followed by a descent, indicating that the information contained in the object is starting to flow out. However, our approach is limited by the necessary semiclassical approximation, which breaks down when quantum effects become dominant, i.e., when $\ell \simeq R_{\rm S}$.

In Chapter I.4, we finally tested a particular model pertaining to our class of metrics, the Fan-Wang black hole, against the S2-star data. This geometry is particularly interesting because of its asymptotics. Indeed, the chosen model has the strongest corrections, among the general class discussed in Chapter I.2, compared to the Schwarzschild black hole. For this reason, the Fan-Wang metric seems to be most suitable to be tested, at the moment, with the data relative to the orbits of stars around the Saggitarius A*. In order to actually constrain the additional parameter of the model, the quantum hair ℓ, we first studied the deviations the orbits of massive particles in our model, Specifically, we find that the precession angle decreases linearly with ℓ, is zero when $\ell = GM$, and becomes negative (the precession is retrograde) when $\ell > GM$. Exploiting this fact, we have been able to constrain this parameter through a Markov-chain Monte Carlo, setting the upper bound at $\ell < 0.47GM$ at 95% confidence level. This value does not exclude the thermodynamically stable configurations.

Finally, in Chapter I.5, we discuss the effect of the deviations from general relativity in a rotating

spacetime, with a particular focus on the imprint of these modifications on the superradiant scattering of electromagnetic and scalar test fields. The idea, here, was again to investigate completely the phenomenological differences between the general-relativistic solutions and the possible alternatives. We focused on the Konoplya-Zhidenko metric, pertaining to the much more general one presented in Ref. [91, 92], as a proxy for generic rotating spacetimes presenting an ergoregion. The advantage of this metric is that the deviations, encoded in a single parameter, η, leads to a spacetime with a rich structure without modifying the asymptotics and the symmetries in relation to the Kerr spacetime. Regarding superradiance, we found that superradiance is still present in these kind of spacetimes, but it is strongly suppressed for large values of the deformation parameter. We also investigated the superradiant instability, happening when the black hole is surrounded by a cloud of massive scalar particles. We found that for $\eta > 0$ the instability time decreases. These results, however, should be taken as indicative due to the several assumptions made to obtain an analytical estimation and we leave further investigation for future work.

Appendices—Part I

I.A Geodesic completeness

In this appendix, we show that spacetimes described by Eq. (I.2.22) are geodesically complete. We start with Raychaudhuri's equation, which describes the evolution of a time-like geodesic congruence Θ

$$\frac{\mathrm{d}\Theta}{\mathrm{d}\tau} = -\frac{1}{3}\Theta^2 - \sigma^{\mu\nu}\sigma_{\mu\nu} + \omega^{\mu\nu}\omega_{\mu\nu} - R_{\mu\nu}u^\mu u^\nu, \tag{I.6.1}$$

where τ is the proper time, $u^\mu = \mathrm{d}x^\mu/\mathrm{d}\tau$ the proper time-like velocity, while $\sigma_{\mu\nu} = \Theta_{\mu\nu} - \Theta h_{\mu\nu}/3$ is the shear tensor ($h_{\mu\nu} = g_{\mu\nu} + u_\mu u_\nu$ is the transverse metric) and $\omega_{\mu\nu} = h^\rho_\mu h^\sigma{}_\nu \nabla_{[\sigma}u_{\rho]}$ is the vorticity tensor. If we consider geodesics to be hypersurface orthogonal, then $\omega_{\mu\nu} = 0$. Since both the shear and the vorticity tensors are purely spatial, i.e., $\omega_{\mu\nu}\omega^{\mu\nu} \geq 0$, $\sigma_{\mu\nu}\sigma^{\mu\nu} \geq 0$, and if we assume the SEC to hold, i.e., $R_{\mu\nu}u^\mu u^\nu \geq 0$, we expect in all generality a focusing of the geodesic congruence, i.e., $\mathrm{d}\Theta/\mathrm{d}\tau \leq 0$ and the formation of caustics, which represent singularities of the congruence. This is the essence of the original Penrose singularity theorem [114]. Let us now show that caustics cannot form for the models described by Eq. (I.2.22). We start by considering a generic static spacetime described by the metric function A. We study time-like geodesics, focusing on those lying on the plane $\theta =$ cons. and $\varphi =$ constant, for which $u^\theta = u^\varphi = 0$, and

$$g_{\mu\nu}u^\mu u^\nu = -A(r)(u^0)^2 + \frac{(u^r)^2}{A(r)} = -1. \tag{I.6.2}$$

Here $u^0 = \mathrm{d}t/\mathrm{d}\tau = 1/A(r)$ since the metric redshift factor determines the relation between the coordinate and proper time, therefore

$$-\frac{1}{A(r)} + \frac{(u^r)^2}{A(r)} = -1 \Rightarrow u^r = \pm\sqrt{1 - A(r)}. \tag{I.6.3}$$

This yields the congruence

$$\Theta = \frac{1}{r^2}\partial_r\left(r^2u^r\right) = \frac{1}{r^2}\left(2ru^r + r^2\frac{du^r}{dr}\right) = \pm\left[\frac{2}{r}\sqrt{1 - A(r)} - \frac{A'(r)}{2\sqrt{1 - A(r)}}\right]. \tag{I.6.4}$$

The geodesic congruence evolution as a function of the proper time can therefore be written as

$$\frac{\mathrm{d}\Theta}{\mathrm{d}\tau} = \frac{\mathrm{d}\Theta}{\mathrm{d}r}\frac{\mathrm{d}r}{\mathrm{d}\tau} = \Theta' u^r = -\frac{2(1 - A(r))}{r^2} - \frac{A'(r)}{r} - \frac{A''(r)}{2} - \frac{A'(r)^2}{4(1 - A(r))}, \tag{I.6.5}$$

where we used the fact that Θ is a function of r only.

We can now express Eq. (I.6.5) in terms of the function F in Eq. (I.2.22), where we wrote

$$A(r) = 1 - \frac{2GM\ell}{r}F(\frac{r}{\ell}). \tag{I.6.6}$$

Eq. (I.6.5) now reads

$$\frac{\mathrm{d}\Theta}{\mathrm{d}\tau} = -\frac{2\alpha F(y)}{y^2\ell^2} + \frac{\alpha}{y\ell^2}F'(y) + \frac{\alpha}{2\ell^2}F''(y) - \frac{\alpha}{4\ell^2}\frac{F'(y)^2}{F(y)} \tag{I.6.7}$$

Since, for large y, our general model behaves essentially as the Schwarzschild BH, we focus on the behavior of the geodesics bundle in the core of the object, i.e., for $y \to 0$, where $F \sim y^2$ according to Eq. (I.2.24). Therefore, $F' \sim 2y$ and $F'' \sim 2$, and thus

$$\frac{\mathrm{d}\Theta}{\mathrm{d}\tau} \sim -\frac{2\alpha}{\ell^2} + \frac{2\alpha}{\ell^2} + \frac{\alpha}{\ell^2} - \frac{\alpha}{\ell^2} \sim 0, \tag{I.6.8}$$

so that there are no caustics in the center, the bundle of geodesics is defocused and therefore they can be extended beyond $r = 0$. This is consistent with the form of the Penrose diagram for such models (see, e.g., Refs. [84, 240]), which shows that, apart from the presence of the central singularity, the maximal extension of these spacetimes is similar to that of RN BHs. These results can be further confirmed by computing $\mathrm{d}\Theta/\mathrm{d}\tau$ for the two specific models investigated in detail in Chapter I.2, namely the Hayward and the Gaussian-core BHs.

For the Hayward BH, plugging the function F (I.2.50) into Eq. (I.6.7) yields

$$\frac{\mathrm{d}\Theta}{\mathrm{d}\tau} = -\frac{9\alpha y^3\left(y^3+4\right)}{4\ell^2\left(1+y^3\right)^3}. \tag{I.6.9}$$

Near $y \sim 0$, we have $\frac{d\Theta}{d\tau} \sim -\frac{9\alpha y^3}{\ell^2} + \mathcal{O}(y^4)$, so no caustic is present in the interior, at $r = 0$.

In the Gaussian-core BH case, using the function F (I.2.70) into Eq. (I.6.7), we get

$$\frac{\mathrm{d}\Theta}{\mathrm{d}\tau} = \frac{\alpha}{\ell^2}\left\{\frac{e^{-y^2}\left(6-4y^2\right)}{\sqrt{\pi}} - \frac{4e^{-2y^2}y^3}{\pi - 2\sqrt{\pi}\Gamma\left(\frac{3}{2},y^2\right)} - \frac{9}{4\sqrt{\pi}y^3}\left[\sqrt{\pi} - 2\Gamma\left(\frac{3}{2},y^2\right)\right]\right\} \tag{I.6.10}$$

Near $y \sim 0$, we have $\frac{\mathrm{d}\Theta}{\mathrm{d}\tau} \sim -\frac{4\alpha y^2}{\sqrt{\pi}\ell^2} + \mathcal{O}(y^4)$, so that again caustics do not form and the spacetime is geodesically complete.

I.B Parameter estimation for the S2-star orbits

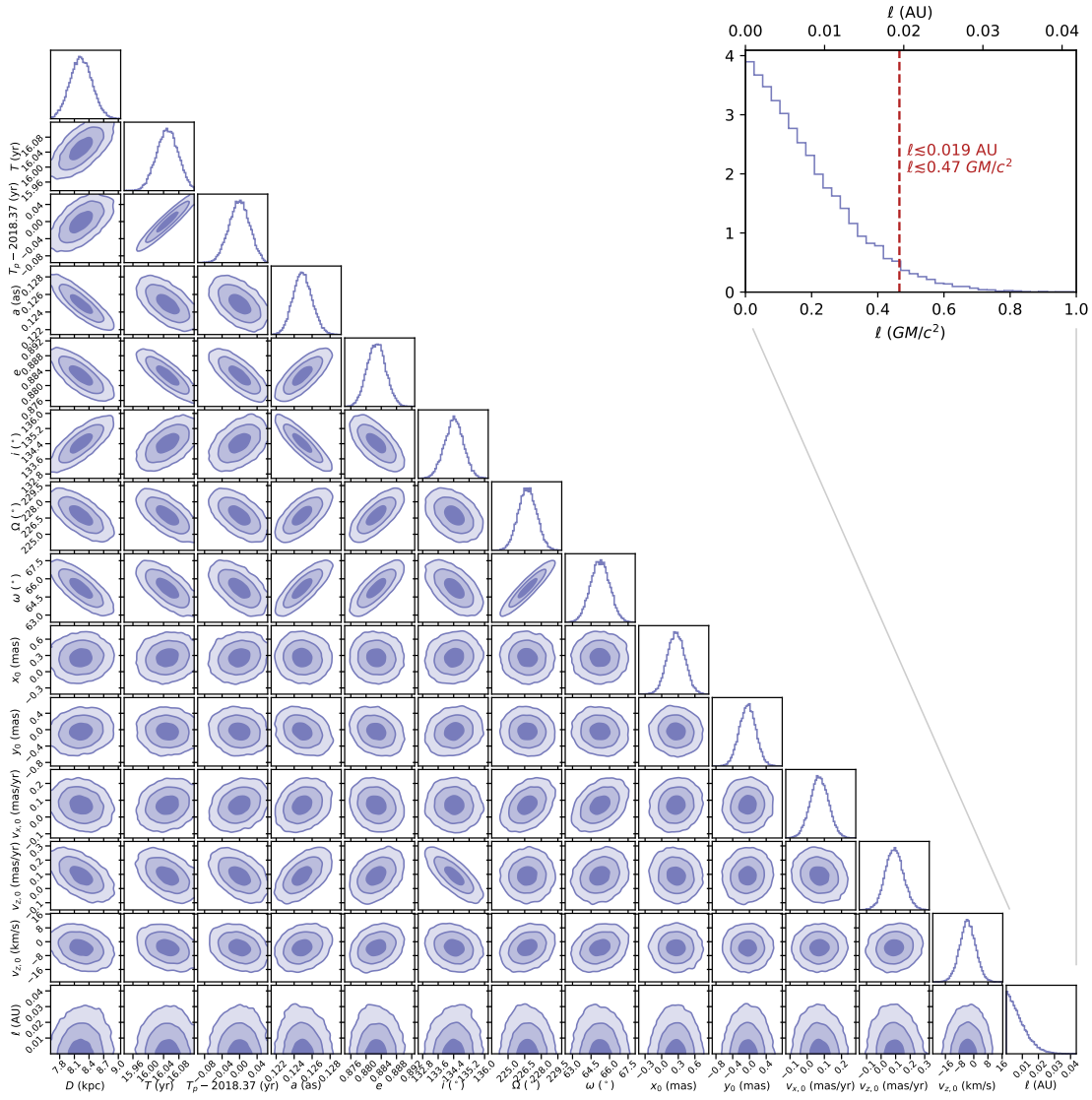

Figure I.6.1: Full 14-dimensional posterior probability distribution for the parameter space of our orbital model. The contour plots report the 68%, 95%, and 99.7% confidence regions (lighter to darker colors, respectively) for each parameter pair, while the marginalized posterior distributions are reported, for each parameter, in the first-row histograms. The inset plot zooms into the posterior distribution for our parameter of interest, ℓ, reporting, as a red dashed line, the upper limit that we derived at the 95% of the confidence level.

I.C No divergences in the ground state stress-energy tensor

In Ref. [279], counterterms are added to the Polyakov action (as in Eq. (I.3.73)) to eliminate a divergence in the stress-energy tensor of the GS $\langle T_{\mu\nu}\rangle \sim \phi^{2a}$, which, for $a > 0$ diverges at asymptotic infinity $\phi \to \infty$. We show that in our case the rapid fall of the potential at infinity allows to avoid this divergent behavior.

We consider, as an example, $\langle T_{+-}\rangle_{\rm GS}$, but similar considerations also hold for the other components of $T_{\mu\nu}$. Using Eq. (I.3.66), we have

$$\langle T_{+-}\rangle_{\rm GS} = -\frac{N}{12}\partial_+\partial_-\rho\Big|_{\rm GS}\,, \tag{I.6.11}$$

where ρ, computed at the GS, is given by Eq. (I.3.60)

$$\rho_{\rm GS} = \frac{1}{2}\ln\left(\frac{2\mathcal{M}_{\rm ext}}{\lambda} + \mathcal{J}_{\rm GS}\right)\,, \qquad \mathcal{J} \equiv \frac{1}{\lambda^2}\int^{\phi} \mathrm{d}\psi\, \mathcal{V}(\psi)\,. \tag{I.6.12}$$

Therefore

$$\partial_-\rho_{\rm GS} = \frac{1}{2}\frac{\partial_-\mathcal{J}_{\rm GS}}{\frac{2\mathcal{M}_{\rm ext}}{\lambda} + \mathcal{J}_{\rm GS}} = \frac{1}{2}\frac{\partial_-\phi_{\rm GS}\,\mathcal{J}_{{\rm GS},\phi}}{\frac{2\mathcal{M}_{\rm ext}}{\lambda} + \mathcal{J}_{\rm GS}} = -\frac{1}{4\lambda}\mathcal{V}_{\rm GS}\,, \tag{I.6.13}$$

where $\mathcal{J}_{,\phi} = \lambda^{-2}\mathcal{V}$ and we used the vacuum solution Eq. (I.3.55b). Differentiating with respect to x^+ yields

$$\partial_+\partial_-\rho_{\rm GS} = -\frac{1}{4\lambda}\partial_+\phi\,\mathcal{V}_{{\rm GS},\phi} = -\frac{1}{8}e^{2\rho}\mathcal{V}_{{\rm GS},\phi}\,. \tag{I.6.14}$$

For $\phi \to \infty$, $e^{2\rho} \to$ constant, while $\mathcal{V}_{,\phi} \sim -\phi^{-3} \to 0$. So we do not have divergences.

I.D Boundary conditions for numerical integration

I.D.1 Boundary condition at $x^+ = x_0^+$

For our numerical integration, we set $\lambda = 1$ and $\ell = 1$.

When the shock wave is turned on, the solution is set equal to the extremal configuration (I.3.60). Our procedure to implement this boundary condition is the following:

1. We first integrate the equation for the dilaton (expression on the right of Eq. (I.3.60)), leading to an implicit relation between the dilaton and the coordinates;
2. We numerically invert it to have explicitly $\phi = \phi(x^+, x^-)$;
3. We plug the result into the equation for $e^{2\rho}$.

The first point is achieved by solving the differential equation

$$\frac{\mathrm{d}r_*}{\mathrm{d}\psi} = \frac{1}{\frac{2\mathcal{M}_{\rm ext}}{\lambda} + \mathcal{J}(\psi)}\,. \tag{I.6.15}$$

This integral can be done analytically. With $\mathcal{M}_{\rm ext} = \sqrt[3]{2}\,\ell/3$ and $\ell = \lambda = 1$ it reads

$$r_{*,\rm ext} = 2^{5/3}\ln\left(\left|\sqrt[3]{2} - \phi\right|\right) + \frac{3\phi}{2^{2/3}} + \frac{3}{\sqrt[3]{2} - \phi} + \frac{\ln\left(2\phi + \sqrt[3]{2}\right)}{2\sqrt[3]{2}}\,. \tag{I.6.16}$$

We then numerically invert the result to get $\phi = \phi(x^+, x^-)$ and plug the result into Eq. (I.3.60) to get $\rho = \rho(x^+, x^-)$, both evaluated at extremality.

I.D.2 Boundary condition at $x^- \to -\infty$

The procedure is exactly the same as before, with $\mathcal{M}_{\rm ext}$ replaced by a different value of the mass. Here, we choose $\mathcal{M} = 0.1\,\lambda$.

The coordinate r_* as a function of ϕ in this case reads

$$r_* \simeq -1.37\ln(|0.47-\phi|) + 25.42\ln(|4.96-\phi|) + 5\phi + 0.95\ln(\phi+0.43)\,. \tag{I.6.17}$$

Again, we numerically invert this expression, to get $\phi = \phi(x^+, x^-)$. In this case, however, the quantity we are (improperly) calling r_* contains the function $F(x^-)$, which has to be computed to fully obtain ϕ as a function of the coordinates. Starting from

$$\mathcal{F}[\phi(x^+,x^-)] \equiv \int^{\phi} \frac{\mathrm{d}\psi}{\frac{2\mathcal{M}}{\lambda}+\mathcal{J}} = \frac{\lambda}{2}\left[x^+ - x_0^+ - F(x^-)\right]\,, \tag{I.6.18}$$

we note that, when evaluated at $x^+ = x_0^+$, it reads

$$\mathcal{F}[\phi(x_0^+,x^-)] = -\frac{\lambda}{2}F(x^-)\,, \tag{I.6.19}$$

from which we get

$$\phi(x_0^+,x^-) \equiv \phi_0(x^-) = \mathcal{F}^{-1}\left[-\frac{\lambda}{2}F(x^-)\right]\,. \tag{I.6.20}$$

This expresssion of $\phi(x_0^+,x^-)$ can be used in Eq. (I.3.63) to compute $\mathcal{J}_0$. This gives us a differential equation in terms of F which reads

$$F'(x^-) = \frac{\frac{2\mathcal{M}_{\rm ext}}{\lambda}+\mathcal{J}_{0,\rm ext}(x^-)}{\frac{2\mathcal{M}}{\lambda}+\mathcal{J}_0\left[\phi_0(x^-)\right]} \equiv \frac{\frac{2\mathcal{M}_{\rm ext}}{\lambda}+\mathcal{J}_{0,\rm ext}(x^-)}{\frac{2\mathcal{M}}{\lambda}+\mathcal{J}_0\left(\mathcal{F}^{-1}\left[-\frac{\lambda}{2}F(x^-)\right]\right)}\,. \tag{I.6.21}$$

This equation is solved numerically. The integration constant is chosen so that, once the solution of F is plugged into the dilaton solution (I.3.63), at $x^+ = x_0^+$, the dilaton is equal to the extremal one computed at x_0^+. This guarantees the continuity of the scalar field across the shock wave.

Once $F(x^-)$ is computed, we plug it into $\phi = \phi(x^+,x^-)$. With this and Eq. (I.3.63), we obtain also $\rho = \rho(x^+,x^-)$ above extremality.

I.E The Klein-Gordon and Maxwell equations in Kerr-like backgrounds

Being s the spin weight of the test field, in linear perturbation theory the scalar ($s=0$) and Maxwell ($s=\pm1$) fields propagate in the background metric. The Klein–Gordon equation for a massless scalar field Φ is easily obtained from $\Box\Phi = 0$, where the D'Alambert operator is built out of the metric (I.5.2). We follow the method proposed in Ref. [381] to derive the Maxwell equations in such spacetime.

First we choose a suitable null tetrad $e^{\ \mu}_{(a)} = \{l^\mu, n^\mu, m^\mu, \bar{m}^\mu\}$ that easily reduces to the Kinnersley tetrad [382] in the Kerr spacetime, i.e.,

$$l^\mu = \frac{1}{\Delta}\left[r^2 R_\Sigma + a^2, \frac{\Delta}{R_B}, 0, a\right]\,, \tag{I.6.22a}$$

$$n^\mu = \frac{1}{2\Sigma}\left[r^2 R_\Sigma + a^2, -\frac{\Delta}{R_B}, 0, a\right]\,, \tag{I.6.22b}$$

$$m^\mu = \frac{1}{\sqrt{2}\bar{\rho}}\left[\mathrm{i}a\sin\theta, 0, 1, \mathrm{i}\csc\theta\right]\,, \tag{I.6.22c}$$

where $\Delta = r^2\,R_\Sigma - R_M\,r + a^2$, $\Sigma = r^2 R_\Sigma + a^2\cos^2\theta$ and $\rho = r\sqrt{R_\Sigma} - \mathrm{i}a\cos\theta$. The tetrad vectors satisfy

$$e^{\ \mu}_{(a)} e_{(b)\,\mu} = \begin{pmatrix} 0 & -1 & 0 & 0 \\ -1 & 0 & 0 & 0 \\ 0 & 0 & 0 & 1 \\ 0 & 0 & 1 & 0 \end{pmatrix}\,. \tag{I.6.23}$$

The non-vanishing spin coefficients are

$$\varrho = -\frac{\left(r^2 R_\Sigma\right)'}{2R_B\Sigma} - \frac{\mathrm{i}a\cos\theta}{\Sigma}, \tag{I.6.24a}$$

$$\epsilon = -\frac{\mathrm{i}a\cos\theta}{4rR_B\Sigma}\left[2rR_B - \frac{\left(r^2R_\Sigma\right)'}{\sqrt{R_\Sigma}}\right], \tag{I.6.24b}$$

$$\mu = -\frac{\Delta}{4R_B\Sigma^2}\left[\left(r^2R_\Sigma\right)' + 2\mathrm{i}aR_B\cos\theta\right], \tag{I.6.24c}$$

$$\gamma = \frac{\Delta'}{4R_B\Sigma} - \frac{\Delta}{8\Sigma^2}\left[\frac{\left(\bar\rho + r\sqrt{R_\Sigma}\right)}{rR_B\sqrt{R_\Sigma}}\left(r^2R_\Sigma\right)' + 2\mathrm{i}a\cos\theta\right], \tag{I.6.24d}$$

$$\tau = \frac{a\sin\theta}{2\sqrt{2}R_B\Sigma\bar\rho}\left[2aR_B\cos\theta - \mathrm{i}\left(r^2R_\Sigma\right)'\right], \tag{I.6.24e}$$

$$\begin{aligned}\alpha = \frac{1}{8\sqrt{2}\Sigma\rho}\Big[&\cot\theta\left(\Sigma - 5a^2 - 5r^2R_\Sigma\right)\\ &+ \frac{2\mathrm{i}a\sin\theta}{R_B}\left(r^2R_\Sigma\right)' + \sin\theta\left(7\mathrm{i}ar\sqrt{R_\Sigma} - 3\mathrm{i}a\rho\right)\Big],\end{aligned} \tag{I.6.24f}$$

$$\pi = \frac{\mathrm{i}a\sin\theta}{\sqrt{2}\Sigma\rho}\left[r\sqrt{R_\Sigma} + \frac{\left(r^2R_\Sigma\right)'}{2R_B} - \rho\right], \tag{I.6.24g}$$

$$\beta = \frac{1}{2\sqrt{2}\Sigma\bar\rho}\left\{\mathrm{i}a\sin\theta\left[r\sqrt{R_\Sigma} - \frac{\left(r^2R_\Sigma\right)'}{2R_B}\right] + \Sigma\cot\theta\right\}. \tag{I.6.24h}$$

The sourceless decoupled Newman–Penrose equations for the massless spin-1 field are given by [381]

$$\left[\left(\boldsymbol{D} - \epsilon + \bar\epsilon - 2\varrho - \bar\varrho\right)\left(\boldsymbol{\Delta} + \mu - 2\gamma\right) - \left(\boldsymbol{\delta} - \beta - \bar\alpha - 2\tau + \bar\pi\right)\left(\bar{\boldsymbol{\delta}} + \pi - 2\alpha\right)\right]\phi_0 = 0\,, \tag{I.6.25a}$$

$$\left[\left(\boldsymbol{\Delta} + \gamma - \bar\gamma + 2\mu + \bar\mu\right)\left(\boldsymbol{D} - \varrho + 2\epsilon\right) - \left(\bar{\boldsymbol{\delta}} + \alpha + \bar\beta + 2\pi - \bar\tau\right)\left(\boldsymbol{\delta} - \tau + 2\beta\right)\right]\phi_2 = 0\,, \tag{I.6.25b}$$

where $\boldsymbol{D} = l^\mu\nabla_\mu$, $\boldsymbol{\Delta} = n^\mu\nabla_\mu$ and $\boldsymbol{\delta} = m^\mu\nabla_\mu$, and the complex fields are defined as $\phi_0 = F_{\mu\nu}\,l^\mu m^\nu$ and $\phi_2 = F_{\mu\nu}\,\bar m^\mu n^\nu$, being $F_{\mu\nu}$ the electromagnetic field tensor.

Differently from the Kerr case, the spin coefficient ϵ is generally non-zero; consequently, Eqs. (I.6.25) are not separable into a radial and angular part. However, one can always perform a null rotation of the tetrad to set $\epsilon = 0$ [383]. Alternatively, we can restrict our metric performing a change of the radial coordinate such that $R_B = 1$ and solving $\epsilon = 0$ for R_Σ,

$$R_\Sigma = \left(1 + \frac{\xi}{r}\right)^2, \tag{I.6.26}$$

where ξ is a constant parameter.

Under the above assumptions, decomposing the test fields as $\mathrm{e}^{-\mathrm{i}\omega t}\,\mathrm{e}^{\mathrm{i}m\varphi}\,S(\theta)\,R_s(r)$, the scalar and electromagnetic wave equations separate, with the angular part described by the spin-weighted spheroidal harmonics equation

$$\begin{aligned}&\frac{1}{\sin\theta}\frac{\mathrm{d}}{\mathrm{d}\theta}\left(\sin\theta\,\frac{\mathrm{d}S}{\mathrm{d}\theta}\right)\\ &\qquad + \left(a^2\omega^2\cos^2\theta - \frac{m^2}{\sin^2\theta} - 2a\omega s\cos\theta - \frac{2ms\cos\theta}{\sin^2\theta} - s^2\cot^2\theta + s + A\right)S = 0\,,\end{aligned} \tag{I.6.27}$$

while the radial part by the following equation,

$$\Delta^{-s}\frac{\mathrm{d}}{\mathrm{d}r}\left(\Delta^{s+1}\frac{\mathrm{d}R_s}{\mathrm{d}r}\right) + \left[\frac{K^2 - \mathrm{i}s\Delta' K}{\Delta} + 4\mathrm{i}srR_\Sigma\omega - \lambda + \frac{s(s+1)\left(\Delta'' - 2\right)}{2}\right]R_s = 0\,, \tag{I.6.28}$$

where $K = \left(r^2R_\Sigma + a^2\right)\omega - am$ and $\lambda = A + a^2\omega^2 - 2am\omega$. The radial functions R_0, R_1 and R_{-1} correspond to Φ, ϕ_0 and ϕ_2/ρ^2.

Eq. (I.6.27) together with regular boundary conditions at $\theta = \{0,\ \pi\}$ is an eigenvalue problem for the separation constant A. For each value of s, m and $a\omega$, the eigenvalues are identified by a number l, whose smallest value is $\max(|m|, |s|)$. The eigenfunctions form a complete and orthonormal set in $\theta \in [0, \pi]$. For $a\omega = 0$, Eq. (I.6.27) reduces to the spin-weighted spherical harmonics equation and $A = (l - s)(l + s + 1)$ [384]; for $a\omega \ll 1$, Eq. (I.6.27) can be solved perturbatively [385], but in general it must be solved numerically [386].

To integrate Eq. (I.6.28) it is necessary to give boundary conditions at the horizon and at infinity. Therefore, we first introduce a tortoise-like coordinate given by $dr_*/dr \equiv (r^2\, R_\Sigma + a^2)/\Delta$ and the radial function $Y_s(r) = \sqrt{r^2\, R_\Sigma + a^2}\Delta^{s/2} R_s(r)$. With these substitutions, Eq. (I.6.28) becomes

$$\frac{\mathrm{d}^2 Y_s}{\mathrm{d}r_*^2} + \left\{ \frac{\Delta\left[s(s+1)\left(\Delta'' - 2\right)/2 - \lambda + 4\mathrm{i}s\omega(r+\xi)\right]}{\left[(r+\xi)^2 + a^2\right]^2} + \frac{K^2 - \mathrm{i}Ks\Delta'}{\left[(r+\xi)^2 + a^2\right]^2} - \frac{\mathrm{d}G}{\mathrm{d}r_*} - G^2 \right\} Y_s = 0, \tag{I.6.29}$$

where $G = s\Delta'/2(r^2 R_\Sigma + a^2) + r\sqrt{R_\Sigma}\Delta/(r^2 R_\Sigma + a^2)^2$ and r is an implicit function of r_*.

At infinity ($r_* \to \infty$), Eq. (I.6.29) can be approximated as

$$\frac{\mathrm{d}^2 Y_s}{\mathrm{d}r_*^2} + \left(\omega^2 + \frac{2\mathrm{i}s\omega}{r}\right) Y_s = 0\,, \tag{I.6.30}$$

from which we see that $Y_s \sim r^{\pm s}\mathrm{e}^{\mp \mathrm{i}\omega r_*}$, where the upper (lower) sign refers to outgoing (ingoing) waves.

Near the event horizon r_0 ($r_* \to -\infty$), Eq. (I.6.29) becomes

$$\frac{\mathrm{d}^2 Y_s}{\mathrm{d}r_*^2} + (k - \mathrm{i}s\sigma)^2\, Y_s = 0\,, \tag{I.6.31}$$

where

$$k = \omega\left(1 + \frac{\xi(2r_0 + \xi)}{(r_0+\xi)^2 + a^2}\right) - m\Omega_0\,, \tag{I.6.32}$$

$$\sigma = \frac{r_0^2\left(1 - R'_M(r_0)\right) - \xi^2 - a^2}{2r_0\left[(r_0+\xi)^2 + a^2\right]}\,. \tag{I.6.33}$$

The purely ingoing solution at the horizon is given by $Y_s \sim \exp\left[\mathrm{i}(k - \mathrm{i}\sigma)r_*\right] \sim \Delta^{-s/2}\mathrm{e}^{-\mathrm{i}kr_*}$.

Teukolsky and Press showed that one solution of the Teukolsky equation with spin-weight s contains the same physical information of that with spin-weight $-s$ [372]. This result is a consequence of the fact that the Kerr spacetime is stationary and axisymmetric. This fact holds for this class of deformed metrics too, in fact, repeating the same derivation for Eq. (I.6.28) but starting with the tetrad

$$\tilde{l}^\mu = -\frac{2\Sigma}{\Delta}\, n^\mu\,, \quad \tilde{n}^\mu = -\frac{\Delta}{2\Sigma}\, l^\mu\,, \quad \tilde{m}^\mu = \frac{r\sqrt{R_\Sigma} - \mathrm{i}a\cos\theta}{r\sqrt{R_\Sigma} + \mathrm{i}a\cos\theta}\, \bar{m}^\mu\,, \tag{I.6.34}$$

related to Eqs. (I.6.22) by the simultaneous transformation $\varphi \to -\varphi$, $t \to -t$, one finds that, after the separation of the radial and angular variables, the radial function $\tilde{R}_s$ satisfies Eq. (I.6.28) with $s \to -s$ and it is related to R_{-s} through

$$\tilde{R}_s = \left(\frac{2}{\Delta}\right)^s R_{-s}\,. \tag{I.6.35}$$

I.F Einstein tensor, geodesic equations, and ZAMO for the Konoplya-Zhidenko spacetime

The non-zero components of the Einstein tensor for the Konoplya–Zhidenko metric read

$$G_{tt} = \eta\,\frac{r^2\left(3\cos^2\theta-5\right)a^2+2r\left(-r^3+2Mr^2+\eta\right)-a^4\cos^2\theta\sin^2\theta}{r^3\left(r^2+a^2\cos^2\theta\right)^3}\,, \tag{I.6.36a}$$

$$G_{t\varphi} = a\eta\sin^2\theta\,\frac{a^2\left(r^2+a^2\right)\cos^2\theta+r\left(5r^3-4Mr^2+5a^2r-2\eta\right)}{r^3\left(r^2+a^2\cos^2\theta\right)^3}\,, \tag{I.6.36b}$$

$$G_{rr} = \frac{2\eta}{r\Delta\left(r^2+a^2\cos^2\theta\right)}\,, \tag{I.6.36c}$$

$$G_{\theta\theta} = -\frac{\eta\left(3r^2+a^2\cos^2\theta\right)}{r^3\left(r^2+a^2\cos^2\theta\right)}\,, \tag{I.6.36d}$$

$$G_{\varphi\varphi} = -\eta\sin^2\theta\,\frac{a^2\left(a^4-r^4+4Mr^3+2r\eta\right)\cos^2\theta+r\left[3r^5+5a^4r-2a^2\left((2M-4r)r^2+\eta\right)\right]}{r^3\left(r^2+a^2\cos^2\theta\right)^3}\,. \tag{I.6.36e}$$

The geodesic equations can be obtained via the Euler-Lagrange equations from the Lagrangian $\mathcal{L}=\frac{1}{2}g_{\mu\nu}\dot{x}^\mu\dot{x}^\nu$, where a dot indicates differentiation with respect to an affine parameter λ. However, it is simpler to use the integrals of motion, two of which are related to the obvious symmetries of the metric, i.e., stationarity and axisymmetry, that can be expressed respectively by

$$p_t \equiv g_{tt}\dot{t}+g_{t\varphi}\dot{\varphi}=-E\,,\quad p_\varphi \equiv g_{\varphi\varphi}\dot{\varphi}+g_{t\varphi}\dot{t}=L_z\,, \tag{I.6.37}$$

where E and L_z represent the energy and the angular momentum along the φ axis of the particle. Another constant of motion can be obtained observing that the Hamiltonian $\mathcal{H}=\frac{1}{2}g_{\mu\nu}p^\mu p^\nu$, where $p^\mu=\partial\mathcal{L}/\partial\dot{x}^\mu$, is independent of the affine parameter. Therefore we can write $\mathcal{H}=-\frac{1}{2}\epsilon^2$, where ϵ^2 is a constant parameter that can be $+1,0,-1$, respectively, for timelike, null and spacelike geodesics. The last integral of motion is less obvious and it is related to the separability of the Hamilton–Jacobi equation

$$\dot{S}=\frac{1}{2}g^{\mu\nu}\frac{\partial S}{\partial x^\mu}\frac{\partial S}{\partial x^\nu}\,, \tag{I.6.38}$$

where S is a function of λ and the coordinates. In fact, with the ansatz $S=-\frac{\epsilon^2}{2}\lambda-Et+S_\theta(\theta)+S_r(r)+L_z\varphi$, Eq. (I.6.38) separates into an angular and a radial part. The (generalized) Carter constant $Q=K-(aE-L_z)^2$ is related to the separation constant K associated to the hidden symmetry of the metric generated by a second-order Killing tensor $K^{\mu\nu}$ that satisfies $\nabla_{(\rho}K_{\mu\nu)}=0$, where the round parentheses denote symmetrization with respect to the indices. The explicit form of $K^{\mu\nu}$ is

$$K^{\mu\nu}=2\Sigma\,l^{(\mu}n^{\nu)}+r^2g^{\mu\nu}\,, \tag{I.6.39}$$

where $\Sigma=r^2+a^2\cos^2\theta$ while l^μ and n^μ are the vectors defined in Eqs. (I.6.22) with $R_\Sigma=R_B=1$ and $R_M=2M+\eta/r^2$.

Using these four integrals of motion it is possible to write the geodesic equations as

$$\dot{t}=E+\frac{\left(2Mr^2+\eta\right)\left((r^2+a^2)E-aL_z\right)}{r\Delta\Sigma}\,, \tag{I.6.40a}$$

$$\dot{\varphi}=\frac{1}{r\Sigma}\left(\frac{a\left(2Mr^2+\eta\right)E-a^2L_zr}{\Delta}+\frac{r\,L_z}{\sin^2\theta}\right), \tag{I.6.40b}$$

$$\Sigma^2\dot{r}^2=\left[aL_z-E\left(a^2+r^2\right)\right]^2-\Delta\left[(aE-L_z)^2+Q+r^2\epsilon^2\right], \tag{I.6.40c}$$

$$\Sigma^2\dot{\theta}^2=a^2\cos^2\theta\left(E^2-\epsilon^2\right)-L_z^2\cot^2\theta+Q\,. \tag{I.6.40d}$$

The four-velocity of a zero-angular-momentum observer in the equatorial plane is readily obtained,

$$u^t = \frac{r^5 + a^2\left(r^3 + 2Mr^2 + \eta\right)}{r^3\Delta}\,, \tag{I.6.41a}$$

$$u^r = -\sqrt{\frac{\left(a^2 + r^2\right)\left(\eta + 2Mr^2\right)}{r^5}}\,, \tag{I.6.41b}$$

$$u^\varphi = \frac{a\left(2Mr^2 + \eta\right)}{r^3\Delta}\,. \tag{I.6.41c}$$

I.G Frequency eigeinvalues in the low-frequency, small-mass and small-deformation limit

In the low-frequency regime, i.e., $M\omega \ll 1$ and $a\omega \ll 1$, the amplification factor for waves scattered off a Kerr black hole can be computed analytically [387–389]. The angular equation reduces to the scalar spherical harmonics equation and the angular eigenvalue λ can be approximated as $l(l+1)$. For massive scalar field a similar technique can be applied in the small mass limit $M\mu_s \ll 1$ [355]. We extend this result to the Konoplya–Zhidenko black hole in the limit $\eta/M^3 \ll 1$.

The asymptotic matching technique consists in solving the radial equation in the asymptotic and near-horizon regions and relies on the existence of an overlap region in which the two solutions can be matched.

In the large r limit the radial equation for a massive scalar field in the Konoplya–Zhidenko background becomes

$$R_0''(r) + \frac{2}{r}\,R_0'(r) + \left(-\frac{l(l+1)}{r^2} + \frac{2M\mu_s^2}{r} + \omega^2 - \mu_s^2\right) R_0(r) = 0\,. \tag{I.6.42}$$

Defining $k^2 = \mu_s^2 - \omega^2$, $\nu = M\mu_s^2/k$, and $x = 2kr$ the above equation reads

$$xR_0''(x) + 2R_0'(x) + \left(-\frac{l(l+1)}{x} + \nu - \frac{x}{4}\right) R_0(x) = 0\,, \tag{I.6.43}$$

i.e., the same equation which governs an electron in the hydrogen atom. For large x the two independent solutions of Eq. (I.6.43) behave as $R_0(x) \sim x^{\pm(\nu+1)}\,\mathrm{e}^{\mp x/2}$. Since we are interested in the unstable modes we take the solution with the upper signs, and the complete solution to Eq. (I.6.43) with such asymptotic behaviour is

$$R_0(x) = \mathrm{e}^{-x/2} x^l U(l - \nu + 1, 2l + 2, x) \tag{I.6.44}$$

being U the confluent hypergeometric function.

The regularity of the electron wave-function in $x = 0$ implies that the bound states of the hydrogen atom corresponds to integer values of ν as $\nu = l + 1 + n$ with n positive. As the boundary conditions in this case are slightly different from the quantum mechanics problem (ingoing waves at the horizon) we guess $\nu = l + 1 + n + \delta\nu$ where $\delta\nu$ is a small complex number.

In the small x limit, Eq. (I.6.44) is

$$R_0(x) \approx \frac{\Gamma(-2l-1)}{\Gamma(-l-\nu)}\,x^l + \frac{\Gamma(2l+1)}{\Gamma(l-\nu+1)}\,x^{-l-1}\,. \tag{I.6.45}$$

In terms of the coordinate r and in the small $\delta\nu$ limit

$$R_0(r) \approx (-1)^n \frac{(2l+n+1)!}{(2l+1)!}\,(2kr)^l + (-1)^{n+1}\delta\nu(2l)!n!(2kr)^{-l-1}\,. \tag{I.6.46}$$

In the near-horizon region we write $R_0(r) = \mathring{R}_0(r) + \eta\,\delta R_0(r)$ and we solve order by order in η/M^3. We define a new dimensionless coordinate $x \equiv (r - r_+)/(r_+ - r_-)$ and the quantity $q \equiv (am - 2Mr_+\omega)/(r_+ - r_-)$ where $r_\pm = M \pm \sqrt{M^2 - a^2}$ are the radial location of the Kerr event and Cauchy horizon.

At zeroth order, the radial equation reduces to

$$x^2(x+1)^2\mathring{R}_0''(x)+x(2x+1)(x+1)\mathring{R}_0'(x) \\ +\left(q^2-l(l+1)x(x+1)\right)\mathring{R}_0(x)=0\,, \tag{I.6.47}$$

whose general solution is a combination of the associated Legendre functions $c_1 P^l_{2\mathrm{i}q}(1+2x)+c_2 Q^l_{2\mathrm{i}q}(1+2x)$ which represent, respectively, the ingoing and outgoing waves at the horizon.

Now assume there exists an intermediate region in which the two solutions calculated asymptotically and close to the horizon overlap. Then the small x limit of the asymptotic solution (I.6.46) must be equal to the large x limit of the near-horizon solution, supplied with the requirement of no outgoing waves at the horizon ($c_2=0$). We have

$$P^l_{2\mathrm{i}q}(1+2x)\sim\frac{(2l)!\,x^l}{l!\Gamma(l+1-2\mathrm{i}q)}+\frac{(-1)^{-1-l}l!\,x^{-l-1}}{(2l+1)!\Gamma(-l-2\mathrm{i}q)}\,. \tag{I.6.48}$$

The constant c_1 can be determined by comparing the r^l terms,

$$c_1=\frac{(2k)^l(r_+-r_-)^l(-1)^n l!(2l+n+1)!\Gamma(l+1-2\mathrm{i}q)}{(2l+1)!(2l)!}\,, \tag{I.6.49}$$

while by comparing the r^{-l-1} terms we get

$$\delta\nu=2\mathrm{i}q\left[2k(r_+-r_-)\right]^{2l+1}\left(\frac{l!}{(2l)!(2l+1)!}\right)^2\times \\ \frac{(2l+n+1)!}{n!}\prod_{j=1}^{l}\left(j^2+4q^2\right). \tag{I.6.50}$$

Finally, the relation among n, $\delta\nu$ and $\omega=\sigma+\mathrm{i}\gamma$ gives $\sigma\approx\mu_s$ from the real part, while from the imaginary part

$$\mathrm{i}\gamma=\left(\frac{M\mu_s}{l+1+n}\right)^3\frac{\delta\nu}{M}\,. \tag{I.6.51}$$

Now we are able to give an estimate for the growth time of the instability. At zeroth order, combining Eqs. (I.6.50) and (I.6.51) we notice that for $m>0$ the imaginary part of the frequency is positive and hence the mode is unstable. In particular, for the most unstable mode, $l=m=1$ and $n=0$, at leading order

$$\gamma=\mu_s\frac{a}{M}\frac{(M\mu_s)^8}{24}\,, \tag{I.6.52}$$

and the growth time, for an axion with mass $m_{\mathrm{axion}}=\mu_{\mathrm{axion}}\hbar=10^{-20}$ eV,

$$\tau\equiv1/\gamma=\left(1.58\cdot10^{-6}\ \mathrm{s}\right)\left(\frac{\mu_{\mathrm{axion}}}{\mu_s}\right)\frac{M}{a}\frac{1}{(M\mu_s)^8}\,. \tag{I.6.53}$$

At first order, the zeroth-order solution enters as a "source term",

$$x^2(x+1)^2\delta R_0''(x)+x(2x+1)(x+1)\delta R_0'(x) \\ +\left(q^2-l(l+1)x(x+1)\right)\delta R_0(x)=T(x)\,, \tag{I.6.54}$$

where

$$r_+(r_+-r_-)^2T(x)=-\mathring{R}_0'(x) \\ -\left(\frac{2q^2}{x}+\frac{q^2\left(r_-^2-5r_-r_++2r_+^2\right)}{Mr_+}-l(l+1)\right)\mathring{R}_0(x)\,, \tag{I.6.55}$$

with $R_0 = c_1 P^l_{2iq}(1+2x)$ and c_1 given by Eq. (I.6.49).

The homogenous problem associated to Eq. (I.6.54) for δR_0 is the same as in Eq. (I.6.47) for $\mathring{R}_0$, meaning that its general solution is again a combination of the associated Legendre functions, $c_3 P^l_{2iq}(1+2x) + c_4 Q^l_{2iq}(1+2x)$. Again, c_4 can be set to zero by the request of no outgoing waves at the horizon. The particular solution can be obtained with the method of variation of constants,

$$\begin{aligned}\delta R_{0,\mathrm{p}} = &- \delta R_{0,1} \int \mathrm{d}z \, \frac{T(z)\, \delta R_{0,2}(z)}{z^2(1+z)^2 W(z)} \\ &+ \delta R_{0,2} \int \mathrm{d}z \, \frac{T(z)\, \delta R_{0,1}(z)}{z^2(1+z)^2 W(z)} \,,\end{aligned} \tag{I.6.56}$$

where $W(x)$ is the Wronskian associated with $\delta R_{0,1}(x) = P^l_{2iq}(1+2x)$ and $\delta R_{0,2}(x) = Q^l_{2iq}(1+2x)$.

As in the zeroth-order calculation, assume that there exists an intermediate overlapping region in which the solution in Eq. (I.6.46) is glued with the large r behaviour of the near-horizon solution.

At this stage, we focus on the $l = m = 1$ and $n = 0$ mode which is, at zeroth order, the most unstable. Using Eq. (I.6.48) with $l = 1$ and

$$\delta R_{0,\mathrm{p}} \sim - \frac{c_1 x \left[\mathfrak{R}_1 M r_+ + \mathfrak{R}_2 r_-^2 + \mathfrak{R}_3 r_- r_+ + \mathfrak{R}_4 r_+^2\right]}{2M r_+^2 (r_+ - r_-)^2 q^2 (1+2\mathrm{i}q)\,(1-2\mathrm{i}q)^3\,\Gamma(1-2\mathrm{i}q)} \,, \tag{I.6.57}$$

where

$$\mathfrak{R}_1 = 8\mathrm{i}q(1-2\mathrm{i}q)\left(2q^2+1\right)\left[\psi\left(-2\mathrm{i}q\right) + \gamma_{\mathrm{E}}\right], \tag{I.6.58a}$$

$$\mathfrak{R}_2 = q^2(1-2\mathrm{i}q)\left(28q^2 - 4\mathrm{i}q + 1\right), \tag{I.6.58b}$$

$$\mathfrak{R}_3 = 280\mathrm{i}q^5 - 120q^4 + 70\mathrm{i}q^3 - 32q^2 + 5\mathrm{i}q - 2\,, \tag{I.6.58c}$$

$$\mathfrak{R}_4 = -112\mathrm{i}q^5 + 20q^4 + 28\mathrm{i}q^3 - 25q^2 + 5\mathrm{i}q - 2\,, \tag{I.6.58d}$$

being $\psi(z)$ the digamma function, γ_{E} the Euler–Mascheroni constant and q is now meant to be computed for $m = 1$, we repeat what we have done for the zeroth-order solution, but matching Eq. (I.6.46) with $c_1 \mathring{R}_0 + \eta\left(c_3 \delta R_{0,1} + \delta R_{0,\mathrm{p}}\right)$. We first solve for c_3 and find that $\delta\nu$ gains a correction proportional to η, whose imaginary part sums up to γ computed at zeroth order,

$$\delta\gamma = \frac{\eta k^3 M \mu_s^3 (r_+ - r_-)}{48 r_+^2 q\,(4q^2+1)} \left[\mathfrak{g}_1 M r_+ + \mathfrak{g}_2 r_-^2 + \mathfrak{g}_3 r_- r_+ + \mathfrak{g}_4 r_+^2\right], \tag{I.6.59}$$

where

$$\mathfrak{g}_1 = 8q\left(2q^2+1\right)\left(4q^2+1\right)\Im\psi(-2\mathrm{i}q)\,, \tag{I.6.60a}$$

$$\mathfrak{g}_2 = -q^2\left(4q^2+1\right)\left(28q^2+1\right), \tag{I.6.60b}$$

$$\mathfrak{g}_3 = 2\left(280q^6 + 130q^4 + 21q^2 + 1\right), \tag{I.6.60c}$$

$$\mathfrak{g}_4 = -\left(224q^6 - 36q^4 - 35q^2 - 2\right). \tag{I.6.60d}$$

We can now evaluate how this correction contributes to the growth time of the instability. At leading order, for an axion,

$$\delta\tau = -\left(7.89 \times 10^3\ \mathrm{s}\right)\left(\frac{\mu_{\mathrm{axion}}}{\mu_s}\right)\left(\frac{\eta/M^3}{0.01}\right)\left(\frac{M}{a}\right)^3 \frac{1}{(M\mu_s)^8}\,. \tag{I.6.61}$$

Part II

The geometry of quantum delocalized sources and microscopic models

In this second part, we review our efforts in introducing the notion of quantum delocalization in Einstein's theory and and in constructing microscopic quantum models for black holes in terms of ensembles of harmonic oscillators. We tackle this problem from two different perspectives. The first aims to considering the source of the gravitational field to be in a quantum superposition of position states and then use a sort of semiclassical approximation: the delocalized gravitational masses are taken as sources of a clasical gravitational field described by general relativity. In particular, when we consider a quantum particle of mass M in a delocalized state, we observe that the classical gravitational field sourced by this system corresponds to a regular-black-hole or a wormhole, depending from the value of the parameters of the model. The second approach, instead, inspired by what we know about quasi normal modes spectra, models the internal structure of the compact object in terms of an ensemble of quantum harmonic oscillators. Adopting this perspective, we first show that the Bekenstein-Hawking entropy of a Schwarzschild black hole is the same of an ensamble of N noninteracting oscillators with proper frequency given by the quasinormal frequencies of the hole. We then study a similar system in 2D Jackiw-Teitelboim gravity finding the same relation between a 2D black hole and a set of oscillators. Moreover, since these black holes also admit a dual description in terms of a conformal field theory, we study the relation between the set of harmonic oscillators and the quasinormal modes, finding a natural correspondence between the latter and the de Alfaro-Fubini-Furlan conformally invariant quantum mechanics, which corresponds to the conformal generalization of the harmonic oscillator.

This part is mainly based on:

A. Akil et al. "Semiclassical spacetimes at super-Planckian scales from delocalized sources". *Phys. Rev. D* **108**.4 (2023), 044051. arXiv: 2211.01657 [gr-qc] for Chapter II.2,

M. Cadoni et al. "Quasinormal modes and microscopic structure of the Schwarzschild black hole". *Phys. Rev. D* **104**.12 (2021), L121502. arXiv: 2109.10744 [gr-qc] for Chapter II.3,

M. Cadoni et al. "Quasi-normal modes and microscopic description of 2D black holes". *JHEP* **01** (2022), 087. arXiv: 2111.07763 [gr-qc] for Chapter II.4.

Chapter II.1

Hints for a microscopic description of gravity

General relativity and quantum mechanics stand as two of the most triumphant and remarkable theories ever conceived by the physics community. On one hand, the latter explains the behaviors of fundamental particles existing within a spacetime that serves as the stage upon which quantum systems interact with one another. On the other hand, spacetime itself, as delineated by general relativity, plays a dynamic role, not only dictating the motion of particles but also reacting to their presence. Nevertheless, the domains of applicability of these theories diverge significantly: the former proficiently characterizes the behavior of macroscopic bodies, which can be treated classically and their quantum nature can be safely neglected. In contrast, the latter exhibits extraordinary precision in describing microscopic phenomena, where gravity is completely negligible. In light of these vastly distinct scopes, a fundamental question arises: what happens in regimes where these two descriptions must be used together? Regrettably, and yet intriguingly, we lack a definitive answer to this puzzle, as the two theories are very different both from a physical point of view and in the formalism they use, and we lack any experimental signatures of what a putative quantum-gravity effect could look like. This is mainly due to the fact that it is very hard to probe the regimes where the two descriptions must be used together. As discussed in the previous part of this thesis, a plausible physical system in which general relativity and quantum mechanics could, instead, talk to each other are black holes.

Over the past seven decades, extensive efforts within the literature have aimed at understanding how classical gravity can be modified to align with a quantum framework. The initial steps gave rise to the (incomplete) semiclassical framework, where quantum field theories are considered in a curved, classical spacetime [390]. Despite its incompleteness, this approximation allowed for deeper exploration of fundamental aspects and resulted in the prediction of novel effects, such as Hawking radiation [41]. Subsequently, numerous theories and frameworks have emerged to address the challenge of describing a quantum theory of gravity. Examples include string theory [27–29], supergravity [391, 392], loop quantum gravity [33, 34], euclidean quantum gravity [393], noncommutative geometry [134, 394, 395], asymptotic safety [193, 396], and corpuscular quantum gravity [35–40]. However, despite these extensive efforts, a complete and fully convincing quantum theory of gravity remains elusive, and every theory we concieved fails at describing some of the phenomenology we observe in the universe.

Over the years, various physical systems have been proposed as probes for quantum gravity. These systems include gamma-ray bursts, which offer the potential to investigate modifications of the dispersion relations of electromagnetic radiation [397]; ultra-high-energy cosmic rays [45] and particle-physics experiments [45, 46], where one can explore modifications of the uncertainty principle, which is expected to be influenced by quantum gravity effects [47–50], or modifications to the cross sections of some scattering processes; and gravitational waves, which may provide insights into the quantum structure of spacetime near event horizons [51, 52]. Nevertheless, current experiments still lack evidence of quantum-gravity effects, making the construction of a comprehensive theory of gravity in the microscopic regime a formidable challenge (for a more exhaustive discussion, see, e.g., Ref. [398] and references therein).

The absence of experimental evidence has been long attributed to the difficulty of probing the Planck scale, at which quantum mechanics and gravity are expected to play comparable roles [44]. However, as we already discussed in the Introduction and in Part I, in more recent times, we

have gained more theoretical evidence about the fact that some of the interesting phenomenology arising from quantum gravity could be measured even at larger scales. This new view, motivated by the corpuscular approach to quantum gravity, also stems from the fact that the underlying theory could show a multi-scale behavior, which is expected to generate some infrared scales effectively encoding quantum effects at the Schwarzschild radius R_S [1, 2, 5], or even at galactic or cosmological distances [64, 65, 71, 72, 399].

Another interesting perspective in studying the quantum gravity problem is to use a bottom-up approach, similarly to what we did in Part I, in particular in Chapter I.2. In the previous chapters, we discussed the possibility of parameterizing some beyond-general-relativity effects. For instance, assuming that quantum effects can be effectively described by an anisotropic fluid (see Chapter I.2 and Ref. [1]), we showed that the most interesting phenomenology arises when the length scale at which these deviations take place is of the order of the classical horizon radius R_S. Using the same logic, one could try to start from general relativity and insert some level of "quantumness" into Einstein's theory (see, e.g., Refs. [400–406]), or, on the contrary, to begin with quantum mechanics in order to see that is the impact of the quantum description on the dynamics of the gravitational field (see, e.g., Refs. [47–50, 402, 404, 407, 408]).

In this second part of the present dissertation, we choose to follow this idea in two distinct ways. On one hand, in Chapter II.2, we use the uncertainty principle to derive a quantum-regular-black-hole metric. On the other hand, in Chapters II.3 and II.4, we adopt the opposite perspective, in which we start from quantum mechanics and we try to reproduce the Bekenstein-Hawking entropy formula modelling a black hole as a set of oscillators.

Chapter II.2

Regular geometries sourced by quantum delocalized sources

The presence of singularities in general relativity (GR) [86, 87, 114], both for black holes and cosmology or even deviations from Newtonian dynamics at galactic scales or the accelerated expansion of the universe [39, 64, 70–72], can be regarded as a problem that could possibly find a natural resolution in a quantum theory of gravity.

In this chapter, instead of trying to construct a fully consistent, i.e., finite or renormalizable, theory of quantum gravity (QG), we follow a bottom-up approach, starting from GR and quantum theory and trying to gradually insert more "quantumness" into gravity. This is suited, for instance, to study quantum superpositions of reference frames or detectors [402, 404, 407, 408], entanglement of quantum systems mediated by gravitational fields [409, 410], and the investigation of the behavior of gravitational sources (and even spacetimes) in quantum superpositions [400–406]. The advantage of these approaches is that they do not rely on a definite ultraviolet (UV) formulation of QG, so that they are likely to be experimentally tested in the foreseeable future. In fact, there is a number of table-top experiments, not only being designed and discussed in the literature [409–413], but attempts to implement them are ongoing as well [414–416]. On the other hand, deviations from GR could be also probed and measured in the strong gravity regime, i.e., via gravitational-wave (GW) experiments (see, e.g., Refs. [343, 365, 417–419]) or, potentially, in black-hole shadow observations (see, e.g., Refs. [13, 420–422]).

This bottom-up approach faces, however, a number of difficulties. For instance, it was argued in [423, 424] that gravity may cause decoherence, forcing the collapse of the quantum wave functions of matter, hence leaving no space for quantum superpositions of gravitational states. According to Penrose, the fundamental problem lies in the inconsistency between general covariance and the equivalence principle with the linearity of quantum mechanics. This idea was further explored for quantum states near a black hole [425–427]. It was, however, shown in [428] that, when the black hole is put in a superposition of masses, this decoherence of the quantum state largely decreases. Penrose's arguments were also challenged in [407, 429], where a unitary locally-inertial-reference-frame transformation was derived within a set of assumptions, supporting the validity of the equivalence principle for observers in a quantum superposition of reference frames.

The main goal of the present chapter is trying to build a bridge between these different approaches. Without making any assumption about the underlying fundamental quantum theory of gravity, we derive an effective description of gravity emerging from quantum superposition of configurations of the source. We first follow a simplified approach by working in a Newtonian framework and regarding the standard gravitational potential as an operator acting on a Hilbert space spanned by states of the source of the gravitational field. We consider the source in a superposition of different locations in space, with a general isotropic probability amplitude $\phi(r)$. We then derive the effective Newtonian potential by taking the expectation value of the gravitational-potential operator, and the effective metric is derived using a covariant uplifting method. We then reproduce and extend the previous results by using a more general approach. We still consider a source in a quantum superposition of different locations, but we assume, in addition, that the metric is described by the classical Schwarzschild solution in each branch of the superposition. We then derive the explicit form of the effective metric by assuming that the

source is in a quantum state described by a Gaussian wave-packet of width R.

The resulting spacetime metric is asymptotically flat and quickly tends to the Schwarzschild one at large distances. However, important differences emerge in the inner core of the solutions. The metric is invariant under reflection of the radial coordinate $r \longleftrightarrow -r$, so that it describes two asymptotically-flat and equivalent regions. Moreover, due to the quantum uncertainty $\Delta r \sim R$ in the position of the source, the radius of the transverse S^2 in the metric does not shrink to zero for $r \to 0$, but reaches a non-zero R-dependent value. The latter represents the radius of a throat connecting the two asymptotically-flat regions, and thus resembles the throat of a wormhole. Depending on the strength of the quantum-superposition effects, our metric describes three classes of objects: (1) nonsingular black holes with an event horizon and a "quantum hair"; (2) one-way critical wormholes; (3) traversable (in the sense of Morris-Thorne [82]) wormholes.

Our approach does not rely on a would-be specific microscopic theory of gravity. The simplest and more general guess for the effective theory is GR sourced by an anisotropic fluid. This type of fluid has been extensively used to construct stellar and black-hole models (both singular and regular) and in cosmology to address the dark matter and dark energy problems (for an incomplete list, see, e.g., Refs. [1, 71, 73, 75, 77, 118, 145, 147–149, 151, 152, 155, 197, 430–432] and references therein). We therefore compute the stress-energy tensor and discuss the associated energy conditions by assuming our effective metric to represent an exact solution of Einstein's field equations, sourced by an anisotropic fluid. As expected, we find that all the usual energy conditions are violated in all the three models.

We then study the thermodynamic properties of the black-hole model. We find two thermodynamic branches of black-holes: those in the "Hawking branch", which are unstable with respect to their radiation (they have negative specific heat), and those which, instead, represent thermodynamically stable configurations and have positive specific heat. By computing the free energy, we show that the latter are always thermodynamically preferred. Using the general entropy formula recently proposed in Ref. [1] we show that the extremal black hole configuration not only has zero temperature, but also is a zero-entropy state. We also revisit the Hawking radiation spectrum and show it is Planckian, but with a different surface gravity. We compute the evaporation time, which turns out to be infinite in the extremal limit, thus confirming the thermodynamic stability of this configuration.

Finally, we extensively analyze the phenomenological properties of our spacetimes, which could possibly give observable signatures in the near future. We study the geodesic structure in detail, focusing on time-like and null geodesics. In both cases, we analyze the evolution of the geodesic congruence, showing that in neither of the two cases we have formation of caustics, which thus further confirms the geodesic completeness of our spacetime. This is a clear consequence of the violation of the energy conditions, which allows to circumvent Penrose's singularity theorems. Additionally, we compute the position of the light ring, i.e., the position of the last unstable photon orbit, showing that the presence of R causes potentially detectable deviations from the standard Schwarzschild prediction.

We also study scalar perturbations in this spacetime. While for small values of R, the effective potential in the Klein-Gordon equation has a single peak, for the stellar wormhole we observe a double peak. This indicates the possibility of having characteristic signatures in the quasi-normal modes (QNMs) spectrum, namely echoes [51, 175, 343, 433–435]. For models with a single peak, we exploit the construction of Ref. [234] to derive an analytical expression of the quasi-normal frequencies in the eikonal regime.

The chapter is organized as follows. In Section II.2.1, we derive the metric for our models following the two approaches mentioned above. The general geometric properties of the metric are studied in Section II.2.2, where we also investigate the usual energy conditions and find violation of all of them. We also explicitly prove that the horizonless wormhole is traversable. Section II.2.3 contains an extensive analysis on the thermodynamic properties of the black-hole model, its Hawking radiation and the evaporation time. In Section II.2.4, we investigate the phenomenological properties of our models.Specifically, we analyze the time-like and null geodesics and the evolution of their congruence and we show that the spacetime is geodesically complete. In the case of null-geodesics, we also compute the position of the light ring. Finally, we compute the analytical expression of the quasi-normal frequencies in the black-hole case in the eikonal regime.

In this chapter, we use units in which $c = \hbar = k_{\rm B} = 1$.

II.2.1 The derivation of the metric

Localized gravitational sources have been studied for centuries, and can be described through Newtonian mechanics or GR, depending on the physical settings. However, quantum mechanics showed that matter cannot be completely localized. Therefore, it is natural to study quantum delocalized gravitational sources. Here, we consider a point-like particle in a quantum superposition of different locations, and we probe its gravitational field. We will first study the quantum corrected Newtonian potential, and do a covariant uplifting to derive the spacetime metric that it generates. The resulting "quantum" metric will turn out to be a regular black hole that has interesting properties. We will then proceed by considering the superposition in a full covariant framework. We will use the formalism established in [429, 436], through which one can construct a quantum superposition of classical spacetimes. We assume GR to hold in each branch of the superposition. Then, we will use the resulting state to compute the expectation value of the metric operator and get the effective quantum spacetime metric. In principle, in such a situation, the probe would get in a joint superposition (entanglement) with the source, as shown in [436] and as intuitively expected. However, we are here only interested in an average/statistical description of the source, which is the heart of semi-classical approximation, and thus we will treat the probe *classically*.

II.2.1.1 Quantum Newtonian potential uplifting

In this section we will work in the framework of Newtonian gravity. We assume that a point source of mass M interacts gravitationally with a probe P of mass m through the Newtonian potential. While the latter is treated as a classical particle, the source is assumed to be in a quantum superposition of different locations. We use a spherical coordinate system where r indicates the radial distance from the origin. The gravitational-potential operator describing the system is

$$\hat{V} = -\frac{GMm}{|\hat{r}_M - I_M\,\mathbf{r}_m|} \tag{II.2.1}$$

where $\hat{r}_M$ is the position operator for the source, while $\mathbf{r}_m$ is treated as a c-number giving the three-dimensional vector position of the probe. I_M, instead, is the identity operator acting in the Hilbert space $\mathcal{H}_M$ pertaining to the source. Moreover, the operator being in the denominator simply denotes the inverse of that operator, i.e., in our notation $\frac{1}{\hat{A}+\hat{I}b} = (\hat{A}+\hat{I}b)^{-1}$.

In $\mathcal{H}_M$, we define the state of the source as

$$|\psi\rangle_M = \int \mathrm{d}^3r\ \phi(\mathbf{r})\,|r\rangle_M\,, \tag{II.2.2}$$

i.e., we express it in terms of a superposition of the complete set of orthonormal generalized eigenstates of $\hat{r}_M$, being $\phi(\mathbf{r})$ a complex function whose modulus gives the probability amplitude for the position of the source.

The quantum corrected potential is given by the expectation value of $\hat{V}$ with respect to the state $|\psi\rangle_M$, which gives[1]

$$\langle\hat{V}\rangle = -{}_M\langle\psi|\frac{GM}{|\hat{r}_M - I_M\,\mathbf{r}_m|}|\psi\rangle_M \tag{II.2.3}$$

$$= -GM\int \mathrm{d}^3r\,\frac{|\phi(\mathbf{r})|^2}{|\mathbf{r}-\mathbf{r}'|} \tag{II.2.4}$$

$$= -2\pi GM\int_0^\pi \mathrm{d}\theta\sin\theta\int_0^\infty \mathrm{d}r\,r^2\frac{|\phi(r)|^2}{\sqrt{r^2+r'^2-2rr'\cos\theta}} \tag{II.2.5}$$

$$= -\frac{2\pi GM}{r'}\int_0^\infty \mathrm{d}r\,r\,(r'+r-|r-r'|)\,|\phi(r)|^2, \tag{II.2.6}$$

[1] We note that there are strong similarities with the approaches based on the Newton-Schrödinger (NS) equation [437–441] (however, see, e.g., Refs. [440, 442, 443] for challenges to this approach). These analogies are mostly embodied by Eq. (II.2.4), which is the usual way to write the potential appearing in the NS equation. Despite this, it is important to stress that in our approach we do not rely here on any dynamics described by the NS equation.

where, to lighten the notation, we indicated with $\mathbf{r}$ and $\mathbf{r}'$ the positions of the source and the probe, respectively, while the last two equalities are valid only if we assume $\phi(\mathbf{r})$ to be isotropic. Given the spherical symmetry of the case under consideration, this assumption is satisfied. Notice that $\langle\hat{V}\rangle$ does not depend on the relative phases between the states $|r\rangle_M$. The latter commonly arise due to a unitary time-evolution of a would-be joint state of the probe, which gets entangled with the source [436]. In this work, however, we are not interested in a fine-grained picture describing the quantum state of one particle and its entanglement with the gravitational field, but rather in the effective description of how, on average, classical localized test particles behave in presence of quantum delocalized sources. This is fully consistent with our choice of treating sources as quantum objects and test particles classically. In this "semiclassical" framework, computing the expectation value Eq. (II.2.3) in eigenstates of $\hat{V}$, erases completely all information regarding possible relative phases in the superposition (II.2.2).

Following the standard method of covariant uplifting, one can use this potential to construct some components of the spacetime metric. The idea is that this potential can be seen as some weak field limit of a general relativistic metric, which can be guessed from the potential as

$$-g_{00} = g_{rr}^{-1} \equiv f(r') = 1 + 2\langle\hat{V}(r')\rangle. \tag{II.2.7}$$

Note that the conventional minus sign is already inserted in the definition of $\langle\hat{V}\rangle$.

Looking at Eq. (II.2.2), the most basic requirement we can impose on $\phi(r)$ is L^2-integrability (so that the state (II.2.2) can be correctly normalized). This requirement is sufficient to guarantee asymptotic flatness (more precisely, an asymptotic Schwarzschild form) of the resulting metric at spatial infinity, as we now show. Using Eqs. (II.2.3) and (II.2.7), we write the metric function in terms of the probability amplitude $\phi(r)$ of the position of the source

$$f(r') = 1 - \frac{4\pi GM}{r'}\int_0^\infty \mathrm{d}r\, r\,(r' + r - |r - r'|)\,|\phi(r)|^2. \tag{II.2.8}$$

To get rid of the absolute value, we separate the integral into two parts, one for $r < r'$, for which $|r - r'| = -(r - r')$, and the other for $r > r'$, for which $|r - r'| = r - r'$. Therefore, the integral in the metric function is separated accordingly

$$\frac{1}{r'}\int_0^\infty \mathrm{d}r\, r\,(r' + r - |r - r'|)\,|\phi(r)|^2 = \frac{2}{r'}\int_0^{r'} \mathrm{d}r\, r^2\,|\phi(r)|^2 + 2\int_{r'}^\infty \mathrm{d}r\, r\,|\phi(r)|^2. \tag{II.2.9}$$

L^2-integrability and normalization of the $\phi(r)$ distribution gives a constraint on the form of the probability amplitude, namely

$$4\pi\int_0^\infty \mathrm{d}r\, r^2\,|\phi(r)|^2 = 1. \tag{II.2.10}$$

We will consider the behavior at asymptotic infinity first. Indeed, by taking the $r' \to \infty$ limit of Eq. (II.2.9), the second integral goes to zero, since the two integral extrema become identical. This is true as long as the integral converges, so that the $r' \to \infty$ limit and the integral commute, which is guaranteed by virtue of Eq. (II.2.10). Indeed, $\phi(r)$ is L^2-integrable when the minimal condition

$$|\phi(r)|^2 \sim \frac{1}{r^4} + \mathcal{O}(r^{-5}), \qquad \text{for } r \to \infty \tag{II.2.11}$$

is satisfied. In this case, the integral in Eq. (II.2.9) reduces to

$$\int_{r'}^\infty \mathrm{d}r\, r\,|\phi(r)|^2 \sim \int_{r'}^\infty \mathrm{d}r\,\frac{1}{r^3} \sim \frac{1}{r'^2} \to 0 \qquad \text{for } r' \to \infty. \tag{II.2.12}$$

The first integral, on the other hand, is equal to $1/4\pi$ by virtue of Eq. (II.2.10). In other words, the metric reduces to $f(r') = 1 - (4\pi GM/r')(1/2\pi) = 1 - 2GM/r'$, which is the usual, asymptotically-flat, Schwarzschild metric.

One can also show that L^2-integrability of $\phi(r)$ is only a necessary condition[2] to have a nonsingular metric, i.e., a spacetime without a central singularity at $r' = 0$. However, the analysis is more involved than before. We first separate the integral in the condition (II.2.10) into two parts

$$\int_0^{r'} \mathrm{d}r\, r^2\, |\phi(r)|^2 + \int_{r'}^{\infty} \mathrm{d}r\, r^2\, |\phi(r)|^2 = \frac{1}{4\pi}. \tag{II.2.13}$$

Next, we use this decomposition to rewrite the right-hand side of Eq. (II.2.9) as follows

$$\frac{2}{r'}\int_0^{r'} \mathrm{d}r\, r^2\, |\phi(r)|^2 + 2\int_{r'}^{\infty} \mathrm{d}r\, r\, |\phi(r)|^2 = \frac{1}{2\pi r'} - \frac{2}{r'}\int_{r'}^{\infty} \mathrm{d}r\, r^2\, |\phi(r)|^2 + 2\int_{r'}^{\infty} \mathrm{d}r\, r\, |\phi(r)|^2. \tag{II.2.14}$$

The second integral on the right-hand side is well-behaved by virtue of L^2-integrability and, in the $r' \to 0$ limit, the divergent factor $2/r'$ in front of it cancels the other divergent term $1/2\pi r'$. The last integral, instead, can be evaluated by parts to yield

$$2\int_{r'}^{\infty} \mathrm{d}r\, r\, |\phi(r)|^2 = \left[r^2|\phi(r)|^2\Big|_{r'}^{\infty} - \int_{r'}^{\infty} \mathrm{d}r\, r^2\, \partial_r|\phi(r)|^2\right]. \tag{II.2.15}$$

As long as we consider ϕ as a function and not as a distribution (thus, as long as we have smearing effects), the first "boundary" term will always be zero. Therefore, we see that the requirement of also $\partial_r|\phi(r)|^2$ being an L^2-function seems to guarantee absence of singularities for $r' \to 0$. This additional condition alone, however, is still insufficient, as it does not automatically prevent the presence of conical singularities. The latter can be avoided if the spacetime is endowed with a throat, i.e., the angular part of the metric does not shrink to zero for $r' \to 0$ [116]. In Section II.2.2, we will argue that an important consequence of superposing sources in different locations, together with the related uncertainty principle, guarantees the presence of a throat whenever $\phi(r)$ is L^2-integrable and sharply peaked at $r = 0$.

The specific spacetime describing the local behavior of the metric near $r' \to 0$ will, of course, strongly depend on the function of r'

$$\mathcal{F}(r') \equiv \int_{r'}^{\infty} \mathrm{d}r\, r^2\, \partial_r|\phi(r)|^2\,, \tag{II.2.16}$$

and on the precise form of the angular part of the metric. This is a clear manifestation of the nonlocal nature of the quantum-mechanical approach we are using. The fact that the angular part of the metric is unspecified in this construction prevents us from performing a complete analysis of the different possibilities.

II.2.1.2 A simple realization: Gaussian distribution

Our approach does not allow to determine the probability amplitude function $\phi(r)$. In fact, we are not making any assumption on the fundamental QG dynamics, which should determine ϕ. The latter is only weakly constrained by general quantum mechanical principles. It must be L^2-integrable, implying that it must decrease sufficiently fast as $r \to \infty$. Moreover, the existence of a classical limit, in which the mass M behaves as a point particle in the Newtonian theory (or GR), requires $|\phi|^2$ to be peaked in $r = 0$. The most natural and simple candidate, respecting these and the other requirements listed in the previous subsection, is a Gaussian distribution of width R centered in $r = 0$. That is

$$|\psi\rangle_M = \left(\frac{2\sqrt{2}}{\pi^{3/2}R^3}\right)^{\frac{1}{2}} \int \mathrm{d}^3r\, e^{-\frac{r^2}{R^2}}\, |r\rangle_M\,. \tag{II.2.17}$$

Physically, this means that we are using a wave packet with uncertainty $\Delta r \sim R$ as a quantum state describing the superposition of the source location states. The resulting momentum uncertainty

[2] L^2-integrability alone is not sufficient to guarantee regularity of the metric. For example, a distribution like $\delta(r)/r^2$, which is L^2-integrable, generates the usual Schwarzschild singularity when plugged into Eq. (II.2.8).

reads $\Delta P \sim 1/R$. We can therefore associate to our superposition state a De Broglie length $\lambda_{\text{DB}} \sim R$. As we will show in the following sections, a comparison of λ_{DB} with the gravitational (Schwarzschild) radius of the source will allow us to measure the strength of quantum effects.

Plugging Eq. (II.2.17) into Eq. (II.2.3) we get

$$\langle \hat{V} \rangle = -\frac{GM}{r} \text{Erf}\left(\sqrt{2}\frac{r}{R}\right). \tag{II.2.18}$$

Here and in the rest of the present work, unless otherwise specified, we have dropped the prime symbol to simplify the notation. Eq. (II.2.18) gives, upon covariant uplifting,

$$-g_{00} = g_{rr}^{-1} = 1 - \frac{2GM}{r} \text{Erf}\left(\sqrt{2}\frac{r}{R}\right). \tag{II.2.19}$$

As we shall see in Section II.2.2, for particular values of the width R, this metric has a horizon at $r = r_{\text{H}}$, where $g_{00}(r_{\text{H}}) = 0$, but no divergences at $r = 0$, as expected. The classical Schwarzschild solution, compatible with a classical source exactly placed at $r = 0$, is only recovered when the uncertainty in the position, quantified by R, is sent to zero.

Interestingly, the same metric function was found also in other works dealing with non-local gravity effects and black-hole mimickers in this framework [319, 444–447].

II.2.1.3 A more general approach

In the previous section we derived the expectation value of the potential operator, given a source in a quantum superposition and a localized probe. Here we will take a slightly different approach which will turn out to give the same results, but further allowing for a derivation of the angular part of the metric as well. The main difference is that we will now work in a full covariant framework and the source is treated as being in a superposition of different locations of a given classical manifold. The mathematical formalism needed to do this was introduced in [448], and further developed by Giacomini, Brukner and others [407, 429, 449] in a series of papers focused on quantum observers in a superposition of different reference frames. In their approach, they also consider the possibility of having a superposition of different *classical* manifolds.

They start with the state $|\Psi^{(i)}\rangle$ describing a delocalized gravitational source in a *single* manifold, labeled by a fixed index i, and the gravitational field associated with it

$$|\Psi^{(i)}\rangle = \frac{1}{2}\int \mathrm{d}^4 x_S \sqrt{-g^{(i)}(x_S)}\, \phi_i(x_S) |g^{(i)}(x_S - x_P)\rangle |x_S^{(i)}\rangle. \tag{II.2.20}$$

Here, $|x_S^{(i)}\rangle$ is the position eigenstate of the source, while we are again treating the probe classically, at a position x_P. This implies that also here the source coordinate x_S is an operator, whereas x_P is a number. As in the previous section, $\phi_i(x_S)$ describes the probability amplitude of the source position x_S in the i-th manifold, whereas $|g^{(i)}(x)\rangle$ is the state describing the spacetime metric. The factor $1/2$ is due to the symmetry under the exchange of x_S and x_P. Moreover, $|g^{(i)}(x)\rangle$ describes a classical spacetime $\mathcal{M}_i$, with i running through the manifolds of the superposition, i.e., $\mathcal{M} = \{\mathcal{M}_i\}_{i=1,\dots,N}$. By summing over the states labelled by i, as well as by integrating over x_S, we construct a quantum superposition of classical spacetimes described by the state $|\Psi\rangle = \sum_i |\Psi^{(i)}\rangle$. We stress, again, the fact that this is not meant to represent a fully consistent second quantization of the gravitational field, but it just represents a way to build a quantum superposition of classical geometries in a first-quantization framework. Thus, summing over manifolds has not the meaning of summing over different spacetime geometries in a diffeomorphism-invariant way, but it is just a formal definition of such superposition.

Now we assume that, in each manifold $\mathcal{M}_i$, there exists a metric operator $\hat{g}_{\mu\nu}^{(i)}(\hat{x})$ acting on the Hilbert space spanned by its generalized eigenstates $|g^{(i)}(x)\rangle$ as

$$\hat{g}_{\mu\nu}^{(i)}(\hat{x})|g^{(i)}(x)\rangle = g_{\mu\nu}^{(i)}(\hat{x})|g^{(i)}(x)\rangle. \tag{II.2.21}$$

The eigenvalues $g_{\mu\nu}^{(i)}(\hat{x})$ are not numbers, but rather operators acting on the Hilbert space spanned by the eigenstates of the coordinates $|x\rangle$. When acting on a position eigenstate, it gives the usual

spacetime metric as eigenvalues

$$g^{(i)}_{\mu\nu}(\hat{x})|x\rangle = g^{(i)}_{\mu\nu}(x)|x\rangle. \tag{II.2.22}$$

Describing states of the gravitational field as a quantum superposition of positions and spacetimes is not straightforward and can be controversial [423]. However, there was a very nice argument presented in Ref. [436] supporting the validity of this construction. The authors start with a massive object (the source) in a superposition of 2 locations, and a localized probe falling through. They do not construct an *a priori* superposition of spacetimes, like $|g_1\rangle+|g_2\rangle$. Instead, they construct a quantum-reference-frame transformation which makes the source localized and leaves the free-falling probe in a superposition of 2 locations. In that case, the physics is described by the semiclassical approach. They then evolve the superposed probe state on the determined curved background, and, at the end of the evolution, they transform back to the original frame in which the source is in a superposition. The result turns out to be in exact accordance with the case where the whole process is done with the source being in a superposition of the two locations, described by the state $|g_1\rangle + |g_2\rangle$.

The state $|\Psi\rangle$ defined above can now be used to compute the metric operator expectation value,

$$\begin{aligned}\langle\hat{g}_{\mu\nu}(\hat{x})\rangle \equiv \langle\Psi|\hat{g}_{\mu\nu}(\hat{x})|\Psi\rangle &= \frac{1}{4}\sum_{i,j=1}^{N}\int \mathrm{d}^4x'_S\sqrt{-g^{(j)}(x'_S)}\phi^*_j(x'_S)\langle g^{(j)}(x'_S - x_P)|\langle x'^{(j)}_S|\hat{g}^{(i)}_{\mu\nu}(\hat{x}) \\ &\quad\times\int \mathrm{d}^4x_S\sqrt{-g^{(i)}(x_S)}\phi_i(x_S)|g^{(i)}(x_S - x_P)\rangle|x^{(i)}_S\rangle \\ &= \sum_{i=1}^{N}\int \mathrm{d}^4x_S\,\sqrt{-g^{(i)}(x_S)}\,|\phi_i(x_S)|^2\,g^{(i)}_{\mu\nu}(x_S - x_P),\end{aligned} \tag{II.2.23}$$

where we assumed that the metric and the position eigenstates of the source are orthogonal to each other, and specifically (see also Refs. [429, 449])

$$\frac{1}{4}\langle g^{(j)}|g^{(i)}\rangle\langle x'^{(j)}_S|x^{(i)}_S\rangle = \frac{\delta^{(4)}(x_S - x'_S)}{\sqrt{-g^{(i)}(x_S)}}\delta^{ij}\,, \tag{II.2.24}$$

where the Kronecker delta emphasizes the fact that gravitational fields on different manifolds are perfectly distinguishable. On a curved background, the distribution $|\phi_i(x)|^2$ now satisfies the normalization condition $\int \mathrm{d}^4x\,\sqrt{-g^{(i)}(x)}\,|\phi_i(x)|^2 = 1$. Note also that we are summing over different manifolds in order to account for extra physical parameters which can as well be in quantum superpositions. That sum can also be an integral for continuous parameters. The mass of the source or the probe being in a superposition is a simple example (see the end of the present Section).

As previously noticed, summing over geometries, even in a first quantization framework, is a quite involved procedure. The completeness of the space spanned by these geometries and diffeomorphism invariance are important issues one should address before performing the summing [450]. In order to avoid these problems and to keep things as simple as possible, we just consider superposition of the positions of a gravitational source in a single given geometry and in a given coordinate system. We fix therefore a particular gauge, requiring that the spacetime metric is the Schwarzschild metric. We also fix the parametrization by writing the latter in the Eddington-Finkelstein coordinates (v, r, θ, φ) for simplicity. Therefore, Eq. (II.2.23) becomes

$$\langle\hat{g}_{\mu\nu}(\hat{x})\rangle = \mathcal{N}^2\frac{2\sqrt{2}}{\pi^{\frac{3}{2}}R^3}\int \mathrm{d}v\,\mathrm{d}r\,\mathrm{d}\theta\,\mathrm{d}\varphi\,r^2\sin\theta\,e^{-2r^2/R^2}g_{\mu\nu}(r - r_P). \tag{II.2.25}$$

Given that the metric is static, i.e., invariant under v-translations in each branch of the superposition, we have to renormalize the integral over v with a renormalization factor $\mathcal{N}^2$. Moreover, given the spherical symmetry of the metrics $g^{(i)}$, we can also integrate over φ. This yields

$$\langle\hat{g}_{\mu\nu}(\hat{x})\rangle = \frac{4\pi\sqrt{2}}{\pi^{\frac{3}{2}}R^3}\int \mathrm{d}r\,\mathrm{d}\theta\,r^2\sin\theta\,e^{-2r^2/R^2}g_{\mu\nu}(r - r_P). \tag{II.2.26}$$

Plugging the explicit expressions of $g_{\mu\nu}$ in terms of the Schwarzschild metric into the above, the expectation value of the metric operator reads

$$\langle \mathrm{d}s^2 \rangle = \left[-1 + \frac{2GM}{r} \mathrm{Erf}\left(\sqrt{2} \frac{r}{R} \right) \right] \mathrm{d}v^2 + 2\mathrm{d}v\mathrm{d}r + \left(r^2 + \frac{3R^2}{4} \right) \mathrm{d}\Omega^2, \quad \mathrm{d}\Omega^2 = \mathrm{d}\theta^2 + \sin^2\theta \mathrm{d}\varphi^2, \tag{II.2.27}$$

where now the radial coordinate r corresponds to the distance of the probe to the source. Interestingly, thus, for a Gaussian distribution of the probability amplitude of the source, one gets the same metric components computed in the previous section, supporting the result, and, in addition, interesting angular components emerge.

Transforming to the Schwarzschild coordinates yields

$$\langle \mathrm{d}s^2 \rangle = \left[-1 + \frac{2GM}{r} \mathrm{Erf}\left(\sqrt{2} \frac{r}{R} \right) \right] \mathrm{d}t^2 + \frac{1}{1 - \frac{2GM}{r} \mathrm{Erf}\left(\sqrt{2} \frac{r}{R} \right)} \mathrm{d}r^2 + \left(r^2 + \frac{3R^2}{4} \right) \mathrm{d}\Omega^2. \tag{II.2.28}$$

Note that we can also introduce a superposition of masses. In a simplified formulation, one can promote the mass in the Schwarzschild metric to an operator, and let it act on a state vector accounting for the dependence of the system from its ADM mass. In this way, we can consider a quantum superposition of mass eigenstates. Note that the mass operator corresponds to an observable in quantum gravity, since it is an explicitly gauge-invariant quantity. Its nonlocal nature is here inherited from the superposition of the different eigenstates. We start therefore by writing the state as

$$|\Psi\rangle = \frac{1}{2} \int \mathrm{d}^4 x_S \sqrt{-g(x_S)}\, \phi(x_S) |g(x_S - x_P))\rangle |x_S\rangle \int \mathrm{d}M\, \psi(M) |M\rangle. \tag{II.2.29}$$

where $\psi(M)$ describes the distribution of different masses. The previously defined metric operator, on the other hand, will be promoted to $\hat{g}_{\mu\nu}(\hat{x}, \hat{M})$. Then, assuming the Schwarzschild metric in each branch of the superposition, and focusing on the mass state, we have

$$\langle g_{\mu\nu}(\hat{x}, \hat{M}) \rangle = \int \mathrm{d}M'\, \psi^*(M') \langle M' |\, \hat{g}_{\mu\nu}(\hat{x}, \hat{M}) \int \mathrm{d}M\, \psi(M)\, |M\rangle. \tag{II.2.30}$$

Substituting the zeroth component of the metric as an example reads

$$\langle g_{00} \rangle = \int \mathrm{d}M'\, \psi^*(M') \langle M' | \left(1 - \frac{2G\hat{M}}{\hat{r}} \right) \int \mathrm{d}M\, \psi(M)\, |M\rangle. \tag{II.2.31}$$

Assuming $\psi(M)$ to be normalized to 1, we have

$$\int \mathrm{d}M\, |\psi(M)|^2 = 1 \tag{II.2.32}$$

$$\int \mathrm{d}M\, |\psi(M)|^2 M = \langle M \rangle \equiv M_{\mathrm{cl}}, \tag{II.2.33}$$

where we have identified the classical mass M_{cl} with the expectation value of the operator $\hat{M}$. When plugged together into Eq. (II.2.30), one easily finds

$$\langle g_{\mu\nu}(\hat{x}, \hat{M}) \rangle = 1 - \frac{2GM_{\mathrm{cl}}}{\hat{r}}. \tag{II.2.34}$$

The same works for the other components of the metric tensor. An important remark is that these results are totally independent of the details of the superposition, i.e., of the explicit form of the distribution $\psi(M)$. Eq. (II.2.28) is again recovered when we compute the expectation value of the operator (II.2.34) with the position states of the source.

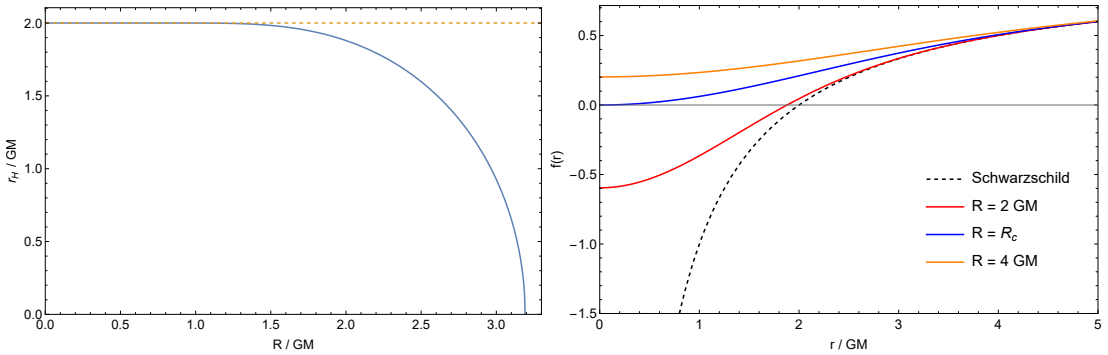

Figure II.2.1: **Left panel**: Horizon radius as a function of the smearing parameter R, both in units of GM. We see that, for values of R greater than $R_c \simeq 3.19\,GM$, the horizon disappears and we are left with a horizonless object. The horizontal dashed line corresponds to the position of the classical Schwarzschild horizon $2GM$. **Right panel**: Behavior of the metric function (II.2.35) as a function of the radial coordinate for different value of R: $R = 2GM$ (solid red line), $R = R_c$ (solid blue line) and $R = 4GM$ (solid orange line). The first case corresponds to a solution with an event horizon (regular black holes), the second to a "critical" wormhole with a null throat, while the latter to a horizonless object, which is a two-way wormhole.

II.2.2 Metric Structure

In the remainder of the work, we will use $f(r)$ to indicate the metric function in Eq. (II.2.28), i.e.,

$$f(r) = 1 - \frac{2GM}{r}\mathrm{Erf}\left(\sqrt{2}\frac{r}{R}\right). \tag{II.2.35}$$

The metric tends to the standard Schwarzschild metric for $r \gg R$. As also mentioned at the end of Section II.2.1.2, this last result can also be obtained in the $R \to 0$ limit, i.e., in the limit in which the width of the Gaussian position distribution goes to zero, which yields the standard Dirac-delta distribution, thus recovering the classical central singularity.

In the $r \to 0$ limit, instead, the metric function behaves as

$$f(r) \simeq 1 - \frac{4GM\sqrt{2/\pi}}{R} + \frac{8GM\sqrt{2/\pi}}{3R^3}r^2 + \mathcal{O}(r^3). \tag{II.2.36}$$

We see that there are no spacetime singularities at $r = 0$. This suggests the relevance of the present approach to the construction of nonsingular black-hole models, which have recently gained increasing attention (see, e.g., Refs. [1, 116, 118, 451]). The local $r = 0$ behavior of the metric function f is similar, except for the constant term, to that of the anti-de-Sitter case. We have explicitly computed the curvature invariants for our spacetime metric (see Appendix II.A) and showed that they remain finite at $r = 0$. One can also easily show that the $r =$ constant-time slices of our spacetime have a surface with area $\mathcal{A} = 4\pi\left(r^2 + \frac{3}{4}R^2\right)$, which is minimized at $r = 0$. The radius of the two-sphere does not shrink to zero, but to the minimal non-vanishing value $\sqrt{3/4}\,R$. This means that, near $r = 0$, the $t =$ constant sections of our spacetime exhibit a $\mathbb{R} \times S^2$ local topology. Additionally, we have an invariance of the metric under $r \longleftrightarrow -r$. Altogether this means that the metric (II.2.28) describes two asymptotically-flat equivalent regions, connected through a long throat of minimal radius $\sqrt{3/4}\,R$, i.e., a wormhole. Indeed, in the $M \to 0$ limit, our metric reduces to the standard Morris-Thorne wormhole [82, 452]

$$\mathrm{d}s^2 = -\mathrm{d}t^2 + \mathrm{d}r^2 + \left(r^2 + \frac{3R^2}{4}\right)\mathrm{d}\Omega^2. \tag{II.2.37}$$

The $r \to 0$ behavior of the metric is what distinguishes our solution from other either phenomenological [1, 84, 118] or "quantum-inspired" regular models [132, 136, 192, 207, 453]. Similarly to our case, these solutions are parametrized by a quantum hair R and are usually endowed with a de Sitter core, which determines the presence of two (or, more generally, an even number of) horizons. Inspection of Eq. (II.2.36) reveals that $f(0)$ changes sign at the critical value of

$R = R_c = 4\sqrt{2/\pi}\, GM \simeq 3.19\, GM$. This signalizes the presence of horizons, whose position can be easily found by computing the zeroes of $f(r)$. For $R < R_c$, we have one horizon, while for $R > R_c$ we have no horizons (see Fig. II.2.1). At $R = R_c$, instead, the metric function has a zero at $r = 0$ and we have an "extremal configuration", separating solutions with and without horizons.

The occurrence of different solutions for different values of the parameter R has a nice explanation in terms of the strength of quantum effects characterizing our quantum superposition of spacetimes. R and R_c are of the order of magnitude of the De Broglie length λ_{DB} of our quantum state and of the classical gravitational radius of the source $R_S = 2GM$, respectively. Thus, $R \ll R_c$ means that quantum effects are completely negligible and we are describing the classical limit of a fully localized source. Correspondingly, the solutions of the effective theory are indistinguishable from the classical Schwarzschild black hole with its singularity at $r = 0$. When $R \sim R_c$, instead, quantum effects become relevant and the solution of the gravitational theory is a "quantum-deformed" Schwarzschild black hole: R plays the role of a quantum hair and the classical singularity at $r = 0$ is resolved. Finally, $R > R_c$ corresponds to a regime that is fully dominated by the quantum effects generated by the superposition of the source location states. On the effective gravitational theory, we have now a horizonless wormhole solution. This is a quite intriguing result, reminiscent of the ER = EPR conjecture [306, 454]. When quantum effects become fully dominant, both the singularity and the horizon disappear, leaving behind a fully regular traversable wormhole. Notice that the relation between quantum effects and wormhole geometries is not completely new (see, for an incomplete list, e.g., [455–460]), instead, our result seems to align with those already present in literature.

One could ask whether the presence of a wormhole in the effective theory is generic or a consequence of assuming the Gaussian form (II.2.17) for the distribution $\phi(r)$. We can easily show that a wormhole solution will always be present, regardless of the specific form of $\phi(r)$, whenever the latter is L^2-integrable and sharply peaked at $r = 0$ (as required by a meaningful quantum picture and for consistency with the classical description in terms of localized source-particle) and whenever the metric is Schwarzschild in every branch of the superposition. Indeed, from Eq. (II.2.23) we see that the $g_{\theta\theta}$ component of the effective metric can be written as

$$\langle g_{\theta\theta}\rangle = 2\pi \int_0^\pi \mathrm{d}\theta \int_0^\infty \mathrm{d}r_S\, r_S^2\, \sin\theta\, |\phi(r_S)|^2\, (r^2 + r_S^2 - 2r r_S \cos\theta), \tag{II.2.38}$$

where r_S indicates the radial coordinate of the source. The integral over θ can be done immediately, giving

$$\langle g_{\theta\theta}\rangle = 4\pi \int_0^\infty \mathrm{d}r_S\, r_S^2\, |\phi(r_S)|^2\, (r^2 + r_S^2) = 4\pi r^2 \int_0^\infty \mathrm{d}r_S\, r_S^2\, |\phi(_S)|^2 + 4\pi \int_0^\infty \mathrm{d}r_S\, r_S^4\, |\phi(r_S)|^2\,. \tag{II.2.39}$$

Using Eq. (II.2.10), the first integral gives $1/4\pi$. By defining a new dimensionless variable $\xi = r_S/R$, the second one, can be written in the form,

$$\int_0^\infty \mathrm{d}r_S\, r_S^4\, |\phi(_S)|^2 = R^5 \int_0^\infty \mathrm{d}\xi\, \xi^4\, |\phi(\xi)|^2\,. \tag{II.2.40}$$

If we assume the integral to be convergent, as it is the case for a sharply peaked function, simple counting of dimensions in the normalization of ϕ, gives $\phi \sim R^{-3/2}$. This implies in turn that integral (II.2.40) gives a^2R^2, where a^2 is some real constant. Therefore, the metric can always be written in the form

$$\mathrm{d}s^2 = -f(r,R)\mathrm{d}t^2 + \frac{\mathrm{d}r^2}{f(r,R)} + (r^2 + a^2R^2)\mathrm{d}\Omega^2. \tag{II.2.41}$$

Additionally, if ϕ has a narrow maximum at $r = 0$, the first integral in Eq. (II.2.12) is dominated by the contribution near this maximum, so that this integral, and hence the metric function $f(r)$ in Eq. (II.2.41), are even functions of r. Finally, L^2-integrability guarantees that the metric is asymptotically flat, as shown in Section II.2.1.1. Altogether, these features tell us that the metric (II.2.41) represents a wormhole.

II.2.2.1 Effective theory and energy conditions

From Birkhoff's theorem, the only static, vacuum solution of Einstein's equations is the Schwarzschild metric. Therefore, if we interpret our spacetime as a solution of standard GR equations, it must be sourced by some non-zero stress-energy tensor. As previously stated, we are not making any assumption about the fundamental quantum theory of gravity underlying our quantum description of spacetime. Our goal is restricted to deriving the effective description of gravity emerging from quantum superposition of positions of the source. Owing to our lack of knowledge about the underlying theory of QG, the simplest, and more general, guess on the emerging effective theory is that of GR sourced by an anisotropic fluid [197, 430], which is characterized by profiles for the energy density ϵ and for the radial and transverse components of the fluid pressure, respectively given by $p_\parallel$ and $p_\perp$. This means that the effect of the quantum superposition of spacetimes allows for an effective classical description in terms of an anisotropic fluid. This kind of fluids are very promising for parametrizing QG effects both for black holes/compact objects [1, 77, 84, 118, 132, 151, 152, 155, 431, 432, 453] and for galactic dynamics and cosmology [71–73, 75, 147–149]. The information about the effective theory will be encoded in the profile $\epsilon(r)$ and the equation of state $p_\parallel = p_\parallel(\epsilon)$, whereas $p_\perp$ is determined by the conservation equation for the stress energy tensor. Using Einstein's equations, we can compute the explicit expressions of the density and the pressure components for the anisotropic fluid

$$\epsilon = \frac{-3R^3 + 4e^{-2r^2/R^2} GM\sqrt{\frac{2}{\pi}}\left(3R^2+4r^2\right) + \frac{6GMR^3}{r}\mathrm{Erf}\left(\sqrt{2}\frac{r}{R}\right)}{2\pi GR\left(3R^2+4r^2\right)^2}, \tag{II.2.42a}$$

$$p_\parallel = \frac{-3R^3 - 4e^{-2r^2/R^2} GM\sqrt{\frac{2}{\pi}}\left(3R^2+4r^2\right) + \frac{6GMR^3}{r}\mathrm{Erf}\left(\sqrt{2}\frac{r}{R}\right)}{2\pi GR\left(3R^2+4r^2\right)^2}, \tag{II.2.42b}$$

$$\begin{aligned} p_\perp = {} & \frac{6R^5r^3 + 2e^{-2r^2/R^2} GM\sqrt{\frac{2}{\pi}}r\left(9R^6+30R^4r^2+48R^2r^4+32r^6\right)}{4\pi GR^3r^3\left(3R^2+4r^2\right)^2} \\ & - \frac{3GMR^5\left(3R^2+8r^2\right)\mathrm{Erf}\left(\sqrt{2}\frac{r}{R}\right)}{4\pi GR^3r^3\left(3R^2+4r^2\right)^2}. \end{aligned} \tag{II.2.42c}$$

We now analyze the energy conditions, focusing on the Null Energy Condition (NEC). In order for this condition to be satisfied, we have to require both $\epsilon + p_\parallel \geq 0$ and $\epsilon + p_\perp \geq 0$ to hold globally. It is sufficient to consider that, from Eqs. (II.2.42a) and (II.2.42b), it follows

$$\epsilon + p_\parallel = -\frac{3R^2 f(r)}{G\pi\left(3R^2+4r^2\right)^2}, \tag{II.2.43}$$

with $f(r)$ given by Eq. (II.2.35). For $R > R_c$, i.e., for horizonless objects, the NEC is always violated, since $f(r) > 0$ everywhere (see Fig. II.2.1). This means that the wormhole is potentially traversable [82, 110] (see Section II.2.2.2). For $R = R_c$, the NEC is always violated except from the point $r = 0$. This means that this model represents a one-way wormhole with a null throat at $r = 0$, which poses restrictions to its traversability as we will see in detail in the following section.

In the black-hole case, things are a little more subtle. In the exterior region, the NEC is always violated, since $f(r) > 0$. In the interior, we have that the time and the radial coordinates swap, so that we now have $\epsilon = -T^r_r$ and $p_\parallel = T^0_0$, while $p_\perp$ remains unchanged. Therefore, the right-hand side of (II.2.43) changes sign. This implies that also in the interior, $f(r) < 0$, and thus the NEC is violated.

For $R \to 0$ (the limit in which our spacetime reduces to the standard Schwarzschild solution), we have that $\epsilon + p_\parallel = 0$ and the NEC is of course satisfied. Violation of the NEC is a sufficient condition for violating all the other energy conditions [110, 119]. Indeed, it has been proved [119] that, for a general metric of the form $\mathrm{d}s^2 = -f(r)\mathrm{d}t^2 + f^{-1}(r)\mathrm{d}r^2 + \Sigma(r)\mathrm{d}\Omega^2$, there is a violation of all energy conditions (regardless of whether t is a temporal or a spatial coordinate, i.e., regardless of whether we are inside or outside the horizon) whenever $f(r) \neq 0$ and $\Sigma(r)$ is non-zero everywhere and satisfies $\Sigma(r) > 0$ and $\Sigma''(r) > 0$, which is indeed the case here.

We have explicitly checked that the other energy conditions are also violated. It is worth noting that the weak energy condition $\epsilon \geq 0$ is typically strongly violated in the region near the

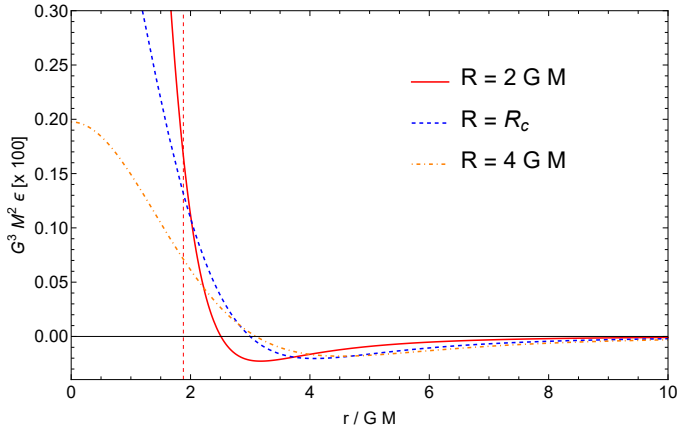

Figure II.2.2: Density ϵ as a function of the radial coordinate r in the three cases: black-hole (solid red line), "critical wormhole" (dashed blue line) and wormhole (dot-dashed blue line). In the first case, the dashed red vertical line corresponds to the position of the event horizon.

Schwarzschild radius, whereas it holds both inside the latter and in the asymptotic ($r \to \infty$) region (see Fig. II.2.2).

II.2.2.2 Wormhole traversability

The violation of the standard energy conditions is only a necessary, but not sufficient, condition to have an "in-principle" traversable wormhole. An additional condition, commonly referred to as "flaring-out", needs to be satisfied. To properly explain the physical meaning and implications of this requirement, we write a general-wormhole metric in the standard form

$$\mathrm{d}s^2 = -e^{2\Phi(r)}\mathrm{d}t^2 + \frac{\mathrm{d}r^2}{1-\frac{b(r)}{r}} + r^2\mathrm{d}\Omega^2 \tag{II.2.44}$$

where $\Phi(r)$ and $b(r)$ are functions of r only. $b(r)$ controls the spatial shape of the wormhole and is therefore called the "shape function", while $\Phi(r)$ is the "redshift function".

The "flaring-out" condition guarantees the existence of a throat connecting the two asymptotic regions, where the radius of spherical shells, as a function of the proper radial distance from the throat itself $\mathcal{L}$, attains a minimum [82, 110, 461]. We, thus, compute the proper radial distance from the throat in the wormhole spacetime (II.2.44), which is

$$\mathcal{L}(r) = \pm\int_{r_{\text{throat}}}^{r} \frac{\mathrm{d}r}{\sqrt{1-\frac{b(r)}{r}}}. \tag{II.2.45}$$

The radius of the throat r_{throat} is given by the minimum of $r\,(\mathcal{L})$, which translates to imposing

$$\frac{\mathrm{d}r}{\mathrm{d}\mathcal{L}} = \pm\sqrt{1-\frac{b(r_{\text{throat}})}{r_{\text{throat}}}} = 0, \tag{II.2.46}$$

which gives r_{throat} as the solution of $b(r_{\text{throat}}) = r_{\text{throat}}$. Finally, in order for the proper distance to be strictly increasing on both sides of the minimum r_{throat}, we require

$$\frac{\mathrm{d}^2 r}{\mathrm{d}\mathcal{L}^2} = \frac{1}{2r_{\text{throat}}}\left(-b'(r_{\text{throat}}) + \frac{b(r_{\text{throat}})}{r_{\text{throat}}}\right) > 0. \tag{II.2.47}$$

Since $b(r_{\text{throat}}) = r_{\text{throat}}$, the "flaring-out" condition translates to requiring $b'(r_{\text{throat}}) < 1$.

To explicitly analyze this condition in our model, we need first to recast our metric (II.2.28) into the form of Eq. (II.2.44). This is simply realized by the coordinate change $r' \equiv \sqrt{r^2 + \frac{3R^2}{4}}$,

and the metric (II.2.28) becomes

$$\begin{aligned} \mathrm{d}s^2 = &-\left[1-\frac{2GM}{\sqrt{r'^2-\frac{3R^2}{4}}}\mathrm{Erf}\left(\frac{\sqrt{2}}{R}\sqrt{r'^2-\frac{3R^2}{4}}\right)\right]\mathrm{d}t^2 \\ &+\frac{r'^2\,\mathrm{d}r'^2}{\left(r'^2-\frac{3R^2}{4}\right)\left[1-\frac{2GM}{\sqrt{r'^2-\frac{3R^2}{4}}}\mathrm{Erf}\left(\frac{\sqrt{2}}{R}\sqrt{r'^2-\frac{3R^2}{4}}\right)\right]} \\ &+r'^2\mathrm{d}\Omega^2, \end{aligned} \tag{II.2.48}$$

from which we immediately read the "redshift" and the "shape" functions

$$\Phi(r') = \frac{1}{2}\ln\left[1-\frac{2GM}{\sqrt{r'^2-\frac{3R^2}{4}}}\mathrm{Erf}\left(\frac{\sqrt{2}}{R}\sqrt{r'^2-\frac{3R^2}{4}}\right)\right]; \tag{II.2.49a}$$

$$b(r') = r' - \frac{1}{r'}\left(r'^2-\frac{3R^2}{4}\right)\left[1-\frac{2GM}{\sqrt{r'^2-\frac{3R^2}{4}}}\mathrm{Erf}\left(\frac{\sqrt{2}}{R}\sqrt{r'^2-\frac{3R^2}{4}}\right)\right]. \tag{II.2.49b}$$

The position of the throat is given by solving the equation $b(r_{\text{throat}}) = r_{\text{throat}}$, so that

$$\left(r_{\text{throat}}^2-\frac{3R^2}{4}\right)\left[1-\frac{2GM}{\sqrt{r_{\text{throat}}^2-\frac{3R^2}{4}}}\mathrm{Erf}\left(\frac{\sqrt{2}}{R}\sqrt{r_{\text{throat}}^2-\frac{3R^2}{4}}\right)\right] = 0. \tag{II.2.50}$$

Regularity of the redshift function (II.2.49a) *everywhere* [82, 110], required to have traversability, implies that the quantity in square brackets in Eq. (II.2.50) is different from zero, which isolates the throat radius $r_{\text{throat}} = \sqrt{3/4}\,R$, as expected.

Taking the derivative of $b(r)$ with respect to r' and evaluating it at $r' = \sqrt{3/4}\,R$ yields

$$b'\left(\sqrt{\frac{3}{4}}R\right) = -1+\frac{8GM}{R}\sqrt{\frac{2}{\pi}}. \tag{II.2.51}$$

For $b'(\sqrt{3/4}\,R) < 1$, i.e., for $R > 4\sqrt{2/\pi}\,GM$, we have a traversable wormhole, while it is non-traversable otherwise. It is interesting to note that the same value of R discriminating between traversable and non-traversable wormholes is the same discriminating between the presence or absence of an event horizon, which correspond, respectively, to $R < R_{\text{c}}$ and $R > R_{\text{c}}$, with, we recall, $R_{\text{c}} = 4\sqrt{2/\pi}\,GM$ the critical value corresponding to the extremal configuration. Specifically, horizonless wormholes will be traversable, while those with an event horizon will not. The object with $R = R_{\text{c}}$ falls in this last category as a particular configuration with a null throat.

This is consistent with the usual Morris and Thorne's requirement [82] of the absence of event horizons to guarantee traversability, as the presence of a horizon prevents two-way travel through the wormhole. This is of course a consequence of the requirement of the regularity of the redshift function (II.2.49a), which implies the absence of a horizon. Indeed, if we had fixed r_{throat} as the zero of the square bracket in Eq. (II.2.50), we would have had $\Phi(r) \to -\infty$ and thus a horizon (since we would have had $e^{2\Phi} \to 0$ in Eq. (II.2.44)).

II.2.3 Thermodynamics and Hawking evaporation

The discussion of the present section is focused on configurations endowed with an event horizon, namely configurations with $R \leq R_{\text{c}}$.

II.2.3.1 Thermodynamic properties

From the metric function (II.2.35), using the standard black-hole thermodynamic relations, we can compute both the black-hole mass and the Hawking temperature T_{H} as functions of the event

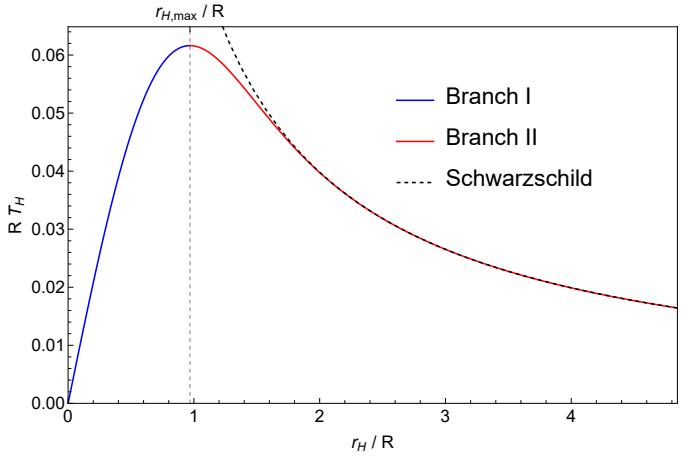

Figure II.2.3: Qualitative behavior of the temperature as a function of the event horizon radius. We highlighted the two thermodynamic branches: thermodynamic stable configurations (blue line) and the unstable (Hawking) branch (orange line).

horizon radius $r_{\rm H}$ and the position uncertainty R

$$M(r_{\rm H},R)=\frac{r_{\rm H}}{2G\,\mathrm{Erf}\left(\frac{\sqrt{2}}{R}r_{\rm H}\right)}, \tag{II.2.52a}$$

$$T_{\rm H}(r_{\rm H},R)=\frac{1}{4\pi}\frac{\mathrm{d}f(r)}{\mathrm{d}r}\bigg|_{r=r_{\rm H}}=\frac{GM(r_{\rm H},R)}{2\pi^{3/2}r_{\rm H}^2}\left[-\frac{2\sqrt{2}\,e^{-2r_{\rm H}^2/R^2}}{R}r_{\rm H}+\sqrt{\pi}\,\mathrm{Erf}\left(\frac{\sqrt{2}}{R}r_{\rm H}\right)\right]. \tag{II.2.52b}$$

Specifically, Eq. (II.2.52a) is the implicit relation between the ADM mass and the event-horizon radius. Plugging it into Eq. (II.2.52b) yields the explicit expression of the temperature

$$T_{\rm H}(r_{\rm H},R)=\frac{1}{4\pi r_{\rm H}}-\frac{\sqrt{\frac{2}{\pi}}\,e^{-2r_{\rm H}^2/R^2}}{2\pi R\,\mathrm{Erf}\left(\frac{\sqrt{2}}{R}r_{\rm H}\right)}. \tag{II.2.53}$$

The first term corresponds to the standard Hawking result. Indeed, it is easy to see that, in the $R\to 0$ limit, $r_{\rm H}\to 2GM$ and $T_{\rm H}\to 1/(8\pi GM)$. In the $r_{\rm H}\to 0$ limit, instead, the temperature goes as $T_{\rm H}\simeq r_{\rm H}/3\pi R^2+\mathcal{O}(r_{\rm H}^2)$, so it goes to zero linearly. The temperature also vanishes as $r_{\rm H}\to\infty$. This signals the non-monotonic behavior of the temperature, which must have at least an extremum somewhere. Indeed, solving $\mathrm{d}T_{\rm H}/\mathrm{d}r_{\rm H}=0$ yields the position of the maximum $r_{\rm H,\,max}\simeq 0.97\,R$. A qualitative plot of the temperature is shown in Fig. II.2.3.

As expected, the divergence of the temperature at $r_{\rm H}\to 0$ of the Schwarzschild black hole is cured. The $r_{\rm H}=0$ configuration corresponds to the "extremal" wormhole, which, therefore, is a perfectly regular, zero-temperature state. In the limit $r_{\rm H}\to 0$, $M(r_{\rm H},R)\to M_{\rm c}\equiv(1/4G)\sqrt{\pi/2}\,R$, which is a non-zero value. This signals the transition from an object with an event horizon to a horizonless one.

An important remark is that R has to be considered as a quantum deformation parameter that, contrary to M, is not associated with conserved charges defined at infinity. This makes our quantum black hole solution drastically different from other two-parameter classes of solutions, like, e.g., the charged Reissner-Nordström solution, for which *both* parameters are associated with thermodynamic potentials. Owing to this feature, we expect a first law of thermodynamics of the form $\mathrm{d}M=T_{\rm H}\mathrm{d}S$, where S is the black-hole entropy. It is known that the presence of a quantum deformation parameter R, not associated with a thermodynamic potential, implies violation of the area-law for the entropy [1]. An entropy formula, which generalises the area-law and applies to "quantum-deformed" black holes, has been proposed in Ref. [1]

$$S=4\pi\int_{r_{\rm min}}^{r_{\rm H}}M(r'_{\rm H})\,\mathrm{d}r'_{\rm H}. \tag{II.2.54}$$

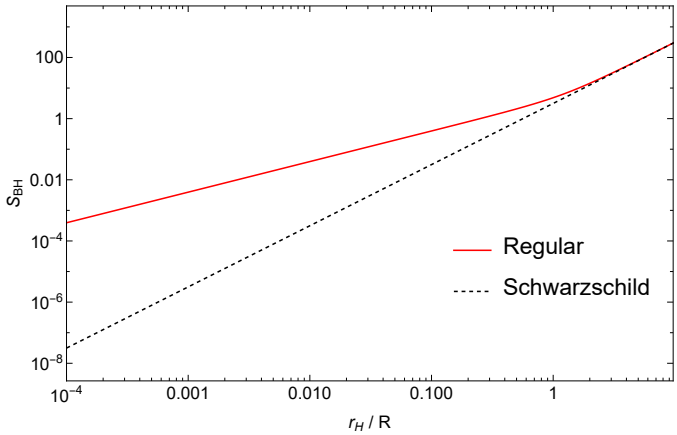

Figure II.2.4: Numerical evaluation of the entropy of the quantum black hole (solid blue line), compared to Hawking's standard result $S_{\rm H} = \mathcal{A}_{\rm H}/(4G)$ (with $\mathcal{A}_{\rm H}$ the area of the event horizon), as a function of the event horizon radius in R units $y_{\rm H} \equiv r_{\rm H}/R$. We set $G = 1$.

where $r_{\rm min}$ is the minimum value $r_{\rm H}$ can attain, corresponding to the radius of the extremal-state event horizon. One can easily check that Eqs. (II.2.52a) and (II.2.52b) imply the validity of the relation $\mathrm{d}M = 4\pi M T_{\rm H} \mathrm{d}r_{\rm H}$, from which it follows that the entropy (II.2.54) satisfies the first principle $\mathrm{d}M = T_{\rm H}\mathrm{d}S$. In the case under consideration, $r_{\rm min} = 0$ and, therefore, the entropy of the extremal, $T_{\rm H} = 0$, configuration vanishes. This $T_{\rm H} = S = 0$, $M \neq 0$ extremal state separates solutions with horizons from horizonless wormholes. In Fig. II.2.4 we plotted the result of the numerical integration of the entropy expression (II.2.54).

As mentioned before, the entropy formula (II.2.54) is a consequence of the validity of the first law of black-hole thermodynamics in its standard formulation, i.e., with $M(r)$ identified as the internal energy of the system. This eventually led to deviations from the entropy area law. It is worth stressing that a parallel, but conceptually different, thermodynamic description can be given [289], in which instead the area-law is satisfied, but the first law gets modified: the internal energy is not identified with M anymore, but also the matter-fields contribution is taken into account. This is due to the extra dependence on M contained in the stress-energy tensor, which leads to a first law of the form

$$C(r_{\rm H}, M)\, \mathrm{d}M = T_{\rm H}\, \mathrm{d}\left(\frac{\mathcal{A}_{\rm H}}{4}\right), \qquad C(r_{\rm H}, M) \equiv 1 + 4\pi \int_{r_{\rm H}}^{\infty} \mathrm{d}r\, r^2\, \frac{\partial T_0^0}{\partial M}, \tag{II.2.55}$$

where $\mathcal{A}_{\rm H}$ is the area of the event horizon. In the standard case, $\partial T_0^0/\partial M = 0$, $C(r_{\rm H}, M) = 1$ and we recover the usual formulation of the first law.

However, this discussion is limited to an analysis of the equations of motion and a Lagrangian description of these models is clearly required to have a precise thermodynamic interpretation of the internal energy of the system and of the entropy (see Ref. [462]), which would allow one to prefer one approach over the other.

Let us end this section by briefly discussing the behavior of our solutions near the "extremal" configuration, i.e., the configuration with $r_{\rm H} = 0$, $T_{\rm H} = 0$, to gain some insights into the transition between the black-hole and the horizonless wormhole models. Expanding around this critical value, at leading order we get, for the mass and the temperature

$$M \simeq M_{\rm c} + \beta r_{\rm H}^2, \tag{II.2.56a}$$

$$T_{\rm H} \simeq \gamma r_{\rm H}, \tag{II.2.56b}$$

where we have defined $\beta \equiv (1/2)\mathrm{d}^2 M/\mathrm{d}r_{\rm H}^2|_{r_{\rm H}=0}$ and $\gamma \equiv \mathrm{d}T_{\rm H}/\mathrm{d}r_{\rm H}|_{r_{\rm H}=0}$. Combining the two expressions together, we find the scaling of the mass above extremality in terms of the temperature

$$M - M_{\rm c} \sim \frac{\beta}{\gamma^2} T_{\rm H}^2. \tag{II.2.57}$$

This scaling of the mass above extremality with the temperature squared is typical of several black-hole models [216, 217].

II.2.3.2 Particle production and evaporation time

In this section we will study the Hawking radiation for our regular black hole. We will give a lightning presentation of the derivation, following the original computation in Ref. [41]. Since the geometric optics approximation is valid in both cases, the equations of motion will be identical, the only differences being in the metric matching, which will—as we shall show—appear only in the expression of the surface gravity. We start by assuming a Vaidya-like gravitational collapse of a null-shell at the lightcone coordinate $v = v_0$ that leads to the metric (II.2.28)[3]. For such a collapse, there is an "in" region described by the Minkowski metric

$$\mathrm{d}s^2_{\text{in}} = -\mathrm{d}t^2 + \mathrm{d}r^2 + r^2\mathrm{d}\Omega^2, \tag{II.2.58}$$

and an "out" region where the metric reads

$$\mathrm{d}s^2_{\text{out}} = -\left[1 - \frac{2GM}{r}\mathrm{Erf}\left(\sqrt{2}\frac{r}{R}\right)\right]\mathrm{d}t^2 + \frac{\mathrm{d}r^2}{1 - \frac{2GM}{r}\mathrm{Erf}\left(\sqrt{2}\frac{r}{R}\right)} + \left(r^2 + \frac{3R^2}{4}\right)\mathrm{d}\Omega^2. \tag{II.2.59}$$

We consider a massless scalar field $\phi(x)$ obeying the usual Klein-Gordon (KG) equation in the fixed spacetime background given by the previous metric. The field can be expanded in terms of both in and out wave-mode functions

$$\Psi(x) = \sum_k a_k u_k(x) + a_k^\dagger u_k^*(x) \tag{II.2.60}$$

$$= \sum_k b_k v_k(x) + b_k^\dagger v_k^*(x), \tag{II.2.61}$$

where a_k is the particle annihilation operator in the "in" region, b_k in the "out" region. u_k and v_k are thus the corresponding "in" and "out" wave modes. Each set of modes is a complete basis and the two sets can be related to each other through the Bogoliubov transformations

$$v_k(x) = \sum_j \alpha_{kj} u_j(x) + \beta_{kj} u_j^*(x). \tag{II.2.62}$$

One can then easily check that

$$\alpha_{kj} = (v_k, u_j) \quad \text{and} \quad \beta_{kj} = -(v_k, u_j^*), \tag{II.2.63}$$

where the canonical inner product (v_k, u_j) is defined by

$$(v_k(x), u_j(x)) = \int \mathrm{d}\Xi\, n^\mu \left[v_k(x)\partial_\mu u_j^*(x) - u_j^*(x)\partial_\mu u_k(x)\right]. \tag{II.2.64}$$

Ξ is a Cauchy hypersurface, and n^μ its normal vector. This product can be shown to be independent of the choice of the hypersurface (see, e.g., Ref. [463]).

Similarly, also the "in" and "out" creation and annihilation operators are related through Bogoliobov transformations. We can now compute the expectation value of the number operator of "out" modes in the "in" vacuum and we find

$$\langle N^{\text{out}}\rangle = \sum_j |\beta_{kj}|^2. \tag{II.2.65}$$

Information about the number of Hawking quanta of each mode k is encoded in the β coefficient, which requires evaluating the integral in (II.2.63). To do so, one has to find both the "in" and "out" wave-modes that are solutions of the KG equation, each in its corresponding spacetime geometry. Following Hawking's computations [41, 464], one arrives at[4]

$$\langle N^{\text{out}}_\omega\rangle = \sum_{\omega'} |\beta_{\omega\omega'}|^2 = \frac{1}{e^{-2\pi\omega\kappa} - 1}. \tag{II.2.66}$$

[3] A dynamic study of the formation of objects with such metrics from gravitational collapse is an important issue, which is left to future investigations.

[4] In the following, we will adopt the s-wave approximation in which all Hawking modes propagate freely. This is a reasonable approximation since the KG potential appearing in Eq. (II.2.97) vanishes both at $\mathcal{I}^+$ and near the horizon, where it is believed that relevant physics happens. Therefore we will not include the backscattering effects by the potential in the KG equation, which usually determine the greybody factors and only affect luminosity.

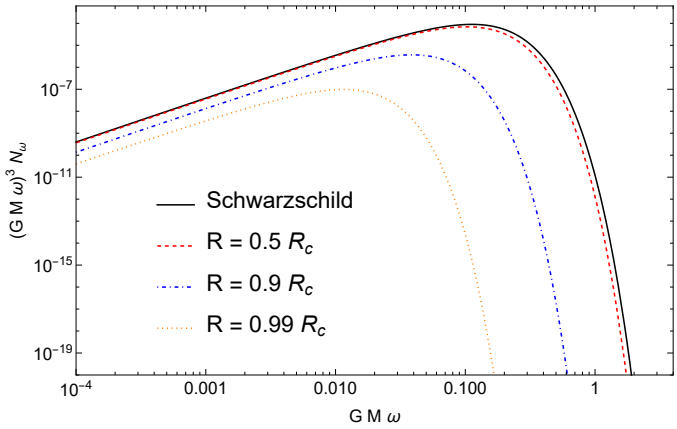

Figure II.2.5: Spectral radiance of the black holes for different values of R (in units of GM), in comparison with the Schwarzschild case.

As it is known, the equation for $N_\omega^{\rm out}$ describes a thermal flux of particles with a Planckian spectrum at temperature $T = \kappa/2\pi$. The only difference with respect to the original Hawking calculation is the explicit expression of the surface gravity κ evaluated at the horizon, which also depends on R, which, therefore, also alters the spectral radiance (see Fig. II.2.5). Specifically, from the temperature (II.2.53), the surface gravity reads

$$\kappa = \frac{1}{2r_{\rm H}} - \frac{\sqrt{\frac{2}{\pi}}\, e^{-2r_{\rm H}^2/R^2}}{R\,{\rm Erf}\left(\frac{\sqrt{2}}{R}r_{\rm H}\right)}\,. \tag{II.2.67}$$

Since the spectrum of the quantum corrected black holes is Planckian, we can use the Stefan-Boltzmann law to compute the luminosity,

$$L = \sigma_{\rm SB}\mathcal{A}_{\rm H}T_{\rm H}^4, \tag{II.2.68}$$

where $\sigma_{\rm SB}$ is the Stefan-Boltzmann constant and $\mathcal{A}_{\rm H} = 4\pi\left(r_{\rm H}^2 + 3R^2/4\right)$ is the surface area of the 2-sphere computed at $r_{\rm H}$. We then use this to compute the mass loss rate which is simply

$$\frac{{\rm d}M(t)}{{\rm d}t} = -L = -4\pi\,\sigma_{\rm SB}\left(r_{\rm H}^2 + \frac{3}{4}R^2\right)T_{\rm H}^4. \tag{II.2.69}$$

The main problem is the absence of an analytic formula isolating $r_{\rm H}$ as a function of the black-hole mass M. We however get around this difficulty by expressing M in terms of $r_{\rm H}$ as in Eq. (II.2.52a). Thus, the variation of $M(t)$ with time is

$$\frac{{\rm d}M}{{\rm d}t} = \left[\frac{1}{2G{\rm Erf}\left(\frac{\sqrt{2}r_{\rm H}(t)}{R}\right)} - \frac{\sqrt{\frac{2}{\pi}}r_{\rm H}(t)e^{-\frac{2r_{\rm H}(t)^2}{R^2}}}{G\,R\,{\rm Erf}\left(\frac{\sqrt{2}r_{\rm H}(t)}{R}\right)^2}\right]\frac{{\rm d}r_{\rm H}(t)}{{\rm d}t}\,. \tag{II.2.70}$$

Plugging Eqs. (II.2.53) and (II.2.70) into Eq. (II.2.69) and integrating from an initial radius $r_{\rm H,\,0}$ down to $r_{\rm H} = 0$ yields

$$\Delta t = -\int_{r_{\rm H,\,0}}^{0} \frac{128\pi^5 r_{\rm H}^4\,R^3\,e^{6r_{\rm H}^2/R^2}\,{\rm Erf}\left(\frac{\sqrt{2}r_{\rm H}}{R}\right)^2\left[R\,e^{2r_{\rm H}^2/R^2}\,{\rm Erf}\left(\frac{\sqrt{2}r_{\rm H}}{R}\right) - 2\sqrt{\frac{2}{\pi}}\,r_{\rm H}\right]}{G\sigma_{\rm SB}\left(4r_{\rm H}^2+3R^2\right)\left(\sqrt{\pi}\,R\,e^{2r_{\rm H}^2/R^2}{\rm Erf}\left(\frac{\sqrt{2}r_{\rm H}}{R}\right) - 2\sqrt{2}\,r_{\rm H}\right)^4}\,{\rm d}r_{\rm H}. \tag{II.2.71}$$

Since we are interested in the final part of the evaporation process, i.e., $r_{\rm H} \sim 0$ (which coincides with the extremal configuration), we look at the expansion of the integrand near this point. We get, after integration, $\Delta t \sim \left[\frac{R^5}{G\,r_{\rm H}^2} + \mathcal{O}(r_{\rm H}^{-3})\right]\Big|_{r_{\rm H,0}}^{0}$, which diverges in $r_{\rm H} = 0$. This is perfectly consistent with the thermodynamic behavior analyzed in Section II.2.3.1: for values of $r_{\rm H}$ smaller than that in correspondence with the temperature peak (see Fig. II.2.3), we have stable remnants.

II.2.4 The phenomenology

The aim of this section is to compute phenomenological observables and to compare them to the Schwarzschild case. In fact, despite the simplicity of our derivation, the presence of the additional parameter R entering the wave function for the source may have observational signatures, which could be tested in the near future by black-hole imaging and GWs observations. In particular, we will analyze the geodesic structure of our spacetime, focusing on null and time-like geodesics, and the QNMs for a scalar perturbations in the eikonal regime.

II.2.4.1 Geodesic structure

In order to study the geodesics equation, we start by considering the following Lagrangian in the usual (t, r, θ, φ) Schwarzschild coordinates, which can be easily derived from the metric (II.2.28)

$$\mathcal{L} = \frac{1}{2} g_{\mu\nu} \dot{x}^\mu \dot{x}^\nu = \frac{1}{2} \left[-f(r) \dot{t}^2 + \frac{\dot{r}^2}{f(r)} + \left(r^2 + \frac{3R^2}{4} \right) \left(\dot{\theta}^2 + \sin^2\theta \, \dot{\phi}^2 \right) \right], \tag{II.2.72}$$

where the dot indicates differentiation with respect to some affine parameter λ. The equations of motion of a particle in such a spacetime are given by

$$\left(\frac{\partial}{\partial \lambda} \frac{\partial}{\partial \dot{x}^\mu} - \frac{\partial}{\partial x^\mu} \right) \mathcal{L} = 0, \tag{II.2.73}$$

and the conjugate momenta are given by

$$p_t = \partial_{\dot{t}} \mathcal{L} = -f(r) \dot{t}, \qquad p_r = \partial_{\dot{r}} \mathcal{L} = \frac{\dot{r}}{f(r)}, \tag{II.2.74a}$$

$$p_\theta = \partial_{\dot{\theta}} \mathcal{L} = \left(r^2 + \frac{3}{4} R^2 \right) \dot{\theta}, \qquad p_\varphi = \partial_{\dot{\phi}} \mathcal{L} = \left(r^2 + \frac{3}{4} R^2 \right) \sin^2\theta \, \dot{\phi}. \tag{II.2.74b}$$

Notice that the lagrangian is not explicitly dependent on t and φ. The corresponding quantities $p_t = -E$ and $p_\varphi = L$ are conserved, a clear consequence of the isometries of the metric. Moreover, from the equations of motion, it follows that

$$\frac{\partial p_\theta}{\partial \lambda} = \frac{\partial}{\partial \lambda} \left(r^2 \dot{\theta} \right) = -\frac{\partial \mathcal{L}}{\partial \theta} = \left(r^2 + \frac{3}{4} R^2 \right) \sin\theta \cos\theta \, \dot{\phi}^2, \tag{II.2.75}$$

so that, if we choose $\theta = \pi/2$ when $\dot{\theta}$ is zero, $\ddot{\theta}$ will be zero as well, and the motion will be constrained on the equatorial plane since θ will remain constant at the assigned value. In order to find another integral of motion, we can build the hamiltonian corresponding to the lagrangian (II.2.72) as

$$\mathcal{H} = p_\mu \dot{x}^\mu - \mathcal{L}. \tag{II.2.76}$$

It is straightforward to see that neither the lagrangian nor the hamiltonian depend on the affine parameter, therefore $\mathcal{H} = \mathcal{L} = \text{const.} = -\epsilon^2/2$, where $\epsilon = 0$ or $\epsilon = \pm 1$ for null and time-like geodesics, respectively. From the constancy of the lagrangian, we can write

$$\dot{r}^2 + f(r) \left(\epsilon^2 + \frac{L^2}{r^2 + 3R^2/4} \right) = E^2, \tag{II.2.77}$$

which is the desired equation for geodesics in the spacetime (II.2.28).

II.2.4.2 Time-like geodesics

Proper time of radially infalling time-like particles

We want to compute the proper-time interval a massive particle in radial free-fall in the metric (II.2.28) takes to reach $r = 0$ starting from some finite distance $r = r_0$. We take radially (infalling) time-like geodesics, which therefore satisfy the constraint

$$g_{\mu\nu} u^\mu u^\nu = -1, \tag{II.2.78}$$

together with $u^\theta = u^\varphi = 0$. Using the geodesic integral of motion $\dot{t} = E/f$, Eq. (II.2.78) translates to

$$-\frac{E^2}{f(r)} + \frac{\dot{r}^2}{f(r)} = -1 \qquad \Rightarrow \qquad \dot{r}^2 = E^2 - f(r)\,. \tag{II.2.79}$$

Since the value of E will not alter the qualitative results of this section, we can choose $E = 1$, which means that the particle starts at infinity at rest (marginally bound geodesics). Since we are interested in the behavior near $r = 0$, we expand Eq. (II.2.79) around $r = 0$

$$\left(\frac{\mathrm{d}r}{\mathrm{d}\tau}\right)^2 \simeq \frac{4GM}{R}\sqrt{\frac{2}{\pi}} - \frac{8GM}{3R^3}\sqrt{\frac{2}{\pi}}r^2 \equiv \frac{R_\mathrm{c}}{R} - \frac{2R_\mathrm{c}}{3R^3}r^2 \tag{II.2.80}$$

where we defined $\lambda = \tau$ as the proper time and R_c is the critical value of R at which we have the transition to a horizonless wormhole, i.e., $4\sqrt{2/\pi}GM$. Therefore, the proper time, as measured by a particle moving from r_0 to r, is given by the integral

$$\Delta\tau(r) = -\int_{r_0}^{r} \frac{\mathrm{d}r'}{\sqrt{\frac{R_\mathrm{c}}{R} - \frac{2R_\mathrm{c}}{3R^3}r'^2}} \tag{II.2.81}$$

where the minus accounts for radial infalling geodesics. This integral is analytical. Evaluating it in the limit $r \to 0$ yields the finite results

$$\Delta\tau(r \to 0) = \sqrt{\frac{3}{2}}\frac{R^{3/2}}{\sqrt{R_\mathrm{c}}}\,\mathrm{arctg}\left[\frac{\sqrt{2R_\mathrm{c}}\,r_0}{\sqrt{R_\mathrm{c}(-2r_0^2 + 3R^2)}}\right]. \tag{II.2.82}$$

This result is particularly important in the horizonless wormhole case, since it confirms that indeed it is traversable, as massive particles can reach the throat in a finite interval of proper time.

Time-like geodesic congruence

We can now study the expansion rate of the metric to check whether the spacetime is geodesically complete or not. To do so, we need to compute the geodesic congruence's expansion rate as

$$\frac{\mathrm{d}\Theta}{\mathrm{d}\tau} = \dot{r}\frac{\mathrm{d}\Theta}{\mathrm{d}r} = \dot{r}\frac{\mathrm{d}}{\mathrm{d}r}\left[\frac{1}{\sqrt{-g}}\partial_\mu\left(\sqrt{-g}u^\mu\right)\right], \tag{II.2.83}$$

where u^μ is the 4-velocity of a particle orbiting the quantum black hole. If we consider time-like radial geodesics, the components of the vector u^μ read

$$u^\mu = \left(\frac{1}{f(r)}, \pm\sqrt{1 - f(r)}, 0, 0\right), \tag{II.2.84}$$

where the upper (lower) sign refers to outgoing (ingoing) geodesics. Therefore, Eq. (II.2.83) becomes just

$$\frac{\mathrm{d}\Theta}{\mathrm{d}\tau} = \dot{r}\,\frac{\mathrm{d}}{\mathrm{d}r}\left[\frac{1}{\rho^2}\frac{\mathrm{d}}{\mathrm{d}r}\left(\rho^2\,u^r\right)\right], \tag{II.2.85}$$

where $\rho^2 = r^2 + 3R^2/4$. The evaluation of Eq. (II.2.85) in terms of the metric functions around $r = 0$ gives

$$\frac{\mathrm{d}\Theta}{\mathrm{d}\tau} = -4\left(\frac{2}{\pi}\right)^{1/4}\sqrt{\frac{GM}{R^5}}\,\dot{r} + O(r^2), \tag{II.2.86}$$

which indicates that the solution is regular near this point and caustics cannot form.

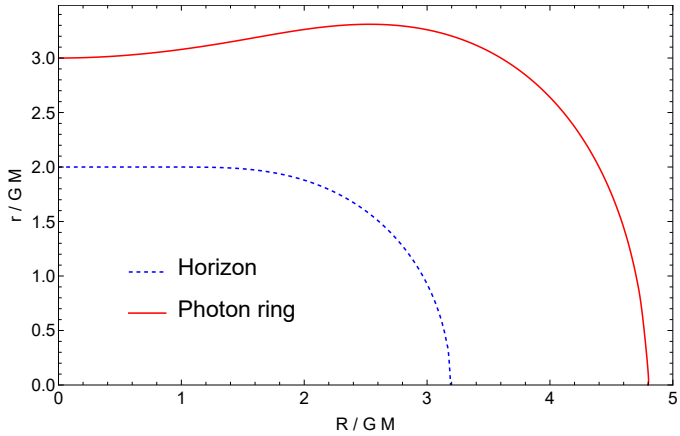

Figure II.2.6: Position of the light ring and horizon radius as a function of R, both in units of GM.

II.2.4.3 Null geodesics

Null-geodesic congruence

We start from a null vector field $k^\mu = \mathrm{d}x^\mu/\mathrm{d}\lambda$ (where λ is as usual the affine parameter), satisfying the normalization condition $k_\mu k^\mu = 0$, tangent to a bundle of radial in-going null geodesics. The null-geodesic congruence therefore reads

$$\Theta = \nabla_\mu k^\mu = \frac{1}{\sqrt{-g}}\partial_\mu\left(\sqrt{-g}k^\mu\right). \tag{II.2.87}$$

We first need to compute the components of the vector field k^μ. To do so, we consider again radial null geodesics, setting $\theta =$ constant and $\varphi =$ constant. Also in this case it is useful to introduce the Eddington-Finkelstein coordinates

$$u = t - r_*, \quad v = t + r_*, \quad r_* = \int f^{-1}\mathrm{d}r. \tag{II.2.88}$$

We see that the vector field $k_\mu = -\partial_\mu u$ is tangent to the outgoing geodesics, while $k_\mu = -\partial_\mu v$ is tangent to the ingoing ones. We are interested in the latter, whose components are $k_\mu = (-1, -f^{-1}, 0, 0)$. So, we also have $k^\mu = g^{\mu\nu}k_\nu = (f^{-1}, -1, 0, 0)$, and we see that the constraint $k_\mu k^\mu = 0$ is satisfied. Therefore, the congruence reads

$$\Theta = -\frac{1}{r^2 + \frac{3R^2}{4}}\partial_r\left(r^2 + \frac{3R^2}{4}\right) = -\frac{8r}{4r^2 + 3R^2}. \tag{II.2.89}$$

The null-geodesic expansion thus reduces to

$$\frac{\mathrm{d}\Theta}{\mathrm{d}\lambda} = \frac{\mathrm{d}\Theta}{\mathrm{d}r}k^r = \frac{8\left(4r^2 - 3R^2\right)}{\left(4r^2 + 3R^2\right)^2}, \tag{II.2.90}$$

which near $r = 0$ behaves as

$$\frac{\mathrm{d}\Theta}{\mathrm{d}\lambda} \simeq -\frac{8}{3R^2} + \frac{32}{3R^4}r^2 + \mathcal{O}(r^3). \tag{II.2.91}$$

As in the previous case, no caustics form.

Photon sphere

The second term in the left-hand side of Eq. (II.2.77) (for null geodesics), i.e.,

$$V(r) = f(r)\frac{L^2}{r^2 + 3R^2/4}, \tag{II.2.92}$$

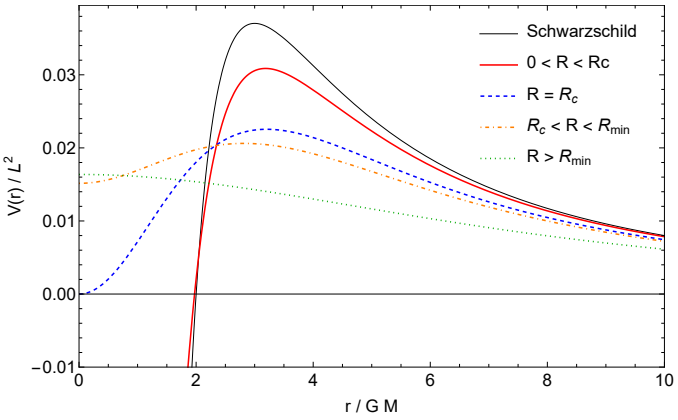

Figure II.2.7: Typical qualitative behavior of the effective potential V for null geodesics as a function of r for $R < R_{\rm c}$, $R = R_{\rm c}$, $R_{\rm c} < R < R_{\rm min}$ and $R > R_{\rm min}$.

can be thought of as an effective potential felt by massless particles orbiting around either the black hole or the wormhole. Therefore, minima and maxima of this potential correspond to the radii of stable and unstable orbits, respectively. In order to determine the position of such points, we have to find the zeroes of $\mathrm{d}V(r)/\mathrm{d}r$, i.e., the roots of the equation

$$-3GMR\,e^{\frac{2r^2}{R^2}}\left(4r^2+R^2\right)\mathrm{Erf}\left(\sqrt{2}\frac{r}{R}\right)+2\sqrt{\frac{2}{\pi}}GMr\left(4r^2+3R^2\right)+4r^3R\,e^{\frac{2r^2}{R^2}}=0. \tag{II.2.93}$$

Inspection of Eq. (II.2.92) shows that the potential has always a maximum for values of R less than a minimum value $R_{\rm min}\simeq 4.8GM$, while, for larger values, the maximum shifts to $r=0$. The maximum corresponds to the so-called photon sphere (or light ring) $r_{\rm LR}$. The numerical solution of Eq. (II.2.93) is shown in Fig. II.2.6 as a function of R, from which we see that there could be potentially detectable deviations from the standard Schwarzschild value $3GM$.

The qualitative behaviors of the effective potential for different values of R is instead depicted in Fig. II.2.7. We note that both the "extremal" configuration with $R = R_{\rm c}$ and the traversable wormhole with $R_{\rm c} < R < R_{\rm min}$ have also a minimum, corresponding to a stable photon orbit at $r = 0$ (at the throat), which is however excluded.

II.2.4.4 Scalar perturbations and quasi-normal modes

In this section we investigate QNMs for scalar perturbations in the fixed background given by our solutions. We will then use the eikonal approximation to give an analytical estimate of the quasi-normal frequencies for the black-hole model.

In order to discuss scalar perturbations and QNMs in our gravitational background, we start from the KG equation for a scalar field in spherical coordinates $\Psi=\Psi(t,r,\theta,\varphi)$

$$\Box\Psi=\frac{1}{\sqrt{-g}}\partial_\mu\left(\sqrt{-g}\,g^{\mu\nu}\partial_\nu\right)\Psi=0 \tag{II.2.94}$$

where $\sqrt{-g}$ is the square root of the determinant of the metric (II.2.28). Due to the spherical symmetry of the metric, we can separate the angular dependence of Ψ from its radial and temporal dependence, i.e., $\Psi(t,r,\theta,\varphi)\equiv R_{\ell m}(t,r)\mathcal{Y}^{\ell m}(\theta,\varphi)$. The angular part is given in terms of spherical harmonics, while the radial part satisfies a Schrödinger-like equation

$$\left[\partial^2_{r_*}-\partial^2_t-V_{\rm eff}(r)\right]\psi=0. \tag{II.2.95}$$

Here $\psi(t,r)$ is related to $R(t,r)$ by

$$R_{\ell m}(t,r)\equiv\frac{\psi_{\ell m}(t,r)}{\sqrt{r^2+\frac{3R^2}{4}}}, \tag{II.2.96}$$

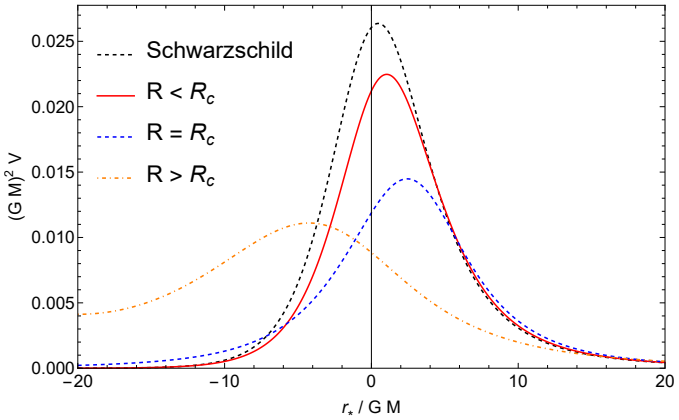

Figure II.2.8: Qualitative behavior of the effective potential (II.2.97), with $\ell = 0$, for the black-hole model ($R < R_c$), the "extremal model" ($R = R_c$) and the wormhole ($R > R_c$).

while $V_{\text{eff}}(r)$ is the effective potential, namely

$$V_{\text{eff}}(r) = \frac{12R^2 f^2}{\left(4r^2 + 3R^2\right)^2} + \frac{4f}{4r^2 + 3R^2}\left[\ell(\ell+1) + rf'\right], \tag{II.2.97}$$

where primes indicate derivation with respect to r. We see that the presence of both R and a non-trivial angular metric function introduce an additional term in the effective potential with respect to the Schwarzschild case, which goes to zero as R^2 in the limit $R \to 0$. In Fig. II.2.8, we plot some examples for different values of R. The traversable-wormhole case is particularly interesting, as the double peak in the potential always signals the possibility of having echoes in the QNMs spectrum [51, 175, 343, 433–435].

II.2.4.5 Analytic expression of QNMs in the eikonal limit

We can exploit the construction of Ref. [234] to find an analytic expression of the quasi-normal frequencies in the eikonal regime, i.e., in the $\ell \gg 1$ limit. This construction only works in the case in which the effective potential in the KG equation has a *single* peak (the presence of the double peak in the horizonless-wormhole case invalidates a direct application of this algorithm [465]). The basics of the construction of Ref. [234] is to exploit a relation between the ringing modes of black holes and photons on the unstable light ring. Specifically, the black-hole vibration modes, whose energy is gradually being radiated away, are interpreted as photons moving along an unstable null-geodesics and slowly leaking out. The real part of the quasi-normal spectrum ω_{R} (corresponding to the periodic oscillations of the modes) is given by the angular velocity of photons on the light ring, whose position is at r_{LR}, namely $\Omega = \dot{\phi}/\dot{t}|_{r=r_{\text{LR}}}$. The imaginary part of the quasi-normal frequencies ω_{I}, instead, responsible for the damping of the modes, is associated to the inverse of the time-scale of the instability of the circular null geodesics, given by the Lyapunov exponent, whose form reads

$$\lambda = \sqrt{-\frac{V''(r)}{2\dot{t}^2}}\bigg|_{r=r_{\text{LR}}}, \tag{II.2.98}$$

where $V(r)$ is the potential for null geodesics (II.2.92), while the minus sign is required since the light ring corresponds to an unstable orbit. Therefore, the spectrum of QNMs reads, in the eikonal regime

$$\omega_{\text{QNMs}} = \omega_{\text{R}} + \text{i}\,\omega_{\text{I}} = \Omega\,\ell - \text{i}\left(n + \frac{1}{2}\right)\lambda \tag{II.2.99}$$

with n an integer (the overtone number). Ω can be easily computed exploiting Eq. (II.2.74) and the fact that $p_t = E$ and $p_\phi = L$. Moreover, using Eq. (II.2.77), setting $\epsilon = 0$ to consider null geodesics,

R/GM	$GM\Omega$	$GM\lambda$
10^{-4}	0.19245	0.19245
0.5	0.19048	0.19179
1	0.18508	0.18978
1.2	0.18219	0.18861
1.4	0.17901	0.18716
1.6	0.17562	0.18511
1.8	0.17211	0.18201
2	0.16856	0.17754
2.2	0.16506	0.17171
2.4	0.16167	0.16470
2.6	0.15845	0.1567
2.8	0.15542	0.14803
3	0.15262	0.13877
$R_{\rm c}$	0.15015	0.12945

Table II.2.1: Values of Ω and λ, which determine the QNMs frequencies in the eikonal limit through Eq. (II.2.99), for different values of the quantum-deformation parameter R (in units of GM).

and making use of the fact that $\dot{r}=0$ at the light ring, yield a relation between E and L

$$\frac{E}{L}=\pm\sqrt{\frac{f(r_{\rm LR})}{r_{\rm LR}^2+\frac{3R^2}{4}}}\,. \tag{II.2.100}$$

Therefore, Ω reads

$$\Omega=\frac{\dot{\phi}}{\dot{t}}\bigg|_{r=r_{\rm LR}}=\sqrt{\frac{f(r_{\rm LR})}{r_{\rm LR}^2+\frac{3R^2}{4}}}=2\sqrt{\frac{f(r_{\rm LR})}{4r_{\rm LR}^2+3R^2}}\,. \tag{II.2.101}$$

To compute λ, we start from Eq. (II.2.98). Using the fact that $V'(r_{\rm LR})=0$, we simplify the expression for $V''(r_{\rm LR})$ and we get

$$\lambda=\sqrt{-\frac{f(r)\left[-8f(r)+f''(r)\left(4r^2+3R^2\right)\right]}{8r^2+6R^2}\bigg|_{r=r_{\rm LR}}}\,. \tag{II.2.102}$$

By numerically solving Eq. (II.2.93) to find the position of the light ring for different values of R (limited to the black-hole and the "extremal" model cases), one can find the explicit values of the quasi-normal frequencies (II.2.99), given the values of Ω and λ reported in Table II.2.1. We also checked that, in the small R limit (the first value in Table II.2.1), the quasi-normal frequencies are consistent with the Schwarzschild ones in the eikonal regime, for which $\Omega=|\lambda|=1/(3\sqrt{3}\,GM)$ [466].

Finally, we can study how QNMs behave near the extremal configuration. We can expand both Ω and λ around $R=R_{\rm c}$ (before computing them at $r_{\rm LR}$). We get

$$\Omega\simeq a+b\ (R-R_{\rm c})\sim a+b'\ (M-M_{\rm c}); \tag{II.2.103a}$$
$$\lambda\simeq d+e\ (R-R_{\rm c})\sim d+e'\ (M-M_{\rm c}), \tag{II.2.103b}$$

where we have defined $a\equiv\Omega\,(R_{\rm c})$, $b\equiv{\rm d}\Omega/{\rm d}R|_{R=R_{\rm c}}$, $d\equiv\lambda(R_{\rm c})$, $e\equiv{\rm d}\lambda/{\rm d}R|_{R=R_{\rm c}}$. If we take the near-horizon[5] limit together with the near-extremal limit, it is easy to see that both the constant and the linear term $R-R_{\rm c}$ of λ go to zero, and therefore we are left with

$$\omega_{\rm I}\propto\lambda\propto M-M_{\rm c}\propto T_{\rm H}, \tag{II.2.104}$$

[5]A problem of the near-horizon limit is that the minimum of the null-geodesic effective potential gets shifted inside the event horizon at soon as we move away from "extremality".

where we took cognisance of Eq. (II.2.57). This scaling of the imaginary part of the quasi-normal frequencies with the temperature is consistent with some conjectures [181, 183, 184, 186, 187]. These zero-damped (or nearly zero-damped) modes [187] would therefore represent a clear phenomenological signature of the extremal configuration.

Chapter II.3

The Schwarzschild black hole as a set of quantum harmonic oscillators

Classically, a perturbed black hole reacts dynamically, producing characteristic oscillations, called quasi-normal modes (QNMs), which decay exponentially in time. At linear perturbation level, QNMs correspond to complex eigenfunctions of the system, namely modes characterized by complex frequencies, whose imaginary part describes the damping of the mode in time (see, e.g., Refs. [467–469]). Moreover, boundary conditions at infinity and at the horizon imply a discrete spectrum for the frequencies ω_n, with the imaginary part depending on an integer n, the overtone number.

In the high-damping regime (large-n limit), the spectrum of QNMs for a Schwarzschild black hole (SBH), with mass M, is independent of l, the angular momentum "quantum" number, and reads[1] [236, 470–472] (see Refs. [467–469, 473] for reviews)

$$8\pi GM\omega_{\rm n} \sim \ln 3 + 2\pi {\rm i}\left(n+\frac{1}{2}\right) + \mathcal{O}\left(n^{-1/2}\right). \tag{II.3.1}$$

By studying the system's response to external perturbations, in principle we could also have access to its internal microscopic structure. Therefore, despite being classical, QNMs could contain signatures of quantum gravity effects, encoding information about the quantum properties of black holes and their horizons [474]. This is particularly true in the large-n limit, which is expected to probe the black hole at short distances.

There are several indications supporting this perspective. On one hand, QNMs could be useful to understand the AdS/CFT conjecture. In fact, in the case of AdS black holes, the damping of QNMs can be mapped into the thermalization of the conformal field theory on the boundary [475]. On the other hand, the emergent and corpuscular gravity scenarios suggest that black holes could be characterized by long-range quantum gravity effects of N quanta building the black hole [35–40]. Similarly to what happens for the surface gravity of a black hole (see Ref. [39]), the quantum nature of Eq. (II.3.1) is obscured (the Planck constant $\hbar$ does not appear) by expressing ω_n in terms of the black-hole mass M, but becomes fully evident when we express it in terms of the black hole temperature $T_{\rm H}$. Thus, the QNMs spectrum could represent a coarse-grained description of the response of these N microscopic degrees of freedom to external perturbations, in the same spirit as the spectrum of the black body radiation is a manifestation of the collective behavior of a photon gas.

However, the no-hair theorem [476, 477] makes a black hole drastically different from a black body. In the latter case the extensive thermodynamic parameters scale with the volume, while the number of photons, i.e., the number of microscopic degrees of freedom, is independent of the size of the system. For a black hole, on the other hand, the mass M and the entropy S are fixed by the temperature or, equivalently, by the horizon radius r_h. From a corpuscular gravity point of view, moreover, we can consider the black hole as a macroscopic quantum state that saturates a maximally packaging condition [40, 66–68], which has been shown to be equivalent to

[1] here and in the remainder of the chapter, we adopt natural units, $c = \hbar = 1$.

the holographic scaling of N [39]. Essentially, in a black hole of a given mass, we can "pack" a maximum amount of degrees of freedom, which is constrained by the size of the system.

The proposal of using QNMs to capture some microscopic properties of black holes is not completely new, but was first proposed by Maggiore in [69]: the linear scaling of the QNMs frequencies with the overtone number n suggests that a SBH can be described, in the high-damping limit, as a harmonic oscillator, with proper frequency

$$\omega = \sqrt{\omega_{\mathrm{R}}^2 + \omega_{\mathrm{I}}^2}, \tag{II.3.2}$$

where ω_{R} and ω_{I} are the real and imaginary parts of the frequencies (II.3.1) respectively[2].

Until now, the high-damped QNMs spectrum has been used in the quantum gravity context to explain and fix the area spectrum of the event horizon (see, e.g., Refs. [471, 478–480]), whose quantization was first suggested by Bekenstein in [481, 482]. This also allowed to fix the Barbero-Immirzi parameter [478], which is essential to correctly account for the Bekenstein-Hawking (BH) entropy in Loop Quantum Gravity [483, 484].

In this chapter, we use Maggiore's result to model the SBH as a canonical ensemble of N harmonic oscillators and derive the black-hole entropy using the QNMs frequencies only, without assuming horizon-area quantization. Consistently with the no-hair theorem, for an asymptotic observer, the only physical observable is the black-hole mass M, which also determines the QNMs frequency spectrum. On the other hand, we assume that, quantum mechanically, the horizon area and the temperature can fluctuate independently from M. This will allow us to consistently define the canonical ensemble and to circumvent the no-hair theorem at quantum level.

In this chapter, we use units in which $c = \hbar = k_{\mathrm{B}} = 1$.

II.3.1 The model

In the high-damping regime, $\omega_{\mathrm{I}} \gg \omega_{\mathrm{R}}$, QNMs probe the internal structure of the black hole, as the wavelength of each oscillator gets smaller and smaller as n grows. From Eqs. (II.3.1) and (II.3.2), we easily get the frequency spectrum

$$\omega_n \simeq |\omega_{\mathrm{I}}| = \frac{1}{4GM}\left(n + \frac{1}{2}\right) + \mathcal{O}(n^{-1/2}). \tag{II.3.3}$$

Following Maggiore's proposal, we model the black hole as a statistical ensemble of $N \gg 1$ indistinguishable non-interacting (at least in a first approximation) quantum harmonic oscillators with frequencies

$$\omega_n = \omega_0\left(n + \frac{1}{2}\right), \tag{II.3.4}$$

where $\omega_0 = 1/(4GM)$ is the proper frequency of each oscillator.

Our derivation relies entirely on equilibrium statistical mechanics, without resorting to usual black-hole thermodynamics. The black hole will be regarded as an ensemble in thermal equilibrium with its surroundings at temperature $T = 1/\beta$. We will therefore work entirely in the canonical ensemble and consider the number of oscillators N fixed. This is motivated by the no-hair theorem, which tells us that the chemical potential of a SBH is zero, being the mass M the only classical hair of the hole. Considering the SBH as a system at fixed temperature is also consistent with the fact that the QNMs spectrum is computed at fixed black-hole mass. For the asymptotic observer, the latter is related to the Hawking temperature, which is therefore fixed.

It is very important to stress that, in our statistical description, we treat β and ω_0 as *independent* variables, i.e., the temperature of the ensemble can change independently from the black-hole mass. At first sight, this may seem at odds with standard black-hole thermodynamics. However, we argue that quantum mechanically this is fully consistent.

In standard black-hole thermodynamics, the Hawking temperature T_{H} can be defined as the coefficient of proportionality between the entropy (the area of the black-hole event horizon, $\mathcal{A}_{\mathrm{H}}$)

[2] A similar proposal for the description of a black hole as a harmonic oscillator, from a corpuscular gravity perspective, can be found in [241].

and its energy (the mass M). Classically, $\mathcal{A}_{\rm H}$ is a function of M, i.e., $\mathcal{A}_{\rm H} = 16\pi G^2 M^2$. The latter, however, should be considered as the mean value, measured at infinity, of the area of the event horizon, which can fluctuate around its expectation value, from a quantum mechanical point of view [481, 482, 485][3]. Only local measurements would allow to probe these fluctuations [485]. An observer at infinity therefore would not have access to them, as the only degree of freedom he/she can measure is the classical hair of the black hole, i.e., its mass. This tells us that, at least quantum mechanically, the area of the event horizon can fluctuate *independently* from M. Hence, only the observer at infinity can make the identification $\beta = \beta_{\rm H} = 1/T_{\rm H} = 8\pi GM$.

Using the spectrum (II.3.3), the statistical Boltzmann weight of each harmonic oscillator black hole microstate is therefore

$$e^{-\beta\omega_n} = e^{-\beta\omega_0\left(n+\frac{1}{2}\right)} e^{-\beta\frac{\kappa}{\sqrt{n}}}, \tag{II.3.5}$$

where κ is a dimensionful constant, proportional to ω_0 on dimensional grounds, parametrizing the low-n behavior of the damping modes. As long as we consider the limit of large-mass black holes $\omega_0 \to 0$ (or the high-temperature limit, $\beta \to 0$), the factor $e^{-\beta\kappa n^{-1/2}}$ can be set equal to 1 and the partition function will be insensible to the subleading terms $\mathcal{O}(n^{-1/2})$.

Being the SBH effectively featureless, except from its mass, and having zero chemical potential, the probability of occupying a given energy level will be the same for all oscillators. The partition function for the composite system of N oscillators therefore reads

$$\mathcal{Z} = \left(\sum_{n=0}^{\infty} e^{-\beta\omega_0\left(n+\frac{1}{2}\right)}\right)^N = \left(\frac{e^{\beta\omega_0/2}}{e^{\beta\omega_0}-1}\right)^N, \tag{II.3.6}$$

$$\ln\mathcal{Z} = \frac{N\omega_0}{2}\beta - N\ln\left(e^{\beta\omega_0}-1\right). \tag{II.3.7}$$

Using standard statistical mechanics relations, we compute the mean energy and the entropy

$$\langle E\rangle = -\partial_\beta \ln\mathcal{Z} = \frac{N\omega_0}{2}\text{cotgh}\left(\frac{\beta\omega_0}{2}\right), \tag{II.3.8}$$

$$S = \ln\mathcal{Z} + \beta\langle E\rangle = -N\ln\left(e^{\beta\omega_0}-1\right) + \frac{N\beta\omega_0 e^{\beta\omega_0}}{e^{\beta\omega_0}-1}. \tag{II.3.9}$$

As expected for consistency, the expressions above satisfy the first law of thermodynamics, $d\langle E\rangle = TdS$.

Let us now focus on macroscopic black holes, by considering the large M limit, i.e., $\omega_0 \to 0$. By expanding the mean energy (II.3.8) and the entropy (II.3.9), we get:

$$\langle E\rangle = \frac{N}{\beta} + \frac{N}{12}\beta\omega_0^2 + \mathcal{O}(\omega_0^3), \tag{II.3.10}$$

$$S = N - N\ln\left(\beta\omega_0\right) + \frac{N}{24}\beta^2\omega_0^2 + \mathcal{O}(\omega_0^3). \tag{II.3.11}$$

We see that the leading terms in the expansions satisfy $\langle E\rangle = TS$, hence they capture only the purely thermal extensive contribution TS to the mean energy. However, for $\beta \to \infty$ (zero-temperature limit), the sub-leading terms in Eq. (II.3.10) diverge at fixed ω_0. The same problem appears in standard black-hole thermodynamics, where a zero Hawking temperature implies a divergence of the black-hole mass M. However, this is an artefact of the expansion. This divergence problem can be simply solved in our approach by first taking the $\beta \to \infty$ limit in the exact expression for $\langle E\rangle$ given by Eq. (II.3.8). We get $\langle E\rangle = N\omega_0/2$. This is a finite value, which cures the divergence appearing in Eq. (II.3.10) and has the simple physical interpretation of the zero-point energies $\omega_0/2$ of the N oscillators, representing therefore the contribution of the vacuum. Notice that this contribution cancels out when we perform first the $\omega_0 \to 0$ limit and keep the leading terms only.

The black-hole mass M measured by an observer at infinity can be seen as the sum of the purely extensive contribution of Eq. (II.3.10) and the contribution of the vacuum E_V. Our microscopic

[3] This is also supported by the fuzzball proposal for black holes in string theory [61].

description of the SBH in terms of N non-interacting harmonic oscillators holds in the large-n limit. Thus, we may expect deviation of E_V from the naive value $N\omega_0/2$. Owing to the absence of an external scale different from the thermal one $\beta_{\rm H} = 1/T_{\rm H}$, we nevertheless expect E_V to get only order-one corrections, and M to take the form

$$M = \frac{N}{\beta} + c\frac{N\omega_0}{2}, \tag{II.3.12}$$

where c is a $\mathcal{O}(1)$ constant, which can be fixed using symmetry arguments. The expansions (II.3.10) and (II.3.11) can be also obtained by considering the limit $\beta \to 0$ instead of $\omega_0 \to 0$ in Eqs. (II.3.8) and (II.3.9). Despite being mathematically equivalent, these two limits have a very different physical meaning. While the latter corresponds to black holes with large masses, the former is related to small-mass SBHs. Treating ω_0 and β separately introduces some kind of duality between small and large black holes, which is again a consequence of the absence of an external scale different from $\beta_{\rm H}$. This implies that in our microscopic description there is no difference between the thermodynamic properties of small- and large-mass black holes (a behavior very different from AdS black holes [219]).

Since the asymptotic observer can only measure the classical hair M, both the limits $\beta \to 0$ and $\beta \to \infty$ in Eq. (II.3.12) must lead to the same result, giving $c = 1/\pi$.

For the asymptotic observer, the black-hole equilibrium temperature is $T_{\rm H}$, so that Eq. (II.3.12) gives

$$N = \frac{\beta_{\rm H} M}{2} = 4\pi G M^2. \tag{II.3.13}$$

Seen by the distant observer, therefore, the number of oscillators scales holographically with the area of the event horizon. The leading term of Eq. (II.3.11), together with Eq. (II.3.13), yields

$$S = N = 4\pi G M^2 \tag{II.3.14}$$

which is exactly the BH entropy. The sub-leading term in Eq. (II.3.11) represents a logarithmic correction $N \ln T$, which is consistent with several results in the literature (see, e.g., Refs. [485–498]).

Our description of the black hole in terms of a canonical ensemble of harmonic oscillators, with frequency given by the fundamental QNMs frequency ω_0, is fully consistent with the corpuscular description [35, 65]; the latter sees the black hole as a coherent state of particles with occupation numbers $n_j(p)$ sharply peaked around the characteristic momentum $p \sim 1/R_{\rm H}$, with j labeling some internal microscopic degrees of freedom (DOF). The relation $\omega_0 \sim p$ is a highly non-trivial check of this consistency. Unfortunately, our thermodynamic treatment based on the QNMs spectrum does not give any information about the origin of these internal DOF and their occupation numbers $n_j(p)$. This is mainly due to the fact that the oscillators are treated as indistinguishable from the beginning, coherently with the no-hair theorem. Consequently, we do not have any chemical potential and the only observable is the total number of oscillators $N = \sum_j n_j$. It is quite obvious that, in order to gain information about n_j, we need some further insight, beyond the QNMs spectrum, on the "quantum hair" associated with the internal DOF.

Chapter II.4

Two-dimensional black holes as sets of harmonic oscilaltors

In recent times, we have gained growing theoretical evidence that some peculiar and puzzling features of the gravitational interaction could be addressed by assuming the underlying microscopic quantum theory of gravity to have a *multi-scale* behavior, with the generation of different infrared (IR) length-scales, both at the black hole horizon and at galactic and cosmological level [64, 65, 71, 72, 399]. The holographic principle, the information paradox for black holes, the deviation from Newtonian dynamics at galactic scales and the origin of dark energy stand out among these puzzles.

Evidence along this direction came out few years ago from the proposal to describe a black hole with mass M and radius $R_{\rm S} = 2GM$ as a condensate of a large number $N_{\rm g} \sim \ell_{\rm P}^2 M^2$ (where $\ell_{\rm P} = \sqrt{G}$ is the Planck length)[1] of soft gravitons with typical energy $\epsilon \sim 1/R_{\rm S}$ [35, 36, 39, 499, 500]. This is tightly connected to the *classicalization* idea, according to which gravity achieves UV-completion by using classical objects of size $R_{\rm S} \gg \ell_{\rm P}$, but composed by a huge number of weakly coupled soft quanta of momenta $p \sim 1/R_{\rm S}$ [35, 67, 68]. In this way, a strong 't Hooft-like coupling $\lambda = \alpha N_{\rm g}$ (with α the running coupling) is traded for a large number of weak interacting particles, generating an IR length-scale $\ell \sim \ell_{\rm P}\sqrt{N_{\rm g}}$ [35, 65, 399].

The same idea can be applied at cosmological and galactic scales. Indeed, in the former case, the de Sitter universe can be seen as a bound state of a huge number of soft particles with typical energy $\epsilon \sim 1/L$, with L the size of the cosmological horizon. In the latter case, long-range quantum gravity effects could generate an IR length-scale of galactic size $r_0 = \ell_{\rm P}\sqrt{N_{\rm G}}$, at which the dynamics deviates from the Newtonian behavior [64, 71, 72]. Here, $N_{\rm G} \sim \ell_{\rm P}^2 M_{\rm G}^2$ is the number of particles associated with the mass $M_{\rm G}$ of the galaxy.

A quite similar black hole description emerged also in the string-theory context, and led to the fuzzball proposal [61, 143, 144, 501]. Specifically, a black hole is considered as a bound state of a large number of extended objects (fuzzballs) of size $R \sim R_{\rm S} + \ell_{\rm P}$. These configurations receive contributions also from virtual fluctuations of the quantum gravity vacuum, dubbed as VECROs [62, 63].

Altogether, these results may be seen as a strong indication of the existence of an internal, non-trivial, microscopic black hole structure, which should represent the starting point for explaining the black hole macroscopic behavior. Unfortunately, owing to the classical no-hair theorems, it is almost impossible for a distant observer to have direct access to this internal microscopic information. The only direct window an asymptotic observer has on the microscopic black-hole structure is the way the hole responds to external perturbations. This response is codified in the quasi-normal modes (QNMs) spectrum [467–469]. QNMs are the characteristic oscillations produced by a perturbed black hole and they decay exponentially in time. Their spectrum can be experimentally detected, by observing the gravitational wave signal originated in the ringdown phase of two compact objects merging to form a black hole.

QNMs correspond to complex eigenfunctions of the linearized system. They are characterized by complex frequencies, where the imaginary part describes the damping of the mode caused

[1] We adopt natural units, $c = \hbar = 1$.

by purely ingoing boundary conditions at the horizon. Moreover, Dirichlet boundary conditions at infinity imply a discrete spectrum for the frequencies $\omega = \omega_{\rm R} + {\rm i}\omega_{\rm I}$, with the imaginary part depending on an integer n, the overtone number.

Despite QNMs being classical, there has been strong indications that they could contain information about the quantum properties of black holes [69], their horizons and their internal microscopic structure. In particular, this is true in the high-damped (large-n) regime, when QNMs are expected to probe the black hole at very short distances.

The high-damped QNMs spectrum, together with an analogue of Bohr's correspondence principle, has been used by Hod to explain and fix the area spectrum of the event horizon (see, e.g., Refs. [471, 478–480]), whose quantization was first suggested by Bekenstein in Refs. [481, 482]. The QNMs spectrum has been also used in the Loop Quantum Gravity framework to fix the Barbero-Immirzi parameter [478], which is essential to correctly account for the Bekenstein-Hawking (BH) entropy [483, 484].

The next, crucial, step along this direction was done by Maggiore [69], who showed that the QNMs spectrum for the Schwarzschild black hole, in the high-damping limit, can be interpreted as a damped harmonic oscillator, with proper frequency $\omega = \sqrt{\omega_{\rm R}^2 + \omega_{\rm I}^2}$. Moreover, he argued that this result corresponds to the dispersion relation of a massive particle quantized on a circle with length given by the inverse of the black-hole Hawking temperature.

In Ref. [6], building on Maggiore's result, we have proposed a microscopic description of the Schwarzschild black hole in terms of a canonical ensemble of N decoupled harmonic oscillators. Using this model, we have reproduced the BH entropy as the leading contribution to the Gibbs entropy, in the large-mass black hole limit. We have also derived subleading, logarithmic corrections to the BH result, in agreement with several results in the literature. We additionally found that the number of oscillators scales holographically with the area of the event horizon.

The natural question that now arises is how general the results of Ref. [6] are. Do they represent a peculiarity of the Schwarzschild black hole or are they, instead, a feature common to all black holes? Since the imaginary part of ω always scales linearly with n in the high-damping regime, we expect the main results of Ref. [6] to generally hold.[2]

In this work, we tackle this issue by considering a two-dimensional (2D) dilaton gravity model, namely Jackiw-Teitelboim (JT) gravity [93, 94, 218]. Despite being particularly simple, this model allows for AdS_2 black holes, i.e., 2D solutions with anti de Sitter asymptotic behavior. Because of its simplicity, the model has been used in several contexts [218], like for instance the Hawking evaporation process [279, 294, 502–504] and the related information puzzle [54, 55, 176, 304, 505–508], AdS/CFT correspondence and computation of entanglement entropy; it is also closely related to the Sachdev-Ye-Kitaev (SYK) model [96].

We first extend previous results for the QNMs spectrum of the JT black hole [180] to include the case of massive scalar perturbations. We show that, for generic (massless or massive) scalar perturbations, the quasi-normal frequencies are purely imaginary and scale linearly with the overtone number.

We then show that the QNMs spectrum agrees with the dispersion relation of a massless particle, quantized on a circle of length given by half of the inverse Hawking temperature of the hole. We use the same approach of Ref. [6] to model the JT black hole first as coherent state with occupation numbers sharply peaked on the characteristic QNMs frequency $\hat{\omega}$, and then as a statistical ensemble of N decoupled quantum harmonic oscillators of frequency $\hat{\omega}$. This latter description enables us to derive the BH entropy of the hole as the leading contribution to the Gibbs entropy, in the high-temperature regime. Sub-leading corrections are also computed and shown to behave logarithmically. Further, we find that N equals the BH entropy.

Furthermore, apart from its simplicity, the JT black hole is interesting because it allows for a dual description in terms of a conformal field theory (CFT). Motivated by this, we investigate the relationship between our description in terms of a set of harmonic oscillators and the dual CFT. We find a natural holographic correspondence between QNMs in the AdS_2 bulk and de Alfaro-Fubini-Furlan (DFF) conformally invariant quantum mechanics, which gives a conformally-invariant generalization of the usual quantum harmonic oscillator.

[2] A general description of a black hole as a set of quantum harmonic oscillators has been also proposed in Ref. [241], by modelling the black hole as a spherical cavity.

The present chapter is organised as follows. In Section II.4.1 we briefly review the main features of black-hole solutions in JT gravity. In Section II.4.2 we review the calculations of the QNMs spectrum for external massless scalars and extend these to massive scalar perturbations. The microscopic descriptions of the JT black hole in terms of quantum particles and a canonical ensemble of decoupled harmonic oscillators are presented in Sections II.4.3 and II.4.4, respectively.

In this chapter, we use units in which $c = \hbar = k_{\mathrm{B}} = 1$.

II.4.1 2D AdS black holes

In this work we consider AdS_2 black-hole solutions of Jackiw-Teitelboim (JT) gravity, a well-known gravity theory in two space-time dimensions, described by the action

$$\mathcal{S}_{\mathrm{JT}} = \frac{1}{2\pi}\int d^2x\sqrt{g}\,\phi\left(R + 2\Lambda^2\right), \tag{II.4.1}$$

where ϕ is a scalar field (the dilaton), R the 2D Ricci scalar, $2\Lambda^2$ the cosmological constant. In the Schwarzschild gauge, where the line element can be written as $ds^2 = -f(r)dt^2 + dr^2/f(r)$, the vacuum solutions for the metric and the dilaton read

$$ds^2 = -\left(\frac{r^2}{L^2} - a^2\right)dt^2 + \left(\frac{r^2}{L^2} - a^2\right)^{-1} dr^2, \qquad \phi(r) = \phi_0\frac{r}{L}, \tag{II.4.2}$$

where $L = 1/\Lambda$ is the AdS length, ϕ_0 and a^2 are integration constants, parametrizing the solutions. Since ϕ_0 is not relevant for our discussion, we will set it to 1 for simplicity in the following. The Arnowitt-Deser-Misner (ADM) mass of the solution, therefore, takes the form [294, 509]

$$M = \frac{a^2}{2L}. \tag{II.4.3}$$

In this work, we will only consider solutions with $a^2 \geq 0$, which have positive ADM mass and a Killing horizon at $r = r_{\mathrm{H}} = aL$, and describe asymptotically AdS black holes, with an event horizon at $r = r_{\mathrm{H}}$ and a singularity at $r = 0$ [294].

Using the standard procedure, one easily finds the temperature T_{H} and the entropy S associated with the black hole [509]

$$T_{\mathrm{H}} = \frac{r_{\mathrm{H}}}{2\pi L^2} = \frac{1}{2\pi}\sqrt{\frac{2M}{L}}, \tag{II.4.4a}$$

$$S = 4\pi\sqrt{\frac{ML}{2}} = 2\pi\frac{r_{\mathrm{H}}}{L}. \tag{II.4.4b}$$

To conclude this section, let us briefly discuss the causal structure of AdS_2. The maximal extension of our black hole geometry, the full AdS_2 space-time, is regular and has two disconnected parts. In the Penrose diagram, the black-hole geometry represents only one of the two wedges building the maximally extended AdS_2 up [294]. We will use this causal structure in Section II.4.4, when dealing with the microscopic derivation of the black-hole entropy.

II.4.2 Scalar perturbations and quasi-normal modes

Quasi-normal modes (QNMs) represent the characteristic oscillations of a black hole reacting to external perturbations. In the linear regime, one finds that QNMs are characterized by a discrete spectrum of complex frequencies, whose imaginary part describes the damping of the mode in time, once appropriate boundary conditions at infinity and at the horizon are imposed (see, e.g., Refs. [467–469]).

The 2D case is peculiar since pure Einstein gravity is topological in two space-time dimensions. In JT gravity, the presence of a further degree of freedom (DOF), i.e., the dilaton, allows for the existence of global modes, but not for vectorial nor tensorial propagating ones. Thus, in this theory, QNMs are linked only to external scalar perturbations of the black hole space-time (II.4.2). The QNMs spectrum for massless scalar perturbations in 2D-gravity has been already investigated

in the literature, by imposing either usual boundary conditions or monodromy conditions around the black-hole horizon [177–180, 510]. In this section, we will briefly review the relevant results and extend them to the case of massive scalar perturbation.

Consider a perturbing, external, massless scalar field Φ in the black hole space-time (II.4.2). This perturbation satisfies a generalized Klein-Gordon equation

$$\frac{1}{\sqrt{-g}\,h(\phi)}\partial_\mu\left(\sqrt{-g}\,h(\phi)g^{\mu\nu}\partial_\nu\Phi\right)=0, \tag{II.4.5}$$

where $h(\phi)$ is a generic arbitrary coupling between the dilaton and the perturbing field Φ. Since the background dilaton solution is a function of the radial coordinate (see Eq. (II.4.2)), we have $h(\phi)\equiv h(r)$. The presence of the coupling $h(\phi)$ is justified in a general setting. Moreover, it is fully natural if one considers the JT black hole as a dimensional reduction of higher-dimensional models– and in particular of the 3D BTZ black hole [511]. In this case, $h(\phi)$ encodes the information on the higher-dimensional theory.

Decomposing $\Phi(t,r)$ into Fourier modes, we can redefine the perturbing field as

$$\Phi(t,r)=e^{\mathrm{i}\omega t}\frac{R(r)}{\sqrt{h(r)}}. \tag{II.4.6}$$

Eq. (II.4.5) can then be written in terms of the radial function $R(r)$ only, which satisfies

$$\frac{d^2R}{dr_*^2}+\left[\omega^2-V(r)\right]R=0, \tag{II.4.7}$$

where we introduced the tortoise coordinate r_*, defined by $dr_*/dr=L^2/(r^2-r_{\rm H}^2)$ or, equivalently, by $r=-r_{\rm H}\coth\left(r_{\rm H}r_*/L^2\right)$. This transformation maps the horizon $r=r_{\rm H}$ into $r_*\to-\infty$ and spatial infinity $r\to\infty$ into $r_*=0$. Moreover, the potential $V(r)$ is given by

$$V(r)=\frac{f(r)}{2h(r)}\left[f(r)\frac{d^2h}{dr^2}+\frac{df}{dr}\frac{dh}{dr}-\frac{f(r)}{2h(r)}\left(\frac{dh}{dr}\right)^2\right]. \tag{II.4.8}$$

We adopt usual boundary conditions for QNMs requiring Dirichlet conditions at infinity, i.e., the radial function has to behave as $R(r)\sim0$ at $r\to\infty$, and we must have purely ingoing modes at the horizon. Eq. (II.4.7), together with boundary conditions, represents an eigenvalue problem in the frequency ω, which can be solved once the function $h(\phi)$ is chosen.

As expected in view of the non-existence of vectorial and tensorial propagating modes in pure JT gravity, a non-trivial coupling function between the scalar field Φ and the dilaton is required to have non-trivial propagating solutions. In fact, when $h(r)=$ constant, the potential $V(r)$ vanishes and Eq. (II.4.7) is solved by a freely propagating perturbation, which is not compatible with the QNMs boundary conditions.

The most natural choice for the coupling function h is a power law in ϕ (hence in r: $h(r)=(r/L)^\alpha$. This is motivated not only by simplicity arguments, but also by regarding JT gravity as the dimensional reduction of a $d+2$ dimensional theory. Indeed, in the latter case, we have $h(r)=\phi(r)=r/L$ [179, 288]. Adopting the power-law form for h, the potential (II.4.8) becomes

$$V(r)=\frac{1}{4}\alpha(\alpha+2)\frac{r^2}{L^4}+\frac{(\alpha-2)\alpha r_{\rm H}^4}{4L^4r^2}-\alpha^2\frac{r_{\rm H}^2}{2L^4}, \tag{II.4.9}$$

which, in terms of the tortoise coordinate, reads

$$V(r_*)=\frac{r_{\rm H}^2\alpha}{4L^4\sinh^2\left(r_{\rm H}r_*/L^2\right)\cosh^2\left(r_{\rm H}r_*/L^2\right)}\left[\alpha+2\cosh\left(2r_{\rm H}r_*/L^2\right)\right]. \tag{II.4.10}$$

As already mentioned at the beginning of the section, the QNMs spectrum for ω can be obtained either by solving Eq. (II.4.7) with usual boundary conditions at infinity and at the horizon [512], or by imposing a monodromy condition around the black hole horizon (see, e.g., Ref. [179]). In the following, we will briefly review the computations of Ref. [512] and then we will apply them to derive the frequency spectrum for scalar perturbations.

The Klein-Gordon equation (II.4.7), together with the potential (II.4.10), can be recast in a more suitable form by introducing a new radial coordinate $x = 1/\cosh(r_{\rm H} r_*/L^2)$. This coordinate change maps the horizon and spatial infinity respectively to $x = 0$ and $x = 1$. Moreover, it is useful to factorize the asymptotic behavior of $R(x)$ in these two limits. Since boundary conditions require $R(x)$ to be purely ingoing at the horizon and to vanish at spatial infinity, one can write $R(x) = (x-1)^{(\alpha+2)/4} x^{-{\rm i}L^2\omega/2r_{\rm H}} F(x)$, so that Eq. (II.4.7), once written in terms of $F(x)$, takes the form

$$x(1-x)\frac{{\rm d}^2F}{{\rm d}x^2} + \left[1 - \frac{{\rm i}\tilde{\omega}}{r_{\rm H}} - \frac{1}{2}\left(\alpha - \frac{2{\rm i}\tilde{\omega}}{r_{\rm H}} + 5\right)x\right]\frac{{\rm d}F}{{\rm d}x} - \frac{(2r_{\rm H} - {\rm i}\tilde{\omega})\left[(\alpha+1)r_{\rm H} - {\rm i}\tilde{\omega}\right]}{4r_{\rm H}^2}F(x) = 0, \tag{II.4.11}$$

where $\tilde{\omega} = L^2\omega$. The solution of this equation is a combination of hypergeometric functions. By selecting purely ingoing modes at the horizon, we are left with

$$\begin{aligned} F(x) &= \mathcal{C}\,{}_2F_1\left(1 - \frac{{\rm i}\tilde{\omega}}{2r_{\rm H}}, \frac{1+\alpha}{2} - \frac{{\rm i}\tilde{\omega}}{2r_{\rm H}}, 1 - \frac{{\rm i}\tilde{\omega}}{r_{\rm H}}, x\right) = \\ &= \mathcal{C}(1-x)^{-\frac{\alpha+1}{2}}\,{}_2F_1\left(-\frac{{\rm i}\omega}{2r_{\rm H}}, \frac{1-\alpha}{2} - \frac{{\rm i}\omega}{2r_{\rm H}}, \frac{1+\alpha}{2} - \frac{{\rm i}\omega}{2r_{\rm H}}, x\right), \end{aligned} \tag{II.4.12}$$

where $\mathcal{C}$ is a constant. Eq. (II.4.12) still does not automatically satisfy boundary conditions at infinity. Requiring

$${}_2F_1\left(-\frac{{\rm i}\,\tilde{\omega}}{2r_{\rm H}}, \frac{1-\alpha}{2} - \frac{{\rm i}\,\tilde{\omega}}{2r_{\rm H}}, \frac{1+\alpha}{2} - \frac{{\rm i}\,\tilde{\omega}}{2r_{\rm H}}, 1\right) = \frac{\Gamma\left(\frac{1+\alpha}{2}\right)\Gamma\left(1 - \frac{{\rm i}\tilde{\omega}}{r_{\rm H}}\right)}{\Gamma\left(1 - \frac{{\rm i}\tilde{\omega}}{2r_{\rm H}}\right)\Gamma\left(\frac{1+\alpha}{2} - \frac{{\rm i}\tilde{\omega}}{2r_{\rm H}}\right)} = 0, \tag{II.4.13}$$

and by solving Eq. (II.4.13), we get the desired behavior. Eq. (II.4.13) is satisfied only when α is a non-even real number and ω is

$$\omega \equiv \omega_n = -\frac{2{\rm i}r_{\rm H}}{L^2}\left(n + \frac{\alpha+1}{2}\right), \tag{II.4.14}$$

where n is the overtone number, an integer labelling the mode.

Notice that the quasi-normal frequencies are purely imaginary and the resulting modes purely damped. This fact derives from the asymptotic AdS_2 behavior of the JT black hole, which is reflected in the form of the potential and in the related boundary conditions.

II.4.2.1 Quasi-normal modes for massive scalar perturbations

Previously, we considered the evolution of external massless scalar perturbations in the fixed gravitational background (II.4.2). Let us now consider external perturbations due to a scalar field Φ of mass m and a coupling function with the dilaton $h(\phi)$. The equation for the perturbation is now

$$\left[\frac{1}{\sqrt{-g}\,h(\phi)}\partial_\mu\left(\sqrt{-g}\,h(\phi)g^{\mu\nu}\partial_\nu\right) - m^2\right]\Phi = 0. \tag{II.4.15}$$

We will consider the same coupling function $h(\phi) = (r/L)^\alpha$ used for the massless case. Our results will therefore generalize those in Ref. [178], derived considering a trivial coupling $h(\phi) =$ constant. This choice, together with the ansatz (II.4.6), leads to the equation

$$\frac{d^2R}{dr_*^2} + \left[\omega^2 - V(r) - m^2(r^2 - r_{\rm H}^2)\right]R = 0, \tag{II.4.16}$$

where $V(r)$ has been defined in Eq. (II.4.9). Following the same procedure described in the previous subsection when dealing with the massless case, we get the spectrum of QNMs for massive scalar perturbations

$$\omega_n = -\frac{2\,\mathrm{i} r_\mathrm{H}}{L^2}\left(n + \frac{1+\alpha}{4} + \frac{1}{4}\sqrt{(1+\alpha)^2 + 4L^2m^2}\right). \tag{II.4.17}$$

The results of this section show that, for both massless and massive scalar perturbations, the QNMs spectrum of JT black holes takes the general form $\omega_n = -\frac{2\mathrm{i}\, r_\mathrm{H}}{L^2}\,(n+\gamma)$, where γ is some real number of order one. The frequencies are purely imaginary and grow linearly with the overtone number n. This latter behavior is reminiscent of the energy spectrum of a one-dimensional quantum harmonic oscillator [69].

In the high-damping regime, we can neglect γ. The relevant information here is the linear scaling of ω_n with n. We can now exploit Maggiore's argument, originally used for the Schwarzschild black hole [69], to suggest a correspondence between the QNM frequencies $\omega_\mathrm{R} + \mathrm{i}\omega_\mathrm{I}$ and the proper frequency ω of an harmonic oscillator via the relation $\omega = \sqrt{\omega_\mathrm{R}^2 + \omega_\mathrm{I}^2}$. In the present case, this gives

$$\omega_n \equiv |\omega_\mathrm{I}| = \hat{\omega}\,(n+\gamma)\,,\ \hat{\omega} = \frac{2r_\mathrm{H}}{L^2}, \tag{II.4.18}$$

where the characteristic frequency $\hat{\omega}$ if defined in terms of the fundamental frequency of the oscillator ω_0 as $\hat{\omega} \equiv \omega_0/\gamma$. $\hat{\omega}$ can also be written in terms of the black hole temperature (II.4.4a) as $\hat{\omega} = 4\pi T_\mathrm{H}$. This relation differs by a factor of 2 from the one pertaining to 4D black holes, $\hat{\omega} = 2\pi T_\mathrm{H}$ [69, 236, 470–472, 513–515]. This fact seems to be a peculiarity of black-hole solutions in 2 and 3 space-time dimensions [180, 512, 516, 517].

Finally, we notice that, in the large-n regime, the QNMs are probing the JT black hole at small distances. This should provide us with information about its microscopic structure, similarly to what happens for the Schwarzschild case. On the other hand, the small-n behavior corresponds to probing large distances, of order of the horizon size. This regime is instead not universal, but depends on γ, i.e., on the mass of the scalar field and on the form of the coupling function $h(\phi)$ (see the parameter α in the spectra (II.4.14) and (II.4.17)).

We will use this information in the next two sections, first to give a corpuscular description of the black hole, then to improve such a description by considering the black hole as a statistical ensemble of harmonic oscillators.

II.4.3 Corpuscular description

A black hole can be considered as a macroscopic quantum system, built up by a large number N of microscopic DOFs [35–40]. The theoretical evidence supporting the validity of this corpuscular description is mounting. Specifically, a black hole can be seen as a coherent quantum state, which *classicalizes* for $N \gg 1$, and satisfies a *maximally packaging* condition, relating the maximal amount of DOFs one can pack in the system to its size [35, 36]. This condition has been shown to be equivalent to the holographic scaling of N [39]. The possible existence of macroscopic quantum gravity states emerged also in investigations concerning galactic dynamics [70–72]. The latter perspective is further supported by the formulation of a *generalized thermal equivalence principle* (GTEP), which relates the temperature of the statistical ensemble of the N DOFs to the surface gravity of a black hole or to the cosmological acceleration [72].

Recently, this corpuscular hypothesis gained support also from an apparent relation between the form of the QNMs spectrum of the Schwarzschild black hole and its microscopic description in terms of an ensemble of quantum harmonic oscillators [6].

This corpuscular interpretation, finds strong support in the Maggiore proposal [69], according to which in the large overtone number-regime, the proper frequency of the harmonic oscillator describing the QNMs spectrum of the Schwarzschild black hole $\omega = \sqrt{\omega_\mathrm{R}^2 + \omega_\mathrm{I}^2}$ can be recast as the dispersion relation of a relativistic particle, i.e., $\omega_n = \sqrt{m^2 + p_n^2}$. Specifically, the particle mass m is defined in terms of the real part of the frequency, $m = \ln 3\, T_\mathrm{H}$, with T_H the Hawking temperature of the hole, while the particle momentum p_n is defined in terms of ω_I (hence its dependence on the overtone number) and reads $p_n = 2\pi T_\mathrm{H}\left(n + \frac{1}{2}\right)$. The latter expression, in particular, is pertinent to a particle quantized on a circle, with length $L = 1/T_\mathrm{H}$, with antiperiodic boundary conditions. Applying the same reasoning to the QNMs spectrum of the JT black hole (II.4.18) considered in

this work, we can rewrite it in the form of a dispersion relation for a relativistic particle with vanishing rest mass

$$\omega_n = p_n, \quad p_n = \frac{4\pi}{\beta_{\rm H}}\left(n+\gamma\right), \tag{II.4.19}$$

where now $\beta_{\rm H} = 1/T_{\rm H}$ is the inverse of the black hole temperature (II.4.4a). As in Ref. [69], the form of p_n is that pertaining to a particle described by a wave function, Ψ, quantized on a circle of length $\beta_{\rm H}/2$, with boundary conditions

$$\Psi\left(x+\frac{\beta_{\rm H}}{2}\right) = e^{2\pi {\rm i}\gamma}\Psi(x). \tag{II.4.20}$$

In a corpuscular description, we can therefore consider the JT black hole as a coherent state representing a classical configuration localized in a region of size $r_{\rm H}$, with occupation numbers $n_j(p)$ sharply peaked around the characteristic QNMs frequency $p = \hat{\omega}$. Being $\hat{\omega} \propto T_{\rm H}$, this is fully in agreement with a thermal, coarse grained, description of the system, according to which the statistical occupation number distribution should be peaked at energies around $T_{\rm H}$.

Since the system is expected to be weakly coupled in the regime $N \gg 1$, on a first approximation we can neglect the interactions. We can consequently consider the JT black hole as a bound state of free particles, each with typical energy $\hat{\omega} = 4\pi T_{\rm H}$. This yields

$$M = N\hat{\omega}, \tag{II.4.21}$$

where M is the black hole mass.

Eqs. (II.4.4a) and (II.4.4b) give the scaling of M and S with the temperature $T_{\rm H}$: $M = 2\pi^2 L T_{\rm H}^2$, $S = 4\pi^2 L T_{\rm H}$, typical of a two-dimensional CFT. This is, therefore, a manifestation of the AdS/CFT correspondence for JT gravity [518, 519]. By using Eq. (II.4.21) together with these scaling relations, one can now easily find that the black hole entropy S is proportional to N

$$S \propto N. \tag{II.4.22}$$

This is fully consistent with the corpuscular description of the JT black hole as a bound state of N particles, whose thermodynamic entropy roughly scales as the number of DOFs.

In view of the discussion of the next section, it is quite interesting to compare the behavior of the JT and of the Schwarzschild black holes. As remarked above, in the latter case, the QNMs spectrum, in the large-n limit, has the same form given in Eq. (II.4.18), with $\hat{\omega} = 1/(2r_{\rm H}) = 2\pi T_{\rm H}$ and $\gamma = 1/2$, where now $T_{\rm H} = 1/(4\pi r_{\rm H})$, corresponding to a particle quantized on a circle of length $\beta_{\rm H}$, with antiperiodic boundary conditions. The corpuscular interpretation of the Schwarzschild black hole is quite the same as the JT case: it can be regarded as a coherent bound state of N particles with occupation numbers sharply peaked at $\hat{\omega} \sim T_{\rm H}$, such that $M = N\hat{\omega}$ and $S \propto N$ on a first approximation.

On the other hand, the scaling of M and S with the Hawking temperature $T_{\rm H}$ is quite different: $M = 1/(8\pi G T_{\rm H})$, $S = 1/(16\pi G T_{\rm H}^2)$. This behavior reflects the fact that we do not have a thermal CFT, dual to the black hole, in the Schwarzschild case. This can also be seen as a consequence of the presence of two different length-scales in the two gravity theories. In JT gravity, the gravitational coupling constant is dimensionless and we have an external length-scale, i.e., the AdS length L. Conversely, in general relativity, the gravitational coupling constant has dimensions of length squared and we have no external length-scale. In the next section, we will show that these features have a deep impact on the black hole description in terms of harmonic oscillators.

Let us conclude this section by noticing an intriguing relationship between our QNMs-motivated corpuscular description of black holes and the recently proposed GTEP [72]. As already mentioned, the latter explains acceleration in gravitational systems, such as the surface gravity κ for black holes and the cosmological acceleration for the de Sitter universe, as a universal macroscopic effect of a large number of thermalized quantum gravity DOFs. The proportionality relation $\hat{\omega} \propto T_{\rm H}$ we found for both the Schwarzschild and the JT black holes also implies $\hat{\omega} \propto \kappa$. This result, therefore, could be seen not as a mere coincidence, but as a consequence of the GTEP.

II.4.4 The JT black hole as statistical ensemble of oscillators

In the previous section, we gave a corpuscular description of the JT black hole in terms of a coherent state of a large number N of particles, with occupation numbers sharply peaked around the characteristic quasi-normal frequency $\hat{\omega}$. In this section, we will give support to this microscopic picture of the black hole. Motivated by the form of the QNMs spectra (II.4.14) and (II.4.17), we will model the black hole as a statistical (canonical) ensemble of N harmonic oscillators of frequency $\hat{\omega}$. We will follow here the same procedure adopted in Ref. [6] for the Schwarzschild black hole.

Similarly to the Schwarzschild case, we are mainly interested in macroscopic black holes, i.e., in their large-mass ($M \to \infty$) behavior. There is, however, a crucial difference between the four-dimensional Schwarzschild and the JT black hole. In the latter case, the large-M limit corresponds to large temperatures $T_{\rm H}$, whereas in the former it corresponds to the small-temperature regime. This is a simple consequence of the scaling of M in terms of $T_{\rm H}$, discussed in the previous section. In the JT case, the large-M behavior will be independent, at leading order, from the vacuum, i.e., from the value of γ in Eq. (II.4.18).

The spectrum will be dominated by the linear behavior in the overtone number n, so that in the large mass limit we can effectively model the JT black hole as an ensemble of $N \gg 1$ decoupled harmonic oscillators. At first sight, modelling the black hole as a set of free particles may seem at odds with the naive intuition of a black hole as a strongly coupled gravitational system. However, one should keep in mind that the system is strongly coupled in terms of the 't Hooft coupling $\lambda = \alpha N$, but it is weakly coupled in terms of the running coupling constant α [35, 65–67].

We adopt a description in terms of a canonical ensemble: the black hole is taken to be in thermal equilibrium with its surroundings at temperature $T = 1/\beta$. Owing to its *negative* specific heat and being asymptotically flat, a Schwarzschild black hole cannot be in stable thermodynamical equilibrium with a thermal bath. Consequently, the canonical ensemble is ill defined and requires the system to be confined within artificial external boundaries [219, 485]. Conversely, the canonical ensemble is perfectly defined in asymptotically AdS space-times, because its asymptotic timelike boundary naturally acts as a confining box. Notice that, although the AdS_2 black hole space-time is not geodesically complete for radial null geodesics, one can impose perfectly-reflecting boundary conditions at the asymptotic timelike boundary of the spacetime. Thus, a large AdS_2 black hole is kept at thermal equilibrium with its radiation and is therefore naturally described in terms of the canonical ensemble.

In addition, motivated by the fact that the solutions can be fully characterized by a single observable, the mass M, we take the number of oscillators N fixed. Following Ref. [6], we consider β and $\hat{\omega}$ as *independent* variables, so that the temperature T and the black hole mass M can vary independently. This is justified by the fact that the observer at infinity, who only measures the QNMs, has access to the mass of the black hole only, due to the absence of any chemical potential, whereas the horizon radius can fluctuate quantum mechanically; only local measurements would allow to probe these fluctuations [485].

In the canonical ensemble, the partition function of a single oscillator, with spectrum given by Eq. (II.4.18), is

$$\mathcal{Z}_1 = \sum_{n=0}^{\infty} e^{-\beta\omega_n} = \frac{e^{\frac{2\beta r_{\rm H}}{L^2}(1-\gamma)}}{e^{\frac{2\beta r_{\rm H}}{L^2}} - 1}. \tag{II.4.23}$$

We consider the JT black hole as a system of N, non-interacting, indistinguishable oscillators. The total partition function is therefore $\mathcal{Z}_N = \mathcal{Z}_1^N$. The average energy and the entropy are

$$\langle E\rangle = -\partial_\beta \ln \mathcal{Z}_N = -\frac{2Nr_{\rm H}}{L^2}(1-\gamma) + \frac{2Nr_{\rm H}}{L^2}\frac{e^{\frac{2\beta r_{\rm H}}{L^2}}}{e^{\frac{2\beta r_{\rm H}}{L^2}} - 1}, \tag{II.4.24a}$$

$$S = \ln \mathcal{Z}_N + \beta\langle E\rangle = -N \ln\left(e^{\frac{2\beta r_{\rm H}}{L^2}} - 1\right) + \frac{2Nr_{\rm H}}{L^2}\beta\frac{e^{\frac{2\beta r_{\rm H}}{L^2}}}{e^{\frac{2\beta r_{\rm H}}{L^2}} - 1}. \tag{II.4.24b}$$

In the large-temperature limit, i.e., $\beta \to 0$, we get:

$$\langle E\rangle \simeq \frac{N}{\beta} + \frac{2Nr_{\rm H}}{L^2}\left(\gamma - \frac{1}{2}\right) + \mathcal{O}(\beta). \tag{II.4.25}$$

$$S \simeq N - N \ln\left(2\frac{r_{\rm H}}{L^2}\beta\right) + \mathcal{O}(\beta^2). \tag{II.4.26}$$

Notice that, consistently with our previous statement, the vacuum contribution (parametrized by γ) enters only in the subleading terms in the $\beta \to 0$ expansion. Thus, for the asymptotic observer, which identifies $T = T_{\rm H}$, the leading term in the large-mass expansion gives a purely extensive contribution to the energy, satisfying $\langle E \rangle = TS$, which is completely unaffected by the zero-point energies of the oscillators. This behavior has to be compared with that of the Schwarzschild black hole, for which also the vacuum energy provides a non-negligible contribution to $\langle E \rangle$ in the large-mass limit, consistently with the scaling $M \sim T_{\rm H}^{-1}$ [6].

The leading term in Eq. (II.4.25) has to be identified with the the black-hole mass M measured by an observer at infinity, who sees the system at thermal equilibrium at the Hawking temperature (II.4.4a). This fixes the number of oscillators to $N = \beta_{\rm H} M = \pi r_{\rm H}/L$. Plugging this result into the leading term of Eq. (II.4.26) gives

$$S = \pi \frac{r_{\rm H}}{L}, \tag{II.4.27}$$

which is half of the Bekenstein-Hawking (BH) entropy (II.4.4b) of the JT black hole. The next-to-leading-order term in the entropy expansion (II.4.26) is a logarithmic correction, in agreement with several results in the literature (see, e.g., Refs. [486–497]). These corrections are positive when expressed in terms of the temperature and have a pure thermodynamic origin, as they arise from the high-temperature expansion, and causes an increase in the entropy, as expected (see, e.g., Ref. [492] for a discussion about thermal corrections to the entropy in general two-dimensional dilatonic models).

The origin of the mismatch of a factor of 2 between the leading term in the Gibbs entropy for the N-oscillator system and the BH entropy (II.4.4b) could be traced back to the peculiar topology of the AdS_2 space-time. The JT black hole represents just one of the two disconnected wedges of full AdS_2. The BH entropy of the hole can be thought as resulting from tracing out the DOFs on the invisible edge of the full AdS_2 [256, 497]. This means that, in our microscopic description in terms of harmonic oscillators, we should double N, keeping however the black hole mass unchanged. In this way, we find $S = 2N = 2\pi r_{\rm H}/L$, matching exactly the BH entropy (II.4.4b).

II.4.5 Quasi-normal modes and Conformal Symmetry

In the previous sections, we derived and discussed the QNMs spectrum for the JT black hole and used it to build a microscopic description both in terms of a coherent state of a large number of particles and as a statistical ensemble of harmonic oscillators. Until now, this perspective has been motivated only by the form of the QNMs spectrum (II.4.18). On the other hand, it is well known that in the AdS/CFT framework, JT gravity allows for a dual description in terms of a CFT. In two spacetime dimensions, the correspondence has both a bulk realization in terms of a 2D CFT [518, 519] and an holographic one in terms of conformal quantum mechanics living on the 1D time-like boundary of AdS_2 [284, 520–522]. It is therefore tempting to see to what extent the microscopic description of the JT black hole in terms of harmonic oscillators finds support in the dual 1D boundary, quantum mechanical description. This will be the subject of this section.

AdS_2 gravity induces a conformally invariant dynamics on the 1D space-time boundary at spatial infinity $r \to \infty$ [523, 524]. Specifically, the boundary theory has the same form of the conformal quantum mechanics proposed by de Alfaro, Fubini and Furlan (DFF) in [525], coupled to an external source. The boundary dynamics is generated by the asymptotic symmetry group of AdS_2, the Diff_1 group (time reparametrizations), namely the set of transformations which leave the following asymptotic expressions of the metric and the dilaton invariant

$$g_{tt} \sim -\frac{r^2}{L^2} + \gamma_{tt}(t) + \mathcal{O}\left(\frac{1}{r^2}\right), \tag{II.4.28}$$

$$g_{rr} \sim \frac{L^2}{r^2} + \frac{L^4 \gamma_{rr}(t)}{r^4} + \mathcal{O}\left(\frac{1}{r^6}\right), \tag{II.4.29}$$

$$\phi \sim \left(\rho(t)\frac{r}{L} + \frac{L\gamma_\phi(t)}{2r}\right) + \mathcal{O}\left(\frac{1}{r^3}\right), \tag{II.4.30}$$

where γ_{tt}, γ_{rr}, γ_ϕ and ρ represent the boundary and the dilaton deformations, respectively. The equations of motion, stemming from the action (II.4.1), together with (II.4.28), give the dynamical equations

$$\frac{\ddot{\rho}}{L^2} - \rho\gamma + \beta = 0, \qquad \dot{\rho}\gamma + \dot{\beta} = 0, \tag{II.4.31}$$

where $\gamma \equiv \gamma_{tt} - \gamma_{rr}/2$, $\beta \equiv \rho\gamma_{rr}/2 + \gamma_\phi$ and the dot indicates differentiation with respect to t.

We can now use the Diff$_1$ gauge freedom to fix $\gamma =$ constant in (II.4.31), and get the equation for the harmonic oscillator

$$\ddot{\rho} = \frac{2\gamma}{L^2}\rho. \tag{II.4.32}$$

γ is a function of the ADM mass (II.4.3), $\gamma = -ML$, and depending on its sign, (II.4.32) describes an harmonic oscillator with real frequency ($M < 0$), a free particle ($M = 0$) or an harmonic oscillator with imaginary frequency ($M > 0$), signalizing the presence of dissipative effects. Specifically, in the black hole solution ($M > 0$), (II.4.32) describes an harmonic oscillator with frequency $\omega = \mathrm{i}\hat{\omega}$, with $\hat{\omega}$ given by (II.4.18). This result corroborates the microscopic description of the JT black hole in terms of harmonic oscillators, based on the QNMs spectrum, from the dual holographic theory point of view.

The gauge fixing, leading to (II.4.32), breaks the full Diff$_1$ invariance group, leaving unbroken only the time-translation subgroup. This is a quite strong condition, because one would like to keep unbroken at least the isometry of AdS$_2$, which is isomorphic to SL(2,R). This group is generated by the transformation

$$G = u\mathcal{H} + v\mathcal{D} + w\mathcal{K} \tag{II.4.33}$$

where $\mathcal{H}$, $\mathcal{D}$, and $\mathcal{K}$ generate translations, dilatations and conformal transformations, respectively.

The spectrum of G can be characterized by the sign of the determinant $\Delta \equiv v^2 - 4uw$. Specifically, for $\Delta < 0$, G is compact, its spectrum is discrete and bounded from below and its eigenstates are normalizable. For $\Delta = 0$, the spectrum is continuous and bounded from below. For $\Delta > 0$, G is non-compact and its spectrum is unbounded from below. The action, invariant under the conformal transformations generated by G, takes the form [525]

$$\mathcal{S} = \frac{1}{2}\int d\tau \left(\dot{q}^2 + \frac{\Delta}{4}q^2 - \frac{g}{q^2}\right). \tag{II.4.34}$$

The parameter Δ in the action (II.4.34) plays the same role of the parameter γ in (II.4.32).

The case of interest in our discussion is $\Delta > 0$, i.e., a non-compact G with an unbounded-from-below spectrum, which corresponds to the $\gamma > 0$ behavior, i.e., the harmonic oscillator with *imaginary* frequencies $\omega = \mathrm{i}\hat{\omega}$, dual to the JT black hole space-time. This is a consequence of the fact that this space-time is endowed with an event horizon and we can describe it in terms of a thermal quantum harmonic oscillator at the horizon temperature (II.4.4a) [523].

The last point shows, in particular, that the black hole space-time is holographically dual to a 1D conformally symmetric *thermal* system on the boundary, which is of course perfectly consistent with the AdS/CFT correspondence.

The next step is to look for a correspondence between the spectrum of the DFF boundary operator (II.4.33) on the boundary and the JT QNMs spectrum in the bulk. This is quite natural also in consideration of the fact that QNMs are dual to the response of a thermal system to external perturbations on the boundary [475]. In view of the holographic nature of the correspondence, we expect a matching of the spectra in the $r \to \infty$ ($r_* \to 0$) limit of the bulk radial coordinate.

Let us then focus on the eigenvalue equation for G [525]

$$\left(-\frac{d^2}{dx^2} + W(x)\right)\psi = 2\mathcal{G}\psi, \quad W(x) = \frac{g}{x^2} - \frac{\Delta}{4}x^2 \tag{II.4.35}$$

where $2\mathcal{G}$ are the eigenvalues and ψ the eigenfunctions. (II.4.35) has the form of a time-independent Schrödinger equation, with potential given by $W(x)$.

The spectrum of the eigenvalues and the normalizability of the eigenfunctions are therefore determined by the coupling g in the $x \to 0$ region. Specifically, $g > 0$ provides an infinite repulsive well, which keeps the particle confined in the internal region $0 < x < \infty$. On the other hand, $g < 0$ corresponds to an attractive potential, giving unphysical solutions. The uncoupled case $g = 0$ provides non-normalizable eigenfunctions, coherently with the free particle, whose wavefunction is defined on all the line $-\infty < x < \infty$.

The parameter Δ rules, instead, the behavior at $x \to \infty$. If $\Delta > 0$, the potential is monotonically decreasing as $x \to \infty$ and is unbounded from below. If $\Delta = 0$, the potential approaches to zero in this limit, thus producing a continuous spectrum bounded from below. If $\Delta < 0$ and the coupling g is positive, the potential has a minimum at $x_{\min} = (2g/|\Delta|)^{1/4}$, and goes to $+\infty$ both for $x \to 0$, ∞. It means that the eigenfunctions will be renormalizable and the eigenvalues spectrum discrete and bounded from below. Specifically, this spectrum is equivalent to the harmonic oscillator one with *real* frequencies, with eigenvalues scaling linearly with an integer n.

Let us now compare the potential $W(x)$ in (II.4.35) with the QNMs potential of (II.4.10). In general, the two potentials will be different. However, as already anticipated, the relationship with the asymptotic symmetries, discussed at the beginning of this section, implies that the QNMs and the operator G spectra are expected to match in the limit $r \to \infty$ ($r_* \to 0$).

The $r_* \to 0$ expansion of the potential (II.4.10) gives

$$V(r_*) = \frac{\alpha(1-\alpha)}{3}\frac{r_{\rm H}^2}{L^4} + \frac{\alpha(\alpha+2)}{4r_*^2} + \frac{\alpha(4\alpha-7)}{15}\frac{r_{\rm H}^4 r_*^2}{L^8} + \mathcal{O}(r_*^3). \tag{II.4.36}$$

In order to make a direct comparison with the DFF model, we now define the dimensionless variable

$$x^2 \equiv \frac{r_{\rm H}^2 r_*^2}{L^4}, \tag{II.4.37}$$

which brings the asymptotic potential (II.4.36) into the form

$$V(x) = \frac{r_{\rm H}^2}{L^4}\left[\frac{\alpha(1-\alpha)}{3} + \frac{\alpha(\alpha+2)}{4x^2} + \frac{\alpha(4\alpha-7)}{15}x^2\right]. \tag{II.4.38}$$

Comparing now the potential $V(x)$ with the DFF one $W(x)$ of (II.4.35), we can easily identify the DFF couplings Δ, g in terms of the dilaton coupling parameter α:

$$g = \frac{\alpha(\alpha+2)}{4}, \tag{II.4.39a}$$

$$-\frac{\Delta}{4} = \frac{\alpha(4\alpha-7)}{15}. \tag{II.4.39b}$$

Notice that, apart from these identifications, the matching between the QNMs and the DFF operator eigenevalue equations requires also a shift of the values of ω^2 by a α-dependent term. Interestingly, however, this shifting term becomes zero when $\alpha = 1$, i.e., using the most natural coupling $h(\phi) = \phi$ (see (II.4.2)).

The sign of Δ determines whether the frequencies are real or imaginary. We see that, for dilaton couplings $0 < \alpha < 7/4$, $\Delta > 0$, and we have a correspondence with a thermal harmonic oscillator, with imaginary frequencies on the boundary. If $\alpha > 7/4$, $\Delta < 0$ and we have the spectrum of a standard harmonic oscillator, with *real* frequencies.

Eqs. (II.4.39a) and (II.4.39b) clearly show that a non-trivial dilaton coupling h in the Klein-Gordon equation (II.4.5) is needed to have also a non-trivial boundary dynamics. $h =$ constant implies $\alpha \to 0$, so that both $g \to 0$ and $\Delta \to 0$, yielding a free-particle boundary dynamics. Correspondingly, the form of the bulk wavefunction is not compatible with the QNMs boundary conditions. On other hand, we see that, as long as $\alpha > 0$, g is positive, so no unphysical eigenstates are present.

II.4.5.1 Eigenvalue problem for the DFF model with $\Delta > 0$

We showed above that, in the asymptotic $r_* \to 0$ regime, the QNMs spectrum for the JT black hole can be put in correspondence with the eingevalue problem for the DFF operator G with $\Delta > 0$.

Let us, therefore, consider the eigenvalue equation (II.4.35) in our specific case. As we saw before, in this case the spectrum of G is unbounded from below. From a quantum mechanical point of view, these states do not have a physical interpretation and were therefore excluded in the analysis of Ref. [525].

Eq. (II.4.35) can be solved in terms of special functions. The solution reads

$$\psi(x) = A\, 2^{b-\frac{1}{4}}\, e^{-\frac{z}{2}} \left(\frac{\mathrm{i}z}{\sqrt{\Delta}}\right)^{\frac{b}{2}-\frac{1}{4}} \mathcal{U}\left(a,b,z\right) + B\, 2^{b-\frac{1}{4}}\, e^{-\frac{z}{2}} \left(\frac{\mathrm{i}z}{\sqrt{\Delta}}\right)^{\frac{b}{2}-\frac{1}{4}} \mathcal{L}_{-a}^{b-1}\left(z\right), \tag{II.4.40}$$

where A and B are two integration constants, $\mathcal{U}(a,b,z)$ is the confluent hypergeometric function, $\mathcal{L}_n^{\alpha}(z)$ are the generalized Laguerre polynomials, and we have defined

$$a \equiv \frac{-4\mathrm{i}\mathcal{G}\sqrt{\Delta} + 2\Delta + \Delta\sqrt{1+4g}}{4\Delta}, \qquad b \equiv 1 + \frac{\sqrt{1+4g}}{2}, \qquad z \equiv -\frac{\mathrm{i}}{2}\sqrt{\Delta}\, x^2. \tag{II.4.41}$$

Let us now impose the boundary conditions. The correspondence between the DFF conformal quantum mechanics and QNMs in the bulk, discussed in the previous subsection, implies that, to solve the former, we have to use here the same boundary conditions at $x = 0$ and $x = \infty$, used to solve the latter in the bulk. Regularity of the solution and selection of purely ingoing waves at $x = \infty$ (corresponding to the horizon in the bulk) requires $B = 0$. On the other hand, the confluent hypergeometric functions diverge in $x = 0$. Near $x = 0$, the first term of Eq. (II.4.40) therefore behaves as (we neglect non-relevant numerical factors)

$$x^{b-\frac{1}{2}}\, \mathcal{U}(a,b,z) \sim\ x^{b-\frac{1}{2}} \frac{\Gamma\left(1-b\right)}{\Gamma\left(1+a-b\right)} + c_1\, x^{b-\frac{1}{2}} x^{2(1-b)} \frac{\left(\frac{1}{2}-\frac{\mathrm{i}}{2}\right)^{2(b-1)} \Delta^{\frac{1}{2}-\frac{b}{2}} \Gamma\left(b-1\right)}{\Gamma\left(a\right)} \tag{II.4.42}$$

with c_1 a numerical factor. Owning to the fact that $g > 0$, the first term goes to zero for $x \to 0$. The second term, however, being proportional to $x^{\frac{1}{2}-\frac{\sqrt{1+4g}}{2}}$, diverges as $x \to 0$. To prevent this, we require the Gamma function to diverge, from which we are able to compute the spectrum of $\mathcal{G}$

$$\frac{1}{2} + \frac{\sqrt{1+4g}}{4} - \frac{\mathrm{i}\mathcal{G}}{\sqrt{\Delta}} = -n, \qquad\qquad n = 0, 1, 2, \ldots \tag{II.4.43}$$

$$\mathcal{G} = -\mathrm{i}\sqrt{\Delta}\left(n + \frac{1}{2} + \frac{\sqrt{1+4g}}{4}\right). \tag{II.4.44}$$

We see that the eigenvalues are purely imaginary and they scale linearly with n, as expected.

Using Eq. (II.4.39a), the previous equation becomes

$$\mathcal{G} = -\mathrm{i}\sqrt{\Delta}\left(n + \frac{1}{2} + \frac{\alpha+1}{4}\right), \tag{II.4.45}$$

which has the same form of the analytic results (II.4.14), (II.4.17) obtained for QNMs in the bulk, with $\hat{\omega} = \sqrt{\Delta}$. Notice that, however, the expressions for the frequency ω_0 are quite different in the two cases. For QNMs, ω_0 in Eq. (II.4.18) is a function of the horizon radius only (or, equivalently, of the black hole mass), whereas ω_0 depends on α only in Eq. (II.4.45) (see Eq. (II.4.39b)). This discrepancy is due to the fact that the correspondence QNMs/DFF quantum mechanics holds only in the $r \to \infty$ asymptotic regime, where we expect the spectrum to be determined by the perturbation, i.e., the parameter α defining the dilatonic coupling function h.

Chapter II.5

Summary of part II

In this second part of the thesis we tackled the problem of understanding regular and singular black-hole systems from a quantum perspective, using toy models and effective parameterization of quantum effects. Here we briefly summary our main results.

In Chapter II.2, we derived a class of models encoding, at the classical level, the effects of a generic quantum superposition of the source of the gravitational field. We proposed a formalism, that resembles the Newton-Schrödinger one, with which it is possible to obtain a regular, asymptotically-flat metric starting from the probability distribution of some particle in a superposition of locations. As a simple example, we considered the case of a Gaussian wave packet of width R which represents the uncertainty in the position of the source. Not only is this uncertainty responsible for the smearing of the classical singularity, but also prevents the radius of the two sphere from shrinking to zero near the classical singularity. The resulting spacetime reduces to the Schwarzschild spacetime in the limit $R \to 0$ and at great distances from the source. Moreover, similarly to what we have shown in Chapter I.2, the spacetime has a different behavior depending on the value of the ratio $R/R_{\rm S}$. In particular, when the quantum effects are negligible and the source is well localized, i.e., when $R/R_{\rm S} \ll 1$, the spacetime is indistinguishable from the classical Schwarzschild one, even very near to the horizon. When r and $R_{\rm S}$ become comparable, namely for $R/R_{\rm S} \simeq 1$, the quantumness of the source produces relevant and measurable effects, modifying the geometry in some neighborhood of the horizon and the physical observables related to it. Finally, when $R/R_{\rm S} \gg 1$ and the quantum effects become dominant, the horizon disappears and the spacetime becomes a traversable wormhole. As done in Chapter I.2, we also investigated the thermodynamics of this spacetime, which seems to behave in the same way the static models presented in Part I. We then concentrated on some more phenomenological features, finding that both the spectrum of the quasinormal modes and the photon orbits are affected by the uncertainty in the position of the source. Moreover, when the spacetime becomes horizonless, we expect the spacetime to produce echoes [51] when perturbed. One intrinsic limitation of our approach is that the probability distribution for the position of the source is not dynamically determined but fixed a priori. In order to formulate a fully dynamical theory we would need to introduce some kind of dynamics (for instance, some Schrödinger-like equation) determing the quantum wave function describing superposition of positions.

Chapters II.3 and II.4 are devoted to the description of the black holes as sets of oscillators with typical frequencies given by the quasinormal modes, motivated by Maggiore's interpretation of the quasinormal-mode spectrum [69]. This possibility is also reasonable in light of the fact that the quasinormal modes represent the linear response of black holes to external perturbations which, in principle, should carry information about the structure of the system involved.

Using this idea, in Chapter II.3 we studied the link between this description and the Schwarzschild black hole. We first built a partition function where the statistical weight of each possible state of the oscillators is given by $\mathrm{e}^{-\omega_n/T_{\rm H}}$, where ω_n is the n-th quasinormal frequency. Notice that, in this description, we let the temperature be free to fluctuate, independently from the black-hole mass, near the average value $T = T_{\rm H}$. We first showed that when we consider large mass black holes the contribution of the first, low-damped modes can be neglected. Using this approximation, we are able to obtain the partition function in a closed form and to compute the internal energy and the entropy of the black hole in terms of the proper frequency of the oscillators $\omega_0 = 1/4GM$. Setting

the internal energy of the hole to the mass of the system, we are able to find the leading and the first subleading terms in the Bekenstein-Hawking entropy. The latter, in particular, is given by the logarithm of the temperature, in line with previous results in literature. Moreover, we showed that the holographic scaling of the entropy is a natural consequence of the relation between the number of oscillators and the area of the system.

In Chapter II.4 we applied a similar approach to two-dimensional AdS black holes, with the twofold objective of checking whether our conjecture is valid even for other systems, and of finding a deeper link between the description in terms of oscillators and the actual microscopic behavior of the system. Using the same tecnique as in Chapter II.3, we again found that the description in terms of N harmonic oscillators naturally reproduce the Bekenstein-Hawking entropy formula and its holografic scaling. In this case, however, we no longer need to limit ourselves to consider only the highly-damped modes due to the simpler, analytical form of the quasinormal-mode spectrum. Additioinally, we corroborated our microscopic description using the holographic correspondence between the 2D bulk gravity theory and the boundary quantum mechanics. We found that the duel description of the spectrum can be given in terms of a DFF conformally-invariant quantum-mechanical model. The Schrödinger-like equation describing the perturbations in the bulk reduces to an eigenvalue problem for the noncompact DFF generator G, whose spectrum reproduces the linear scaling of the frequencies with the overtone number n.

Appendices—Part II

II.A Curvature invariants

Computing the Ricci tensor for the metric Eq. (II.2.28), one easily finds the Ricci scalar

$$\mathcal{R} = -\frac{4e^{-\frac{2r^2}{R^2}}}{R^3r^3\left(3R^2+4r^2\right)^2}\left[-3GMR^5e^{\frac{2r^2}{R^2}}\left(3R^2+8r^2\right)\mathrm{Erf}\left(\sqrt{2}\frac{r}{R}\right)\right.$$
$$\left.+2\sqrt{\frac{2}{\pi}}GMr\left(9R^6+18R^4r^2+32R^2r^4+32r^6\right)+6R^5r^3e^{\frac{2r^2}{R^2}}\right]. \tag{II.5.1}$$

At $r=0$, we have

$$\mathcal{R}(r=0) = \frac{8\left(6\sqrt{\frac{2}{\pi}}GM-R\right)}{3R^3}, \tag{II.5.2}$$

which shows no divergences. We have also computed the other curvature invariants, $\mathcal{R}_{\mu\nu}\mathcal{R}^{\mu\nu}$, the Kretschmann scalar $\mathcal{R}_{\mu\nu\rho\sigma}\mathcal{R}^{\mu\nu\rho\sigma}$, and the Weyl contraction $C_{\mu\nu\rho\sigma}C^{\mu\nu\rho\sigma} = \mathcal{R}_{\mu\nu\rho\sigma}\mathcal{R}^{\mu\nu\rho\sigma} - 2\mathcal{R}_{\mu\nu}\mathcal{R}^{\mu\nu} + \mathcal{R}^2/3$. The first one reads

$$\begin{aligned}\mathcal{R}_{\mu\nu}\mathcal{R}^{\mu\nu} = {}& \frac{8e^{-\frac{4r^2}{R^2}}}{\pi r^6R^6\left(4r^2+3R^2\right)^4}\\
&\times\left\{8r^2\left[G^2M^2\left(4r^2+3R^2\right)^2\left(64r^8+96r^6R^2+100r^4R^4+36r^2R^6+9R^8\right)\right.\right.\\
&\left.+3\sqrt{2\pi}GMr^2R^5e^{\frac{2r^2}{R^2}}\left(32r^6+48r^4R^2+30r^2R^4+9R^6\right)+9\pi r^4R^{10}e^{\frac{4r^2}{R^2}}\right]\\
&-12GMrR^5e^{\frac{2r^2}{R^2}}\mathrm{Erf}\left(\sqrt{2}\frac{r}{R}\right)\\
&\times\left[\sqrt{2\pi}GM\left(256r^8+480r^6R^2+384r^4R^4+162r^2R^6+27R^8\right)+9\pi r^2R^5e^{\frac{2r^2}{R^2}}\left(4r^2+R^2\right)\right]\\
&\left.+9\pi G^2M^2R^{10}e^{\frac{4r^2}{R^2}}\left(80r^4+48r^2R^2+9R^4\right)\mathrm{Erf}\left(\sqrt{2}\frac{r}{R}\right)^2\right\},\end{aligned} \tag{II.5.3}$$

which, evaluated at $r=0$ gives

$$\mathcal{R}_{\mu\nu}\mathcal{R}^{\mu\nu}|_{r=0} = \frac{64\left(36G^2M^2-6\sqrt{2\pi}GMR+\pi R^2\right)}{9\pi R^6}. \tag{II.5.4}$$

The Kretschmann scalar instead reads

$$\begin{aligned}\mathcal{R}_{\mu\nu\rho\sigma}\mathcal{R}^{\mu\nu\rho\sigma} = &\frac{16e^{-\frac{4r^2}{R^2}}}{\pi r^6 R^6\left(4r^2+3R^2\right)^4}\\ &\Big\{8G^2M^2r^2\left(4r^2+3R^2\right)^2\left(64r^8+160r^6R^2+164r^4R^4+60r^2R^6+9R^8\right)\\ &-96\sqrt{2\pi}GMr^6R^7e^{\frac{2r^2}{R^2}}\left(4r^2+3R^2\right)+108\pi r^6R^{10}e^{\frac{4r^2}{R^2}}-4GMrR^3e^{\frac{2r^2}{R^2}}\,\mathrm{Erf}\left(\sqrt{2}\frac{r}{R}\right)\\ &\times\Big[\sqrt{2\pi}GM\left(512r^{10}+2048r^8R^2+2688r^6R^4+1728r^4R^6+594r^2R^8+81R^{10}\right)\\ &+12\pi r^4R^5e^{\frac{2r^2}{R^2}}\left(3R^2-8r^2\right)\Big]+3\pi G^2M^2R^6e^{\frac{4r^2}{R^2}}\,\mathrm{Erf}\left(\sqrt{2}\frac{r}{R}\right)^2\\ &\times\left(256r^8+256r^6R^2+336r^4R^4+144r^2R^6+27R^8\right)\Big\}\,,\end{aligned}\tag{II.5.5}$$

which at $r=0$ reduces to

$$\mathcal{R}_{\mu\nu\rho\sigma}\mathcal{R}^{\mu\nu\rho\sigma}|_{r=0}=\frac{64\left(72G^2M^2-16\sqrt{2\pi}GMR+3\pi R^2\right)}{9\pi R^6}.\tag{II.5.6}$$

We see that $\mathcal{R}$, $\mathcal{R}_{\mu\nu}\mathcal{R}^{\mu\nu}$ and $\mathcal{R}_{\mu\nu\rho\sigma}\mathcal{R}^{\mu\nu\rho\sigma}$ are all regular at $r=0$. This is a sufficient condition to have also a regular Weyl contraction in this point.

Conclusions

In this thesis we investigated several aspects of black hole physics, with a particular focus on constructing models for black-hole mimickers, solving the singularity problem, modelling the black hole interior, investigating some possible quantum effects producing deformations of the black hole geometries, and characterizing the resulting phenomenology. In doing so, we studied some classes of regular and singular spacetimes, their phenomenology and the physical interpretation of their most important features.

In Part I we investigated two classes of mimickers, namely a set of de Sitter-core regular models and the Konoplya-Rezzolla-Zhidenko black holes. We mainly focused on one-parameter modifications of the Schwarzschild and Kerr metrics, which allow for a simple analytical treatment but, at the same time, enrich the phenomenology. We computed several observed quantities showing that they are and will be testable (position of the light ring, quasinormal mode spectrum, orbits of massive particles, and superradiant scattering).

In Chapter I.2, we developed a class of regular, asymptotically-flat, static, de Sitter-core black holes sourced by an anisotropic fluid with equation of state $p_\parallel = -\rho$. The anisotropicities are here identified as a parameterization of some (still unspecified) quantum effects, whose microscopic dynamics are effectively encoded in the coarse-grained, hydroninamical quantities ρ, $p_\parallel$, $p_\perp$, and the related equation of state. Such a parameterization allowed us to circumvent Penrose's theorems since the fluid does not satisfy the strong energy condition. Our class of black holes depend on a single additional parameter, the quantum hair ℓ, and on a function whose form depend on the functional form of the energy density. The additional hair ℓ is here interpreted as the scale at which quantum effects are important. Under these assumptions, we find that, in general, our class of black holes admits an even number of horizons, although we only considered models with, at most, two horizons. We find that when this parameter is much smaller than the Schwarzschild radius of the object, $R_{\rm S}$, the geometry resembles that of the Schwarzschild black hole, when $\ell \simeq R_{\rm S}$ the configuration has two distinct or coinciding horizons, and when $\ell \gtrsim R_{\rm S}$ the model becomes horizonless. The extremal configuration, i.e., the one with two coinciding horizons is particularly interesting. Indeed, by studying the thermodynamics we found that classical configurations, that is with $\ell \ll R_{\rm S}$, are always thermodynamically less favored than those near extremality, where we quantum effects are visible at the horizon scale. We also studied the motion of particles in this geometry. In particular, we found that the presence of the additional parameter ℓ could largely modify the orbits allowing for tests general relativity. Finally, we studied the quasinormal-mode spectrum in the eikonal limit, finding that, again, the presence of quantum effects can have a strong impact on the ringdown signal which could be, in principle, measured and used to test Einstein's theory against putative alternatives.

In Chapter I.3, we studied in greater detail the semiclassical dynamics (like the black-hole evaporation process) of these regular spacetimes. In order to give a semianalytical treatment of the problem, we chose to work in two spacetime dimensions, with which we expect to capture the main dynamics of the evaporation process but keeping the physical description simple. We first rebuilt the class of models discussed above in the Jackiw-Teitelboim theory, where we find a similar thermodynamic behavior to the four-dimensional case. We then proceed with investigating the evaporation process focusing on the Hayward model, which is included in our general class, both analytically, under the quasistatic approximation, and numerically, where we account for

the backreaction of the geometry. The results of both methods indicate that the final state of the evaporation is an extremal, zero-entropy, regular configuration, and that this is reached in a finite amount of time. Moreover, we built the Page curve, which clearly shows the presence of a maximum followed by a descent representing a clear indication that the information can be recovered in the final part of the evaporation process. Unfortunately, we are not able to reconstruct the full curve because of the breakdown of the semiclassical approximation right after the appearence of the maximum.

Moreover, in Chapter I.4, we tested our class of metrics against the S2-star orbital data, under the hypothesis that Sagittarius A*, the supermassive black hole in our galactic center, is a de Sitter-core regular object. Due to the fact that the typical size of the orbit is much grater than $R_{\rm S}$, we can safely neglect any effect introduced by the spin of the compact object and test the class of models developed in Chapter I.2. Moreover, in order ot obtain the strongest constraint on the quantum parameter ℓ, we chose to work with the Fan-Wang model, which pertains to our general class, and has the property of exhibiting the greatest corrections to Schwarzschild at infinity. We proceeded to study the orbits of massive particles around this geometry, finding that the precession angle decreases proportionally to the quantum parameter ℓ, becomes zero when $\ell = R_{\rm S}/2$ and is negative (retrograde precession) when $\ell > R_{\rm S}/2$. This feature was also verified numerically by directly integrating the geodesic equations. By building a Markov-chain-Monte-Carlo simulation, we have also been able to fit the S2-star data, constraining the quantum parameter to $\ell \lesssim 0.47GM$ at 95% confidence level. This constraint does not exclude thermodynamically favored configurations but rules out most of the horizonless configurations.

This rich field allows for a number of future investigations from both the fundamental and more phenomenological side. From the fundamental side, an important issue is the microscopic origin of the *quantum hair* ℓ parametrizing the deformation of the geometry. In our effective, coarse grained, description this is hidden in the form of the free function ρ, the energy density. However, one would like to fix the form of ρ using microscopic information, for instance in terms of some elementary fields. From the phenomenological side instead, in order to further test our class of regular black-hole models we need a generalization to the rotating case. This generalization has already been done in Ref. [85], but a deeper investigation on the source of the gravitational field, under the light of our interpretation of the additional length scale, is required. Moreover, we believe our effective description of quantum black holes to be sensible to tidal deformations. Indeed, due to the hydrodynamic, coarse-grained nature of our description, we expect the fluid, encoding any putative quantum effect, to be responsive to tidal forces. This property should be sufficiently general for our class of models, and could allow experiments to test our spacetimes against general relativity. Finally, because of the modifications the quantum parameter ℓ introduces on the orbits of test particles, we expect the shadow to be deformed accordingly. This feature could be observed and tested against the Kerr hypothesis once the generalization of our model to the rotating case is completed.

Finally, in Chapter I.5, we studied the imprint of eventual modifications to the Kerr metric on the superradiant scattering of massless and massive particles. The main idea was to investigate in detail the imprint of the modifications introduced in these metrics on the phenomenology. Starting from the Konoplya-Rezzolla-Zhidenko class, we find a subset of geometries that admit both the separation of the angular from the radial part of the perturbation equations. We then focus on a specific example pertaining to this general class, namely the Konoplya-Zhidenko metric, which is a minimal deformation of the Kerr spacetime sharing the same asymptotics and symmetries with its general-relativistic analogous. We begin by studying in detail the structure of such a model, and we find, again that the experimentally accessible quantities are sensible to the introcution of the new parameter, η characterizing the geometry. We then move to the systematic study of the superradiant scattering of scalar and electromagnetic fields on this black-hole model. We found here that the most interesting modifications are introduced when η is small, in which case the superradiant amplification can be larger than in the Kerr case. Moreover, we investigated the suparradiant instability produced by the presence of massive scalar fields under the small-η approximation. This study suggests that these spacetimes are slightly more unstable than the Kerr spacetime. However, this last assessment should be taken with care because of the large number of used assumptions, and a full numerical simulation is required to correctly claim the magnitude of this effect.

In Part II, we tackled the problem of understanding microscopic and quantum systems in the context of general relativity without relying on a specific theory of quantum gravity, although our approach is similar, in its idea, to that of the corpuscular picture of gravitational interactions. To do so, we developed two distinct models: in the first we consider a quantum delocalized source for the gravitational field, whose position is subject to the uncertainty principle; the second, interprets the Bekenstein-Hawking formula as the entropy of a set of oscillators with typical frequencies given by the quasinormal modes of a black hole.

In particular, Chapter II.2 is devoted to the developement of the first model. We started by considering a system composed of a quantum particle in a delocalized state and a classical probe. The particle position is described by a smooth function of the radial coordinate peaked around the classical position at $r = 0$ and with uncertainty radius R. With this setup, we were able to compute the expectation value of the Newtonian potential, and by covariantly uplifting this quantity we recontructed the metric functions, which depend on the probability density describing the position state of the source. We showed also that the L^2-integrability of the proability density and of the smoothness of its derivative guarantee asymptotic flatness and regularity at the core, respectively. This approach is very similar to a well-known approximation, namely the Newton-Schrödinger formalism, although we do not consider here the dynamics of the quantum particle. However, since this approach leaves the angular part of the metric undetermined, we also adopted a "more covariant" approach in which also the metric is an operator that depends on the positions of the particle and the probe. With this method, we obtain that the radius of the two sphere does not shrink to zero for $r \to 0$ and our spacetime represents a wormhole. As a simple realization of this model, we consider a system where the probability density is given by a Gaussian distribution, and we studied some of its phenomenological features. We found that this model behaves similarly to the general class discussed in Chapter I.2, both from a thermodynamical and a geometrical point of view. In this case, when the quantum scale R, playing the same role as ℓ, is much smaller than the classical gravitational radius $R_{\rm S}$, the configuration behaves as a Schwarzschild black hole, when $R \simeq R_{\rm S}$ it becomes extremal with a single horizon at $r = 0$ and when $R \gtrsim R_{\rm S}$ the model corresponds to a horizonless compact objects. Again, the thermodynamical properties indicate that objects with $R \simeq R_{\rm S}$ are favored with respect to their classical counterparts with $R \ll R_{\rm S}$. We also studied orbits and quasinormal modes of this spacetime, finding results similar to the one in Chapter I.2. An interesting follow-up of this work would be, again, to generalize this method to the rotating case, both through the Janis-Newmann algorithm and by directly applying our formalism to generate an axially-symmetric spacetime, maybe showing some dependence on the spin of the particle. We also hope to be able to test our metric or its rotating version with current or future experimental data in order to put some constraint on the strenght of quantum effects. The weakness of our approach is the lack of knowledge about the dynamics, needed to determine the wave function of the delocalized source. This point deserves further investigations.

In Chapters II.3 and II.4 we discussed the possibility of recovering the Bekenstein-Hawking formula as the entropy of a set of oscillators with frequencies given by the quasinormal modes of the system. Indeed, motivated by Maggiore's idea [69], we started in the former from the Schwarzschild black hole as a canonical ensemble of N oscillators. The statistical weight of each state is given by the Boltzmann factor $\mathrm{e}^{-\omega_n/T}$. Here we assumed the possibility, at quantum level, that the temperature and the mass could oscillate independently around their classical values, though any observer at infinity should see these fluctuations averaged to their classical values. Moreover, in the approximation in which the black-hole mass is large compared to the typical thermal energy, we see that the negligible modes correspond to those with large overtone number, whose approximate expression is analytical. We are then able to compute both the internal energy of the system and its entropy. The former can be identified with the classical mass of the system and gives a holographic scaling of the number of oscillators, while the latter, at first order in the large mass expansion, gives the Bekenstein-Hawking entropy of the black hole and a subdominant logarithmic correction. Notice that the holographic scaling can be perfectly understood in a corpuscular perspective, in which the black hole is identified with a condensate of soft gravitons.

This same idea was used in Chapter II.4, but instead of working with the Schwarzschild spacetime we decided to test this hypothesis with 2D anti-de Sitter black holes. There are two main reasons to choose the simplified 2D environment in this case. First, in the Jackiw-Teitelboim theory we are able to compute analytically the full spectrum of the quasinormal modes and,

therefore, we can compute the entropy without the need of further approxiamtions. Second, two-dimensional black holes are good proxies for the near-extremal and near-horizon geometries of several 4D black holes, reason why we expect these results to be applicable to other cases as well. We proceeded by using the same formalism as in Chapter II.3, this time without expanding for large masses, and found very similar results. Moreover, investigated deeply the connection between the harmonic oscillators and the quasinormal modes of anti-de Sitter 2D black holes by considering at the conformal quantum mechanics at the boundary. In this case, we observed that the equations describing the spectra of the perturbations of these objects correspond to the de Alfaro-Fubini-Furlan formalism, which is a conformally invariant generalization of the harmonic oscillator in quantum mechanics.

Bibliography

[1] M. Cadoni, M. Oi, and A. P. Sanna. "Effective models of nonsingular quantum black holes". *Phys. Rev. D* **106**.2 (2022), 024030. arXiv: 2204.09444 [gr-qc] (cit. on pp. v, 2, 3, 5, 7, 8, 37, 38, 41, 43, 45, 65, 106, 108, 115, 117, 120).

[2] M. Cadoni, M. Oi, and A. P. Sanna. "Evaporation and information puzzle for 2D nonsingular asymptotically flat black holes". *JHEP* **06** (2023), 211. arXiv: 2303.05557 [hep-th] (cit. on pp. v, 5, 7, 20, 106).

[3] M. Cadoni, M. De Laurentis, I. De Martino, R. Della Monica, M. Oi, and A. P. Sanna. "Are nonsingular black holes with super-Planckian hair ruled out by S2 star data?" *Phys. Rev. D* **107**.4 (2023), 044038. arXiv: 2211.11585 [gr-qc] (cit. on pp. v, 5, 7, 37, 38).

[4] E. Franzin, S. Liberati, and M. Oi. "Superradiance in Kerr-like black holes". *Phys. Rev. D* **103**.10 (2021), 104034. arXiv: 2102.03152 [gr-qc] (cit. on pp. v, 5).

[5] A. Akil, M. Cadoni, L. Modesto, M. Oi, and A. P. Sanna. "Semiclassical spacetimes at super-Planckian scales from delocalized sources". *Phys. Rev. D* **108**.4 (2023), 044051. arXiv: 2211.01657 [gr-qc] (cit. on pp. v, 2, 18, 49, 64, 103, 106).

[6] M. Cadoni, M. Oi, and A. P. Sanna. "Quasinormal modes and microscopic structure of the Schwarzschild black hole". *Phys. Rev. D* **104**.12 (2021), L121502. arXiv: 2109.10744 [gr-qc] (cit. on pp. v, 2, 8, 11, 19, 37, 103, 136, 140, 142, 143).

[7] M. Cadoni, M. Oi, and A. P. Sanna. "Quasi-normal modes and microscopic description of 2D black holes". *JHEP* **01** (2022), 087. arXiv: 2111.07763 [gr-qc] (cit. on pp. v, 12, 19, 27, 103).

[8] D. Brundu, M. Cadoni, M. Oi, P. Olla, and A. P. Sanna. "Atmospheric Newtonian noise modeling for third-generation gravitational wave detectors". *Phys. Rev. D* **106**.6 (2022), 064040. arXiv: 2206.02610 [gr-qc] (cit. on p. v).

[9] K. Schwarzschild. "On the gravitational field of a mass point according to Einstein's theory". *Sitzungsber. Preuss. Akad. Wiss. Berlin (Math. Phys.)* **1916** (1916), 189–196. arXiv: physics/9905030 (cit. on p. 1).

[10] R. P. Kerr. "Gravitational field of a spinning mass as an example of algebraically special metrics". *Phys. Rev. Lett.* **11** (1963), 237–238 (cit. on p. 1).

[11] C. M. Will. "The Confrontation between General Relativity and Experiment". *Living Rev. Relativ.* **17** (2014), 4. arXiv: 1403.7377 [gr-qc] (cit. on pp. 1, 3, 75).

[12] C. Bambi. "Testing the Kerr black hole hypothesis". *Mod. Phys. Lett. A* **26** (2011), 2453–2468. arXiv: 1109.4256 [gr-qc] (cit. on pp. 1, 65).

[13] Event Horizon Telescope Collaboration. "Gravitational Test Beyond the First Post-Newtonian Order with the Shadow of the M87 Black Hole". *Phys. Rev. Lett.* **125**.14 (2020), 141104. arXiv: 2010.01055 [gr-qc] (cit. on pp. 1, 65, 107).

[14] P. Kocherlakota et al., Event Horizon Telescope collaboration. "Constraints on black-hole charges with the 2017 EHT observations of M87*". *Phys. Rev. D* **103**.10 (2021), 104047. arXiv: 2105.09343 [gr-qc] (cit. on p. 1).

[15] K. Akiyama et al., Event Horizon Telescope collaboration. "First Sagittarius A* Event Horizon Telescope Results. VI. Testing the Black Hole Metric". *Astrophys. J. Lett.* **930**.2 (2022), L17 (cit. on pp. 1, 65, 66).

[16] B. P. Abbott et al., LIGO Scientific, Virgo collaboration. "Observation of Gravitational Waves from a Binary Black Hole Merger". *Phys. Rev. Lett.* **116**.6 (2016), 061102. arXiv: 1602.03837 [gr-qc] (cit. on pp. 1, 37, 65).

[17] B. P. Abbott et al., LIGO Scientific, Virgo collaboration. "Tests of general relativity with GW150914". *Phys. Rev. Lett.* **116**.22 (2016). [Erratum: Phys. Rev. Lett. **121**, 129902 (2018)], 221101. arXiv: 1602.03841 [gr-qc] (cit. on p. 1).

[18] R. Abbott et al., LIGO Scientific, VIRGO, KAGRA collaboration. "Tests of General Relativity with GWTC-3". (2021). arXiv: 2112.06861 [gr-qc] (cit. on pp. 1, 66).

[19] S. Perlmutter et al., Supernova Cosmology Project collaboration. "Measurements of Ω and Λ from 42 high redshift supernovae". *Astrophys. J.* **517** (1999), 565–586. arXiv: astro-ph/9812133 (cit. on p. 1).

[20] A. G. Riess et al., Supernova Search Team collaboration. "Observational evidence from supernovae for an accelerating universe and a cosmological constant". *Astron. J.* **116** (1998), 1009–1038. arXiv: astro-ph/9805201 (cit. on p. 1).

[21] P. J. E. Peebles and B. Ratra. "The Cosmological Constant and Dark Energy". *Rev. Mod. Phys.* **75** (2003). Ed. by J.-P. Hsu and D. Fine, 559–606. arXiv: astro-ph/0207347 (cit. on p. 1).

[22] I. Antoniadis, J. Rizos, and K. Tamvakis. "Singularity - free cosmological solutions of the superstring effective action". *Nucl. Phys. B* **415** (1994), 497–514. arXiv: hep-th/9305025 (cit. on p. 1).

[23] S. Nojiri and S. D. Odintsov. "Gravity assisted dark energy dominance and cosmic acceleration". *Phys. Lett. B* **599** (2004), 137–142. arXiv: astro-ph/0403622 (cit. on p. 1).

[24] S. Nojiri and S. D. Odintsov. "Introduction to modified gravity and gravitational alternative for dark energy". *eConf* **C0602061** (2006). Ed. by A. Borowiec, 06. arXiv: hep-th/0601213 (cit. on p. 1).

[25] T. Clifton, P. G. Ferreira, A. Padilla, and C. Skordis. "Modified Gravity and Cosmology". *Phys. Rept.* **513** (2012), 1–189. arXiv: 1106.2476 [astro-ph.CO] (cit. on p. 1).

[26] P. O. Mazur. "Black hole uniqueness theorems". (2000). arXiv: hep-th/0101012 (cit. on p. 1).

[27] A. O. Barvinsky. "Quantum Effective Action in Spacetimes with Branes and Boundaries: Diffeomorphism Invariance". *Phys. Rev. D* **74** (2006), 084033. arXiv: hep-th/0608004 (cit. on pp. 2, 105).

[28] G. T. Horowitz. "Spacetime in string theory". *New J. Phys.* **7** (2005), 201. arXiv: gr-qc/0410049 (cit. on pp. 2, 105).

[29] E. Witten. "Comments on string theory". *Challenges to the Standard Paradigm: Fundamental Physics and Cosmology*. 2002. arXiv: hep-th/0212247 (cit. on pp. 2, 105).

[30] J. M. Maldacena. "The Large N limit of superconformal field theories and supergravity". *Adv. Theor. Math. Phys.* **2** (1998), 231–252. arXiv: hep-th/9711200 (cit. on p. 2).

[31] E. Witten. "Anti-de Sitter space and holography". *Adv. Theor. Math. Phys.* **2** (1998), 253–291. arXiv: hep-th/9802150 (cit. on p. 2).

[32] S. S. Gubser, I. R. Klebanov, and A. M. Polyakov. "Gauge theory correlators from noncritical string theory". *Phys. Lett. B* **428** (1998), 105–114. arXiv: hep-th/9802109 (cit. on p. 2).

[33] A. Ashtekar and E. Bianchi. "A short review of loop quantum gravity". *Rept. Prog. Phys.* **84**.4 (2021), 042001. arXiv: 2104.04394 [gr-qc] (cit. on pp. 2, 105).

[34] C. Rovelli. "Loop quantum gravity". *Living Rev. Rel.* **1** (1998), 1. arXiv: gr-qc/9710008 (cit. on pp. 2, 105).

[35] G. Dvali and C. Gomez. "Black Hole's Quantum N-Portrait". *Fortsch. Phys.* **61** (2013), 742–767. arXiv: 1112.3359 [hep-th] (cit. on pp. 2, 8, 11, 19, 37, 105, 131, 134, 135, 140, 142).

[36] G. Dvali and C. Gomez. "Quantum Compositeness of Gravity: Black Holes, AdS and Inflation". *JCAP* **01** (2014), 023. arXiv: 1312.4795 [hep-th] (cit. on pp. 2, 8, 11, 19, 105, 131, 135, 140).

[37] R. Casadio, A. Giugno, O. Micu, and A. Orlandi. "Thermal BEC black holes". *Entropy* **17** (2015), 6893–6924. arXiv: 1511.01279 [gr-qc] (cit. on pp. 2, 8, 11, 19, 105, 131, 140).

[38] R. Casadio, A. Giugno, and A. Giusti. "Matter and gravitons in the gravitational collapse". *Phys. Lett. B* **763** (2016), 337–340. arXiv: 1606.04744 [hep-th] (cit. on pp. 2, 8, 11, 19, 105, 131, 140).

[39] M. Cadoni, M. Tuveri, and A. P. Sanna. "Long-Range Quantum Gravity". *Symmetry* **12**.9 (2020), 1396. arXiv: 2006.16652 [gr-qc] (cit. on pp. 2, 8, 11, 19, 105, 107, 131, 132, 135, 140).

[40] R. Casadio. "A quantum bound on the compactness". *Eur. Phys. J. C* **82**.1 (2022), 10. arXiv: 2103.14582 [gr-qc] (cit. on pp. 2, 105, 131, 140).

[41] S. W. Hawking. "Particle Creation by Black Holes". *Commun. Math. Phys.* **43** (1975). Ed. by G. W. Gibbons and S. W. Hawking. [Erratum: Commun.Math.Phys. 46, 206 (1976)], 199–220 (cit. on pp. 2, 8, 11, 105, 122).

[42] S. W. Hawking. "Breakdown of Predictability in Gravitational Collapse". *Phys. Rev. D* **14** (1976), 2460–2473 (cit. on pp. 2, 8, 12, 22, 37).

[43] D. N. Page. "Information in black hole radiation". *Phys. Rev. Lett.* **71** (1993), 3743–3746. arXiv: hep-th/9306083 (cit. on pp. 2, 8, 12, 22, 37, 38).

[44] G. Amelino-Camelia. "Quantum gravity phenomenology". (2003). arXiv: physics/0311037 (cit. on pp. 2, 105).

[45] S. Hossenfelder, M. Bleicher, S. Hofmann, J. Ruppert, S. Scherer, and H. Stoecker. "Collider signatures in the Planck regime". *Phys. Lett. B* **575** (2003), 85–99. arXiv: hep-th/0305262 (cit. on pp. 2, 105).

[46] E. A. Mirabelli, M. Perelstein, and M. E. Peskin. "Collider signatures of new large space dimensions". *Phys. Rev. Lett.* **82** (1999), 2236–2239. arXiv: hep-ph/9811337 (cit. on pp. 2, 105).

[47] R. J. Adler and D. I. Santiago. "On gravity and the uncertainty principle". *Mod. Phys. Lett. A* **14** (1999), 1371. arXiv: gr-qc/9904026 (cit. on pp. 2, 105, 106).

[48] F. Scardigli. "Generalized uncertainty principle in quantum gravity from micro - black hole Gedanken experiment". *Phys. Lett. B* **452** (1999), 39–44. arXiv: hep-th/9904025 (cit. on pp. 2, 105, 106).

[49] B. Bolen and M. Cavaglia. "(Anti-)de Sitter black hole thermodynamics and the generalized uncertainty principle". *Gen. Rel. Grav.* **37** (2005), 1255–1262. arXiv: gr-qc/0411086 (cit. on pp. 2, 105, 106).

[50] M.-i. Park. "The Generalized Uncertainty Principle in (A)dS Space and the Modification of Hawking Temperature from the Minimal Length". *Phys. Lett. B* **659** (2008), 698–702. arXiv: 0709.2307 [hep-th] (cit. on pp. 2, 105, 106).

[51] V. Cardoso, E. Franzin, and P. Pani. "Is the gravitational-wave ringdown a probe of the event horizon?" *Phys. Rev. Lett.* **116**.17 (2016). [Erratum: Phys. Rev. Lett. **117**, 089902 (2016)], 171101. arXiv: 1602.07309 [gr-qc] (cit. on pp. 2, 7, 75, 105, 108, 128, 147).

[52] G. Calcagni, S. Kuroyanagi, S. Marsat, M. Sakellariadou, N. Tamanini, and G. Tasinato. "Quantum gravity and gravitational-wave astronomy". *JCAP* **10** (2019), 012. arXiv: 1907.02489 [gr-qc] (cit. on pp. 2, 105).

[53] A. Almheiri, D. Marolf, J. Polchinski, and J. Sully. "Black Holes: Complementarity or Firewalls?" *JHEP* **02** (2013), 062. arXiv: 1207.3123 [hep-th] (cit. on pp. 2, 8, 11).

[54] G. Penington, S. H. Shenker, D. Stanford, and Z. Yang. "Replica wormholes and the black hole interior". *JHEP* **03** (2022), 205. arXiv: 1911.11977 [hep-th] (cit. on pp. 2, 8, 22, 37, 61, 63, 136).

[55] A. Almheiri, T. Hartman, J. Maldacena, E. Shaghoulian, and A. Tajdini. "Replica Wormholes and the Entropy of Hawking Radiation". *JHEP* **05** (2020), 013. arXiv: 1911.12333 [hep-th] (cit. on pp. 2, 8, 12, 22, 37, 61, 63, 136).

[56] A. Almheiri, T. Hartman, J. Maldacena, E. Shaghoulian, and A. Tajdini. "The entropy of Hawking radiation". *Rev. Mod. Phys.* **93**.3 (2021), 035002. arXiv: 2006.06872 [hep-th] (cit. on pp. 2, 8, 37, 63).

[57] R. Bousso, X. Dong, N. Engelhardt, T. Faulkner, T. Hartman, S. H. Shenker, and D. Stanford. "Snowmass White Paper: Quantum Aspects of Black Holes and the Emergence of Spacetime". (2022). arXiv: 2201.03096 [hep-th] (cit. on pp. 2, 8).

[58] S. B. Giddings. "Nonviolent nonlocality". *Phys. Rev. D* **88** (2013), 064023. arXiv: 1211.7070 [hep-th] (cit. on pp. 2, 8).

[59] S. B. Giddings. "A 'black hole theorem,' and its implications". *Class. Quant. Grav.* **40**.8 (2023), 085002. arXiv: 2110.10690 [hep-th] (cit. on pp. 2, 8).

[60] S. B. Giddings. "The deepest problem: some perspectives on quantum gravity". (2022). arXiv: 2202.08292 [hep-th] (cit. on pp. 2, 8).

[61] S. D. Mathur. "The Fuzzball proposal for black holes: An Elementary review". *Fortsch. Phys.* **53** (2005). Ed. by E. Kiritsis, 793–827. arXiv: hep-th/0502050 (cit. on pp. 2, 8, 19, 65, 133, 135).

[62] S. D. Mathur. "The nature of the gravitational vacuum". *Int. J. Mod. Phys. D* **28**.14 (2019), 1944005. arXiv: 1905.12004 [hep-th] (cit. on pp. 2, 8, 19, 135).

[63] S. D. Mathur. "The VECRO hypothesis". (2020). arXiv: 2001.11057 [hep-th] (cit. on pp. 2, 8, 19, 135).

[64] E. P. Verlinde. "Emergent Gravity and the Dark Universe". *SciPost Phys.* **2**.3 (2017), 016. arXiv: 1611.02269 [hep-th] (cit. on pp. 2, 8, 11, 13, 14, 18, 19, 23, 106, 107, 135).

[65] G. Dvali. "Entropy Bound and Unitarity of Scattering Amplitudes". *JHEP* **03** (2021), 126. arXiv: 2003.05546 [hep-th] (cit. on pp. 2, 8, 11, 19, 106, 134, 135, 142).

[66] G. Dvali and C. Gomez. "Self-Completeness of Einstein Gravity". (2010). arXiv: 1005.3497 [hep-th] (cit. on pp. 2, 8, 131, 142).

[67] G. Dvali, G. F. Giudice, C. Gomez, and A. Kehagias. "UV-Completion by Classicalization". *JHEP* **08** (2011), 108. arXiv: 1010.1415 [hep-ph] (cit. on pp. 2, 8, 131, 135, 142).

[68] G. Dvali, C. Gomez, and A. Kehagias. "Classicalization of Gravitons and Goldstones". *JHEP* **11** (2011), 070. arXiv: 1103.5963 [hep-th] (cit. on pp. 2, 8, 131, 135).

[69] M. Maggiore. "The Physical interpretation of the spectrum of black hole quasinormal modes". *Phys. Rev. Lett.* **100** (2008), 141301. arXiv: 0711.3145 [gr-qc] (cit. on pp. 2, 4, 8, 11, 19, 132, 136, 140, 141, 147, 153).

[70] M. Cadoni, R. Casadio, A. Giusti, and M. Tuveri. "Emergence of a Dark Force in Corpuscular Gravity". *Phys. Rev. D* **97**.4 (2018), 044047. arXiv: 1801.10374 [gr-qc] (cit. on pp. 2, 13, 18, 107, 140).

[71] M. Cadoni, R. Casadio, A. Giusti, W. Mück, and M. Tuveri. "Effective Fluid Description of the Dark Universe". *Phys. Lett. B* **776** (2018), 242–248. arXiv: 1707.09945 [gr-qc] (cit. on pp. 2, 8, 13, 14, 18, 106, 107, 108, 117, 135, 140).

[72] M. Tuveri and M. Cadoni. "Galactic dynamics and long-range quantum gravity". *Phys. Rev. D* **100**.2 (2019), 024029. arXiv: 1904.11835 [gr-qc] (cit. on pp. 2, 13, 14, 17, 18, 106, 107, 117, 135, 140, 141).

[73] M. Cadoni, A. P. Sanna, and M. Tuveri. "Anisotropic fluid cosmology: An alternative to dark matter?" *Phys. Rev. D* **102**.2 (2020), 023514. arXiv: 2002.06988 [gr-qc] (cit. on pp. 2, 8, 13, 14, 108, 117).

[74] M. Cadoni and A. P. Sanna. "Emergence of a cosmological constant in anisotropic fluid cosmology". *Int. J. Mod. Phys. A* **36**.21 (2021), 2150156. arXiv: 2012.08335 [gr-qc] (cit. on pp. 2, 8, 13, 14).

[75] M. Cadoni and A. P. Sanna. "Unified description of galactic dynamics and the cosmological constant". *Class. Quant. Grav.* **38**.13 (2021), 135004. arXiv: 2101.07642 [gr-qc] (cit. on pp. 2, 8, 13, 14, 108, 117).

[76] V. Cardoso and P. Pani. "Testing the nature of dark compact objects: a status report". *Living Rev. Relativ.* **22**.1 (2019), 4. arXiv: 1904.05363 [gr-qc] (cit. on pp. 2, 7).

[77] G. Raposo, P. Pani, M. Bezares, C. Palenzuela, and V. Cardoso. "Anisotropic stars as ultracompact objects in General Relativity". *Phys. Rev. D* **99**.10 (2019), 104072. arXiv: 1811.07917 [gr-qc] (cit. on pp. 2, 8, 14, 108, 117).

[78] K. Dev and M. Gleiser. "Anisotropic stars: Exact solutions". *Gen. Rel. Grav.* **34** (2002), 1793–1818. arXiv: astro-ph/0012265 (cit. on p. 2).

[79] S. L. Liebling and C. Palenzuela. "Dynamical boson stars". *Living Rev. Rel.* **26**.1 (2023), 1. arXiv: 1202.5809 [gr-qc] (cit. on p. 2).

[80] C. F. B. Macedo, P. Pani, V. Cardoso, and L. C. B. Crispino. "Astrophysical signatures of boson stars: quasinormal modes and inspiral resonances". *Phys. Rev. D* **88**.6 (2013), 064046. arXiv: 1307.4812 [gr-qc] (cit. on p. 2).

[81] P. O. Mazur and E. Mottola. "Gravitational vacuum condensate stars". *Proc. Nat. Acad. Sci.* **101** (2004), 9545–9550. arXiv: gr-qc/0407075 (cit. on p. 2).

[82] M. S. Morris and K. S. Thorne. "Wormholes in space-time and their use for interstellar travel: A tool for teaching general relativity". *Am. J. Phys.* **56** (1988), 395–412 (cit. on pp. 2, 108, 115, 117, 118, 119).

[83] C. Bambi. *Regular Black Holes*. Springer Series in Astrophysics and Cosmology. Springer Singapore, 2023. arXiv: 2307.13249 [gr-qc] (cit. on p. 2).

[84] S. A. Hayward. "Formation and evaporation of regular black holes". *Phys. Rev. Lett.* **96** (2006), 031103. arXiv: gr-qc/0506126 (cit. on pp. 2, 7, 8, 14, 18, 27, 37, 38, 41, 42, 65, 92, 115, 117).

[85] I. Dymnikova. "Regular Rotating Black Holes and Solitons with the de Sitter/Phantom Interiors". (2023) (cit. on pp. 2, 152).

[86] R. Penrose. "Gravitational collapse: The role of general relativity". *Riv. Nuovo Cim.* **1** (1969), 252–276 (cit. on pp. 2, 7, 11, 107).

[87] S. W. Hawking and R. Penrose. "The Singularities of gravitational collapse and cosmology". *Proc. Roy. Soc. Lond. A* **314** (1970), 529–548 (cit. on pp. 2, 7, 11, 37, 65, 107).

[88] N. Franchini and S. H. Völkel. "Parametrized quasinormal mode framework for non-Schwarzschild metrics". *Phys. Rev. D* **107**.12 (2023), 124063. arXiv: 2210.14020 [gr-qc] (cit. on p. 3).

[89] V. Cardoso, M. Kimura, A. Maselli, E. Berti, C. F. B. Macedo, and R. McManus. "Parametrized black hole quasinormal ringdown: Decoupled equations for nonrotating black holes". *Phys. Rev. D* **99**.10 (2019), 104077. arXiv: 1901.01265 [gr-qc] (cit. on p. 3).

[90] T. Johannsen and D. Psaltis. "A Metric for Rapidly Spinning Black Holes Suitable for Strong-Field Tests of the No-Hair Theorem". *Phys. Rev. D* **83** (2011), 124015. arXiv: 1105.3191 [gr-qc] (cit. on pp. 3, 8, 65, 75).

[91] L. Rezzolla and A. Zhidenko. "New parametrization for spherically symmetric black holes in metric theories of gravity". *Phys. Rev. D* **90**.8 (2014), 084009. arXiv: 1407.3086 [gr-qc] (cit. on pp. 3, 8, 75, 90).

[92] R. Konoplya, L. Rezzolla, and A. Zhidenko. "General parametrization of axisymmetric black holes in metric theories of gravity". *Phys. Rev. D* **93**.6 (2016), 064015. arXiv: 1602.02378 [gr-qc] (cit. on pp. 3, 8, 65, 75, 90).

[93] R. Jackiw. "Lower Dimensional Gravity". *Nucl. Phys. B* **252** (1985). Ed. by R. Baier and H. Satz, 343–356 (cit. on pp. 3, 22, 136).

[94] C. Teitelboim. "Gravitation and Hamiltonian Structure in Two Space-Time Dimensions". *Phys. Lett. B* **126** (1983), 41–45 (cit. on pp. 3, 22, 136).

[95] T. G. Mertens and G. J. Turiaci. "Solvable models of quantum black holes: a review on Jackiw–Teitelboim gravity". *Living Rev. Rel.* **26**.1 (2023), 4. arXiv: 2210.10846 [hep-th] (cit. on p. 3).

[96] A. Kitaev and S. J. Suh. "The soft mode in the Sachdev-Ye-Kitaev model and its gravity dual". *JHEP* **05** (2018), 183. arXiv: 1711.08467 [hep-th] (cit. on pp. 3, 12, 22, 136).

[97] J. Maldacena and D. Stanford. "Remarks on the Sachdev-Ye-Kitaev model". *Phys. Rev. D* **94**.10 (2016), 106002. arXiv: 1604.07818 [hep-th] (cit. on p. 3).

[98] Y. B. Zel'dovic. "The Fate of a Star and the Evolution of Gravitational Energy Upon Accretion". *Sov. Phys. Dokl.* **9** (1964), 195 (cit. on p. 7).

[99] E. E. Salpeter. "Accretion of Interstellar Matter by Massive Objects". *Astrophys. J.* **140** (1964), 796–800 (cit. on p. 7).

[100] C. T. Bolton. "Identification of Cygnus X-1 with HDE 226868". *Nature* **235**.5336 (1972), 271–273 (cit. on p. 7).

[101] B. L. Webster and P. Murdin. "Cygnus X-1-a Spectroscopic Binary with a Heavy Companion ?" *Nature* **235** (1972), 37–38 (cit. on p. 7).

[102] R. Genzel, F. Eisenhauer, and S. Gillessen. "The Galactic Center Massive Black Hole and Nuclear Star Cluster". *Rev. Mod. Phys.* **82** (2010), 3121–3195. arXiv: 1006.0064 [astro-ph.GA] (cit. on p. 7).

[103] B. P. Abbott et al., LIGO Scientific, Virgo collaboration. "Observation of Gravitational Waves from a Binary Black Hole Merger". *Phys. Rev. Lett.* **116**.6 (2016), 061102. arXiv: 1602.03837 [gr-qc] (cit. on p. 7).

[104] K. Akiyama et al., Event Horizon Telescope collaboration. "First M87 Event Horizon Telescope Results. I. The Shadow of the Supermassive Black Hole". *Astrophys. J.* **875**.1 (2019), L1. arXiv: 1906.11238 [astro-ph.GA] (cit. on p. 7).

[105] C. Bambi. "Testing black hole candidates with electromagnetic radiation". *Rev. Mod. Phys.* **89**.2 (2017), 025001. arXiv: 1509.03884 [gr-qc] (cit. on pp. 7, 66).

[106] A. Celotti, J. C. Miller, and D. W. Sciama. "Astrophysical evidence for the existence of black holes". *Class. Quantum Grav.* **16** (1999), A3. arXiv: astro-ph/9912186 (cit. on p. 7).

[107] M. Visser. "Physical observability of horizons". *Phys. Rev. D* **90**.12 (2014), 127502. arXiv: 1407.7295 [gr-qc] (cit. on p. 7).

[108] M. A. Abramowicz, T. Bulik, G. F. R. Ellis, K. A. Meissner, and M. Wielgus. "The electromagnetic afterglows of gravitational waves as a test for Quantum Gravity". (2016). arXiv: 1603.07830 [gr-qc] (cit. on p. 7).

[109] E. W. Mielke and F. E. Schunck. "Boson stars: Alternatives to primordial black holes?" *Nucl. Phys. B* **564** (2000), 185–203. arXiv: gr-qc/0001061 (cit. on p. 7).

[110] M. Visser. *Lorentzian wormholes: From Einstein to Hawking*. 1995 (cit. on pp. 7, 117, 118, 119).

[111] P. O. Mazur and E. Mottola. "Gravitational Condensate Stars: An Alternative to Black Holes". *Universe* **9**.2 (2023), 88. arXiv: gr-qc/0109035 (cit. on p. 7).

[112] O. B. Zaslavskii. "Regular black holes and energy conditions". *Phys. Lett. B* **688** (2010), 278–280. arXiv: 1004.2362 [gr-qc] (cit. on p. 7).

[113] V. Cardoso, E. Franzin, A. Maselli, P. Pani, and G. Raposo. "Testing strong-field gravity with tidal Love numbers". *Phys. Rev. D* **95**.8 (2017). [Addendum: Phys.Rev.D 95, 089901 (2017)], 084014. arXiv: 1701.01116 [gr-qc] (cit. on p. 7).

[114] R. Penrose. "Gravitational collapse and space-time singularities". *Phys. Rev. Lett.* **14** (1965), 57–59 (cit. on pp. 7, 11, 37, 65, 91, 107).

[115] R. Carballo-Rubio, F. Di Filippo, S. Liberati, and M. Visser. "Phenomenological aspects of black holes beyond general relativity". *Phys. Rev. D* **98**.12 (2018), 124009. arXiv: 1809.08238 [gr-qc] (cit. on pp. 7, 11).

[116] R. Carballo-Rubio, F. Di Filippo, S. Liberati, and M. Visser. "Geodesically complete black holes". *Phys. Rev. D* **101** (2020), 084047. arXiv: 1911.11200 [gr-qc] (cit. on pp. 7, 11, 111, 115).

[117] H. Maeda. "Quest for realistic non-singular black-hole geometries: regular-center type". *JHEP* **11** (2022), 108. arXiv: 2107.04791 [gr-qc] (cit. on pp. 7, 11).

[118] A. Simpson and M. Visser. "Regular black holes with asymptotically Minkowski cores". *Universe* **6**.1 (2019), 8. arXiv: 1911.01020 [gr-qc] (cit. on pp. 7, 8, 11, 14, 16, 18, 65, 108, 115, 117).

[119] F. S. N. Lobo, M. E. Rodrigues, M. V. de Sousa Silva, A. Simpson, and M. Visser. "Novel black-bounce spacetimes: wormholes, regularity, energy conditions, and causal structure". *Phys. Rev. D* **103**.8 (2021), 084052. arXiv: 2009.12057 [gr-qc] (cit. on pp. 7, 11, 64, 117).

[120] J. Mazza, E. Franzin, and S. Liberati. "A novel family of rotating black hole mimickers". *JCAP* **04** (2021), 082. arXiv: 2102.01105 [gr-qc] (cit. on pp. 7, 11, 65).

[121] E. Franzin, S. Liberati, J. Mazza, A. Simpson, and M. Visser. "Charged black-bounce spacetimes". *JCAP* **07** (2021), 036. arXiv: 2104.11376 [gr-qc] (cit. on pp. 7, 8, 11, 14).

[122] E. Ayon-Beato and A. Garcia. "Nonsingular charged black hole solution for nonlinear source". *Gen. Rel. Grav.* **31** (1999), 629–633. arXiv: gr-qc/9911084 (cit. on pp. 7, 11).

[123] K. A. Bronnikov. "Regular magnetic black holes and monopoles from nonlinear electrodynamics". *Phys. Rev. D* **63** (2001), 044005. arXiv: gr-qc/0006014 (cit. on pp. 7, 11).

[124] I. Dymnikova. "Regular electrically charged structures in nonlinear electrodynamics coupled to general relativity". *Class. Quant. Grav.* **21** (2004), 4417–4429. arXiv: gr-qc/0407072 (cit. on pp. 7, 11).

[125] H. Culetu. "On a regular charged black hole with a nonlinear electric source". *Int. J. Theor. Phys.* **54**.8 (2015), 2855–2863. arXiv: 1408.3334 [gr-qc] (cit. on pp. 7, 11).

[126] I. Banerjee. "Signatures of regular black holes from the quasar continuum spectrum". *Eur. Phys. J. C* **83**.2 (2023), 171. arXiv: 2206.06899 [gr-qc] (cit. on pp. 7, 11).

[127] A. Bokulić, I. Smolić, and T. Jurić. "Constraints on singularity resolution by nonlinear electrodynamics". *Phys. Rev. D* **106**.6 (2022), 064020. arXiv: 2206.07064 [gr-qc] (cit. on pp. 7, 11).

[128] A. A. Tseytlin. "On singularities of spherically symmetric backgrounds in string theory". *Phys. Lett. B* **363** (1995), 223–229. arXiv: hep-th/9509050 (cit. on pp. 8, 11).

[129] A. E. Lawrence and E. J. Martinec. "String field theory in curved space-time and the resolution of space - like singularities". *Class. Quant. Grav.* **13** (1996), 63–96. arXiv: hep-th/9509149 (cit. on pp. 8, 11).

[130] G. T. Horowitz and A. R. Steif. "Space-Time Singularities in String Theory". *Phys. Rev. Lett.* **64** (1990), 260 (cit. on pp. 8, 11).

[131] L. Modesto. "Disappearance of black hole singularity in quantum gravity". *Phys. Rev. D* **70** (2004), 124009. arXiv: gr-qc/0407097 (cit. on pp. 8, 11, 19, 32).

[132] P. Nicolini, A. Smailagic, and E. Spallucci. "Noncommutative geometry inspired Schwarzschild black hole". *Phys. Lett. B* **632** (2006), 547–551. arXiv: gr-qc/0510112 (cit. on pp. 8, 11, 14, 19, 30, 32, 115, 117).

[133] L. Modesto. "Semiclassical loop quantum black hole". *Int. J. Theor. Phys.* **49** (2010), 1649–1683. arXiv: 0811.2196 [gr-qc] (cit. on pp. 8, 11, 19, 32).

[134] P. Nicolini. "Noncommutative Black Holes, The Final Appeal To Quantum Gravity: A Review". *Int. J. Mod. Phys. A* **24** (2009), 1229–1308. arXiv: 0807.1939 [hep-th] (cit. on pp. 8, 11, 19, 32, 38, 41, 42, 105).

[135] S. Hossenfelder, L. Modesto, and I. Premont-Schwarz. "A Model for non-singular black hole collapse and evaporation". *Phys. Rev. D* **81** (2010), 044036. arXiv: 0912.1823 [gr-qc] (cit. on pp. 8, 11, 19, 32).

[136] L. Modesto, J. W. Moffat, and P. Nicolini. "Black holes in an ultraviolet complete quantum gravity". *Phys. Lett. B* **695** (2011), 397–400. arXiv: 1010.0680 [gr-qc] (cit. on pp. 8, 11, 19, 30, 32, 38, 41, 115).

[137] E. Spallucci and S. Ansoldi. "Regular black holes in UV self-complete quantum gravity". *Phys. Lett. B* **701** (2011), 471–474. arXiv: 1101.2760 [hep-th] (cit. on pp. 8, 11, 19, 32).

[138] M. Sprenger, P. Nicolini, and M. Bleicher. "Physics on Smallest Scales - An Introduction to Minimal Length Phenomenology". *Eur. J. Phys.* **33** (2012), 853–862. arXiv: 1202.1500 [physics.ed-ph] (cit. on pp. 8, 11, 19, 32).

[139] C. Bambi, D. Malafarina, and L. Modesto. "Non-singular quantum-inspired gravitational collapse". *Phys. Rev. D* **88** (2013), 044009. arXiv: 1305.4790 [gr-qc] (cit. on pp. 8, 11, 19, 32).

[140] V. P. Frolov. "Information loss problem and a 'black hole' model with a closed apparent horizon". *JHEP* **05** (2014), 049. arXiv: 1402.5446 [hep-th] (cit. on pp. 8, 11, 19, 37).

[141] R. Casadio, O. Micu, and P. Nicolini. "Minimum length effects in black hole physics". *Fundam. Theor. Phys.* **178** (2015), 293–322. arXiv: 1405.1692 [hep-th] (cit. on pp. 8, 11, 19, 32).

[142] E. Binetti, M. Del Piano, S. Hohenegger, F. Pezzella, and F. Sannino. "Effective theory of quantum black holes". *Phys. Rev. D* **106**.4 (2022), 046006. arXiv: 2203.13515 [gr-qc] (cit. on pp. 8, 11, 19).

[143] O. Lunin and S. D. Mathur. "AdS / CFT duality and the black hole information paradox". *Nucl. Phys. B* **623** (2002), 342–394. arXiv: hep-th/0109154 (cit. on pp. 8, 135).

[144] O. Lunin and S. D. Mathur. "Statistical interpretation of Bekenstein entropy for systems with a stretched horizon". *Phys. Rev. Lett.* **88** (2002), 211303. arXiv: hep-th/0202072 (cit. on pp. 8, 135).

[145] A. Simpson and M. Visser. "Black-bounce to traversable wormhole". *JCAP* **02** (2019), 042. arXiv: 1812.07114 [gr-qc] (cit. on pp. 8, 108).

[146] H. Culetu. "On a regular modified Schwarzschild spacetime". (2013). arXiv: 1305.5964 [gr-qc] (cit. on pp. 8, 14).

[147] S. S. Bayin. "Anisotropic fluids and cosmology". *Astrophys. J.* **303** (1986), 101–110 (cit. on pp. 8, 14, 108, 117).

[148] P. Aluri, S. Panda, M. Sharma, and S. Thakur. "Anisotropic universe with anisotropic sources". *JCAP* **12** (2013), 003. arXiv: 1210.3159 [gr-qc] (cit. on pp. 8, 14, 108, 117).

[149] T. Harko and F. S. N. Lobo. "Cosmological anisotropy from non-comoving dark matter and dark energy". *JCAP* **07** (2013), 036. arXiv: 1304.0757 [gr-qc] (cit. on pp. 8, 14, 108, 117).

[150] A. DeBenedictis, D. Horvat, S. Ilijic, S. Kloster, and K. S. Viswanathan. "Gravastar solutions with continuous pressures and equation of state". *Class. Quant. Grav.* **23** (2006), 2303–2316. arXiv: gr-qc/0511097 (cit. on pp. 8, 14).

[151] C. B. M. H. Chirenti and L. Rezzolla. "How to tell a gravastar from a black hole". *Class. Quant. Grav.* **24** (2007), 4191–4206. arXiv: 0706.1513 [gr-qc] (cit. on pp. 8, 14, 108, 117).

[152] R. Chan, M. F. A. da Silva, and P. Rocha. "Gravastars and Black Holes of Anisotropic Dark Energy". *Gen. Rel. Grav.* **43** (2011), 2223–2235. arXiv: 1009.4403 [gr-qc] (cit. on pp. 8, 14, 108, 117).

[153] P. Martin Moruno, N. Montelongo Garcia, F. S. N. Lobo, and M. Visser. "Generic thin-shell gravastars". *JCAP* **03** (2012), 034. arXiv: 1112.5253 [gr-qc] (cit. on pp. 8, 14).

[154] P. Beltracchi and P. Gondolo. "Formation of dark energy stars". *Phys. Rev. D* **99**.4 (2019), 044037. arXiv: 1810.12400 [gr-qc] (cit. on pp. 8, 14).

[155] J. Kumar and P. Bharti. "The classification of interior solutions of anisotropic fluid configurations". (2021). arXiv: 2112.12518 [gr-qc] (cit. on pp. 8, 14, 108, 117).

[156] I. Musco and T. Papanikolaou. "Primordial black hole formation for an anisotropic perfect fluid: Initial conditions and estimation of the threshold". *Phys. Rev. D* **106**.8 (2022), 083017. arXiv: 2110.05982 [gr-qc] (cit. on pp. 8, 14).

[157] J. M. Bardeen, B. Carter, and S. W. Hawking. "The Four laws of black hole mechanics". *Commun. Math. Phys.* **31** (1973), 161–170 (cit. on p. 8).

[158] Z.-Y. Fan and X. Wang. "Construction of Regular Black Holes in General Relativity". *Phys. Rev. D* **94**.12 (2016), 124027. arXiv: 1610.02636 [gr-qc] (cit. on pp. 8, 38, 41, 42, 65, 66).

[159] S. D. Mathur. "The Information paradox: A Pedagogical introduction". *Class. Quant. Grav.* **26** (2009). Ed. by A. M. Uranga, 224001. arXiv: 0909.1038 [hep-th] (cit. on pp. 8, 12, 22, 37).

[160] B. Hasslacher and E. Mottola. "Asymptotically Free Quantum Gravity and Black Holes". *Phys. Lett. B* **99** (1981), 221–224 (cit. on pp. 8, 37).

[161] G. T. Horowitz and J. M. Maldacena. "The Black hole final state". *JHEP* **02** (2004), 008. arXiv: hep-th/0310281 (cit. on pp. 8, 37).

[162] A. Ashtekar and M. Bojowald. "Quantum geometry and the Schwarzschild singularity". *Class. Quant. Grav.* **23** (2006), 391–411. arXiv: gr-qc/0509075 (cit. on pp. 8, 37).

[163] A. Ashtekar, V. Taveras, and M. Varadarajan. "Information is Not Lost in the Evaporation of 2-dimensional Black Holes". *Phys. Rev. Lett.* **100** (2008), 211302. arXiv: 0801.1811 [gr-qc] (cit. on pp. 8, 37).

[164] S. Hossenfelder and L. Smolin. "Conservative solutions to the black hole information problem". *Phys. Rev. D* **81** (2010), 064009. arXiv: 0901.3156 [gr-qc] (cit. on pp. 8, 37).

[165] T. Johannsen. "Regular Black Hole Metric with Three Constants of Motion". *Phys. Rev. D* **88**.4 (2013), 044002. arXiv: 1501.02809 [gr-qc] (cit. on pp. 8, 75, 76).

[166] T. Johannsen, A. E. Broderick, P. M. Plewa, S. Chatzopoulos, S. S. Doeleman, F. Eisenhauer, V. L. Fish, R. Genzel, O. Gerhard, and M. D. Johnson. "Testing General Relativity with the Shadow Size of Sgr A*". *Phys. Rev. Lett.* **116**.3 (2016), 031101. arXiv: 1512.02640 [astro-ph.GA] (cit. on pp. 8, 75).

[167] V. Cardoso, P. Pani, and J. Rico. "On generic parametrizations of spinning black-hole geometries". *Phys. Rev. D* **89** (2014), 064007. arXiv: 1401.0528 [gr-qc] (cit. on pp. 8, 75).

[168] Y. Ni, J. Jiang, and C. Bambi. "Testing the Kerr metric with the iron line and the KRZ parametrization". *JCAP* **09** (2016), 014. arXiv: 1607.04893 [gr-qc] (cit. on pp. 8, 75).

[169] A. Cárdenas-Avendaño, J. Jiang, and C. Bambi. "Testing the Kerr black hole hypothesis: comparison between the gravitational wave and the iron line approaches". *Phys. Lett. B* **760** (2016), 254–258. arXiv: 1603.04720 [gr-qc] (cit. on pp. 8, 75).

[170] S. Nampalliwar, S. Xin, S. Srivastava, A. B. Abdikamalov, D. Ayzenberg, C. Bambi, T. Dauser, J. A. Garcia, and A. Tripathi. "Testing General Relativity with X-ray reflection spectroscopy: The Konoplya-Rezzolla-Zhidenko parametrization". *Phys. Rev. D* **102**.12 (2020), 124071. arXiv: 1903.12119 [gr-qc] (cit. on pp. 8, 75).

[171] Z. Younsi, A. Zhidenko, L. Rezzolla, R. Konoplya, and Y. Mizuno. "New method for shadow calculations: Application to parametrized axisymmetric black holes". *Phys. Rev. D* **94**.8 (2016), 084025. arXiv: 1607.05767 [gr-qc] (cit. on pp. 8, 65, 75).

[172] Y. Mizuno, Z. Younsi, C. M. Fromm, O. Porth, M. De Laurentis, H. Olivares, H. Falcke, M. Kramer, and L. Rezzolla. "The Current Ability to Test Theories of Gravity with Black Hole Shadows". *Nature Astron.* **2**.7 (2018), 585–590. arXiv: 1804.05812 [astro-ph.GA] (cit. on pp. 8, 75).

[173] N. Oshita, Q. Wang, and N. Afshordi. "On Reflectivity of Quantum Black Hole Horizons". *JCAP* **04** (2020), 016. arXiv: 1905.00464 [hep-th] (cit. on p. 11).

[174] Q. Wang, N. Oshita, and N. Afshordi. "Echoes from Quantum Black Holes". *Phys. Rev. D* **101**.2 (2020), 024031. arXiv: 1905.00446 [gr-qc] (cit. on p. 11).

[175] S. Chakraborty, E. Maggio, A. Mazumdar, and P. Pani. "Implications of the quantum nature of the black hole horizon on the gravitational-wave ringdown". *Phys. Rev. D* **106**.2 (2022), 024041. arXiv: 2202.09111 [gr-qc] (cit. on pp. 11, 108, 128).

[176] A. Almheiri, R. Mahajan, J. Maldacena, and Y. Zhao. "The Page curve of Hawking radiation from semiclassical geometry". *JHEP* **03** (2020), 149. arXiv: 1908.10996 [hep-th] (cit. on pp. 12, 22, 136).

[177] A. Lopez-Ortega. "Entropy spectra of single horizon black holes in two dimensions". *Int. J. Mod. Phys. D* **20** (2011), 2525–2542. arXiv: 1112.6211 [gr-qc] (cit. on pp. 12, 27, 138).

[178] R. Cordero, A. Lopez-Ortega, and I. Vega-Acevedo. "Quasinormal frequencies of asymptotically anti-de Sitter black holes in two dimensions". *Gen. Rel. Grav.* **44** (2012), 917–940. arXiv: 1201.3605 [gr-qc] (cit. on pp. 12, 27, 138, 139).

[179] J. Kettner, G. Kunstatter, and A. J. M. Medved. "Quasinormal modes for single horizon black holes in generic 2-d dilaton gravity". *Class. Quant. Grav.* **21** (2004), 5317–5332. arXiv: gr-qc/0408042 (cit. on pp. 12, 27, 138).

[180] S. Bhattacharjee, S. Sarkar, and A. Bhattacharyya. "Scalar perturbations of black holes in Jackiw-Teitelboim gravity". *Phys. Rev. D* **103**.2 (2021), 024008. arXiv: 2011.08179 [gr-qc] (cit. on pp. 12, 27, 136, 138, 140).

[181] S. Hod. "Quasinormal resonances of near-extremal Kerr-Newman black holes". *Phys. Lett. B* **666** (2008), 483–485. arXiv: 0810.5419 [gr-qc] (cit. on pp. 12, 27, 130).

[182] S. Hod. "Slow relaxation of rapidly rotating black holes". *Phys. Rev. D* **78** (2008), 084035. arXiv: 0811.3806 [gr-qc] (cit. on pp. 12, 27).

[183] S. Hod. "Quasinormal resonances of a massive scalar field in a near-extremal Kerr black hole spacetime". *Phys. Rev. D* **84** (2011), 044046. arXiv: 1109.4080 [gr-qc] (cit. on pp. 12, 27, 130).

[184] S. Hod. "Quasinormal resonances of a charged scalar field in a charged Reissner-Nordstroem black-hole spacetime: A WKB analysis". *Phys. Lett. B* **710** (2012), 349–351. arXiv: 1205.5087 [gr-qc] (cit. on pp. 12, 27, 130).

[185] S. Hod. "Universality in the relaxation dynamics of the composed black-hole-charged-massive-scalar-field system: The role of quantum Schwinger discharge". *Phys. Lett. B* **747** (2015), 339–344. arXiv: 1507.01943 [gr-qc] (cit. on pp. 12, 27).

[186] A. Zimmerman and Z. Mark. "Damped and zero-damped quasinormal modes of charged, nearly extremal black holes". *Phys. Rev. D* **93**.4 (2016). [Erratum: Phys.Rev.D 93, 089905 (2016)], 044033. arXiv: 1512.02247 [gr-qc] (cit. on pp. 12, 27, 130).

[187] J. Joykutty. "Existence of Zero-Damped Quasinormal Frequencies for Nearly Extremal Black Holes". *Annales Henri Poincare* **23**.12 (2022), 4343–4390. arXiv: 2112.05669 [gr-qc] (cit. on pp. 12, 27, 130).

[188] S. Ansoldi, P. Nicolini, A. Smailagic, and E. Spallucci. "Noncommutative geometry inspired charged black holes". *Phys. Lett. B* **645** (2007), 261–266. arXiv: gr-qc/0612035 (cit. on p. 12).

[189] L. Modesto and P. Nicolini. "Charged rotating noncommutative black holes". *Phys. Rev. D* **82** (2010), 104035. arXiv: 1005.5605 [gr-qc] (cit. on p. 12).

[190] C. Lan, Y.-G. Miao, and H. Yang. "Quasinormal modes and phase transitions of regular black holes". *Nucl. Phys. B* **971** (2021), 115539. arXiv: 2008.04609 [gr-qc] (cit. on p. 12).

[191] M. Cadoni. "Conformal symmetry of gravity and the cosmological constant problem". *Phys. Lett. B* **642** (2006), 525–529. arXiv: hep-th/0606274 (cit. on p. 13).

[192] A. Bonanno and M. Reuter. "Renormalization group improved black hole space-times". *Phys. Rev. D* **62** (2000), 043008. arXiv: hep-th/0002196 (cit. on pp. 14, 18, 52, 115).

[193] M. Niedermaier and M. Reuter. "The Asymptotic Safety Scenario in Quantum Gravity". *Living Rev. Rel.* **9** (2006), 5–173 (cit. on pp. 14, 105).

[194] A. Bonanno, A. Eichhorn, H. Gies, J. M. Pawlowski, R. Percacci, M. Reuter, F. Saueressig, and G. P. Vacca. "Critical reflections on asymptotically safe gravity". *Front. in Phys.* **8** (2020), 269. arXiv: 2004.06810 [gr-qc] (cit. on p. 14).

[195] A. Adeifeoba, A. Eichhorn, and A. Platania. "Towards conditions for black-hole singularity-resolution in asymptotically safe quantum gravity". *Class. Quant. Grav.* **35**.22 (2018), 225007. arXiv: 1808.03472 [gr-qc] (cit. on p. 14).

[196] J. N. Borissova, A. Held, and N. Afshordi. "Scale-invariance at the core of quantum black holes". *Class. Quant. Grav.* **40**.7 (2023), 075011. arXiv: 2203.02559 [gr-qc] (cit. on p. 14).

[197] M. Cosenza, L. Herrera, M. Esculpi, and L. Witten. "Some models of anisotropic spheres in general relativity". *Journal of Mathematical Physics* **22**.1 (1981), 118–125 (cit. on pp. 14, 108, 117).

[198] S. W. Hawking and G. F. R. Ellis. *The Large Scale Structure of Space-Time*. Cambridge Monographs on Mathematical Physics. Cambridge University Press, 2023 (cit. on p. 15).

[199] E. Poisson and W. Israel. "Inner-horizon instability and mass inflation in black holes". *Phys. Rev. Lett.* **63** (1989), 1663–1666 (cit. on p. 18).

[200] A. Ori. "Inner structure of a charged black hole: An exact mass-inflation solution". *Phys. Rev. Lett.* **67** (1991), 789–792 (cit. on p. 18).

[201] D. Markovic and E. Poisson. "Classical stability and quantum instability of black hole Cauchy horizons". *Phys. Rev. Lett.* **74** (1995), 1280–1283. arXiv: gr-qc/9411002 (cit. on p. 18).

[202] R. Carballo-Rubio, F. Di Filippo, S. Liberati, C. Pacilio, and M. Visser. "On the viability of regular black holes". *JHEP* **07** (2018), 023. arXiv: 1805.02675 [gr-qc] (cit. on pp. 18, 49, 52).

[203] R. Carballo-Rubio, F. Di Filippo, S. Liberati, C. Pacilio, and M. Visser. "Inner horizon instability and the unstable cores of regular black holes". *JHEP* **05** (2021), 132. arXiv: 2101.05006 [gr-qc] (cit. on p. 18).

[204] A. Bonanno, A.-P. Khosravi, and F. Saueressig. "Regular black holes with stable cores". *Phys. Rev. D* **103**.12 (2021), 124027. arXiv: 2010.04226 [gr-qc] (cit. on p. 18).

[205] C. Barceló, V. Boyanov, R. Carballo-Rubio, and L. J. Garay. "Classical mass inflation versus semiclassical inner horizon inflation". *Phys. Rev. D* **106**.12 (2022), 124006. arXiv: 2203.13539 [gr-qc] (cit. on p. 18).

[206] E. Franzin, S. Liberati, J. Mazza, and V. Vellucci. "Stable rotating regular black holes". *Phys. Rev. D* **106**.10 (2022), 104060. arXiv: 2207.08864 [gr-qc] (cit. on pp. 18, 65).

[207] A. Giugno, A. Giusti, and A. Helou. "Horizon quantum fuzziness for non-singular black holes". *Eur. Phys. J. C* **78**.3 (2018), 208. arXiv: 1711.06209 [gr-qc] (cit. on pp. 18, 115).

[208] R. Casadio, A. Giugno, and O. Micu. "Horizon quantum mechanics: A hitchhiker's guide to quantum black holes". *Int. J. Mod. Phys. D* **25**.02 (2016), 1630006. arXiv: 1512.04071 [hep-th] (cit. on p. 18).

[209] R. Casadio, A. Giusti, and J. Ovalle. "Quantum Reissner-Nordström geometry: Singularity and Cauchy horizon". *Phys. Rev. D* **105**.12 (2022), 124026. arXiv: 2203.03252 [gr-qc] (cit. on p. 18).

[210] B. Knorr and A. Platania. "Sifting quantum black holes through the principle of least action". *Phys. Rev. D* **106**.2 (2022), L021901. arXiv: 2202.01216 [hep-th] (cit. on pp. 18, 27, 31).

[211] S. B. Giddings and A. Strominger. "Dynamics of extremal black holes". *Phys. Rev. D* **46** (1992), 627–637. arXiv: hep-th/9202004 (cit. on pp. 20, 43).

[212] J. M. Bardeen and G. T. Horowitz. "The Extreme Kerr throat geometry: A Vacuum analog of AdS(2) x S**2". *Phys. Rev. D* **60** (1999), 104030. arXiv: hep-th/9905099 (cit. on pp. 20, 43).

[213] T. Hartman, K. Murata, T. Nishioka, and A. Strominger. "CFT Duals for Extreme Black Holes". *JHEP* **04** (2009), 019. arXiv: 0811.4393 [hep-th] (cit. on p. 20).

[214] H. K. Kunduri and J. Lucietti. "Classification of near-horizon geometries of extremal black holes". *Living Rev. Rel.* **16** (2013), 8. arXiv: 1306.2517 [hep-th] (cit. on p. 20).

[215] J. M. Maldacena, J. Michelson, and A. Strominger. "Anti-de Sitter fragmentation". *JHEP* **02** (1999), 011. arXiv: hep-th/9812073 (cit. on pp. 22, 37, 48, 51, 64).

[216] A. Almheiri and J. Polchinski. "Models of AdS_2 backreaction and holography". *JHEP* **11** (2015), 014. arXiv: 1402.6334 [hep-th] (cit. on pp. 22, 121).

[217] A. Almheiri and B. Kang. "Conformal Symmetry Breaking and Thermodynamics of Near-Extremal Black Holes". *JHEP* **10** (2016), 052. arXiv: 1606.04108 [hep-th] (cit. on pp. 22, 48, 51, 121).

[218] D. Grumiller, W. Kummer, and D. V. Vassilevich. "Dilaton gravity in two-dimensions". *Phys. Rept.* **369** (2002), 327–430. arXiv: hep-th/0204253 (cit. on pp. 22, 39, 136).

[219] S. W. Hawking and D. N. Page. "Thermodynamics of Black Holes in anti-De Sitter Space". *Commun. Math. Phys.* **87** (1983), 577 (cit. on pp. 22, 134, 142).

[220] D. Pavon. "Phase transition in Reissner-Nordstrom black holes". *Phys. Rev. D* **43** (1991), 2495–2497 (cit. on p. 22).

[221] E. Witten. "Anti-de Sitter space, thermal phase transition, and confinement in gauge theories". *Adv. Theor. Math. Phys.* **2** (1998). Ed. by L. Bergstrom and U. Lindstrom, 505–532. arXiv: hep-th/9803131 (cit. on p. 22).

[222] A. Chamblin, R. Emparan, C. V. Johnson, and R. C. Myers. "Holography, thermodynamics and fluctuations of charged AdS black holes". *Phys. Rev. D* **60** (1999), 104026. arXiv: hep-th/9904197 (cit. on p. 22).

[223] X. N. Wu. "Multicritical phenomena of Reissner-Nordstrom anti-de Sitter black holes". *Phys. Rev. D* **62** (2000), 124023 (cit. on p. 22).

[224] M. Cadoni, G. D'Appollonio, and P. Pani. "Phase transitions between Reissner-Nordstrom and dilatonic black holes in 4D AdS spacetime". *JHEP* **03** (2010), 100. arXiv: 0912.3520 [hep-th] (cit. on p. 22).

[225] D. Kubiznak and R. B. Mann. "P-V criticality of charged AdS black holes". *JHEP* **07** (2012), 033. arXiv: 1205.0559 [hep-th] (cit. on p. 22).

[226] A. Rajagopal, D. Kubizňák, and R. B. Mann. "Van der Waals black hole". *Phys. Lett. B* **737** (2014), 277–279. arXiv: 1408.1105 [gr-qc] (cit. on p. 22).

[227] A. Mandal, S. Samanta, and B. R. Majhi. "Phase transition and critical phenomena of black holes: A general approach". *Phys. Rev. D* **94**.6 (2016), 064069. arXiv: 1608.04176 [gr-qc] (cit. on p. 22).

[228] R. Li, K. Zhang, and J. Wang. "Thermal dynamic phase transition of Reissner-Nordström Anti-de Sitter black holes on free energy landscape". *JHEP* **10** (2020), 090. arXiv: 2008.00495 [hep-th] (cit. on p. 22).

[229] P. Chen, Y. C. Ong, and D.-h. Yeom. "Black Hole Remnants and the Information Loss Paradox". *Phys. Rept.* **603** (2015), 1–45. arXiv: 1412.8366 [gr-qc] (cit. on pp. 23, 37).

[230] R. Banerjee, S. K. Modak, and S. Samanta. "Glassy Phase Transition and Stability in Black Holes". *Eur. Phys. J. C* **70** (2010), 317–328. arXiv: 1002.0466 [hep-th] (cit. on p. 23).

[231] W. H. Press. "Long Wave Trains of Gravitational Waves from a Vibrating Black Hole". *Astrophys. J. Lett.* **170** (1971), L105–L108 (cit. on p. 25).

[232] V. Ferrari and B. Mashhoon. "New approach to the quasinormal modes of a black hole". *Phys. Rev. D* **30** (1984), 295–304 (cit. on p. 25).

[233] B. Mashhoon. "Stability of charged rotating black holes in the eikonal approximation". *Phys. Rev. D* **31**.2 (1985), 290–293 (cit. on p. 25).

[234] V. Cardoso, A. S. Miranda, E. Berti, H. Witek, and V. T. Zanchin. "Geodesic stability, Lyapunov exponents and quasinormal modes". *Phys. Rev. D* **79**.6 (2009), 064016. arXiv: 0812.1806 [hep-th] (cit. on pp. 25, 108, 128).

[235] M. S. Churilova. "Analytical quasinormal modes of spherically symmetric black holes in the eikonal regime". *Eur. Phys. J. C* **79**.7 (2019), 629. arXiv: 1905.04536 [gr-qc] (cit. on p. 25).

[236] B. F. Schutz and C. M. Will. "Black hole normal modes: a semianalytical approach". *Astrophys. J. Lett.* **291** (1985), L33–L36 (cit. on pp. 25, 131, 140).

[237] H. Yang, F. Zhang, A. Zimmerman, D. A. Nichols, E. Berti, and Y. Chen. "Branching of quasinormal modes for nearly extremal Kerr black holes". *Phys. Rev. D* **87**.4 (2013), 041502. arXiv: 1212.3271 [gr-qc] (cit. on p. 27).

[238] V. P. Frolov. "Notes on nonsingular models of black holes". *Phys. Rev. D* **94**.10 (2016), 104056. arXiv: 1609.01758 [gr-qc] (cit. on pp. 27, 38, 41).

[239] M. Molina and J. R. Villanueva. "On the thermodynamics of the Hayward black hole". *Class. Quant. Grav.* **38**.10 (2021), 105002. arXiv: 2101.07917 [gr-qc] (cit. on p. 29).

[240] S. Ansoldi. "Spherical black holes with regular center: A Review of existing models including a recent realization with Gaussian sources". *Conference on Black Holes and Naked Singularities*. 2008. arXiv: 0802.0330 [gr-qc] (cit. on pp. 30, 32, 92).

[241] R. Casadio and A. Orlandi. "Quantum Harmonic Black Holes". *JHEP* **08** (2013), 025. arXiv: 1302.7138 [hep-th] (cit. on pp. 30, 32, 33, 132, 136).

[242] Y. S. Myung, Y.-W. Kim, and Y.-J. Park. "Thermodynamics and evaporation of the noncommutative black hole". *JHEP* **02** (2007), 012. arXiv: gr-qc/0611130 (cit. on p. 34).

[243] R. Banerjee, B. R. Majhi, and S. K. Modak. "Noncommutative Schwarzschild Black Hole and Area Law". *Class. Quant. Grav.* **26** (2009), 085010. arXiv: 0802.2176 [hep-th] (cit. on p. 34).

[244] K. Nozari and S. H. Mehdipour. "Hawking Radiation as Quantum Tunneling from Noncommutative Schwarzschild Black Hole". *Class. Quant. Grav.* **25** (2008), 175015. arXiv: 0801.4074 [gr-qc] (cit. on p. 34).

[245] B. P. Abbott et al., LIGO Scientific, Virgo collaboration. "GW170817: Observation of Gravitational Waves from a Binary Neutron Star Inspiral". *Phys. Rev. Lett.* **119**.16 (2017), 161101. arXiv: 1710.05832 [gr-qc] (cit. on p. 37).

[246] K. Akiyama et al., Event Horizon Telescope collaboration. "First M87 Event Horizon Telescope Results. I. The Shadow of the Supermassive Black Hole". *Astrophys. J. Lett.* **875** (2019), L1. arXiv: 1906.11238 [astro-ph.GA] (cit. on pp. 37, 65).

[247] Event Horizon Telescope Collaboration. "First Sagittarius A* Event Horizon Telescope Results. I. The Shadow of the Supermassive Black Hole in the Center of the Milky Way". *Astrophys. J. Lett.* **930**.2 (2022), L12 (cit. on pp. 37, 65).

[248] A. Strominger and C. Vafa. "Microscopic origin of the Bekenstein-Hawking entropy". *Phys. Lett. B* **379** (1996), 99–104. arXiv: hep-th/9601029 (cit. on p. 37).

[249] A. Ashtekar, J. Baez, A. Corichi, and K. Krasnov. "Quantum geometry and black hole entropy". *Phys. Rev. Lett.* **80** (1998), 904–907. arXiv: gr-qc/9710007 (cit. on p. 37).

[250] S. Carlip. "Near horizon conformal symmetry and black hole entropy". *Phys. Rev. Lett.* **88** (2002), 241301. arXiv: gr-qc/0203001 (cit. on p. 37).

[251] S. Ryu and T. Takayanagi. "Holographic derivation of entanglement entropy from AdS/CFT". *Phys. Rev. Lett.* **96** (2006), 181602. arXiv: hep-th/0603001 (cit. on p. 37).

[252] T. Padmanabhan. "Thermodynamical Aspects of Gravity: New insights". *Rept. Prog. Phys.* **73** (2010), 046901. arXiv: 0911.5004 [gr-qc] (cit. on p. 37).

[253] L. McGough and H. Verlinde. "Bekenstein-Hawking Entropy as Topological Entanglement Entropy". *JHEP* **11** (2013), 208. arXiv: 1308.2342 [hep-th] (cit. on p. 37).

[254] S. B. Giddings. "Constraints on black hole remnants". *Phys. Rev. D* **49** (1994), 947–957. arXiv: hep-th/9304027 (cit. on p. 37).

[255] G. Penington. "Entanglement Wedge Reconstruction and the Information Paradox". *JHEP* **09** (2020), 002. arXiv: 1905.08255 [hep-th] (cit. on pp. 37, 63).

[256] J. M. Maldacena. "Eternal black holes in anti-de Sitter". *JHEP* **04** (2003), 021. arXiv: hep-th/0106112 (cit. on pp. 37, 62, 143).

[257] K. Sueto and H. Yoshino. "Evaporation of a nonsingular Reissner-Nordström black hole and information loss problem". (2023). arXiv: 2301.10456 [gr-qc] (cit. on p. 37).

[258] E. Bianchi, T. De Lorenzo, and M. Smerlak. "Entanglement entropy production in gravitational collapse: covariant regularization and solvable models". *JHEP* **06** (2015), 180. arXiv: 1409.0144 [hep-th] (cit. on pp. 38, 63).

[259] V. P. Frolov and A. Zelnikov. "Quantum radiation from an evaporating nonsingular black hole". *Phys. Rev. D* **95**.12 (2017), 124028. arXiv: 1704.03043 [hep-th] (cit. on pp. 38, 63).

[260] *Abstracts / 5th International Conference on Gravitation and the Theory of Relativity*. eng. Tbilisi: Publ. House of Tbilisi Univ., 1968 (cit. on pp. 38, 41, 42, 65).

[261] I. Dymnikova. "Vacuum nonsingular black hole". *Gen. Rel. Grav.* **24** (1992), 235–242 (cit. on pp. 38, 41).

[262] M. Cadoni and A. P. Sanna. "Nonsingular black holes from conformal symmetries". *Class. Quant. Grav.* **40**.14 (2023), 145012. arXiv: 2302.06401 [gr-qc] (cit. on p. 38).

[263] J.-P. Hu and Y. Zhang. "Orbital motion of test particles in regular Hayward black hole space–time". *Can. J. Phys.* **97**.1 (2019), 58–62. arXiv: 1910.04161 [gr-qc] (cit. on p. 38).

[264] F. Lamy, E. Gourgoulhon, T. Paumard, and F. H. Vincent. "Imaging a non-singular rotating black hole at the center of the Galaxy". *Class. Quant. Grav.* **35**.11 (2018), 115009. arXiv: 1802.01635 [gr-qc] (cit. on p. 38).

[265] S. Guo, G.-R. Li, and E.-W. Liang. "Influence of accretion flow and magnetic charge on the observed shadows and rings of the Hayward black hole". *Phys. Rev. D* **105**.2 (2022), 023024. arXiv: 2112.11227 [astro-ph.HE] (cit. on p. 38).

[266] R. Della Monica and I. de Martino. "Unveiling the nature of SgrA* with the geodesic motion of S-stars". *JCAP* **03**.03 (2022), 007. arXiv: 2112.01888 [astro-ph.GA] (cit. on pp. 38, 71, 72).

[267] D. N. Page. "Time Dependence of Hawking Radiation Entropy". *JCAP* **09** (2013), 028. arXiv: 1301.4995 [hep-th] (cit. on p. 38).

[268] D. Grumiller, R. Ruzziconi, and C. Zwikel. "Generalized dilaton gravity in 2d". *SciPost Phys.* **12**.1 (2022), 032. arXiv: 2109.03266 [hep-th] (cit. on p. 39).

[269] T. Banks and M. O'Loughlin. "Two-dimensional quantum gravity in Minkowski space". *Nucl. Phys. B* **362** (1991), 649–664 (cit. on p. 39).

[270] M. Cavaglia. "A Note on Weyl transformations in two-dimensional dilaton gravity". *Mod. Phys. Lett. A* **15** (2000), 2113–2118. arXiv: hep-th/0011136 (cit. on p. 39).

[271] C. G. Callan Jr., S. B. Giddings, J. A. Harvey, and A. Strominger. "Evanescent black holes". *Phys. Rev. D* **45**.4 (1992), R1005. arXiv: hep-th/9111056 (cit. on pp. 39, 55).

[272] A. Bogojevic and D. Stojkovic. "A Nonsingular black hole". *Phys. Rev. D* **61** (2000), 084011. arXiv: gr-qc/9804070 (cit. on p. 39).

[273] M. Cadoni. "Statistical entropy of the Schwarzschild black hole". *Mod. Phys. Lett. A* **21** (2006), 1879–1888. arXiv: hep-th/0511103 (cit. on p. 39).

[274] V. P. Frolov and A. Zelnikov. "Two-dimensional black holes in the limiting curvature theory of gravity". *JHEP* **08** (2021), 154. arXiv: 2105.12808 [hep-th] (cit. on p. 39).

[275] M. Fitkevich. "Black bounces and remnants in dilaton gravity". *Phys. Rev. D* **105**.10 (2022), 106027. arXiv: 2202.00023 [gr-qc] (cit. on pp. 39, 64).

[276] M. Trodden, V. F. Mukhanov, and R. H. Brandenberger. "A Nonsingular two-dimensional black hole". *Phys. Lett. B* **316** (1993), 483–487. arXiv: hep-th/9305111 (cit. on pp. 39, 64).

[277] T. Banks and M. O'Loughlin. "Nonsingular Lagrangians for two-dimensional black holes". *Phys. Rev. D* **48** (1993), 698–706. arXiv: hep-th/9212136 (cit. on p. 39).

[278] D. A. Lowe and M. O'Loughlin. "Nonsingular black hole evaporation and 'stable' remnants". *Phys. Rev. D* **48** (1993), 3735–3742. arXiv: hep-th/9305125 (cit. on pp. 39, 58).

[279] M. Cadoni. "Trace anomaly and Hawking effect in generic 2-D dilaton gravity theories". *Phys. Rev. D* **53** (1996), 4413–4420. arXiv: gr-qc/9510012 (cit. on pp. 39, 53, 54, 55, 56, 57, 94, 136).

[280] W.-Y. Ai. "Nonsingular black hole in two-dimensional asymptotically flat spacetime". *Phys. Rev. D* **104**.4 (2021), 044064. arXiv: 2006.07962 [hep-th] (cit. on p. 39).

[281] R. B. Mann. "Conservation laws and 2-D black holes in dilaton gravity". *Phys. Rev. D* **47** (1993), 4438–4442. arXiv: hep-th/9206044 (cit. on pp. 39, 40).

[282] M. Cadoni and S. Mignemi. "On the conformal equivalence between 2-d black holes and Rindler space-time". *Phys. Lett. B* **358** (1995), 217–222. arXiv: gr-qc/9505032 (cit. on pp. 40, 55).

[283] S. Mignemi. "Black holes in generalized dilaton gravity in two-dimensions". *Annals Phys.* **245** (1996), 23–36. arXiv: hep-th/9411153 (cit. on p. 40).

[284] J. Navarro-Salas and P. Navarro. "AdS(2) / CFT(1) correspondence and near extremal black hole entropy". *Nucl. Phys. B* **579** (2000), 250–266. arXiv: hep-th/9910076 (cit. on pp. 42, 143).

[285] M. Cadoni, M. Ciulu, and M. Tuveri. "Symmetries, Holography and Quantum Phase Transition in Two-dimensional Dilaton AdS Gravity". *Phys. Rev. D* **97**.10 (2018), 103527. arXiv: 1711.02459 [hep-th] (cit. on pp. 42, 48, 64).

[286] A. Bagchi, D. Grumiller, J. Salzer, S. Sarkar, and F. Schöller. "Flat space cosmologies in two dimensions - Phase transitions and asymptotic mass-domination". *Phys. Rev. D* **90**.8 (2014), 084041. arXiv: 1408.5337 [hep-th] (cit. on pp. 42, 44).

[287] C. R. Nappi and A. Pasquinucci. "Thermodynamics of two-dimensional black holes". *Mod. Phys. Lett. A* **7** (1992), 3337–3346. arXiv: gr-qc/9208002 (cit. on p. 45).

[288] G. Kunstatter, R. Petryk, and S. Shelemy. "Hamiltonian thermodynamics of black holes in generic 2-D dilaton gravity". *Phys. Rev. D* **57** (1998), 3537–3547. arXiv: gr-qc/9709043 (cit. on pp. 45, 138).

[289] M.-S. Ma and R. Zhao. "Corrected form of the first law of thermodynamics for regular black holes". *Class. Quant. Grav.* **31** (2014), 245014. arXiv: 1411.0833 [gr-qc] (cit. on pp. 45, 121).

[290] A. Kumar and K. Ray. "Thermodynamics of two-dimensional black holes". *Phys. Lett. B* **351** (1995), 431–438. arXiv: hep-th/9410068 (cit. on p. 47).

[291] S. M. Carroll, M. C. Johnson, and L. Randall. "Extremal limits and black hole entropy". *JHEP* **11** (2009), 109. arXiv: 0901.0931 [hep-th] (cit. on p. 48).

[292] T. R. Cardoso and A. S. de Castro. "The Blackbody radiation in D-dimensional universes". *Rev. Bras. Ens. Fis.* **27** (2005), 559–563. arXiv: quant-ph/0510002 (cit. on p. 49).

[293] E. Alesci and L. Modesto. "Particle Creation by Loop Black Holes". *Gen. Rel. Grav.* **46** (2014), 1656. arXiv: 1101.5792 [gr-qc] (cit. on p. 49).

[294] M. Cadoni and S. Mignemi. "Nonsingular four-dimensional black holes and the Jackiw-Teitelboim theory". *Phys. Rev. D* **51** (1995), 4319–4329. arXiv: hep-th/9410041 (cit. on pp. 54, 136, 137).

[295] S. M. Christensen and S. A. Fulling. "Trace Anomalies and the Hawking Effect". *Phys. Rev. D* **15** (1977), 2088–2104 (cit. on p. 54).

[296] A. Bilal and C. G. Callan Jr. "Liouville models of black hole evaporation". *Nucl. Phys. B* **394** (1993), 73–100. arXiv: hep-th/9205089 (cit. on p. 56).

[297] J. G. Russo, L. Susskind, and L. Thorlacius. "The Endpoint of Hawking radiation". *Phys. Rev. D* **46** (1992), 3444–3449. arXiv: hep-th/9206070 (cit. on p. 56).

[298] J. G. Russo, L. Susskind, and L. Thorlacius. "Black hole evaporation in (1+1)-dimensions". *Phys. Lett. B* **292** (1992), 13–18. arXiv: hep-th/9201074 (cit. on p. 57).

[299] T. Piran and A. Strominger. "Numerical analysis of black hole evaporation". *Phys. Rev. D* **48** (1993), 4729–4734. arXiv: hep-th/9304148 (cit. on p. 58).

[300] D. A. Lowe. "Semiclassical approach to black hole evaporation". *Phys. Rev. D* **47** (1993), 2446–2453. arXiv: hep-th/9209008 (cit. on p. 58).

[301] A. Ashtekar, F. Pretorius, and F. M. Ramazanoglu. "Evaporation of 2-Dimensional Black Holes". *Phys. Rev. D* **83** (2011), 044040. arXiv: 1012.0077 [gr-qc] (cit. on p. 58).

[302] K. Diba and D. A. Lowe. "Near extremal black hole evaporation in asymptotically flat space-time". *Phys. Rev. D* **66** (2002), 024039. arXiv: hep-th/0202005 (cit. on p. 58).

[303] T. M. Fiola, J. Preskill, A. Strominger, and S. P. Trivedi. "Black hole thermodynamics and information loss in two-dimensions". *Phys. Rev. D* **50** (1994), 3987–4014. arXiv: hep-th/9403137 (cit. on p. 61).

[304] A. Almheiri, R. Mahajan, and J. Maldacena. "Islands outside the horizon". (2019). arXiv: 1910.11077 [hep-th] (cit. on pp. 61, 136).

[305] P. Calabrese and J. Cardy. "Entanglement entropy and conformal field theory". *J. Phys. A* **42** (2009), 504005. arXiv: 0905.4013 [cond-mat.stat-mech] (cit. on p. 61).

[306] J. Maldacena and L. Susskind. "Cool horizons for entangled black holes". *Fortsch. Phys.* **61** (2013), 781–811. arXiv: 1306.0533 [hep-th] (cit. on pp. 62, 116).

[307] X. Wang, R. Li, and J. Wang. "Islands and Page curves of Reissner-Nordström black holes". *JHEP* **04** (2021), 103. arXiv: 2101.06867 [hep-th] (cit. on p. 64).

[308] W. Kim and M. Nam. "Entanglement entropy of asymptotically flat non-extremal and extremal black holes with an island". *Eur. Phys. J. C* **81**.10 (2021), 869. arXiv: 2103.16163 [hep-th] (cit. on p. 64).

[309] K. Goswami and K. Narayan. "Small Schwarzschild de Sitter black holes, quantum extremal surfaces and islands". *JHEP* **10** (2022), 031. arXiv: 2207.10724 [hep-th] (cit. on p. 64).

[310] A. Svesko, E. Verheijden, E. P. Verlinde, and M. R. Visser. "Quasi-local energy and microcanonical entropy in two-dimensional nearly de Sitter gravity". *JHEP* **08** (2022), 075. arXiv: 2203.00700 [hep-th] (cit. on p. 64).

[311] D. S. Ageev, I. Y. Aref'eva, A. I. Belokon, V. V. Pushkarev, and T. A. Rusalev. "Entanglement entropy in de Sitter: no pure states for conformal matter". (2023). arXiv: 2304.12351 [hep-th] (cit. on p. 64).

[312] K. Hashimoto, N. Iizuka, and Y. Matsuo. "Islands in Schwarzschild black holes". *JHEP* **06** (2020), 085. arXiv: 2004.05863 [hep-th] (cit. on p. 64).

[313] F. F. Gautason, L. Schneiderbauer, W. Sybesma, and L. Thorlacius. "Page Curve for an Evaporating Black Hole". *JHEP* **05** (2020), 091. arXiv: 2004.00598 [hep-th] (cit. on p. 64).

[314] T. Hartman, E. Shaghoulian, and A. Strominger. "Islands in Asymptotically Flat 2D Gravity". *JHEP* **07** (2020), 022. arXiv: 2004.13857 [hep-th] (cit. on p. 64).

[315] A. Eckart and R. Genzel. "Stellar proper motions in the central 0.1 PC of the galaxy". *Mon. Not. Roy. Astron. Soc.* **284** (1997), 576–598 (cit. on p. 65).

[316] A. Ghez, M. Morris, E. E. Becklin, T. Kremenek, and A. Tanner. "The Accelerations of stars orbiting the Milky Way's central black hole". *Nature* **407** (2000), 349. arXiv: astro-ph/0009339 (cit. on p. 65).

[317] A. Tripathi, A. B. Abdikamalov, D. Ayzenberg, C. Bambi, V. Grinberg, H. Liu, and M. Zhou. "Testing the Kerr black hole hypothesis with the continuum-fitting and the iron line methods: the case of GRS 1915+105". *JCAP* **01**.01 (2022), 019. arXiv: 2106.10982 [astro-ph.HE] (cit. on p. 65).

[318] A. Perez. "Black Holes in Loop Quantum Gravity". *Rept. Prog. Phys.* **80**.12 (2017), 126901. arXiv: 1703.09149 [gr-qc] (cit. on p. 65).

[319] L. Buoninfante and A. Mazumdar. "Nonlocal star as a blackhole mimicker". *Phys. Rev. D* **100**.2 (2019), 024031. arXiv: 1903.01542 [gr-qc] (cit. on pp. 65, 112).

[320] A. Simpson and M. Visser. "The eye of the storm: a regular Kerr black hole". *JCAP* **03**.03 (2022), 011. arXiv: 2111.12329 [gr-qc] (cit. on p. 65).

[321] L. Sebastiani and S. Zerbini. "Some Remarks on Non-Singular Spherically Symmetric Space-Times". *Astronomy* **1**.2 (2022), 99–125. arXiv: 2206.03814 [gr-qc] (cit. on p. 65).

[322] K. Jusufi. "Regular black holes in Verlinde's emergent gravity". *Annals Phys.* **448** (2023), 169191. arXiv: 2208.12979 [gr-qc] (cit. on p. 65).

[323] I. de Martino, R. della Monica, and M. de Laurentis. "f(R) gravity after the detection of the orbital precession of the S2 star around the Galactic Center massive black hole". *Phys. Rev. D* **104**.10 (2021), L101502. arXiv: 2106.06821 [gr-qc] (cit. on pp. 65, 72).

[324] R. Della Monica, I. de Martino, and M. de Laurentis. "Orbital precession of the S2 star in Scalar–Tensor–Vector Gravity". *Mon. Not. Roy. Astron. Soc.* **510**.4 (2022), 4757–4766. arXiv: 2105.12687 [gr-qc] (cit. on pp. 65, 71).

[325] R. Ghosh, M. Rahman, and A. K. Mishra. "Regularized Stable Kerr Black Hole: Cosmic Censorships, Shadow and Quasi-Normal Modes". (2022). arXiv: 2209.12291 [gr-qc] (cit. on p. 65).

[326] R. Kumar Walia, S. G. Ghosh, and S. D. Maharaj. "Testing Rotating Regular Metrics with EHT Results of Sgr A*". *Astrophys. J.* **939**.2 (2022), 77. arXiv: 2207.00078 [gr-qc] (cit. on p. 65).

[327] S. Vagnozzi et al. "Horizon-scale tests of gravity theories and fundamental physics from the Event Horizon Telescope image of Sagittarius A". *Class. Quant. Grav.* **40**.16 (2023), 165007. arXiv: 2205.07787 [gr-qc] (cit. on p. 65).

[328] S. Riaz, S. Shashank, R. Roy, A. B. Abdikamalov, D. Ayzenberg, C. Bambi, Z. Zhang, and M. Zhou. "Testing regular black holes with X-ray and GW data". *JCAP* **10** (2022), 040. arXiv: 2206.03729 [gr-qc] (cit. on p. 65).

[329] R. Schodel et al. "A Star in a 15.2 year orbit around the supermassive black hole at the center of the Milky Way". *Nature* **419** (2002), 694–696. arXiv: astro-ph/0210426 (cit. on p. 65).

[330] A. M. Ghez et al. "The first measurement of spectral lines in a short - period star bound to the galaxy's central black hole: A paradox of youth". *Astrophys. J. Lett.* **586** (2003), L127–L131. arXiv: astro-ph/0302299 (cit. on p. 65).

[331] L. Hernquist. "An Analytical Model for Spherical Galaxies and Bulges". *Astrophys. J.* **356** (1990), 359 (cit. on p. 66).

[332] W. Jaffe. "A Simple model for the distribution of light in spherical galaxies". *Mon. Not. Roy. Astron. Soc.* **202** (1983), 995–999 (cit. on p. 66).

[333] S. Chandrasekhar. "The Mathematical Theory of Black Holes". *Fundam. Theor. Phys.* **9** (1984). Ed. by B. Bertotti, F. de Felice, and A. Pascolini, 5–26 (cit. on pp. 68, 81).

[334] S. Gillessen, P. M. Plewa, F. Eisenhauer, R. Sari, I. Waisberg, M. Habibi, O. Pfuhl, E. George, J. Dexter, S. von Fellenberg, T. Ott, and R. Genzel. "An Update on Monitoring Stellar Orbits in the Galactic Center". *Astrophysical Journal* **837**.1, 30 (2017), 30. arXiv: 1611.09144 [astro-ph.GA] (cit. on pp. 71, 72).

[335] R. Abuter et al., GRAVITY collaboration. "Detection of the Schwarzschild precession in the orbit of the star S2 near the Galactic centre massive black hole". *Astron. Astrophys.* **636** (2020), L5. arXiv: 2004.07187 [astro-ph.GA] (cit. on pp. 71, 72).

[336] R. Abuter et al., GRAVITY collaboration. "Mass distribution in the Galactic Center based on interferometric astrometry of multiple stellar orbits". *Astron. Astrophys.* **657** (2022), L12. arXiv: 2112.07478 [astro-ph.GA] (cit. on p. 72).

[337] M. Grould, F. H. Vincent, T. Paumard, and G. Perrin. "General relativistic effects on the orbit of the S2 star with GRAVITY". *Astron. Astrophys.* **608** (2017), A60. arXiv: 1709.04492 [astro-ph.HE] (cit. on p. 72).

[338] P. M. Plewa, S. Gillessen, F. Eisenhauer, T. Ott, O. Pfuhl, E. George, J. Dexter, M. Habibi, R. Genzel, M. J. Reid, and K. M. Menten. "Pinpointing the near-infrared location of Sgr A* by correcting optical distortion in the NACO imager". *Monthly Notices of the Royal Astronomical Society* **453**.3 (2015), 3235–3245. URL: https://doi.org/10.1093/mnras/stv1910 (cit. on p. 72).

[339] J. Goodman and J. Weare. "Ensemble samplers with affine invariance". *Communications in Applied Mathematics and Computational Science* **5**.1 (2010), 65–80. URL: https://doi.org/10.2140/camcos.2010.5.65 (cit. on p. 72).

[340] D. Foreman-Mackey, D. W. Hogg, D. Lang, and J. Goodman. "emcee: The MCMC Hammer". *Publ. Astron. Soc. Pac.* **125** (2013), 306–312. arXiv: 1202.3665 [astro-ph.IM] (cit. on p. 72).

[341] V. Ferrari and K. D. Kokkotas. "Scattering of particles by neutron stars: Time evolutions for axial perturbations". *Phys. Rev. D* **62** (2000), 107504. arXiv: gr-qc/0008057 (cit. on p. 75).

[342] J. Abedi, N. Afshordi, N. Oshita, and Q. Wang. "Quantum Black Holes in the Sky". *Universe* **6**.3 (2020), 43. arXiv: 2001.09553 [gr-qc] (cit. on p. 75).

[343] V. Cardoso, S. Hopper, C. F. B. Macedo, C. Palenzuela, and P. Pani. "Gravitational-wave signatures of exotic compact objects and of quantum corrections at the horizon scale". *Phys. Rev. D* **94**.8 (2016), 084031. arXiv: 1608.08637 [gr-qc] (cit. on pp. 75, 107, 108, 128).

[344] V. Cardoso and P. Pani. "Tests for the existence of black holes through gravitational wave echoes". *Nature Astron.* **1**.9 (2017), 586–591. arXiv: 1709.01525 [gr-qc] (cit. on p. 75).

[345] E. Berti, K. Yagi, H. Yang, and N. Yunes. "Extreme Gravity Tests with Gravitational Waves from Compact Binary Coalescences: (II) Ringdown". *Gen. Relativ. Gravit.* **50**.5 (2018), 49. arXiv: 1801.03587 [gr-qc] (cit. on p. 75).

[346] M. Ghasemi-Nodehi and C. Bambi. "Note on a new parametrization for testing the Kerr metric". *Eur. Phys. J. C* **76**.5 (2016), 290. arXiv: 1604.07032 [gr-qc] (cit. on p. 75).

[347] Z. Carson and K. Yagi. "Asymptotically flat, parametrized black hole metric preserving Kerr symmetries". *Phys. Rev. D* **101**.8 (2020), 084030. arXiv: 2002.01028 [gr-qc] (cit. on p. 75).

[348] R. A. Konoplya and A. Zhidenko. "General parametrization of black holes: the only parameters that matter". *Phys. Rev. D* **101**.12 (2020), 124004. arXiv: 2001.06100 [gr-qc] (cit. on p. 76).

[349] Y. B. Zel'dovich. "Generation of Waves by a Rotating Body". *J. Exp. Theor. Phys. Letters* **14** (1971), 180 (cit. on p. 76).

[350] J. D. Bekenstein and M. Schiffer. "The many faces of superradiance". *Phys. Rev. D* **58** (1998), 064014. arXiv: gr-qc/9803033 (cit. on p. 76).

[351] R. Brito, V. Cardoso, and P. Pani. *Superradiance: Energy Extraction, Black-Hole Bombs and Implications for Astrophysics and Particle Physics*. 2nd ed. Vol. 971. Lect. Notes Phys. Springer, 2020, pp. 1–293. arXiv: 1501.06570 [gr-qc] (cit. on p. 76).

[352] W. H. Press and S. A. Teukolsky. "Floating Orbits, Superradiant Scattering and the Black-hole Bomb". *Nature* **238** (1972), 211–212 (cit. on p. 76).

[353] V. Cardoso, Ó. J. C. Dias, J. P. S. Lemos, and S. Yoshida. "The black hole bomb and superradiant instabilities". *Phys. Rev. D* **70** (2004). [Erratum: Phys. Rev. D **70**, 049903 (2004)], 044039. arXiv: hep-th/0404096 (cit. on p. 76).

[354] T. Damour, N. Deruelle, and R. Ruffini. "On Quantum Resonances in Stationary Geometries". *Lett. Nuovo Cim.* **15** (1976), 257–262 (cit. on p. 76).

[355] S. L. Detweiler. "Klein-Gordon equation and rotating black holes". *Phys. Rev. D* **22** (1980), 2323–2326 (cit. on pp. 76, 99).

[356] V. Cardoso, S. Chakrabarti, P. Pani, E. Berti, and L. Gualtieri. "Floating and sinking: The imprint of massive scalars around rotating black holes". *Phys. Rev. Lett.* **107** (2011), 241101. arXiv: 1109.6021 [gr-qc] (cit. on p. 76).

[357] H. Witek, V. Cardoso, A. Ishibashi, and U. Sperhake. "Superradiant instabilities in astrophysical systems". *Phys. Rev. D* **87**.4 (2013), 043513. arXiv: 1212.0551 [gr-qc] (cit. on p. 76).

[358] R. Brito, V. Cardoso, and P. Pani. "Massive spin-2 fields on black hole spacetimes: Instability of the Schwarzschild and Kerr solutions and bounds on the graviton mass". *Phys. Rev. D* **88**.2 (2013), 023514. arXiv: 1304.6725 [gr-qc] (cit. on pp. 76, 87).

[359] R. Brito, S. Ghosh, E. Barausse, E. Berti, V. Cardoso, I. Dvorkin, A. Klein, and P. Pani. "Stochastic and resolvable gravitational waves from ultralight bosons". *Phys. Rev. Lett.* **119**.13 (2017), 131101. arXiv: 1706.05097 [gr-qc] (cit. on pp. 76, 87).

[360] R. Brito, S. Ghosh, E. Barausse, E. Berti, V. Cardoso, I. Dvorkin, A. Klein, and P. Pani. "Gravitational wave searches for ultralight bosons with LIGO and LISA". *Phys. Rev. D* **96**.6 (2017), 064050. arXiv: 1706.06311 [gr-qc] (cit. on p. 76).

[361] V. Cardoso, Ó. J. C. Dias, G. S. Hartnett, M. Middleton, P. Pani, and J. E. Santos. "Constraining the mass of dark photons and axion-like particles through black-hole superradiance". *JCAP* **03** (2018), 043. arXiv: 1801.01420 [gr-qc] (cit. on p. 76).

[362] N. Yunes and X. Siemens. "Gravitational-Wave Tests of General Relativity with Ground-Based Detectors and Pulsar Timing-Arrays". *Living Rev. Relativ.* **16** (2013), 9. arXiv: 1304.3473 [gr-qc] (cit. on p. 76).

[363] E. Berti et al. "Testing General Relativity with Present and Future Astrophysical Observations". *Class. Quant. Grav.* **32** (2015), 243001. arXiv: 1501.07274 [gr-qc] (cit. on p. 76).

[364] R. A. Konoplya, Z. Stuchlík, and A. Zhidenko. "Axisymmetric black holes allowing for separation of variables in the Klein-Gordon and Hamilton-Jacobi equations". *Phys. Rev. D* **97**.8 (2018), 084044. arXiv: 1801.07195 [gr-qc] (cit. on pp. 76, 77).

[365] R. Konoplya and A. Zhidenko. "Detection of gravitational waves from black holes: Is there a window for alternative theories?" *Phys. Lett. B* **756** (2016), 350–353. arXiv: 1602.04738 [gr-qc] (cit. on pp. 76, 77, 107).

[366] S. Wang, S. Chen, and J. Jing. "Strong gravitational lensing by a Konoplya-Zhidenko rotating non-Kerr compact object". *JCAP* **11** (2016), 020. arXiv: 1609.00802 [gr-qc] (cit. on p. 76).

[367] M. Wang, S. Chen, and J. Jing. "Shadow casted by a Konoplya-Zhidenko rotating non-Kerr black hole". *JCAP* **10** (2017), 051. arXiv: 1707.09451 [gr-qc] (cit. on p. 76).

[368] R. A. Konoplya. "Quantum corrected black holes: quasinormal modes, scattering, shadows". *Phys. Lett. B* **804** (2020), 135363. arXiv: 1912.10582 [gr-qc] (cit. on p. 76).

[369] A. G. Suvorov. "A family of solutions to the inverse problem in gravitation: building a theory around a metric". *Gen. Relativ. Gravit.* **53**.1 (2021), 6. arXiv: 2008.02510 [gr-qc] (cit. on p. 81).

[370] A. G. Suvorov and S. H. Völkel. "Exact theory for the Rezzolla-Zhidenko metric and self-consistent calculation of quasinormal modes". *Phys. Rev. D* **103**.4 (2021), 044027. arXiv: 2101.09697 [gr-qc] (cit. on p. 81).

[371] E. Poisson. *A Relativist's Toolkit. The Mathematics of Black-Hole Mechanics*. Cambridge, UK: Cambridge University Press, 2004 (cit. on p. 82).

[372] S. A. Teukolsky and W. H. Press. "Perturbations of a rotating black hole. III. Interaction of the hole with gravitational and electromagnetic radiation". *Astrophys. J.* **193** (1974), 443–461 (cit. on pp. 83, 97).

[373] E. W. Leaver. "An analytic representation for the quasi normal modes of Kerr black holes". *Proc. Roy. Soc. Lond. A* **402** (1985), 285–298 (cit. on p. 84).

[374] C. S. Reynolds. "Observing black holes spin". *Nature Astron.* **3**.1 (2019), 41–47. arXiv: 1903.11704 [astro-ph.HE] (cit. on p. 84).

[375] *SuperradianceKZ GitHub repository*. https://github.com/efranzin/SuperradianceKZ/ (cit. on p. 84).

[376] R. B. Magalhães, L. C. S. Leite, and L. C. B. Crispino. "Absorption by deformed black holes". *Phys. Lett. B* **805** (2020), 135418. arXiv: 2004.08438 [gr-qc] (cit. on p. 85).

[377] R. B. Magalhães, L. C. S. Leite, and L. C. B. Crispino. "Schwarzschild-like black holes: Light-like trajectories and massless scalar absorption". *Eur. Phys. J. C* **80**.5 (2020), 386. arXiv: 2005.04515 [gr-qc] (cit. on p. 85).

[378] S. R. Dolan. "Instability of the massive Klein-Gordon field on the Kerr spacetime". *Phys. Rev. D* **76** (2007), 084001. arXiv: 0705.2880 [gr-qc] (cit. on p. 87).

[379] R. Brito, V. Cardoso, and P. Pani. "Black holes as particle detectors: evolution of superradiant instabilities". *Class. Quantum Grav.* **32**.13 (2015), 134001. arXiv: 1411.0686 [gr-qc] (cit. on p. 87).

[380] A. Arvanitaki, M. Baryakhtar, and X. Huang. "Discovering the QCD Axion with Black Holes and Gravitational Waves". *Phys. Rev. D* **91**.8 (2015), 084011. arXiv: 1411.2263 [hep-ph] (cit. on p. 87).

[381] S. A. Teukolsky. "Perturbations of a rotating black hole. I. Fundamental equations for gravitational electromagnetic and neutrino field perturbations". *Astrophys. J.* **185** (1973), 635–647 (cit. on pp. 95, 96).

[382] W. Kinnersley. "Type D Vacuum Metrics". *J. Math. Phys.* **10** (1969), 1195–1203 (cit. on p. 95).

[383] A. I. Janis and E. T. Newman. "Structure of Gravitational Sources". *J. Math. Phys.* **6** (1965), 902–914 (cit. on p. 96).

[384] J. N. Goldberg, A. J. MacFarlane, E. T. Newman, F. Rohrlich, and E. C. G. Sudarshan. "Spin-s spherical harmonics and $\eth$". *J. Math. Phys.* **8** (1967), 2155 (cit. on p. 97).

[385] W. H. Press and S. A. Teukolsky. "Perturbations of a Rotating Black Hole. II. Dynamical Stability of the Kerr Metric". *Astrophys. J.* **185** (1973), 649–674 (cit. on p. 97).

[386] E. Berti, V. Cardoso, and M. Casals. "Eigenvalues and eigenfunctions of spin-weighted spheroidal harmonics in four and higher dimensions". *Phys. Rev. D* **73** (2006). [Erratum: Phys. Rev. D **73**, 109902 (2006)], 024013. arXiv: gr-qc/0511111 (cit. on p. 97).

[387] A. A. Starobinskii. "Amplification of waves during reflection from a rotating black hole". *J. Exp. Theor. Phys.* **37** (1973), 28–32 (cit. on p. 99).

[388] A. A. Starobinskii and S. M. Churilov. "Amplification of electromagnetic and gravitational waves scattered by a rotating black hole". *J. Exp. Theor. Phys.* **38** (1974), 1–5 (cit. on p. 99).

[389] D. N. Page. "Particle Emission Rates from a Black Hole: Massless Particles from an Uncharged, Nonrotating Hole". *Phys. Rev. D* **13** (1976), 198–206 (cit. on p. 99).

[390] S. A. Fulling. *Aspects of Quantum Field Theory in Curved Space-time*. Vol. 17. 1989 (cit. on p. 105).

[391] H. P. Nilles. "Supersymmetry, Supergravity and Particle Physics". *Phys. Rept.* **110** (1984), 1–162 (cit. on p. 105).

[392] P. Van Nieuwenhuizen. "Supergravity". *Phys. Rept.* **68** (1981), 189–398 (cit. on p. 105).

[393] J. Ambjørn, J. Jurkiewicz, and R. Loll. "Lorentzian and Euclidean Quantum Gravity—Analytical and Numerical Results". *NATO Sci. Ser. C* **556** (2000). Ed. by L. Thorlacius and T. Jonsson, 381–450. arXiv: hep-th/0001124 (cit. on p. 105).

[394] A. Konechny and A. S. Schwarz. "Introduction to M(atrix) theory and noncommutative geometry". *Phys. Rept.* **360** (2002), 353–465. arXiv: hep-th/0012145 (cit. on p. 105).

[395] G. Landi. *An Introduction to noncommutative spaces and their geometry*. Vol. 51. 1997. arXiv: hep-th/9701078 (cit. on p. 105).

[396] R. Percacci. "Asymptotic Safety". (2007), 111–128. arXiv: 0709.3851 [hep-th] (cit. on p. 105).

[397] G. Amelino-Camelia, J. R. Ellis, N. E. Mavromatos, D. V. Nanopoulos, and S. Sarkar. "Tests of quantum gravity from observations of gamma-ray bursts". *Nature* **393** (1998), 763–765. arXiv: astro-ph/9712103 (cit. on p. 105).

[398] F. Coradeschi, A. M. Frassino, T. Guerreiro, J. R. West, and E. Schioppa Junior. "Can We Detect the Quantum Nature of Weak Gravitational Fields?" *Universe* **7**.11 (2021), 414. arXiv: 2110.02542 [gr-qc] (cit. on p. 105).

[399] S. Bose, A. Mazumdar, and M. Toroš. "Infrared scaling for a graviton condensate". *Nucl. Phys. B* **977** (2022), 115730. arXiv: 2110.04536 [gr-qc] (cit. on pp. 106, 135).

[400] M. Carlesso, A. Bassi, M. Paternostro, and H. Ulbricht. "Testing the gravitational field generated by a quantum superposition". *New J. Phys.* **21**.9 (2019), 093052. arXiv: 1906.04513 [quant-ph] (cit. on pp. 106, 107).

[401] M. Christodoulou and C. Rovelli. "On the possibility of laboratory evidence for quantum superposition of geometries". *Phys. Lett. B* **792** (2019), 64–68. arXiv: 1808.05842 [gr-qc] (cit. on pp. 106, 107).

[402] J. Foo, S. Onoe, and M. Zych. "Unruh-deWitt detectors in quantum superpositions of trajectories". *Phys. Rev. D* **102**.8 (2020), 085013. arXiv: 2003.12774 [quant-ph] (cit. on pp. 106, 107).

[403] J. Foo, R. B. Mann, and M. Zych. "Schrödinger's cat for de Sitter spacetime". *Class. Quant. Grav.* **38**.11 (2021), 115010. arXiv: 2012.10025 [gr-qc] (cit. on pp. 106, 107).

[404] J. Foo, C. S. Arabaci, M. Zych, and R. B. Mann. "Quantum Signatures of Black Hole Mass Superpositions". *Phys. Rev. Lett.* **129**.18 (2022), 181301. arXiv: 2111.13315 [gr-qc] (cit. on pp. 106, 107).

[405] J. Foo, R. B. Mann, and M. Zych. "Schrödinger's black hole cat". *Int. J. Mod. Phys. D* **31**.14 (2022), 2242016. arXiv: 2204.00384 [gr-qc] (cit. on pp. 106, 107).

[406] J. Foo, C. S. Arabaci, M. Zych, and R. B. Mann. "Quantum superpositions of Minkowski spacetime". *Phys. Rev. D* **107**.4 (2023), 045014. arXiv: 2208.12083 [gr-qc] (cit. on pp. 106, 107).

[407] F. Giacomini, E. Castro-Ruiz, and Č. Brukner. "Quantum mechanics and the covariance of physical laws in quantum reference frames". *Nature Commun.* **10**.1 (2019), 494. arXiv: 1712.07207 [quant-ph] (cit. on pp. 106, 107, 112).

[408] E. Tjoa and R. B. Mann. "Unruh-DeWitt detector in dimensionally-reduced static spherically symmetric spacetimes". *JHEP* **03** (2022), 014. arXiv: 2202.04084 [gr-qc] (cit. on pp. 106, 107).

[409] S. Bose, A. Mazumdar, G. W. Morley, H. Ulbricht, M. Toroš, M. Paternostro, A. Geraci, P. Barker, M. S. Kim, and G. Milburn. "Spin Entanglement Witness for Quantum Gravity". *Phys. Rev. Lett.* **119**.24 (2017), 240401. arXiv: 1707.06050 [quant-ph] (cit. on p. 107).

[410] C. Marletto and V. Vedral. "Gravitationally-induced entanglement between two massive particles is sufficient evidence of quantum effects in gravity". *Phys. Rev. Lett.* **119**.24 (2017), 240402. arXiv: 1707.06036 [quant-ph] (cit. on p. 107).

[411] R. Howl, R. Penrose, and I. Fuentes. "Exploring the unification of quantum theory and general relativity with a Bose–Einstein condensate". *New J. Phys.* **21**.4 (2019), 043047. arXiv: 1812.04630 [quant-ph] (cit. on p. 107).

[412] R. Howl, V. Vedral, D. Naik, M. Christodoulou, C. Rovelli, and A. Iyer. "Non-Gaussianity as a signature of a quantum theory of gravity". *PRX Quantum* **2** (2021), 010325. arXiv: 2004.01189 [quant-ph] (cit. on p. 107).

[413] T. Krisnanda, G. Y. Tham, M. Paternostro, and T. Paterek. "Observable quantum entanglement due to gravity". (2019). arXiv: 1906.08808 [quant-ph] (cit. on p. 107).

[414] T. Westphal, H. Hepach, J. Pfaff, and M. Aspelmeyer. "Measurement of gravitational coupling between millimetre-sized masses". *Nature* **591**.7849 (2021), 225–228. arXiv: 2009.09546 [gr-qc] (cit. on p. 107).

[415] Y. Y. Fein, P. Geyer, P. Zwick, F. Kiałka, S. Pedalino, M. Mayor, S. Gerlich, and M. Arndt. "Quantum superposition of molecules beyond 25 kDa". *Nature Physics* **15**.12 (2019), 1242–1245. URL: https://doi.org/10.1038/s41567-019-0663-9 (cit. on p. 107).

[416] M. Aspelmeyer. "When Zeh Meets Feynman: How to Avoid the Appearance of a Classical World in Gravity Experiments". *Fundam. Theor. Phys.* **204** (2022), 85–95. arXiv: 2203.05587 [quant-ph] (cit. on p. 107).

[417] L. Barack et al. "Black holes, gravitational waves and fundamental physics: a roadmap". *Class. Quant. Grav.* **36**.14 (2019), 143001. arXiv: 1806.05195 [gr-qc] (cit. on p. 107).

[418] Z. Carson and K. Yagi. "Parametrized and inspiral-merger-ringdown consistency tests of gravity with multiband gravitational wave observations". *Phys. Rev. D* **101**.4 (2020), 044047. arXiv: 1911.05258 [gr-qc] (cit. on p. 107).

[419] J. R. Gair, M. Vallisneri, S. L. Larson, and J. G. Baker. "Testing General Relativity with Low-Frequency, Space-Based Gravitational-Wave Detectors". *Living Rev. Rel.* **16** (2013), 7. arXiv: 1212.5575 [gr-qc] (cit. on p. 107).

[420] H. C. D. Lima Junior., L. C. B. Crispino, P. V. P. Cunha, and C. A. R. Herdeiro. "Can different black holes cast the same shadow?" *Phys. Rev. D* **103**.8 (2021), 084040. arXiv: 2102.07034 [gr-qc] (cit. on p. 107).

[421] Z. Younsi, D. Psaltis, and F. Özel. "Black Hole Images as Tests of General Relativity: Effects of Spacetime Geometry". *Astrophys. J.* **942**.1 (2023), 47. arXiv: 2111.01752 [astro-ph.HE] (cit. on p. 107).

[422] S. Nampalliwar and S. K. "Theory-agnostic tests of gravity with black hole shadows". (2021). arXiv: 2108.01190 [gr-qc] (cit. on p. 107).

[423] R. Penrose. "On gravity's role in quantum state reduction". *Gen. Rel. Grav.* **28** (1996), 581–600 (cit. on pp. 107, 113).

[424] R. Penrose. "On the Gravitization of Quantum Mechanics 1: Quantum State Reduction". *Found. Phys.* **44** (2014). Ed. by F. Scardigli and M. Nespoli, 557–575 (cit. on p. 107).

[425] M. P. Blencowe. "Effective Field Theory Approach to Gravitationally Induced Decoherence". *Phys. Rev. Lett.* **111**.2 (2013), 021302. arXiv: 1211.4751 [quant-ph] (cit. on p. 107).

[426] I. Fuentes-Schuller and R. B. Mann. "Alice falls into a black hole: Entanglement in noninertial frames". *Phys. Rev. Lett.* **95** (2005), 120404. arXiv: quant-ph/0410172 (cit. on p. 107).

[427] E. Martin-Martinez, L. J. Garay, and J. Leon. "Unveiling quantum entanglement degradation near a Schwarzschild black hole". *Phys. Rev. D* **82** (2010), 064006. arXiv: 1006.1394 [quant-ph] (cit. on p. 107).

[428] R. Howl, A. Akil, H. Kristjánsson, X. Zhao, and G. Chiribella. "Quantum gravity as a communication resource". (2022). arXiv: 2203.05861 [quant-ph] (cit. on p. 107).

[429] F. Giacomini and Č. Brukner. "Einstein's Equivalence principle for superpositions of gravitational fields and quantum reference frames". (2020). arXiv: 2012.13754 [quant-ph] (cit. on pp. 107, 109, 112, 113).

[430] R. L. Bowers and E. P. T. Liang. "Anisotropic Spheres in General Relativity". *Astrophys. J.* **188** (1974), 657–665 (cit. on pp. 108, 117).

[431] H. Dehnen, V. D. Ivashchuk, and V. N. Melnikov. "On black hole solutions in model with anisotropic fluid". *Grav. Cosmol.* **9** (2003), 153–158. arXiv: gr-qc/0211049 (cit. on pp. 108, 117).

[432] M. Visser and D. L. Wiltshire. "Stable gravastars: An Alternative to black holes?" *Class. Quant. Grav.* **21** (2004), 1135–1152. arXiv: gr-qc/0310107 (cit. on pp. 108, 117).

[433] J. Abedi, H. Dykaar, and N. Afshordi. "Echoes from the Abyss: Tentative evidence for Planck-scale structure at black hole horizons". *Phys. Rev. D* **96**.8 (2017), 082004. arXiv: 1612.00266 [gr-qc] (cit. on pp. 108, 128).

[434] E. Maggio, L. Buoninfante, A. Mazumdar, and P. Pani. "How does a dark compact object ringdown?" *Phys. Rev. D* **102**.6 (2020), 064053. arXiv: 2006.14628 [gr-qc] (cit. on pp. 108, 128).

[435] E. Maggio, P. Pani, and G. Raposo. "Testing the nature of dark compact objects with gravitational waves". (2021). arXiv: 2105.06410 [gr-qc] (cit. on pp. 108, 128).

[436] A.-C. de la Hamette, V. Kabel, E. Castro-Ruiz, and Č. Brukner. "Falling through masses in superposition: quantum reference frames for indefinite metrics". (2021). arXiv: 2112.11473 [quant-ph] (cit. on pp. 109, 110, 113).

[437] R. Ruffini and S. Bonazzola. "Systems of selfgravitating particles in general relativity and the concept of an equation of state". *Phys. Rev.* **187** (1969), 1767–1783 (cit. on p. 109).

[438] L. Diósi. "Gravitation and quantummechanical localization of macroobjects". *Phys. Lett. A* **105** (1984), 199–202. arXiv: 1412.0201 [quant-ph] (cit. on p. 109).

[439] D. Giulini and A. Grossardt. "The Schrödinger-Newton equation as non-relativistic limit of self-gravitating Klein-Gordon and Dirac fields". *Class. Quant. Grav.* **29** (2012), 215010. arXiv: 1206.4250 [gr-qc] (cit. on p. 109).

[440] M. Bahrami, A. Großardt, S. Donadi, and A. Bassi. "The Schroedinger-Newton equation and its foundations". *New J. Phys.* **16**.11 (2014), 115007. arXiv: 1407.4370 [quant-ph] (cit. on p. 109).

[441] T. Roger, C. Maitland, K. Wilson, N. Westerberg, D. Vocke, E. M. Wright, and D. Faccio. "Optical analogues of the Newton-Schrödinger equation and boson star evolution". *Nature Commun.* **7** (2016), 13492. arXiv: 1611.00924 [physics.optics] (cit. on p. 109).

[442] R. Ligez, R. B. MacKenzie, V. Massart, M. B. Paranjape, and U. A. Yajnik. "What is the Gravitational Field of a Mass in a Spatially Nonlocal Quantum Superposition?" *Phys. Rev. Lett.* **130**.10 (2023), 101502. arXiv: 2110.13866 [gr-qc] (cit. on p. 109).

[443] J. V. B. da Silva, G. H. S. Aguiar, and G. E. A. Matsas. "Disfavoring the Schrödinger-Newton equation in explaining the emergence of classicality". *Phys. Rev. A* **108**.1 (2023), 012214. arXiv: 2307.04914 [quant-ph] (cit. on p. 109).

[444] T. Biswas, A. Mazumdar, and W. Siegel. "Bouncing universes in string-inspired gravity". *JCAP* **03** (2006), 009. arXiv: hep-th/0508194 (cit. on p. 112).

[445] T. Biswas, E. Gerwick, T. Koivisto, and A. Mazumdar. "Towards singularity and ghost free theories of gravity". *Phys. Rev. Lett.* **108** (2012), 031101. arXiv: 1110.5249 [gr-qc] (cit. on p. 112).

[446] N. Burzillà, B. L. Giacchini, T. d. P. Netto, and L. Modesto. "Higher-order regularity in local and nonlocal quantum gravity". *Eur. Phys. J. C* **81**.5 (2021), 462. arXiv: 2012.11829 [gr-qc] (cit. on p. 112).

[447] J. Boos. "Non-singular "Gauss" black hole from non-locality: a simple model with a de Sitter core, mass gap, and no inner horizon". (2021). arXiv: 2104.00555 [gr-qc] (cit. on p. 112).

[448] M. J. Lake, M. Miller, R. F. Ganardi, Z. Liu, S.-D. Liang, and T. Paterek. "Generalised uncertainty relations from superpositions of geometries". *Class. Quant. Grav.* **36**.15 (2019), 155012. arXiv: 1812.10045 [quant-ph] (cit. on p. 112).

[449] F. Giacomini and Č. Brukner. "Quantum superposition of spacetimes obeys Einstein's equivalence principle". *AVS Quantum Sci.* **4**.1 (2022), 015601. arXiv: 2109.01405 [quant-ph] (cit. on pp. 112, 113).

[450] S. B. Giddings, D. Marolf, and J. B. Hartle. "Observables in effective gravity". *Phys. Rev. D* **74** (2006), 064018. arXiv: hep-th/0512200 (cit. on p. 113).

[451] R. Carballo-Rubio, F. Di Filippo, S. Liberati, and M. Visser. "Opening the Pandora's box at the core of black holes". *Class. Quant. Grav.* **37**.14 (2020), 14. arXiv: 1908.03261 [gr-qc] (cit. on p. 115).

[452] M. S. Morris, K. S. Thorne, and U. Yurtsever. "Wormholes, Time Machines, and the Weak Energy Condition". *Phys. Rev. Lett.* **61** (1988), 1446–1449 (cit. on p. 115).

[453] R. Casadio. "Geometry and thermodynamics of coherent quantum black holes". *Int. J. Mod. Phys. D* **31**.16 (2022), 2250128. arXiv: 2103.00183 [gr-qc] (cit. on pp. 115, 117).

[454] M. Van Raamsdonk. "Building up spacetime with quantum entanglement". *Gen. Rel. Grav.* **42** (2010), 2323–2329. arXiv: 1005.3035 [hep-th] (cit. on p. 116).

[455] R. Garattini and F. S. N. Lobo. "Self sustained phantom wormholes in semi-classical gravity". *Class. Quant. Grav.* **24** (2007), 2401–2413. arXiv: gr-qc/0701020 (cit. on p. 116).

[456] R. Garattini and F. S. N. Lobo. "Self-sustained traversable wormholes in noncommutative geometry". *Phys. Lett. B* **671** (2009), 146–152. arXiv: 0811.0919 [gr-qc] (cit. on p. 116).

[457] R. Garattini and F. S. N. Lobo. "Self-sustained wormholes in modified dispersion relations". *Phys. Rev. D* **85** (2012), 024043. arXiv: 1111.5729 [gr-qc] (cit. on p. 116).

[458] R. Garattini. "Casimir Wormholes". *Eur. Phys. J. C* **79**.11 (2019), 951. arXiv: 1907.03623 [gr-qc] (cit. on p. 116).

[459] R. Garattini. "Self sustained traversable wormholes?" *Class. Quant. Grav.* **22** (2005), 1105–1118. arXiv: gr-qc/0501105 (cit. on p. 116).

[460] R. Garattini. "Self sustained traversable wormholes and the equation of state". *Class. Quant. Grav.* **24** (2007). Ed. by P. Apostolopoulos, C. Bona, J. Carot, L. Mas, A. M. Sintes, and J. Stela, 1189–1210. arXiv: gr-qc/0701019 (cit. on p. 116).

[461] A. Kundu. "Wormholes and holography: an introduction". *Eur. Phys. J. C* **82**.5 (2022), 447. arXiv: 2110.14958 [hep-th] (cit. on p. 118).

[462] M. Visser. "Dirty black holes: Entropy versus area". *Phys. Rev. D* **48** (1993), 583–591. arXiv: hep-th/9303029 (cit. on p. 121).

[463] P. K. Townsend. "Black holes: Lecture notes". (1997). arXiv: gr-qc/9707012 (cit. on p. 122).

[464] A. Fabbri and J. Navarro-Salas. *Modeling black hole evaporation*. 2005 (cit. on p. 122).

[465] M. S. Churilova and Z. Stuchlik. "Ringing of the regular black-hole/wormhole transition". *Class. Quant. Grav.* **37**.7 (2020), 075014. arXiv: 1911.11823 [gr-qc] (cit. on p. 128).

[466] H.-J. Blome and B. Mashhoon. "Quasi-normal oscillations of a schwarzschild black hole". *Physics Letters A* **100**.5 (1984), 231–234 (cit. on p. 129).

[467] E. Berti, V. Cardoso, and A. O. Starinets. "Quasinormal modes of black holes and black branes". *Class. Quant. Grav.* **26** (2009), 163001. arXiv: 0905.2975 [gr-qc] (cit. on pp. 131, 135, 137).

[468] K. D. Kokkotas and B. G. Schmidt. "Quasinormal modes of stars and black holes". *Living Rev. Rel.* **2** (1999), 2. arXiv: gr-qc/9909058 (cit. on pp. 131, 135, 137).

[469] R. A. Konoplya and A. Zhidenko. "Quasinormal modes of black holes: From astrophysics to string theory". *Rev. Mod. Phys.* **83** (2011), 793–836. arXiv: 1102.4014 [gr-qc] (cit. on pp. 131, 135, 137).

[470] H.-P. Nollert. "Quasinormal modes of Schwarzschild black holes: The determination of quasinormal frequencies with very large imaginary parts". *Phys. Rev. D* **47** (1993), 5253–5258 (cit. on pp. 131, 140).

[471] S. Hod. "Bohr's correspondence principle and the area spectrum of quantum black holes". *Phys. Rev. Lett.* **81** (1998), 4293. arXiv: gr-qc/9812002 (cit. on pp. 131, 132, 136, 140).

[472] L. Motl. "An Analytical computation of asymptotic Schwarzschild quasinormal frequencies". *Adv. Theor. Math. Phys.* **6** (2003), 1135–1162. arXiv: gr-qc/0212096 (cit. on pp. 131, 140).

[473] H.-P. Nollert. "TOPICAL REVIEW: Quasinormal modes: the characteristic 'sound' of black holes and neutron stars". *Class. Quant. Grav.* **16** (1999), R159–R216 (cit. on p. 131).

[474] I. Agullo, V. Cardoso, A. D. Rio, M. Maggiore, and J. Pullin. "Potential Gravitational Wave Signatures of Quantum Gravity". *Phys. Rev. Lett.* **126**.4 (2021), 041302. arXiv: 2007.13761 [gr-qc] (cit. on p. 131).

[475] G. T. Horowitz and V. E. Hubeny. "Quasinormal modes of AdS black holes and the approach to thermal equilibrium". *Phys. Rev. D* **62** (2000), 024027. arXiv: hep-th/9909056 (cit. on pp. 131, 144).

[476] W. Israel. "Event horizons in static electrovac space-times". *Commun. Math. Phys.* **8** (1968), 245–260 (cit. on p. 131).

[477] S. W. Hawking. "Black holes in general relativity". *Commun. Math. Phys.* **25** (1972), 152–166 (cit. on p. 131).

[478] O. Dreyer. "Quasinormal modes, the area spectrum, and black hole entropy". *Phys. Rev. Lett.* **90** (2003), 081301. arXiv: gr-qc/0211076 (cit. on pp. 132, 136).

[479] G. Kunstatter. "d-dimensional black hole entropy spectrum from quasinormal modes". *Phys. Rev. Lett.* **90** (2003), 161301. arXiv: gr-qc/0212014 (cit. on pp. 132, 136).

[480] C. Corda. "Quasi-Normal Modes: The 'Electrons' of Black Holes as 'Gravitational Atoms'? Implications for the Black Hole Information Puzzle". *Adv. High Energy Phys.* **2015** (2015), 867601. arXiv: 1503.00565 [gr-qc] (cit. on pp. 132, 136).

[481] J. D. Bekenstein. "The quantum mass spectrum of the Kerr black hole". *Lett. Nuovo Cim.* **11** (1974), 467 (cit. on pp. 132, 133, 136).

[482] J. D. Bekenstein and V. F. Mukhanov. "Spectroscopy of the quantum black hole". *Phys. Lett. B* **360** (1995), 7–12. arXiv: gr-qc/9505012 (cit. on pp. 132, 133, 136).

[483] G. Immirzi. "Quantum gravity and Regge calculus". *Nucl. Phys. B Proc. Suppl.* **57** (1997). Ed. by V. de Alfaro, J. E. Nelson, G. Bandelloni, A. Blasi, M. Cavaglia, and A. T. Filippov, 65–72. arXiv: gr-qc/9701052 (cit. on pp. 132, 136).

[484] I. Agullo, J. F. Barbero G., J. Diaz-Polo, E. Fernandez-Borja, and E. J. S. Villasenor. "Black hole state counting in LQG: A Number theoretical approach". *Phys. Rev. Lett.* **100** (2008), 211301. arXiv: 0802.4077 [gr-qc] (cit. on pp. 132, 136).

[485] G. Gour. "Schwarzschild black hole as a grand canonical ensemble". *Phys. Rev. D* **61** (2000), 021501. arXiv: gr-qc/9907066 (cit. on pp. 133, 134, 142).

[486] R. B. Mann and S. N. Solodukhin. "Universality of quantum entropy for extreme black holes". *Nucl. Phys. B* **523** (1998), 293–307. arXiv: hep-th/9709064 (cit. on pp. 134, 143).

[487] M. Akbar and K. Saifullah. "Quantum corrections to the entropy of charged rotating black holes". *Eur. Phys. J. C* **67** (2010), 205–211. arXiv: 1002.3581 [gr-qc] (cit. on pp. 134, 143).

[488] S. Carlip. "Logarithmic corrections to black hole entropy from the Cardy formula". *Class. Quant. Grav.* **17** (2000), 4175–4186. arXiv: gr-qc/0005017 (cit. on pp. 134, 143).

[489] S. Mukherji and S. S. Pal. "Logarithmic corrections to black hole entropy and AdS / CFT correspondence". *JHEP* **05** (2002), 026. arXiv: hep-th/0205164 (cit. on pp. 134, 143).

[490] A. J. M. Medved. "A Comment on black hole entropy or does nature abhor a logarithm?" *Class. Quant. Grav.* **22** (2005), 133–142. arXiv: gr-qc/0406044 (cit. on pp. 134, 143).

[491] M. Domagala and J. Lewandowski. "Black hole entropy from quantum geometry". *Class. Quant. Grav.* **21** (2004), 5233–5244. arXiv: gr-qc/0407051 (cit. on pp. 134, 143).

[492] D. Grumiller. "Logarithmic corrections to the entropy of the exact string black hole". *8th International Conference on Path Integrals from Quantum Information to Cosmology*. 2005. arXiv: hep-th/0506175 (cit. on pp. 134, 143).

[493] D. V. Fursaev. "Temperature and entropy of a quantum black hole and conformal anomaly". *Phys. Rev. D* **51** (1995), 5352–5355. arXiv: hep-th/9412161 (cit. on pp. 134, 143).

[494] M. R. Setare. "Space noncommutativity corrections to the Cardy-Verlinde formula". *Int. J. Mod. Phys. A* **21** (2006), 3007–3014. arXiv: gr-qc/0604119 (cit. on pp. 134, 143).

[495] A. Ghosh and P. Mitra. "Entropy in dilatonic black hole background". *Phys. Rev. Lett.* **73** (1994), 2521–2523. arXiv: hep-th/9406210 (cit. on pp. 134, 143).

[496] R. K. Kaul and P. Majumdar. "Logarithmic correction to the Bekenstein-Hawking entropy". *Phys. Rev. Lett.* **84** (2000), 5255–5257. arXiv: gr-qc/0002040 (cit. on pp. 134, 143).

[497] M. Cadoni. "Entanglement entropy of two-dimensional Anti-de Sitter black holes". *Phys. Lett. B* **653** (2007), 434–438. arXiv: 0704.0140 [hep-th] (cit. on pp. 134, 143).

[498] G. Gour and A. J. M. Medved. "Thermal fluctuations and black hole entropy". *Class. Quant. Grav.* **20** (2003), 3307–3326. arXiv: gr-qc/0305018 (cit. on p. 134).

[499] G. Dvali and C. Gomez. "Black Holes as Critical Point of Quantum Phase Transition". *Eur. Phys. J. C* **74** (2014), 2752. arXiv: 1207.4059 [hep-th] (cit. on p. 135).

[500] G. Dvali and C. Gomez. "Black Hole's 1/N Hair". *Phys. Lett. B* **719** (2013), 419–423. arXiv: 1203.6575 [hep-th] (cit. on p. 135).

[501] T. Ikeda, M. Bianchi, D. Consoli, A. Grillo, J. F. Morales, P. Pani, and G. Raposo. "Black-hole microstate spectroscopy: Ringdown, quasinormal modes, and echoes". *Phys. Rev. D* **104**.6 (2021), 066021. arXiv: 2103.10960 [gr-qc] (cit. on p. 135).

[502] W. T. Kim and J. J. Oh. "Dilaton driven Hawking radiation in AdS(2) black hole". *Phys. Lett. B* **461** (1999), 189–195. arXiv: hep-th/9905007 (cit. on p. 136).

[503] J. Engelsöy, T. G. Mertens, and H. Verlinde. "An investigation of AdS_2 backreaction and holography". *JHEP* **07** (2016), 139. arXiv: 1606.03438 [hep-th] (cit. on p. 136).

[504] T. G. Mertens. "Towards Black Hole Evaporation in Jackiw-Teitelboim Gravity". *JHEP* **07** (2019), 097. arXiv: 1903.10485 [hep-th] (cit. on p. 136).

[505] A. Almheiri, N. Engelhardt, D. Marolf, and H. Maxfield. "The entropy of bulk quantum fields and the entanglement wedge of an evaporating black hole". *JHEP* **12** (2019), 063. arXiv: 1905.08762 [hep-th] (cit. on p. 136).

[506] K. Goto, T. Hartman, and A. Tajdini. "Replica wormholes for an evaporating 2D black hole". *JHEP* **04** (2021), 289. arXiv: 2011.09043 [hep-th] (cit. on p. 136).

[507] E. Verheijden and E. Verlinde. "From the BTZ black hole to JT gravity: geometrizing the island". *JHEP* **11** (2021), 092. arXiv: 2102.00922 [hep-th] (cit. on p. 136).

[508] M. Cadoni and A. P. Sanna. "Unitarity and Page Curve for Evaporation of 2D AdS Black Holes". *Entropy* **24** (2021), 101. arXiv: 2106.14738 [hep-th] (cit. on p. 136).

[509] M. Cadoni and S. Mignemi. "Classical and semiclassical properties of extremal black holes with dilaton and modulus fields". *Nucl. Phys. B* **427** (1994), 669–696. arXiv: hep-th/9312171 (cit. on p. 137).

[510] M. I. Hernandez-Velazquez and A. Lopez-Ortega. "Quasinormal Frequencies of a Two-Dimensional Asymptotically Anti-de Sitter Black Hole of the Dilaton Gravity Theory". *Front. Astron. Space Sci.* **8** (2021), 713422. arXiv: 2108.09559 [gr-qc] (cit. on p. 138).

[511] A. Achucarro and M. E. Ortiz. "Relating black holes in two-dimensions and three-dimensions". *Phys. Rev. D* **48** (1993), 3600–3605. arXiv: hep-th/9304068 (cit. on p. 138).

[512] V. Cardoso and J. P. S. Lemos. "Scalar, electromagnetic and Weyl perturbations of BTZ black holes: Quasinormal modes". *Phys. Rev. D* **63** (2001), 124015. arXiv: gr-qc/0101052 (cit. on pp. 138, 140).

[513] S. Hod and U. Keshet. "Intermediate asymptotics of the Kerr quasinormal spectrum". *Class. Quant. Grav.* **22** (2005), L71–L76. arXiv: gr-qc/0505112 (cit. on p. 140).

[514] U. Keshet and S. Hod. "Analytic study of rotating black-hole quasinormal modes". *Phys. Rev. D* **76** (2007), 061501. arXiv: 0705.1179 [gr-qc] (cit. on p. 140).

[515] G. Panotopoulos and Á. Rincón. "Quasinormal spectra of scale-dependent Schwarzschild–de Sitter black holes". *Phys. Dark Univ.* **31** (2021), 100743. arXiv: 2011.02860 [gr-qc] (cit. on p. 140).

[516] D. Birmingham, I. Sachs, and S. N. Solodukhin. "Conformal field theory interpretation of black hole quasinormal modes". *Phys. Rev. Lett.* **88** (2002), 151301. arXiv: hep-th/0112055 (cit. on p. 140).

[517] Á. Rincón and G. Panotopoulos. "Quasinormal modes of scale dependent black holes in (1+2)-dimensional Einstein-power-Maxwell theory". *Phys. Rev. D* **97**.2 (2018), 024027. arXiv: 1801.03248 [hep-th] (cit. on p. 140).

[518] M. Cadoni and M. Cavaglia. "Open strings, 2-D gravity and AdS / CFT correspondence". *Phys. Rev. D* **63** (2001), 084024. arXiv: hep-th/0008084 (cit. on pp. 141, 143).

[519] M. Cadoni and M. Cavaglia. "Two-dimensional black holes as open strings: A New realization of the AdS / CFT duality". *Phys. Lett. B* **499** (2001), 315–320. arXiv: hep-th/0005179 (cit. on pp. 141, 143).

[520] A. Strominger. "AdS(2) quantum gravity and string theory". *JHEP* **01** (1999), 007. arXiv: hep-th/9809027 (cit. on p. 143).

[521] M. Cadoni and S. Mignemi. "Asymptotic symmetries of AdS(2) and conformal group in d = 1". *Nucl. Phys. B* **557** (1999), 165–180. arXiv: hep-th/9902040 (cit. on p. 143).

[522] M. Cadoni and S. Mignemi. "Symmetry breaking, central charges and the AdS(2) / CFT(1) correspondence". *Phys. Lett. B* **490** (2000), 131–135. arXiv: hep-th/0002256 (cit. on p. 143).

[523] M. Cadoni. "Horizons and the quantum and thermal harmonic oscillator". *Mod. Phys. Lett. A* **20** (2005), 1503–1511. arXiv: hep-th/0405174 (cit. on pp. 143, 144).

[524] M. Cadoni, P. Carta, D. Klemm, and S. Mignemi. "AdS(2) gravity as conformally invariant mechanical system". *Phys. Rev. D* **63** (2001), 125021. arXiv: hep-th/0009185 (cit. on p. 143).

[525] V. de Alfaro, S. Fubini, and G. Furlan. "Conformal Invariance in Quantum Mechanics". *Nuovo Cim. A* **34** (1976), 569 (cit. on pp. 143, 144, 146).